THE UNIVERSITY OF
SYDNEY

Development of Novel Scaffold Systems for Modulating Biotic Activity

A tale of two scaffolds

Alexander Stephen Baume

A thesis submitted in fulfilment of the requirements for the degree of Doctor of Philosphy

Faculty of Engineering & IT

2014

Declaration of Original Work

I hereby declare that the following outlines my work contained in this thesis. All design, analysis, discussions and conclusion are my own, although influenced by my supervisor's opinions and by advice from experts in their respective fields.

- I carried out a thorough literature review to understand the fields study, develop experimental approach and draw conclusions from results obtained.
- I fabricated PCL scaffolds and bioglass along with the team from Biometic Pty Ltd. I manufactured composite scaffolds myself.
- I designed both the wound healing scaffold and the ethylene biofilter themselves as well as the manufacturing routes and the protocols to test these systems.
- I performed all experimental protocols myself or with the assistance of those mentioned in the Methods.
- The results presented were generated from my own experiments and analysis and conclusions drawn were my own.

 The above represents an accurate summary of the candidate's contribution.

Alexander Baume

March 31, 2014

Acknowledgements

Firstly, many thanks to my supervisor Professor Andrew Ruys for his continued support and attention that kept the project running smoothly. Thanks go to my associate supervisors: Dr Philip Boughton for the energy and design expertise he put in and; Dr Nick Coleman for his guidance and knowledge in all things bacterial.

A huge thank-you goes to Associate Professor Sue McLennan and her lab for training me in cell culture and qPCR as well as guidance throughout the project. The Friday morning teas are what kept me going.

I'd like to thank Biometic Pty Ltd, particularly Philip Boughton, Chris Baxter and Peter Lok for providing and supporting such an interesting project.

Thanks go to Jake Cao, Rahmat Kartono, Trevor Shearing, the mechanical engineering workshop, the ACMM and the Biometic production team for technical support throughout the project.

To the Baume and Deegan families: Thank you so much for your love, support and humour.

This thesis is dedicated to my grandparents: Pauline, Edith, Ernest and Max.

Abstract

Composite scaffolds are the core of tissue engineering therapeutics that are being used to revolutionise modern medicine. The porous scaffolds are designed to mimic bodily tissues so as to attract cells and accelerate healing. Recently, microbial interactions with composite scaffolds have become an important area of study as infection has been a major problem for these devices. This study explores means of controlling and modulating biotic activity through the use of differentiated coatings on a biocompatible polymer matrix. Both antibacterial and pro-bacterial scaffold systems were developed for chronic skin wounds and ethylene-mediated spoilage respectively. The processes of scaffold fabrication and testing employed many commonalities for both, thereby allowing a parallel development of the dichotomous designs.

Chronic skin wounds present a major problem for the health sector. Wound dressings and other treatments have many shortfalls making them relatively ineffective. Tissue engineered skin grafts are recognised as having great potential, but as yet these have remained costly and impractical owing in part to short shelf life and refrigerated storage. They have also failed to address wound sepsis. An acellular tissue scaffold that can act as a synthetic graft to facilitate healing of chronic dermal wounds is proposed. The bi-phasic composite is comprised of a bioresorbable aliphatic polyester supporting a polyvinyl alcohol (PVA) hydrogel webbing capable of delivering erythromycin antibiotic and bioactive factors. The use of established synthetic biomaterials minimises the costs associated with biologically derived systems.

Reliable and scalable methods were developed for forming bi-phasic scaffolds. 45S5 bioglass was manufactured, characterised and microparticles were coated on the scaffold surface to further increase tissue attachment. Varying concentrations of PVA solution were then assessed with porosity and morphology evaluated. The PVA was cross-linked using freeze-thaw cycles, dehydrated and sterilized. Erythromycin was loaded into the PVA employing ethanol as a carrier and sustained release assays were performed showing that *Staphylococcus aureus* could be inhibited for up to 5 days. A sophisticated *in vitro* co-culture was designed and used to validate the composite scaffold which proved it could simultaneously prevent bacterial biofilms while allowing for fibroblast adhesion and proliferation.

The price of fresh food is on the rise and spoilage is a key inefficiency in the fresh food value chain. Spoilage is partially attributed to ethylene a simple gaseous molecule that is produced by fruits and acts as an aging hormone. In post-harvest storage facilities ethylene can build up and cause the food to spoil

before it reaches the consumer. Chemical based ethylene scrubbers are currently used to prevent this but they are expensive due to the active agents requiring regular replacement. Biofilters using viable microbes to breakdown ethylene have major advantages including their dramatically longer working lifetimes.

A biofilter system was designed using tissue engineering principles that offers control of biofiltration properties. *Mycobacterium* strain NBB4 cells were immobilised to a highly porous polymer matrix in a thin agar coating. The agar coating contained trace element and minerals to enhance bacteria survival and metabolic efficiency. The coating thickness could be controlled by variations in the agar concentration. 0.4% w/v agar was found to be the optimal concentration, maintain high mass transfer while allowing high NBB4 biomass. The biofilter was able to degrade ethylene efficiently for > 85 days and had a shelf life up to > 60 days when in humidified packaging. The biofilters prevented bananas from rotting for up to 1 month compared to controls that spoiled in 2 weeks.

Table of Contents

Table of Figures

Figures

Tables

Table of Acronyms

BG	45S5 Bioactive glass
BMG	Bulk metallic glass
CAP	Chloramphenicol
cDNA	Complementary DNA
Ct	cycle threshold
DDS	drug delivery system
DMA	Dynamic mechanical analysis
DMEM	Dulbecco's modified Eagle's medium
DNA	Deoxyribonucleic acid
DSC	Dynamic scanning calorimetry
ECM	extra-cellular matrix
EDS	Energy dispersive X-ray spectroscopy
EPS	exopolymeric substances
EPS	exopolymeric substances
Ery	Erthromycin
EtO	Ethyene Oxide sterilization
EtOH	ethanol
FCS	Fetal calf serum
FDA	US Food and Drug Administration
F-T	freeze thaw cycle
GC	Gas Chromatography
HA	Hydroxyapatite
HFb	Human Fibroblasts CRL-2097
LB	Luria-Bertani medium
MIC	Minimum inhibitory concentration
MLC	Minimum lethal concentration
MRSA	Methicilin resistant Staphylococcus aureus
MSM	Mineral salts media
NBB3	*Mycobacterium rhodesiae* strain NBB3
NBB4	*Mycobacterium chubuense strain NBB4*
NO	Nitrogen oxide
OD600	Optical density measured at 600 nm
PCL	Polycaprolactone
PDGF	Platelet derived growth factor
PGA	Polygylocolic acid
PknG	Protein kinase G
PLA	Polylactic acid
ppm/ppmV	Parts per million by volume
PVA	Polyvinyl alcohol
RNA	Ribonucleic acid

rRNA	ribosomal RNA
RT-qPCR	Reverse transcription quantitative polymerase chain reaction
Sa	Staphylococcus aureus ATCC29213
SDIMO	Soluble Di-Iron Monooxygenase
SEM	Scanning electron microscopy
TCP	Tricalcium phosphate
Tg	Glass transition temperature
TSA	Tryptic Soya Broth with 15% agar
TSB	Tryptic Soya Broth
TSG	Tryptic Soya Broth with 10% glucose
ZoI	Zone of Inhibition

Glossary

Adsorption/Adhesion	A surface phenomenon in which particles are held on the surface of solid material
Agar	A natural polymer derived from seaweed
Bioactive	A feature of a material such that host tissues form interfacial bonds with it
Biocatalysis	The use of enzymes to catalyse useful reactions
Biocompatible	A feature of a material such that it does not provoke a negative immune response
Biofilm	A community of bacterial enveloped in bio-synthesised polymers
Biofiltration	The removal of waste from a fluid by bacterial metabolism
Biomimetic	Similar in design to natural biological systems
Biore/absorbable	A feature of a material such that it degrades and can be removed from the body by natural metabolism
Calcination	A process to remove unwanted reactant from a glass reaction
Chitosan	A protein derived from crustacean shells
Collagen	A natural protein component of connective tissue
Composite	A solid construct comprising two or more materials
Cross-linking	The physical/chemical bonding between separate polymer chains
Cytotoxic	Toxic to human cells
Debridement	Removal of necrotic skin and other unwanted material from a wound
Fibroblast	The main cell type of the dermis
Housekeeper gene	A highly conserved essential gene that is expressed at a fairly constant level independent of environmental factors on the organism
Hydrogel	A highly hydrated 3D matrix made up of crosslinked polymers
Hydrophobic	Repels aqueous solution
Immobilization	The fixation of bacteria in or on a support material
Ischemia	Reduction in blood flow to tissue
Keratinocyte	The main cell type of the epidermis
Neuropathy	Nerve damage resulting in loss of stimuli detection and response
Operation stability	The working lifetime of a biofilter
Scaffold	A construct with porous architecture
Sputter coating	The physical deposition of a material in vapour form onto another material as a thin film
Sterilization	The complete destruction of pathogens/1 in 1 million probability of a pathogen existing
Turbidity	The density of suspended solids in a solution/cloudy appearance of a liquid

1 Introduction

Composite scaffolds are key therapeutics being developed by tissue engineers to solve a multitude of health problems: Chronic skin wounds, bone deformations, osteochondral defects and heart valve replacement just to name a few. As tissue engineering solutions are moving from the lab bench to the clinic and finally to the market place companies are looking for solutions to finance the expensive and long-term development of the medical therapeutics they have innovated. Dr. David Mooney reported that some tissue engineering companies are leaping the financial hurdles by employing the capabilities they have developed in other fields, such as dentistry and cosmetics, which do not have as many regulatory barriers (Correspondence: Mooney, TERMIS-AM, 2013). This also serves to meet un-met needs in the market place with innovative designs stemming from the health sector.

This thesis describes the design, fabrication and validation of two scaffold systems: One for treatment of chronic wounds and the other a biofilter for fruit preservation. The work relied on a soft tissue scaffold developed by Elizabeth Boughton. It was reasoned that the capabilities developed and knowledge gained from engineering the antibacterial aspects of the scaffold could be combined to engineer a scaffold where the affinity for bacteria could be modulated. This was taken a step further: Composite scaffolds could be synthesised by coating the same base aliphatic polyester scaffold with coatings that could be used for either antibacterial or pro-bacterial applications based on the nature of the coating. Dr. Nicholas Coleman had previously isolated an environmental *Mycobacterium* strain NBB4 which can degrade a number of harmful hydrocarbon pollutants. It was hypothesised that the NBB4 could be immobilized on the surface of a scaffold could serve as a biofiltration device.

Scaffold systems with dichotomous design aims were developed in parallel to provide insights (see Figure 1). Composite scaffolds were fabricated by applying adjunct coating systems to identical base scaffolds and subsequently characterized for antibacterial activity on the one hand and pro-bacterial activity on the other hand. The results of this dichotomous study were used to refine each system. A number of overlapping theories, features and test methods were used during the dichotomous design study. Similar and contrasting elements were determined. The final scaffold designs were validated with *in vitro* pilot studies: The wound healing scaffold was tested in a co-culture to validate conduction of soft tissue and simultaneous prevention of bacterial infection. The biofilter scaffold system was tested in a fruit preservation study to validate the maintenance of freshness of fruit produce beyond the normal shelf life period.

Both scaffold designs are novel for their respective applications. The wound healing scaffold uses a combination of biomaterials and drugs that has not been utilised previously for wound healing. The biofilter scaffold is the first to utilise NBB4 bacteria as the active agent and is particularly novel in the use of tissue engineering principles and materials for the removal of ethylene gas.

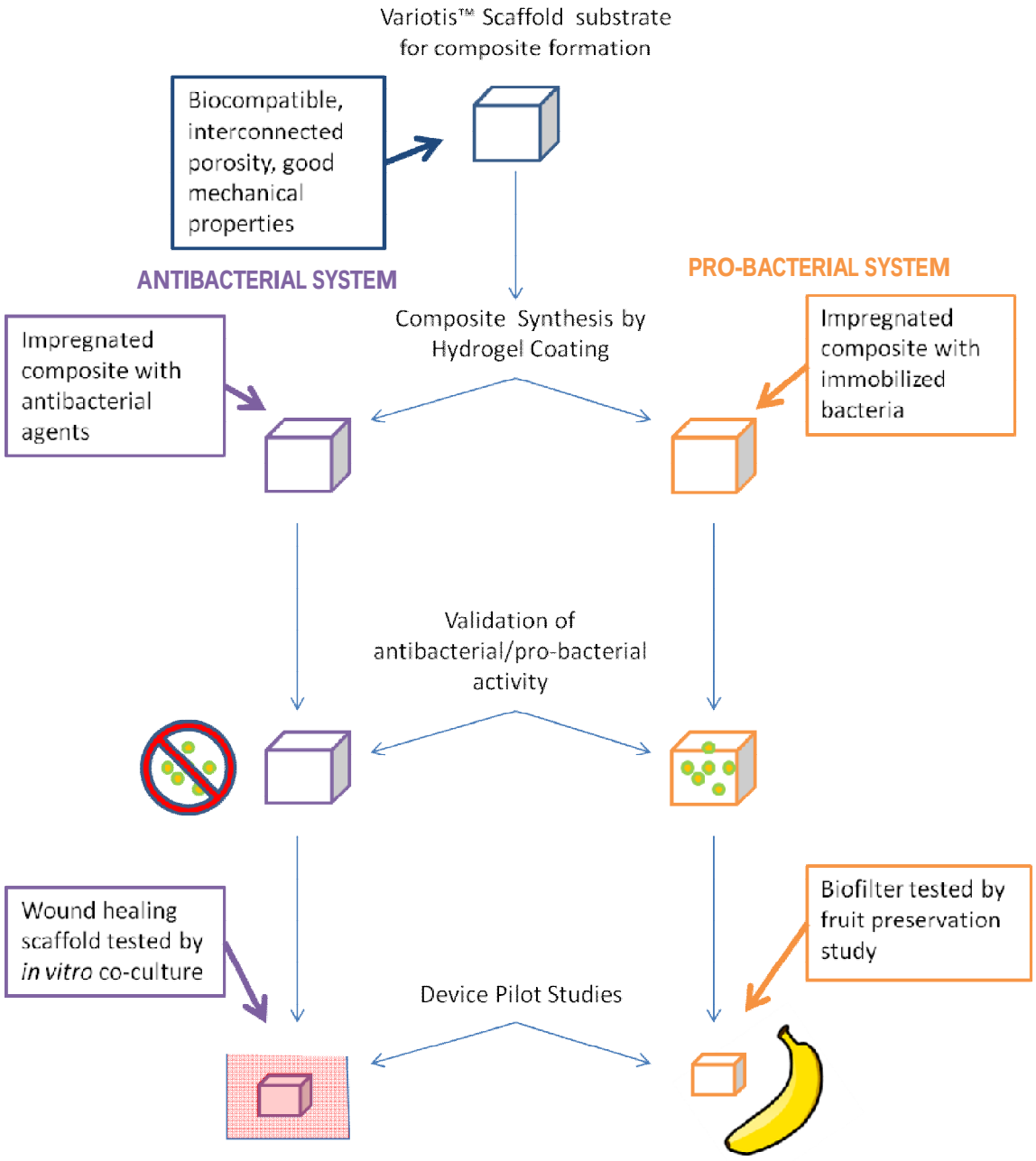

Figure 1. Dichotomous design road map. A schematic representation of the design and development of two separate scaffold systems from the same base scaffold through modulating the biotic activity. The two systems were developed in parallel to take advantage of overlapping features.

1.1 Notes of Reading this Thesis

The simulataneous development of two separate devices is difficult to capture in a single thesis. The thesis has been structured to give the reader a sense of the parallel development and overlap of concepts (see Table 2) while attempting to minimalise confusion from discontinuity of topics. As such the thesis has sections where both devices are discussed and other sections where only a single device is dealt with.

Table 1. Overlapping thesis concepts and their application in each scaffold system.

	Application of Concepts	
Overlapping Concepts	*Wound Healing Device*	*Biofilter Device*
Porous Scaffolds	Transportation of nutrients and waste; cell migration; diffusion of antibiotics.	Diffusion of ethylene; filtration kinetics, elution of waste
Composite formation/Scaffold coatings	Bioglass coating; PVA coating; structural alterations, thickness optimisation, emulating soft tissue modulus.	Agar coating; structural alterations, thickness optimisation, mechanical stability
Hydrogels	Freeze-thaw crosslinking; antibiotic delivery; slow delivery	Gel entrapment; humidified gel environments, Cell nutrition
Biofilms	Antibacterials; antibiofilm surfaces; biofilm inhibition	Bacterial adhesion and immobilization; pro-bacterial activity; long-term biofilm survival

The Background section is broken up into 3 smaller subsections: First composite scaffolds are discussed in a general sense followed by all aspects relating to the wound healing device and finally by the biofilter device. This is to avoid confusion and discontinuity, giving a holistic view of each device. The reader will note however that there is substantial repetition of ideas and concepts. The Methods and Results &

Discussion sections are structured based on the parallel development and as such each subsection contains information relation to both devices in a semi-integrated manner. That is experiments relating to each device is distinct but these are arranged into sections based on design phase rather than device type. A Device Design Summary section is included for each device so the reader can have a summarised view of the design inputs and outputs for each device separately. Finally the Conclusion section briefly deals with the project it its entirety assessing the dichotomous design process and whether bacterial activity could be modulated on the scaffold system. A visualisation of the structure of this thesis can be seen below (Table 2).

Table 2. A guide for reading this thesis. Blue subsections are those common to both devices; purple sections relate specifically to the wound healing device; orange sections relate specifically to the biofilter device.

Section	Subsections	
Background	Composites	
	Wound Healing Grafts	Ethylene Biofilters
Methods	Composite and Material Fabrication Biofilm Formation Antibacterial/Pro-bacterial Activity Device Pilot Studies	
Results and Discussion	Composite and Material Fabrication Biofilm Formation Antibacterial/Pro-bacterial Activity Device Pilot Studies	
Device Design Summary	Synthetic Skin Graft	NBB4 Ethylene Biofilter
Conclusion	Conclusion	

1.2 Aims

- To control the microbiotic interactions of a biocompatible polycaprolactone (PCL) scaffold such that it can support and hinder bacterial activity.
- To design and develop an antibacterial scaffold that will serve as a synthetic skin graft for treatment of chronic skin wounds.
- To design and develop a pro-bacterial scaffold that will serve as a biofilter for ethylene to preserve fruit and minimise fresh produce spoilage.

1.3 Hypotheses

- The microbiotic interactions of a biocompatible PCL scaffold will be able to be modulated by forming composites using specific bioactive coatings.
- An antibacterial composite scaffold can be formed which prevents the attachment and growth of common wound bacteria while facilitating dermal tissue growth.
- A pro-bacterial composite scaffold can be formed which immobilizes viable ethylene degrading microbes while maintaining a high porosity, thus allowing the efficient filtration of ethylene and preservation of fruit.

2 Background

2.1 Composite Scaffolds

A Tissue Engineering scaffold is a medical device which acts as a template to grow biological cells in vitro and in vivo. The scaffold is a biomimetic device that forms the extra-cellular matrix (ECM) providing an initial support framework for cells to attach and grow[1]. There are some characteristics that are common in scaffolds, independent of their final function. These are biocompatibility, porosity, degradability and 3D structure [2]. However, generally the design of a scaffold's properties is dependent on the intended use, which usually relates to the anatomical location the scaffold is trying to mimic and the type of cells it will host [1, 3-6]. The properties dependent on the anatomical location of the scaffold are mechanical properties, structural properties, surface chemistry and degradation rates.

Scaffold properties are controlled by selecting biomimetic materials for the target location. It is rare that one material can provide all the key properties to properly mimic the complexity of the ECM. Therefore biomaterials are usually combined to form composite scaffolds containing multiple materials which each contribute to the scaffolds properties [1-2]. For example hydroxyapatite (HA) has excellent biocompatibility with hard tissues such as bone, but is mechanically brittle. Thus HA/collagen composites are formed to improve strength and further enhance biocompatibility [1].

2.1.1 Generic Properties

2.1.1.1 Biocompatibility

Interactions between implanted materials and their host tissue are of great importance for the fate of the implanted device. The interactions have effects both on the healing response and the long term organization of the surrounding tissue[7]. An ideal scaffold should have excellent biocompatibility with a high affinity for cells to attach and proliferate [1, 3-5]. An implanted scaffold must not trigger an immune response in the patient as this could lead to chronic inflammation posing risk to the patient and resulting in possible rejection of the scaffold [6].

It is implied that the surface properties of the scaffold material play an important role in the biocompatibility [7] and whether an immune reaction will occur. Surface properties also affect the cell attachment sites further impacting the biocompatibility [8]. Biocompatibility of scaffold degradation products, released therapeutics or other diffusible products should also be considered.

Biocompatibility is clearly important, although it is important to note that “biocompatibility” is not an intrinsic property of a material, but depends on the biologic environment and the leeway that exists with respect to tissue reaction. For example, a scaffold that is biocompatible in subcutaneous tissue might not be so in nerve or in the peritoneum [6].

2.1.1.2 Porosity

Scaffolds must have an interconnected porous network for a number of reasons:

1. For transport of nutrients and wastes between cells via the interconnected network of pores.
2. So cells can migrate and have sites for firm attachment.
3. Angiogenesis, the formation of new blood vessels through the scaffold to supply newly formed tissues.
4. To properly mimic the ECM of bodily tissues.

Two types of pores can be differentiated, the micro- and the macropores. The size of the prior one is up to 100 µm, and the latter ranges in 100–500 µm. The pores below 100 µm are to improve the gas, air and nutritive transport, while the macropores are to give mechanical support and a temporary frame for cells to attach and proliferate [1, 5, 9]. A typical porosity of around 90% as well as a pore diameter of at least 100 µm is known to be compulsory for cell penetration and a proper vascularisation of the ingrown tissue [2, 10].

2.1.1.3 Degradability

Initially when a scaffold is implanted it must act wholly as the tissue it is replacing. But, as time goes on and cells begin to inhabit the scaffold and lay down new ECM, the scaffold should degrade letting the new tissue take over. All scaffolds must be biodegradable, so that eventually the native tissue can completely heal and resume its normal function [1, 3-5, 8, 11]. Therefore controlling the degradation rate is crucial. Optimally the degradation of the scaffold should correspond with the natural healing time of the injury [12].

It is believed that degradation occurs in five stages: hydration, depolymerization, mass loss, absorption and elimination. The degradation of scaffolds depends on several parameters, namely the biomaterial’s intrinsic properties and the scaffolds morphology. It is of general acceptance that the higher the water uptake, the higher the hydration rate, the higher the degradation rate [11]. Cunha-Reis *et al* tested the impact of morphology on scaffold degradation rate. They found that scaffolds with smaller fibre

diameter lead to greater water uptake and increased degradation. This was due to the scaffold having a greater surface area of contact with the water. What's more, scaffolds with the same fibre diameter were tested with different porosities; The porosity had no effect on either the water uptake or the degradation [11]. This illustrates the effect of porous scaffold structure on degradation rates.

2.1.1.4 3D structure

Scaffolds are 3D structures just the same as human tissues are [6]. Cells respond to positional cues and mechanical stresses ensuring proper tissue growth. This phenomenon is only seen in 3D culture situations as these stimuli are virtually non-existent in traditional 2D cell culture systems. As a result, contemporary culture methods are being replaced with 3D culture techniques [13]. This is a prominent non-clinical application for tissue engineering.

2.1.2 Biocompatible synthetic polymers

2.1.2.1 Natural vs Synthetic

Biocompatible polymers and naturally occurring biopolymers are the most common biomaterials for scaffold fabrication. Synthetic polymers include relatively hydrophobic materials such as the α-hydroxy acids (polyglycolic acid (PGA) and polylactic acid (PLA)), aliphatic esters (Polycaprolactone (PCL)), polyanhydrides and many others. Naturally occurring biopolymers include hyaluronan, chitosan, elastin and collagen [6]. However, synthetic biopolymers offer an advantage over natural materials in that they can be tailored to give a wide range of properties, are less expensive and easier to manufacture [1]. In particular, many investigations have concentrated on synthetic biodegradable polymers that are already approved by the US food and drug administration (FDA). The most common biodegradable polymers being used or studied include PLA, PGA, and PCL (and their co-polymers) [1, 6, 14].

2.1.2.2 Bioabsorbability

The synthetic polymers mentioned above have excellent biocompatibility; what's more their degradation products of these polymers are present in the human body and are removed by natural metabolic pathways[3]. Thus they are 'bioabsorbale' [15].

When polymers degrade, firstly breaks in the polymer chain occur reducing the molecular weight. Monomers are then released into solution decreasing the mass of the bulk polymer. It has been described that these degradation products are mildly acidic and when released in high concentrations

can result in an immune response in vivo [1]. In terms of the most common synthetic biopolymers, their erosion rates follow the order PGA > PGLA> PLA > PCL. This is mainly due to the polymers' interactions with water, with PGA being the most hydrophilic and PCL being the most hydrophobic [1, 16-17]. The fast degradation rates of α-hydroxy acid biopolymer family (PGA, PGLA and PLA) coupled with acidic monomer products compromises their biocompatibility [3, 6, 8].

Table 3. Synthetic polymer property comparison for tissue engineering: α-Hydroxy Acids vs Polycaprolactone.

α-Hydroxy Acids	Polycaprolactone
Stiff	Flexible
Fast Degradation	Slow Degradation
High mp	Low mp

High molecular weight PCL has mechanical properties that suit hard and soft tissue applications [1, 9, 18]. PCL degrades the slowest out of synthetic biopolymers used for scaffolds, taking over a year to degrade. This is due to the five hydrophobic –CH2 moieties in its repeating units, making it very hydrophobic [16]. Because of this, some have criticised PCL's use as a scaffold, limiting its application to long-term drug delivery or commercial sutures [1, 11, 16]. Furthermore degradation studies become somewhat inefficient to run without the use of a catalyst. *Pseudomonas cepacia* lipase has been reported to greatly increase the degradation rate of PCL, so meaningful results can be obtained within a week [8, 19]. However, slow degradation is not necessarily a disadvantage. Since PCL has a much slower rate of hydrolysis the deposition of acidic monomers is not a problem, as they are removed by the body before accumulating in large amounts [8]. Olah *et al* [9] also saw the potential of PCL as a suitable scaffold material for bone regeneration, because a slower degradation rate is needed due to the slow-healing nature of bone. The very low melting temperature of PCL (60°C) makes it easier to process than other biopolymers. These advantages make PCL a versatile scaffold material.

2.1.2.3 Surface properties

As mentioned synthetic biopolymers have hydrophobic surfaces which adsorb key proteins conditioning the surfaces for cellular attachment – a necessary property for tissue engineering. PCL, PGA and PLA are

all tissue conductive materials that cells can actively attach to [1-2, 17]. However, being synthetic materials they lack the cell recognition signals of natural polymers. Their hydrophobic nature also inhibits cell seeding [20].

Cottam *et al* [8] demonstrated that Bovine chondroprogenitor cells attach and proliferate on PCL surfaces. Zhang et al [20] showed that the addition of hydrophilic collagen to PCL firbres, increased the surface attachment and migration of dermal fibroblasts.

2.1.3 Hydrogels

2.1.3.1 Gels vs Hydrogels

Hydrogels are highly hydrated 3D matrices made up of crosslinked polymers. This is distinct from a gel which is merely a semi-solid arrangement of polymers. The crosslinked network gives hydrogels the unique swelling property. That is, hydrogels remain insoluble in aqueous solution and instead swell up while maintaining their 3D structure while gels dissolve [21]. This has made hydrogels useful in many biomedical applications including wound dressings, contact lenses and drug delivery systems.

2.1.3.2 Structure

Hydrogels are 3D arrangements of hydrophilic crosslinked polymer chains. It is the hydrophilicity of the polymer chains that draws water molecules into the system causing the swelling effect. While swollen, hydrogels form mechanical stable structures, held together by the crosslinks. These structures are elastic in nature due to the inherent shape memory, allowing repeated swelling and drying with negligible permanent deformation[21]. In dried form, hydrogels are often glassy and brittle.

When in hydrated form, hydrogels possess some water-like properties such as permeability of water-soluble substances through the polymer matrix. This is, amongst other things, governed by the nano-porous network existing between the crosslinked polymers [22-23].

2.1.3.3 Fabrication

Synthesis of hydrogels often occurs in three distinct steps:

1. Preparation of polymer solution
2. Crosslinking

3. Casting/forming

In the first step, hydrophilic polymers usually in powdered form are added to water and with the application of heat and agitation made into an aqueous solution. The viscosity of this solution must be controlled as this may be important in casting/forming the desired structures. For example a very low viscosity is required for spray drying, such that Salama *et al* [24] used a relatively low PVA concentration in (1.5% (w/v)) water to achieve this.

The second crosslinking step determines much of the hydrogel's properties. Crosslinking is the chemical or physical process that connects the polymer chains together forming a networked structure and increasing the average molecular weight. Chemical processes act to create free radicals which break and then reconnect the polymer backbones for a net lengthening of the chains. Physical processes create crystal structures, mechanically locking polymer chains together [25-26]. The proportion of crosslinking can depend on the composition of the polymer solution as well as the temperature and other environmental conditions during the reaction.

Casting and forming of hydrogels is usually performed by pouring the aqueous crosslinked hydrogel into a mould to achieve the desired shape. Hydrogels are often quite soft materials when hydrated and can be cut to size once solid.

2.1.3.4 Types

2.1.3.4.1 Natural

Naturally derived hydrogels have been used regularly in tissue engineering and other biomedical devices because they are either biomimetic or components of the natural extra cellular matrix (ECM). This is thought to improve biocompatibility and accelerate tissue growth and differentiation in vivo[27].

Collagen is the most abundant protein in the mammalian extra cellular matrix. Although there are many different types of collagen, they share a common structure of three polypeptide chains coiled around one another forming a rope shape. Collagen can self aggregate forming the network structure necessary for hydrogels. This network can be more densely crosslinked by the addition of physical (freeze-drying, heating) or chemical processes (UV-irradiation, glutaraldehyde, formaldehyde) [27]. Collagen is bioabsorbable since it is broken down collagenases and other proteases in vivo.

Despite advantages such as bioactivity and bioabsorbability, naturally derived hydrogel materials have a limited application because of their high cost and low shelf lives.

2.1.3.4.2 Synthetic

Synthetically derived hydrogels are gaining traction in biomedicine because of their controllable physical and chemical properties, reproducibility and relatively low cost in comparison to their naturally derived counterparts [27-28].

Poly(vinyl alcohol) (PVA) is a widely used hydrogel in drug delivery and space filling. It is biocompatible [29]and bioresorbable [15]. PVA is also known for its film and fibre forming properties [29]. PVA aqueous solutions can be physically crosslinked by freeze-thaw cycles which forms crystallites binding the polymers chains [22, 25, 30-33]. It can also be chemically crosslinked by glutaraldehyde, succinyl chloride, adipoyl chloride, and sebacoyl chloride[27]; as well as by electron beam, gamma [22, 34] and UV irradiation (in the presence of photocrosslinkers, like acrylamide) [35].

2.1.3.5 Hydrogel Properties

The hydrogel materials and the fabrication method dictate the properties of the hydrogel. The material properties such as molecular weight and the chemical structure determine the final network structure and its interaction with the external environment. For example, pH-responsive hydrogels are composed of polymeric backbones with ionic pendant groups[21]. The fabrication method controls the polymer network structure and composition on a molecular level which in turn affects the macro properties [27].

2.1.3.5.1 Molecular

The density of crosslinking is the most important property which will govern the physical function of the hydrogel. Increasing crosslinking will typically increase the hydrogels mechanical properties and decrease the rate of swelling and the network pore size which is important for diffusion and transportation kinetics [22].

The polymer main chain and side chain chemical structure impact the mobility of the polymer and thus affect the T_g. The glass transition temperature (T_g) is the state in which polymer chains can move past one another facilitating the change from a glassy to a rubbery solid. Flexible groups such as ether linkages reduce the T_g, where as stiff chemical groups like benzene rings increase it [21-22].

2.1.3.5.2 Macroscopic

When dehydrated, hydrogels are often glassy solids with collapsed polymer chains. On contact with water or other aqueous media, the macroscopic pores become penetrated with liquid which imposes stresses on the matrix which open up the network. This is seen macroscopically as swelling [21].

T_g is a crucial macroscopic property in hydrogels. T_g is the temperature at which a dehydrated glassy hydrogel will become rubbery and thus be allowed to swell. This property also mediates many of the hydrogels mechanical properties [21-22].

2.1.3.5.3 Biological

Hydrogels mimic biological tissues closely with their highly hydrated structures and soft rubbery consistency and water retentive capabilities [21].

Hydrogels are composed of hydrophilic polymers which relates to low surface tension. This results in a minimal tendency to adsorb proteins in body fluid, prohibiting tissue ingress and platelet adhesion [21, 29].

Adsorption of proteins to the biomaterial surface is almost instant when it contacts the blood plasma. The adsorption of protein is governed by many complex interactions, but generally hydrophobic surfaces adsorb more proteins than hydrophilic ones [36]. Most mammalian cells require attachment to biocompatible substrates to grow and differentiate. Thus protein adsorption to biomaterials is crucial for cell adhesion [37]. However, protein adsorption is also important in mediating clotting and immune response. Thus the protein adsorption should be tailored for the medical device application.

2.1.3.6 Hydrogel Characterisation

Hydrogels can be characterised on a molecular, micro and macro level using a range of techniques and instruments.

Important physical properties such as melting temperature, degree of crystallinity and glass transition temperature can be determined by dynamic scanning calorimetry (DSC) [29, 32, 38]. Melting temperature and degree of crystallinity can be used to validate crosslinking. Lian *et al* showed an

increase in T_g with addition to PEO to PVA hydrogels[32]. As mentioned above T_g is a crucial hydrogel property determining the rate of relaxation of the matrix and thus relates to drug delivery kinetics.

Fourier transform infrared spectroscopy (FTIR) can be used to determine the type of bond used in hydrogel crosslinking [39]. The presence or absence of bonds is shown by the absorbance at specific wavelengths. For example, Basak *et al* crosslinked PVA with maleic acid for colon targeted drug delivery and found by FTIR analysis a sharp peak at 1640 characteristic of the C=C bond. This implied the C=C bond in the maleic acid backbone was preserved and not used in crosslinking. Analysing the full spectra gave a detailed picture of how the molecules interact during crosslinking [38].

The degree of swelling is an important characteristic of the hydrogel and reflects how much the hydrogel swells compared to the dry state. This characteristic is determined by gravimetric analysis. Dried films are pre-weighed then immersed in a liquid phase until swelling equilibrium is achieved. The surface water is removed from swollen films before re-weighing. The degree of swelling is then calculated as follows:

$$Degree\ of\ Swelling\ \% = \frac{w_w - w_d}{w_d} \times 100 \qquad (1)$$

where, w_d and w_w are the initial dry weight and final wet weight of the hydrogel films, respectively [31, 38-39].

The gel fraction of a hydrogel is another property that can be easily determined by gravimetric analysis and provides valuable information about the relative degree of crosslinking within the matrix. Preweighed hydrogels are immersed in solution for a long period to solubilise any un-crosslinked polymers. The samples are then dried and reweighed. The gel fraction is calculated as follows:

$$Gel\ Fraction\ \% = \frac{w_e}{w_0} \times 100 \qquad (2)$$

where, w_e is the dry weight after long term leaching of polymers in solution and w_0 is the initial dry weight [32].

2.1.3.7 Hydrogel/Polyester Composites

Hydrogels do not generally have the blood adsorption properties to support cellular attachment for tissue engineering. This is attributed to the hydrophilic nature of hydrogels affecting the adsorption of key blood proteins such as fibronectin [27]. Synthetic hydrogels in particular are subject to this property

and this has been utilized in other fields of biomedical design. PVA has been used as a non-adhesive in tendon repair. Common ways around this problem that tissue engineers have utilized is introducing a bioactive co-polymer such as collagen and covalently coupling blood protein peptides that can bind directly to cell receptors [27]. Forming composites with hydrophobic polyesters and hydrophilic hydrogels may pose a solution for mimicking the water absorbing and cell binding properties of native ECM.

Hydrogel/Polyester composites may also overcome shortfalls in mechanical stability of ordinary hydrogels. Mechanical properties are important for scaffolds to perform under mechanical strains of surrounding tissue and to support cell growth which is very much dependent on mechanical cues [27]. Pok *et al* [40] designed a multi-layered scaffold with a PCL core which provided mechanical support for the low strength chitosan-gelatin surface layer.

Hydrogel scaffolds often have very small pore sizes. This limits the cell ingrowth and promotes bacterial infiltration of the scaffold which can enter the porous structure and remain protected from host immune cells which cannot follow.

2.1.4 Bioactive Glass

2.1.4.1 Bioactivity

Bioglass is a synthetic, resorbable bioceramic that is highly bioactive. When Bioglass particles come in contact with body fluids a chemical change occurs resulting in a hydroxyapatite layer forming on the glass surface [41-45]. The step-by-step reactions of this process are summarised in Table 4. Native cells will interact with this layer as if it were “self”, binding to it readily and forming a strong adhesion to the material.

Table 4. Reaction Stages of Bioactive Glass [42].

Stage	Reaction
1	Rapid exchange of Na^+or K^+ with H^+ or H_3O^+ from solution: $Si-O-Na^+ + H^+ + OH^- \rightarrow Si-OH^+ + Na^+(solution) + OH^-$ This stage is usually controlled by diffusion and exhibits a $t^{-1/2}$ dependence.
2	Loss of soluble silica in the form of $Si(OH)_4$ to the solution, resulting from breaking of Si–O–Si bonds and formation of Si–OH (silanols) at the glass solution interface: $Si-O-Si + H_2O \rightarrow Si-OH + OH-Si$ This stage is usually controlled by interfacial reaction and exhibits a $t^{1.0}$ dependence.
3	Condensation and repolymerization of a SiO_2-rich layer on the surface depleted in alkalis and alkaline-earth cations: 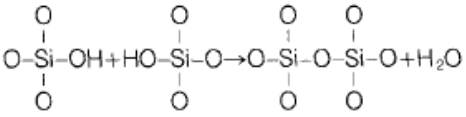
4	Migration of Ca^{2+} and PO_4^{3-} groups to the surface through the SiO_2-rich layer forming a $CaO-P_2O_5$-rich film on top of the SiO_2-rich layer, followed by growth of the amorphous $CaO-P_2O_5$-rich film by incorporation of soluble calcium and phosphates from solution.
5	Crystallization of the amorphous $CaO-P_2O_5$ film by incorporation of OH^-, CO_3^{2-}, or F^- anions from solution to form a mixed hydroxyl, carbonate, fluorapatite layer.

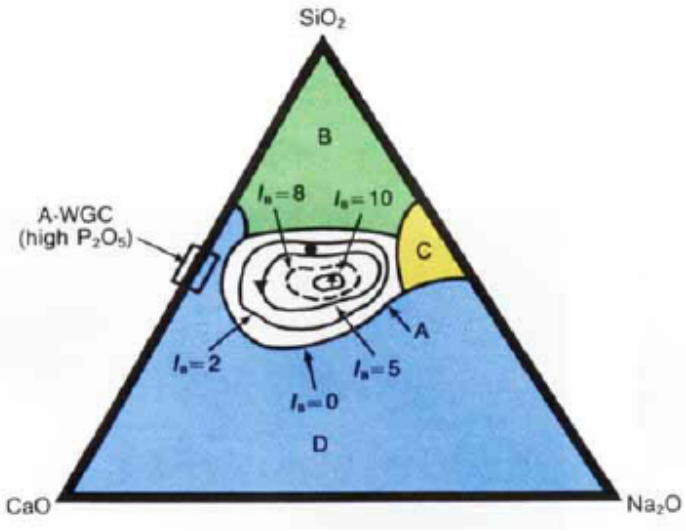

Figure 2. Compositional dependence of bioactive glasses on bone and soft tissue bonding [42]. (A) Bioactive Region; within dashed line soft tissue bonding also occurs (e.g. 45S5). (B) Bioinert Region; non-resorbing glasses, fibrous capsule formation occurs. (C) Unstable; resorb too rapidly. (D) Impractical Glasses; untested.

The main constituents of Bioglass are SiO_2, Na_2O, CaO and P_2O_5. The level and type of bioactivity and stability of the Bioglass can be controlled by altering the chemical composition of these constituents. The bioactivity of different glass compositions has been tested and the results summarised in Figure 2.

It has been found that the 45S5 Bioglass (signifying 45 wt% SiO2 as the network former and a 5 to 1 molar ratio of Ca to P) has optimal bioactivity for both hard and soft tissues [42]. It has been suggested that the silica and phosphate composition of this class of bioactive glass are within the optimal range that allows dissolution and calcium phosphate formation at its surface while maintaining the appropriate rate of degradability. This composition has also been shown to up-regulate osteoblast activity and proliferation via a complex genetic mechanism involving seven gene families [41]. It is because of its versatility and high bioactivity that 45S5 composition is the most commonly used and tested Bioglass.

2.1.4.2 Antibacterial Compositions

More recently, studies have been conducted to dope bioactive glasses with a number of different metal oxides to incorporate antibacterial and other desirable properties into the material [41, 46-52]. When this doped bioglass comes into contact with body fluids, metallic ions will be released and elicit a local antibacterial effect, which is dependent on the doping metal/s chosen. Furthermore, the antibacterial effect will be gradual and long-term because the metallic ions are slowly released as the bioglass is resorbed. Robinson *et al* [52], states the important characteristics of bioresorbable anti-bacterial materials:

i) Broad-spectrum antibacterial activity;

ii) Non-toxic to surrounding host tissue;

iii) Must not be susceptible to microbial resistance.

Since ancient times, silver has been used in medicine for controlling infections [47]. Nowadays, silver is one of the preferred methods to confer microbial resiliency on biomedical materials and devices [41, 47-48]. This is due to its rapid broad-spectrum bacteriostatic and bactericidal effects. Bellantone *et al*, compared the antibacterial action of silver doped bioglass (AgBG: wt %, was as follows: 76% SiO2; 19% CaO; 2% P2O5; and 3% Ag2O) to a novel bioglass (BG: wt% SiO2, 76%; CaO, 22%; P2O5 2%) and 45S5; on three common wound pathogens: *E.coli*, *S. aureus*, and *P. aeruginosa*. It was found that AgBG was

bacteriostatic at concentrations of between 0.05 – 0.2 mg/ml and rapidly bactericidal at 10 mg/ml (Figure 3). At the same concentrations BG and 45S5 had no antibacterial effect [48]. This result was reinforced in a similar study by Balamurugan *et al* [46]. It is important to note that some studies have found 45S5 Bioglass to be antibacterial due to sodium and calcium ions elevating pH [53-54]. However this occurred at much higher concentrations than in the study conducted by Bellantone [47-48, 52-54]. It is commonly mentioned that the optimal composition of AgBG, at which bioactivity is not compromised is 2-5 %wt [41, 43, 46-48].

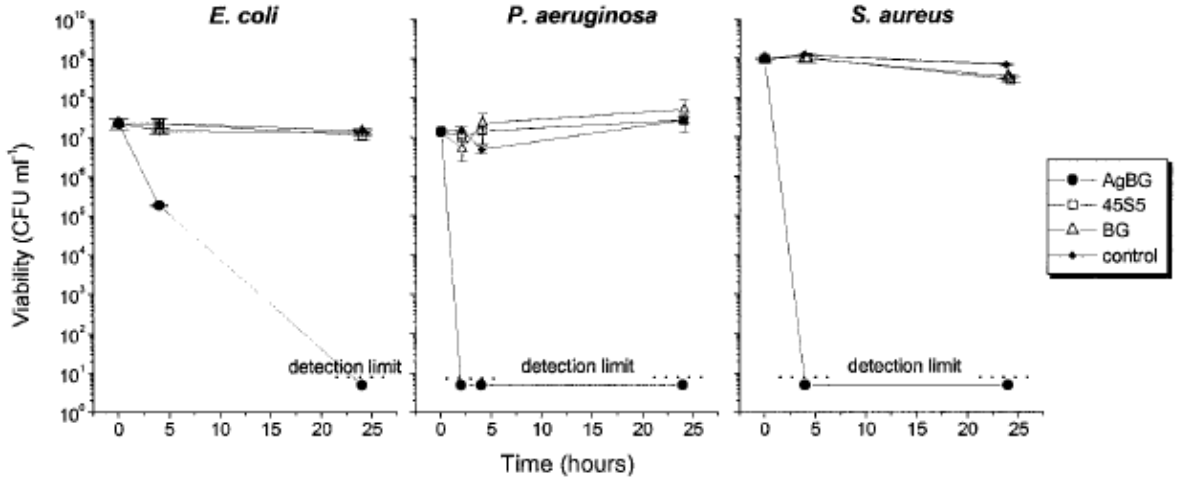

Figure 3. Time-dependent killing of common wound pathogens by bioactive glasses (10 mg/ml) [48].

It is agreed that the antibacterial mechanism of silver is attributed to leaching of Ag+ ions rather than a change in pH because of the obvious uptake of Ag+ ions by bacteria [46-48, 51]. Although the precise interactions between Ag+ ions and microbial cells is not well understood. Balamurugan suggests that the main driving force for the antimicrobial activity are the interactions between silver ions and the bacterial nucleophilic amino acid residues in key proteins causing denaturation resulting in cell death [46]. Whereas Matsumoto [51] states that Ag+ ions that passed through the cell membrane were present in the interior of the cell, and not in the cell membrane; these ions interacted with a ribosomal subunit protein linked to thiol groups, and then they inhibited the expression of enzymes and protein products necessary for the functioning of adenosine triphosphate (ATP), resulting in cell death. Kumar *et al* [55] states that silver nanoparticles target electron transport proteins located on exterior of prokaryotes, but in eukaryotes this protein is inside cell mitochondria and thus requires greater dosage for cytotoxic effect.

In any case, silver doped bioglass is a potent candidate for an antibacterial resorbable material. It has broad-spectrum activity, not susceptible to microbial resistance [41, 46-47, 51], and has a rapid and concentrated bactericidal effect which is essential for a successful anti-biotic agent [46]. Furthermore, silver has been has been shown to aid in healing of sterile skin wounds in rat models, reducing inflammation and granulation tissue [41]. However, silver does have some disadvantages, firstly that it is non-essential to the host and can be cytotoxic [52]; Ag+ is considered a highly toxic metal ion [51]. Secondly, there is a challenge in preserving the 1+ oxidation state of the Ag2O.

Although silver seems to be the most acclaimed antibacterial doping agent, there are a number of other additives to consider. Magnesium was shown to have an antibacterial affect on wound pathogens by Robinson *et al* [52]. Magnesium imposed an antimicrobial effect by leaching Mg2+ ions which in turn caused an increase in pH. High alkalinity cannot easily be resisted by bacteria and is not necessarily cytotoxic to cells. Saboori *et al* doped bioglass with silica and found it increased its stability and mechanical properties. The Mg-bioglass was non-cytotoxic and supported bone marrow stem cells [43, 56]. Zinc and copper are well known antibacterial factors [51-52, 57-58]. Sheng *et al*, found that Zn2+ inhibited the bacterial catabolism of glutamate [57]. Matsumoto *et al* [51] studied the antibacterial effect of co-doped silver, zinc and copper tricalcium phosphate and found that the addition of zinc and copper lead to the creation of free radicals eliciting an enhanced bactericidal effect. Zinc bioglasses show higher surface areas which enhances bioactivity due to the increased number of nucleation sites on the calcium phosphate phase. However, zinc has been shown to decrease glass degradation rates. Both zinc and copper glasses have been suggested in the prevention of inflammation [43]. However, while considered essential to normal homeostasis, both have the potential for toxic sequelae [52]. Titanium is another possible antibacterial bioglass additive [59] and Vrouwenvelder *et al* [45] demonstrated that osteoblasts show superior histological and biochemical parameters grown on Ti-doped 45S5. Although, some report that Titanium has no antibacterial effect [58].

Fluorine is a non-metallic bioglass additive with great antibacterial potential. Fluorine has been demonstrated as a potent antimicrobial toward oral anaerobes in the dental industry [58, 60]. Yoshinari *et al* [58] suggested that metal-fluoride complexes with their inhibition of enzymatic activity have a bactericidal effect on bacteria. When calcium fluoride was incorporated into 45S5, the Bioglass became more stable but exhibited decreased bone bonding [45]. Thus far, the antibacterial effect of Fluorine-doped Bioglass has not been tested.

2.1.4.3 Manufacturing

To date, clinical applications of silica-based bioactive glasses are limited to those materials synthesized by melting processes [43]. The raw ingredients, which normally consist of SiO_2, Na_2CO_3, $CaCO_3$ and $Ca_3(PO_4)_2$ [44, 61-62], are well mixed and heated in a conventional furnace. A platinum crucible is usually used because of its low reactivity and high melting point [44, 61-63]. The heating cycle for melt-derived glass usually includes a calcination phase at around 1000°C before smelting at 1300-1450°C [44, 61-64]. Figure 4 clearly shows the entire process of making melt-derived bioglass.

In the early 1990s bioactive glasses were for the first time prepared by the sol–gel process. Porous bioglasses could be prepared from the hydrolysis and polymerization of metal hydroxides, alkoxides and/or inorganic salts [43]. The induced porosity from the sol-gel process increases the compositional range of bioactivity for these glasses due to the increased surface area. The high porosity also yields excellent degradation properties [43, 47]. The sol-gel method has the added benefit of not being conducted at high temperatures. The disadvantage of porous sol-gel derived glasses is the decreased mechanical strength, which can result in the brittle fracture under rehydration stresses [2, 47].

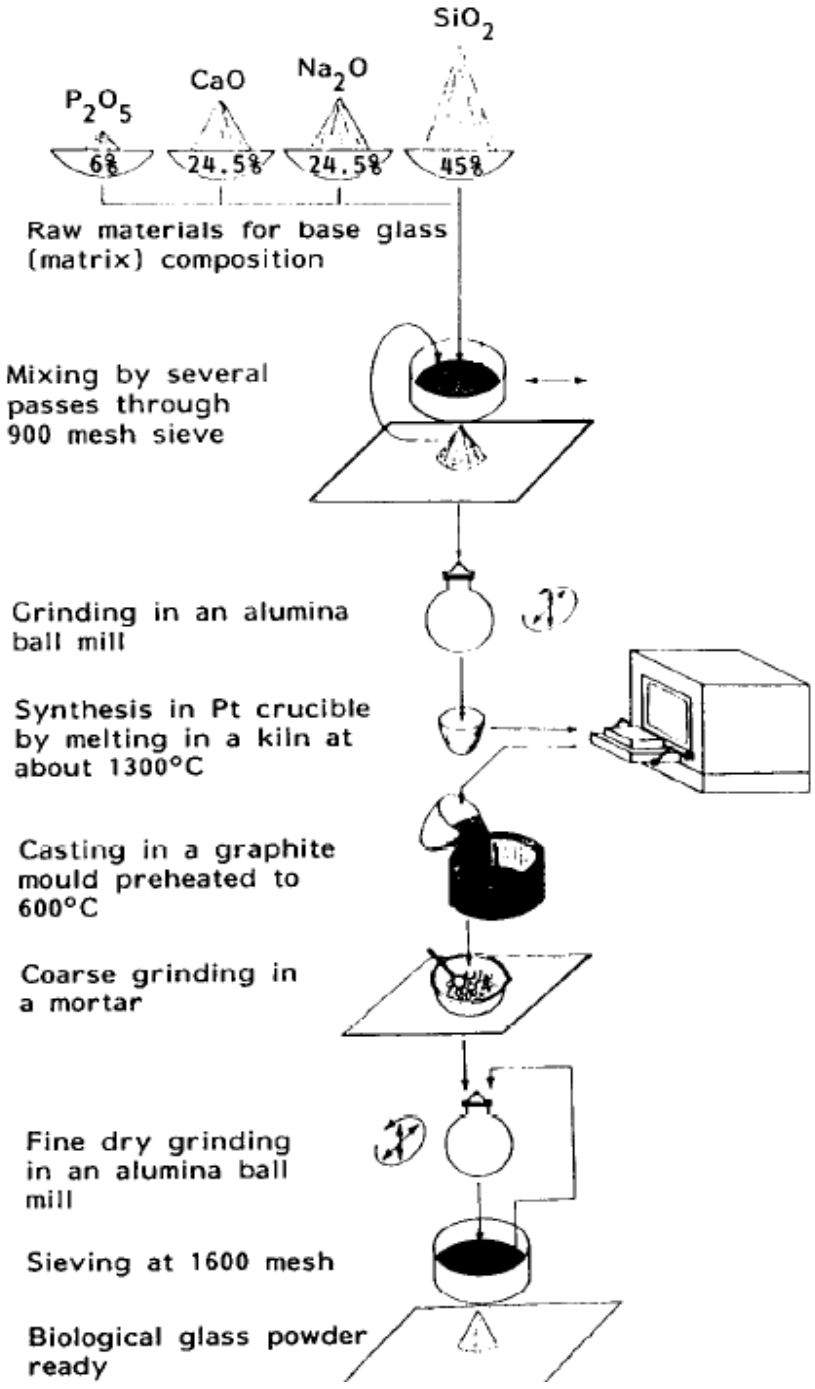

Figure 4. Schematic diagram of a typical melt-derived bioglass synthesis route [63].

Bioglass is usually milled into a fine powder so it can be incorporated into other materials as the bioactive component. This also increases the surface area for bioactive cell adhesion. Bioglass can be pulverized in a number of ways; ball milling, jet milling or flame spraying. The important thing is to limit

the level of contamination from the milling media. Our group has previously shown that the use of an alumina ball mill introduced aluminium contaminants into powdered bioglass [65].

It is mandatory to sterilize all artificial implants, preferably by gamma irradiation. The effect of sterilization on bioglass is an under-studied field. It has been reported that gamma irradiation may create defects in silicate glasses [66-67]. Interestingly Bharati *et al* [66], showed gamma irradiation improves scratch resistance of melt-derived bioactive and improves crystallization resulting in a different glass ceramic material having better set of mechanical properties. Given this information, the effect of sterilization should be considered when using bioactive glasses in particular applications.

2.1.4.4 Polymer/Bioglass Composite Scaffolds

In recent years, tissue engineers have focused on developing tissue scaffold composites. These composites usually consist of a supportive/structural material and a bioactive material [2, 62, 68]. In particular, the development of composite materials comprising a biodegradable polymeric phase and a bioactive inorganic phase, such as hydroxyapatite (HA) or bioactive glass (e.g. 45S5 Bioglass), is seen as a promising approach for scaffold production [69]. Biocompatible polymers are suitable materials for the structural composite phase due to their easily controllable structural and biomimetic mechanical properties [2, 70]. Bioglass is an excellent candidate for the bioactive phase due to its high cell-conductivity and simple processing compared to organic bioactive components (e.g. collagen and BMPs). The addition of bioglass can also be used to modulate mechanical properties and degradation kinetics. Bioglass has been shown to affect hydrophilicity thus increasing water absorption. It has also been shown to have a pH buffering effect against acid bi-products of biopolymer degradation [2, 69].

Biopolymer/bioglass composites have been tested in a number of biomedical applications: Blaker *et al* [41], coated sutures with silver-doped bioglass using a slurry dipping technique and found that the suture became bioactive while maintaining its mechanical properties. Day *et al* [71], used a similar coating method to produce PGA/45S5 scaffolds that greatly increased angiogenesis in rat models. However it was found that the bioglass had an inhibitory effect on fibroblast proliferation, suggesting some optimal concentration. Verrier *et al* [69], cultured human lung epithelial cells and osteosarcoma cells on homogenous PDLLA/45S5 bioglass composites fabricated by thermally induced phase separation and found that bioglass positively effects the growth of these cells and increases cell-scaffold adhesion in a dose dependent manner. Using similar scaffolds Helen *et al* [72], demonstrated increased proliferation and attachment of bovine annulus fibrosis cells. Cannillo *et al* [62], used salt-leaching to

produce 45S5/PCL scaffolds with high porosity and interconnectivity for bone healing. However, the prolonged contact of the 45S5 particles with water used to remove the salt probably induced a reaction which promoted the development of calcite and altered the glass composition, suppressing the development of hydroxyapatite in vitro resulting in loss of bioactivity.

It is plain that the composite fabrication process plays a major factor in determining scaffold properties and bioactivity. A review by Rezwan *et al* [2], neatly assesses current composite scaffold processing techniques (Table 5).

Table 5. Fabrication routes for 3D composite scaffolds with high pore interconnectivity and their advantages and disadvantages [2].

Fabrication route	Advantages	Disadvantages
Thermally induced phase separation (TIPS)	High porosities (~95%) Highly interconnected pore structures Anisotropic and tubular pores possible Control of structure and pore size by varying preparation conditions	Long time to sublime solvent (48 hours) Shrinkage issues Small scale production Use of organic solvents
Solvent casting/particle leaching	Controlled porosity Controlled interconnectivity (if particles are sintered)	Structures generally isotropic Use of organic solvents
Solid free-form	Porous structure can be tailored to host tissue Protein and cell encapsulation possible Good interface with medical imaging	Resolution needs to be improved to the micro-scale Some methods use organic solvents
Microsphere sintering	Graded porosity structures possible Controlled porosity Can be fabricated into complex shapes	Interconnectivity is an issue Use of organic solvents
Scaffold coating	Quick and easy	Clogging of pores, sometimes organic solvents used, coating adhesion to substrate can be too weak

2.1.5 Bulk Metallic Glasses

Bulk Metallic Glass (BMG) is an amorphous metal alloy. The key advantage of BMGs compared with conventional crystalline alloys is that BMGs can be easily cast as opposed to machined to make various metal components. BMGs also have in some cases vastly different thermal, mechanical, corrosive and conductive properties. Many kinds of BMGs have been developed including MgCuY, LaAlNi, ZrAlNiCu, ZrAlNiCu(Ti, Nb), ZrTiCuNiBe, TiNiCuSn, CuZrTiNi, NdFeCoAl, LaAlNi, FeCoNiZrNbB, FeAlGaPCB, PrCuNiAl, PdNiCuP, etc [73].

Recently BMGs have received attention for their biomedical potential due to their high strength and biodegradability. MgZnCa BMGs have been demonstrated to show good biocompatibility, mechanical properties matching bone and excellent corrosion properties [74-75]. Thus these materials have been recognised as outstanding candidates for biodegradable implants such as bone pins. The degradation rates for these alloys is between 0.5 – 3 mm/year [74].

An unrecognised benefit of MgZnCa BMGs may be their biofilm disrupting and antibacterial properties. Mg and Zn ions are both known to have antibacterial effects [56-57]. Biofilms have been shown to be less resistant to metal ions compared to antibiotics [76].

2.1.5.1 Sputter Coating

Sputtering devices are used primarily for blanket metal film deposition. Sputter coating is a physical deposition process wherein noble gas particles are accelerated to a ‘target’ (the desired metal coating) using a strong electrical potential. The gas particles hit the target and in a transfer of momentum eject a particle from the target’s surface. This particle then lands on the ‘substrate’ (the object which is to be coated). Over time as numerous particles are deposited on the substrate a homogenous film is formed. Secondary electrons are ejected from the collisions and are redirected back toward the target by a magnetron – this maintains the plasma and improves the sputtering efficiency. Magnetron sputtering makes a significant impact in application areas including hard, wear-resistant coatings, low friction coatings, corrosion-resistant coatings, decorative coatings and coatings with specific optical or electrical properties [77-79].

Sputter coating may represent a viable method for coating polymer scaffolds with biodegradable metals such as BMGs. These polymer/metal composite scaffolds could be used to deliver antibacterial metal ions and act as a degradable envelope to control the delivery of other bioactive substances.

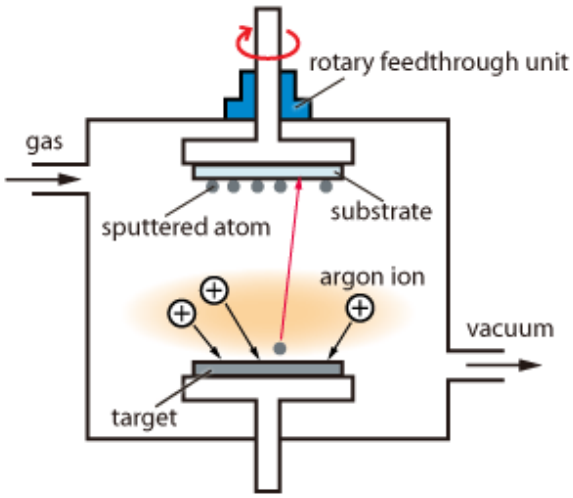

Figure 5.Schematic of standard magnetron sputter coater set-up [80].

2.1.6 Scaffold Mechanics

The mechanical properties of a scaffold must match those of the tissue for which it is intended. Different tissues have different stress states; tensile or compressive. For example, skin is generally under tension whilst bone is under compression [81]. Scaffolds designed for these purposes must have excellent mechanical properties relating to the tissue stress state so the scaffold can properly mimic the native ECM and survive the harsh *in vivo* environments [1-2, 6, 12]. Remarkably few studies have been done performing mechanical testing on scaffolds, almost always bulk materials are used.

A typical compression curve of foams can be described by characteristic points and lines (Figure 6). The modulus of elasticity ($E_{elasticity}$), which is the initial slope of the compression curve, characterizes the scaffold in the linear elastic region where all the deformations are reversible. The yield strength ($s_{elasticity}$) is the intersection of the slope of $E_{elasticity}$ and $E_{plateau}$. $E_{plateau}$ is in the connection with the non-reversible demolishment of the cell structure. Beyond the densification point the material is thought as non-porous material, and the modulus converges to the value of the bulk modulus [9].

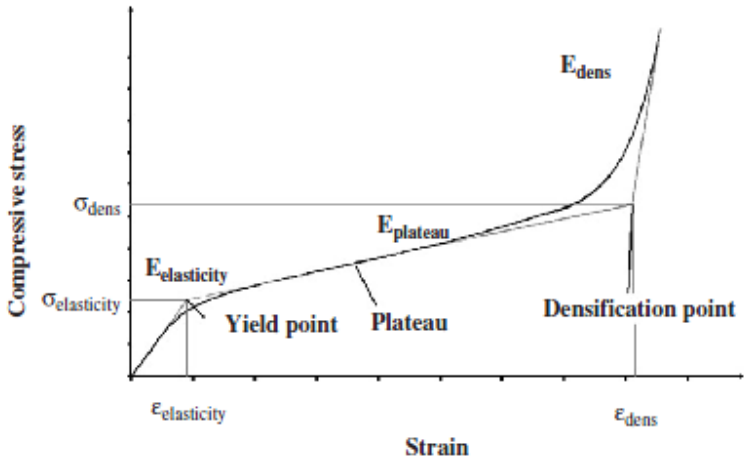

Figure 6. Compression curve of polymer foams, the yield and densification points are indicated [81].

Tension curves for scaffolds appear very similar to ordinary stress-strain tension curves for flexible materials. That is; an initial linear elastic region, the slope of which gives the Young's modulus; a non-linear region of plastic deformation; and a point of failure, where stresses rapidly decrease. Odelius *et al* [82] tested different copolymer scaffolds in tension. An example of a scaffold tension curve from this study is shown in Figure 7.

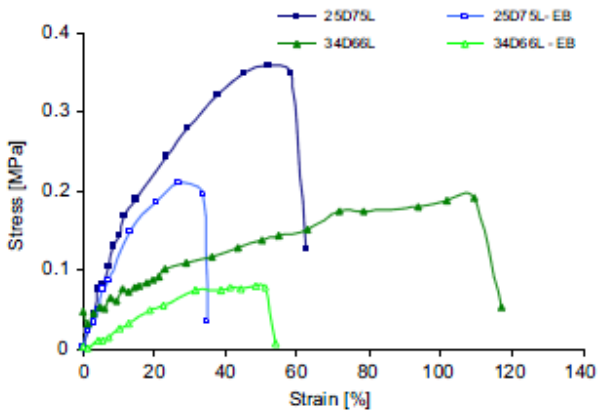

Figure 7. Copolymer scaffold tension stress-strain curve [82].

Scaffold stiffness in particular has been shown to have a profound effect on cell growth, differentiation and migration[83]. The mechanical property relating to stiffness is the Young's Modulus (E). Examination of dermal fibroblast behaviour seeded on biological hydrogels demonstrated the influence of hydrogel stiffness on cell migration and proliferation, where increased stiffness yielded normal proliferation rates

but retarded migration. Moreover, substrate stiffness exhibited a direct effect on actin cytoskeleton reorganization as shown in Figure 8. [84]

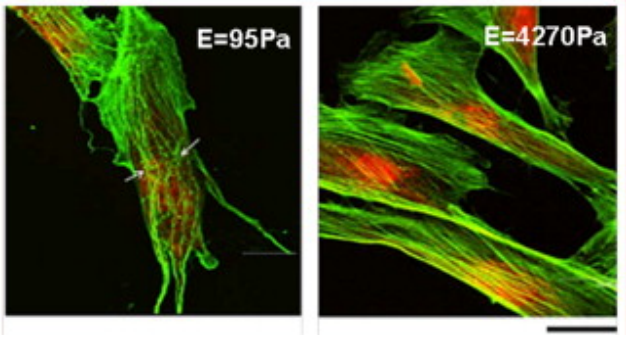

Figure 8. The cytoskeletal organization of dermal fibroblasts seeded on biological hydrogels with two different degrees of stiffness was stained for actin (green). Cells had more linear, stretched arrays of actin microfilaments on stiffer hydrogels in comparison to those associated with compliant hydrogels. Scale bar 16 μm [84].

2.1.7 Scaffold Synthesis

The porous structure of a scaffold is almost completely dependent on the fabrication method used in its synthesis. Table 6 outlines some of the present methods for making scaffolds and the resulting scaffold architectures that can be achieved [1].

Solvent casting, in combination with particulate leaching involves casting a polymer solution with water soluble particulates into a mould. After the evaporation of the solvent, the particulates are leached away using water to form the pores of the scaffold. The process is easy to carry out, but it works only for thin membranes or very thin 3D specimens. In thicker sample preparation, it is very difficult to remove all the soluble particulates from the polymer matrix [85]. The extensive use of solvents (some of which are toxic) in this method also presents a difficulty, as any residuals of the solvent would hinder the cell attachment and proliferation onto the scaffold [86]. A more recent publication which has shown that low toxicity solvents can be used in this technique and residues brought down to acceptable levels for application [1, 87].

Table 6. Fabrication Techniques and there Resultant Structures, Problems and Biomaterials that can be used [1].

Fabrication technique	Requirement for materials	Reproducibility	Scaffold architecture	Biomaterials	Problems	Reference
Impregnate sintering	Withstand high temperature	Sensitive to sintering	Pore size: 200 ~ 1000 μm; porosity: >50% foam dependent	HA, TCP	Brittle	(Lee and Kim, 1996; Liu, 1997; Meenan *et al.*, 2000; Meenen *et al.*, 1992; Wells *et al.*, 1996),
Solvent casting and particulate leaching	Soluble in cell non-toxic solvent	User and materials dependent	Pore size: 50 ~ 1000 μm; porosity: 30 ~ 90%	PLA, PLGA, collagen and so on	Solvent toxicity Particulate remanet	(Chen *et al.*, 2001; Miko *et al.*, 1994)
Phase separation/ emulsion in combination with freezing drying/critical point drying	Soluble in cell non-toxic solvent	Emulsion formation sensitive to stirring	Pore size <200 μm; Porosity: 70 ~ 95%	PLGA, PLA, PLLA and collagen	Solvent toxicity Pore size difficult to control	(Whang *et al.*, 1995; Zhao *et al.*, 2002)
Fiber knitting/ non-woven/ bonding	Fiber	Machine control Solvent sensitive	Interconnected channels, 20 ~ 100 μm in diameter	PVA, PLA, PLGA	Lack of rigidity	(Cooper *et al.*, 2005; Cooper *et al.*, 2005 2000; Ouyang *et al.*, 2003)
Solid free form	Low melting point and thermoplastic	Computer control	Interconnected channels Complex shape and structure >150 μm Customer based	PEG, PLA, PLGA Collagen, starch, HA, TCP	Costly	(Calvert *et al.*, 1998; Chu *et al.*, 2002; Das *et al.*, 2003; Hollister *et al.*, 2002; Hoque *et al.*, 2005; Hutmacher *et al.*, 2004; Khalil *et al.*, 2005; Lin *et al.*, 2004; Sachlos and Czernuszka 2003; Taboas *et al.*, 2003; Woodfield *et al.*, 2004)

Fibre networking technique uses biodegradable fibres to fabricate scaffolds via a textile method, such as non-woven, knitting and fibre bonding routes [88-89]. Electrospinning method is reportedly capable to fabricate polymer fibres range from a few nanometres to hundreds of microns [90-91].

Solid freeform fabrication (SFF) is a developing technology that enables the fabrication of custom made devices directly from computer data such as computer aided design (CAD), computed tomography (CT) and magnetic resonance imaging (MRI) data [92]. The digital information is then converted to a machine specific cross-sectional format, expressing the model as a series of layers. The file is then implemented on the SFF machine, which builds customer designed 3D objects by layered manufacturing strategy [93].

The important message relating to these fabrication techniques is the control over the scaffold structure is related directly to the cost and complexity of the technique; Increased structural control → more costly and complex fabrication method. This is summarised in Table 6. Structural control is important to

ensure manipulation of scaffold properties, since properties are so dependent on the scaffold architecture.

2.1.7.1 Sterilization

Tissue engineering scaffolds are biomimetic structures with carefully controlled chemical and physical properties. Scaffolds are implanted medical therapeutics and as such are required to meet stringent sterility regulations to ensure patient safety [94-95]. Common sterilization methods involve harsh conditions that are required to inactivate tough microscopic pathogens. Unfortunately these conditions will commonly alter the susceptible scaffold biomaterials being sterilized, causing a multitude of chemical, morphological and mechanical changes which ultimately affect the function of the tissue engineering device.

Cell containing scaffolds cannot be terminally sterilized. Growth factors such as bone morphogenic protein (BMP) will become denatured by many terminal sterilization methods. After all, the point of sterilization is to inactivate pathogen proteins and nucleic acids by denaturation and therefore cannot distinguish these materials from protein-based growth factors. A route to circumventing this problem is to aseptically process rather than terminally sterilise growth factors i.e. the recombinant human platelet-derived growth factor-BB (PDGF-BB), GEM 21S™ which is incorporated into a dental bone filler composite has been processed in this way [28, 96]. Unfortunately aseptic processing is far more expensive and more difficult to scale.

Natural polymers are sensitive to most sterilization methods. Collagens are the most widely distributed type of protein in human extracellular matrix (ECM) and are commonly used tissue scaffolds. They are heat sensitive and cannot be autoclaved. Radiation sterilization such as gamma and E-beam attack the molecular structure of collagen resulting in decreased mechanical properties and enzymatic resistance. Chemical methods have proved to be more promising. Ethylene oxide (EtO) sterilization was found to be less damaging than radiation depending on the collagen product [97]. The sterilization of collagen scaffolds has yet to be optimised [98].

Synthetic biocompatible polymers show the best resistance to common sterilization methods. They cannot be heat sterilized but both chemical and radiation techniques have been successful. The residues left behind from EtO sterilization are highly toxic and their complete removal is not always possible [7, 9, 17, 82, 97]. Ionising radiation affects the performance bioresorbable polymer medical devices by making

alterations to the polymer chain organisation. [8-9, 17, 82, 99-100]. It has been found that synthetic biopolymer mechanical properties have actually been improved by gamma sterilization [8, 17, 81].

Tissue engineers need to consider the terminal sterilization method in the initial design process of tissue scaffolds to account for changes in properties and synthesis routes. Designing in this way may overcome the high cost shortfalls of current tissue scaffolds.

2.1.8 Other Applications

Composite scaffolds are used in the medical industry for wound dressings [12, 101], drug delivery [21, 27] and tissue engineering of a number of organs and soft and hard tissues [1, 6, 28]. However, the generic properties and design aspects of composite scaffolds have made them useful for other applications in completely separate industries.

2.1.8.1 Filter Systems

The interconnected porosity of composite scaffolds makes them ideal filter materials. The high porosity and high surface area allows unimpeded diffusion of fluids and high reactivity. The controllable surface properties particularly lend themselves to the field of biofiltration where the surface can be modified to immobilize biocatalysts to perform industrial reactions such as epoxide formation, desulphurization and waste removal. In fact, porous polyurethane foams have been used as tissue engineered wound dressings [101] and for immobilization of bacterial viable cells for biofiltration [102].

2.1.8.2 Advanced Materials

The use of porous structures with controllable architectures similar to tissue scaffolds has been applied to the design of advanced materials. Schaedler *et al* [103] used photo-polymerisation to rapidly create polymer matrices. These were then coated in nickel-phosphorus by electroless plating. Finally the polymer was etched away leaving a metal material that was 99.99% air. The porosity allows the creation of ultra light materials with customisable properties and greatly enhanced mechanics. The Ni-P ‘microlattices’ produced in this study were reported to be the strongest material compared to its density.

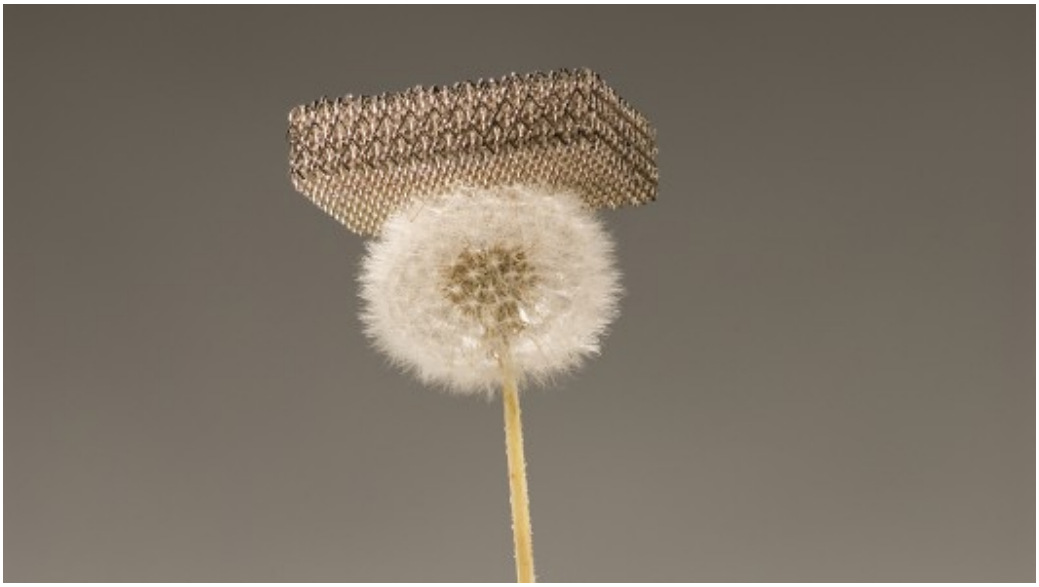

Figure 9. Ultralight Ni-P microlattice rests atop a dandelion (Image: Dan Little, HRL Laboratories, LLC).

.

2.2 Wound Healing Grafts

2.2.1 Skin

2.2.1.1 Structure and Function

Skin is the largest organ in the human body. It acts as the barrier, protecting sensitive tissues from toxins and microorganisms in the external environment as well as preventing dehydration. Skin plays other key roles such as perspiration and sensory detection [12].

Skin is comprised of two main layers: the epidermis and the dermis. The epidermis is comprised mostly of keratinocytes. The cells are constantly dividing. They slowly shift to the outmost part of the epidermis changing their morphology from round to flattened, where they eventually die from lack of blood supply. Once they reach the layer exposed to the environment, the sheets of dead keratinocytes flake off which helps to remove pathogens from the skin [104].

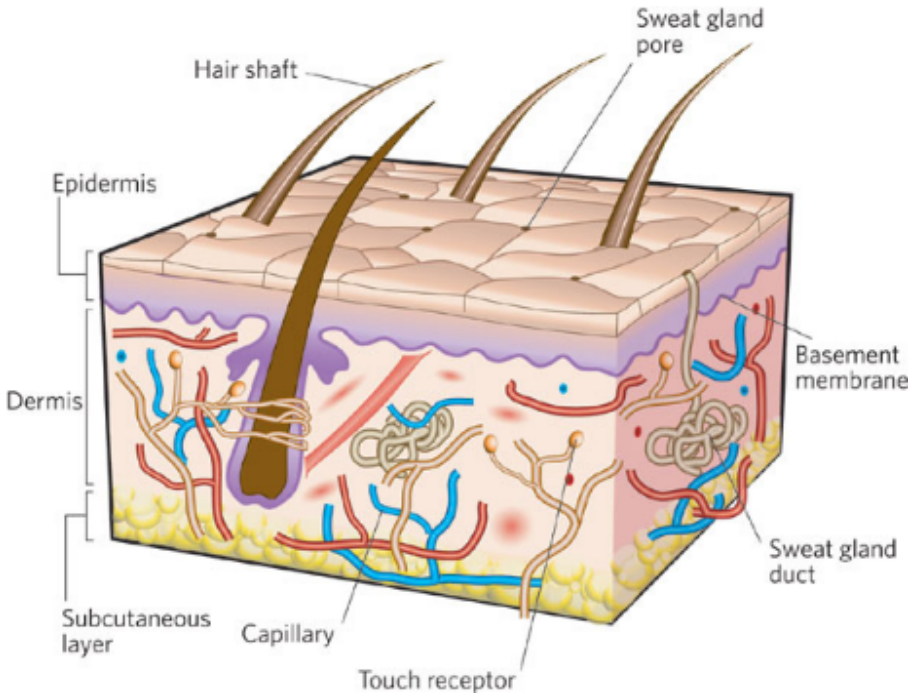

Figure 10. Cross-sectional diagram of human skin [105].

The dermis is comprised mostly of fibroblasts. Fibroblasts produce collagen, the main constituent of the connective tissue giving the skin its mechanical strength [106]. The dermis holds a number of other important structures such as nerve endings, tough receptors and sweat gland ducts. It also contains a wide network of blood vessels and capillaries which provides nutrients and waste removal to surrounding tissues as well as allowing access of the immune system to repair damage and fight infections [107].

2.2.1.2 Mechanical Properties

Mechanical properties of biomaterials and tissues should not be taken as absolutes, as different testing methods usually generate varying results.

Agache *et al* [108] used a torsional set-up to test the tensile properties of a test subject's skin directly and determined the Young's Modulus as 850kPa in older individuals.

Silver *et al* [109] tested human skin allografted samples and computed a modulus of 0.1MPa for strains up to 40% (Table 7). This is more than 8 times less than Agache's calculation of the modulus for human skin.

Table 7. Slopes of incremental stress-strain curves [109].

Sample	Slopes (MPa)			Fibril length (μm)
	Initial elastic	Final elastic	Viscous	
Human skin	0.10	18.8	5.13	54.8
Alloderm®	0.10	18.4	7.05	63.7
Processed dermis	0.10	17.6	4.35	48.8

* Calculated using a fibril diameter of 80 nm.

Animal models of skin have also been used to determine mechanical properties. Common models are mouse and pig [106]. Animal models generally allow a larger amount of samples from an increased number of individuals.

The majority of biomechanical testing of skin has been performed analysing tensile properties with very few analysing compressive properties. This is despite the fact that it is compressive type injuries that more often lead to chronic wounds such as bed sores [106].

2.2.1.3 Wounds and healing

A wound is a defect or a break in the skin, resulting from physical or thermal damage or as a result of the presence of an underlying medical or physiological condition. Acute wounds are those that take < 12 weeks to fully heal. The primary cause for such wounds is mechanical in nature such as cuts, tears and abrasions [101]. When one suffers an acute wound normal wound healing ensues.

Normal wound healing can be thought of in three consecutive stages: the inflammatory stage, the proliferative stage and the maturation stage [110]. During the inflammation stage platelets rapidly form a clot. Neutrophils and macrophage (inflammatory cells) migrate to the clot where they destroy any pathogens and secrete growth factors. This leads to the activation and proliferation of fibroblasts and endothelial cells. These cells migrate to the fibrin clot forming granulation tissue. Tissue ingrowth continues from the dermis providing new vasculature to the clot. The epidermis begins to grow over the clot while physiological function is returned to the wound site [12]. Dysfunction during this fine-tuned physiological process can prevent proper healing and cause a chronic wound (dermal ulcer) (Figure 11).

2.2.2 Chronic Skin Wounds

Chronic Wounds are tissue injuries that persist beyond 12 weeks [101]. The initial injury can be incredibly varied (burn, abrasion, tear, cut, ischemia, etc.), but the slow healing is due to interruption of the healing stages by inhibited blood flow to the wound area and repeated aggravation of the damaged tissue, preventing normal physiological healing and return of function [110]. The result is a chronic opening in the skin called an ulcer that is prone to infection and can often end in amputation [12]. There are different types of ulcers such as diabetic ulcers, venous ulcers and pressure sores, but of these diabetic ulcers are by far the most common and represent the biggest health care challenge for the future [12].

In the US, the prevalence of venous ulcers was 1.5-2 per 1000 individuals, for which the average total medical cost was $9685 [111]. In Australia, there are approximately 10,000 hospitalisations due to diabetic foot ulcers per year and these wounds account for 8% of all diabetic-related deaths [112]. The cost of treating chronic wounds in the US in 2001 was US$25billion. The economic impact is even greater when loss of work is also accounted for [113].

Chronic wounds are on the rise due to the increasing prevalence of obesity, an aging population and diabetes – key risk factors for chronic wounds [107, 113]. Chronic ulcers occur mostly in the elderly as this population often has impaired healing and other pathologies such as diabetes and cardiovascular disease [12, 101, 114]. Obesity is a major risk factor for becoming hyperglycaemic and developing type 2 diabetes. Further obesity puts addition pressure on the feet such that wounds can develop [113].

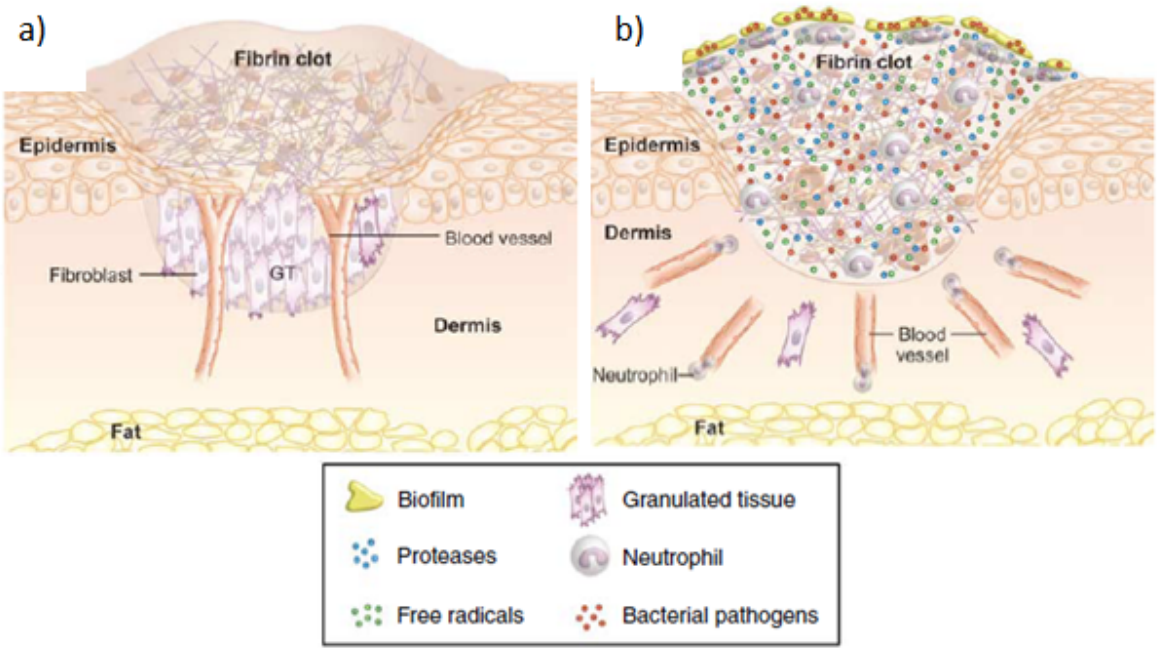

Figure 11. Wound healing pathology. a) Normal acute wound healing: fibrin clot with granulation tissue and neovascular ingress; b) Chronic wound: Dysfunction of normal wound healing processes. Bacterial biofilm growth, inflammatory cells and free radicals saturate fibrin clot preventing normal tissue proliferation [12].

2.2.2.1 Aetiology

2.2.2.1.1 Ischemia

Ischemia is the reduction in blood flow to tissue. In the context of wounds, ischemia prevents adequate delivery of immune cells to carry out normal healing hence forming a chronic wound. The lack of oxygen supply and other nutrients also causes tissue necrosis which further aggravates the problem. Ischemia is a key cause of chronic wounds and must be addressed before proper wound healing can occur [114-115].

2.2.2.1.2 Diabetes

The prevalence of diabetes in the US is 7% of the population and is on the rise [12]. During the period 2005–2007, the total incidence of diabetes increased 13.5% [113]. Diabetics have a 15% chance to develop foot ulcers with 70% recurrence within 5 years [110].

Persons with diabetes are at higher risk of suffering from atherosclerosis resulting ischemia. Sweat glands do not function properly which dries the skin predisposing it to cracking and abrasion. Most importantly diabetics suffer from peripheral neuropathy, or the loss of feeling of the extremities. This loss of feeling includes loss of pain and is the major cause of deep skin traumas which can eventually become chronic [114-115]. Diabetic patients are often hyperglycaemic resulting in the superoxide production which neutralises nitric oxide (NO), a key wound healing factor produced by endothelial cells. This results in an excess of free radicals in the wound, impairing healing [110].

Figure 12. Diabetic foot ulcer in a typical position [114].

2.2.2.1.3 Infection

Infection in chronic wounds is common and can be detrimental to the healing process and even fatal [55, 101]. Invading microorganisms often produce toxins causing local cell death. These pathogens also elicit an inflammation response leading to further tissue destruction, further slowing healing. The fibrous wound milieu and necrotic tissue offer a prime location for microbes to form biofilms, providing resistance to antibiotics and phagocytosis. These biofilms serve as beachheads for pathogens that ultimately result in a systemic infection which can be fatal [116]. Infection can also lead to osteomyelitis, sepsis of the bone making the infection even more difficult to remove [114].

Many different types of bacteria can become pathogenic within a wound. Common wound infecting bacteria include *Pseudomonas aeruginosa*, *Escherichia coli*, *Staphylococcus aureus*, *Streptococcus pyrogenes* and some *Proteus*, *Clostridium* and *Coliform* species [101, 117].

2.2.2.2 Treatments

2.2.2.2.1 Debridement

Debridement is the removal of necrotic tissue from the wound bed. Debridement is important in the diagnosis of a wound, because clearing dead tissue is often necessary to view and assess the underlying wound bed. Further, necrotic tissue increases the risk of infection and sepsis and prolongs the inflammatory phase of healing [101]. Surgical removal using scalpel and scissors are the main method of debridement. A curette is also used to scrape out necrotic tissue on the wound bed. Debridement is the most effective way to remove biofilms [118]. Abundant data shows that regular debridement of ulcer wounds and removal of devitalized tissues is the single most important therapeutic step leading to ulcer healing and limb salvage [115].

2.2.2.2.2 Pressure Off-Loading

Pressure off-loading is an essential part of managing chronic skin wounds in areas that experience mechanical loading, such as the heel of foot. Specially cast orthotic medical-grade shoes fully support the patient's foot and can reduce trauma of the chronic ulcer. This is especially important in the case of foot deformities which can often act as pressure points causing re-occurring wounds. In severe cases, orthopaedic surgical intervention may be required to remove such pressure points and produce improved outcomes. Medical-grade footwear can be very expensive, further adding to the cost of treating chronic wounds [112, 115, 118].

The most effective method of pressure off-loading is inactivity and rest. However, most patients are unlikely to comply with this, due to the inertia of day-to-day activities and the long periods required for healing [114]. Further, peripheral neuropathy prevents a painful reminder of pressure points [118].

2.2.2.2.3 Wound Dressings

Kumar *et al* [55] states that an ideal wound dressing should: keep the wound moist, allow gas exchange, act as a microbial barrier, remove excess exudates, be non-toxic, non-adherent (easy to remove), antimicrobial and promote healing. It has become widely accepted that the wound should be kept moist

to promote an environment wherein epithelial cells can move unimpeded and vital nutrients can be effectively transported [101, 114].

To treat infected wounds, dressings containing antimicrobial agents are used. The most common antimicrobial agent used is silver and most dressings have both normal and silver-containing types [101, 118].

Although wound dressings do improve healing they are not a permanent solution and need to be changed regularly (in many cases daily) depending on the wound pathology [12, 115]. This represents a large burden on health systems to employ clinicians to perform the regular dressing changes required. Currently: “There is no evidence showing that one type of dressing is better than another, or that one type of dressing can be used on all wounds [112] [114].”

2.2.2.2.4 Antibiotics

As previously mentioned the main types of pathogens that infect chronic wounds are gram positive cocci such as *Staphylococcus aureus*. However, other type of pathogens including aerobes and even fungi can infect wounds thus the antibiotic treatment should be broad-spectrum [115]. Methicillin-resistant strains, such as methicillin-resistant *Staphylococcus aureus* (MRSA), are frequently encountered, so newer antibiotics, such as vancomycin, rifampicin and daptomycin, should be considered [114-115].

Topical antibiotics can be used in more superficial wounds but do not properly interact with deeper ulcerations [118] and are not recommended for the treatment of diabetic foot ulcers [115]. Thus systemic antibiotics are used which require higher doses to maintain an impact at the wound site and have harmful side effects [101]. Tobramycin drug delivery devices can be inserted directly into the wound to provide extended and direct antibiotics, however these devices are expensive and introduce a pressure point into the wound which may provoke trauma [118]. Antibiotics including gentamycin and ofloxacin have also been impregnated into hydrogel wound dressings [101].

2.2.2.2.5 Skin Grafting

Autografting (self-donor) and allografting (human donor) of skin is used in wound repair. However, allografting has the substantial disadvantage of host rejection of the transplanted tissue. While autografting requires surgery which has its own risk and the donor site can often be subject to morbidity [12]. Skin grafts are particularly ineffective on weight bearing defects because of the poor durability of the graft [115].

2.2.2.2.6 Tissue Engineered Skin Substitutes

Tissue engineered wound healing devices have shown promise compared with classical dressings in recent studies. Tissue engineered dressings are made of biocompatible scaffolds that mimic skin connective tissue and biodegrade once the local tissue has healed. They also can be used to deliver cells, growth factors, genes, drugs and other antibacterial agents to the wound to expedite healing [101, 107, 111]. Further advantages of tissue engineering scaffolds are they: retain a moist environment, allow permeation of gas, absorption of exudates and are easy to remove without trauma [55]. Highly porous mesh grafts are used so as to not entrap exudates. However, most commercial tissue engineered grafts are not genuine grafts as they are very thin and serve more as a dressing that delivers cells and extracellular matrix components to the granulating wound bed [115]. In essence wound healing scaffolds should provide an environment for cell adhesion and wound regeneration and prevent secondary infection [116].

Currently, tissue engineering skin substitutes have been ineffective at integrating with the wound. Chong *et al* [107] claims the reason to be a combination of low flexibility and high thickness scaffolds. In accordance with this, Chong *et al* designed an approach using a PCL/gelatin matrix, electrospun onto an existing polyurethane dressing (Tegaderm™) to build up the dermis in thin layers, but admits that "Ultimately [it] may be insufficient to replace the lost dermis in terms of thickness". This contradiction, suggests that thickness may not be the issue, but possibly high porosity is needed to bridge the wound. However, some researchers see integration with the wound as a negative. Kumar *et al* used Scanning Electron Microscopy (SEM) to observe cells with globular morphology, indicating weak attachments to the β-Chitin/silver nano-particle hydrogel. This was seen as indicative of a non-adherent wound dressing and thus advantageous [55]. Viewing non-adherence as a positive characteristic affirms the point that most tissue engineered skin substitutes are closer to dressings and would need to be changed regularly.

Kim *et al* [119] showcased the potential of an integrin receptor ligand (peptide RGD)-bound PLLA scaffold for delivery of endothelial progenitor cells. These stem cells that are native in the bone marrow and aid angiogenesis following tissue injury are currently not clinically utilised due to poor bio-distribution and survival even when injected locally. The use of the endothelial cell-seeded RGD-g-PLLA scaffold greatly increased cell survival, targeted adhesion and vascularisation in a mouse wound model compared with local injection.

Breen *et al* [110] optimised a fibrin scaffold to increase the efficiency of adenovirus vector expressing endothelial NO synthase (AdeNOS). AdeNOS had been shown previously to upregulate eNOS expression, but had the disadvantages of short duration of transgene expression as well as a viral immune response. These were obviated by use of the scaffold which was able to deliver the eNOS gene for longer and at lower dosages which was shown to increase NO at the wound, prevent chronic inflammation and accelerate epithelialisation.

Dermagraft™ (Smith and Nephew Plc) is a human fibroblast-derived dermal replacement for wound repair. The origin of the cells is human newborn foreskin. It consists of a bio-absorbable three-dimensional scaffold containing growth factors, matrix proteins and glycosaminoglycans, on which fibroblasts are cultured to produce a living, metabolically active dermal tissue. Possible healing mechanisms include providing the wound bed with a metabolically active dermal matrix and/or promoting the expression of important mediators (VEGF, TGF-b, HGF/SF) and thus stimulating angiogenesis and subsequent wound healing [111].

Table 8. Commercially available tissue engineered skin substitutes [101].

Dressing	Type	Major Components	Manufacturers
Integra™	Artificial skin	Collagen/chondroitin-6 sulphate matrix overlaid with a thin silicone sheet	Integra LifeScience (Plainsborough, NJ)
Biobrane™	Biosynthetic skin substitute	Silicone, nylon mesh, collagen	Dow Hickham/Bertek Pharmaceuticals (Sugar Land, TX)
Alloderm™	Acellular dermal graft	Normal human dermis with all the cellular material removed	Lifecell Corporation (Branchberg, NJ)
Dermagraft™	Dermal skin substitute	Cultured human fibroblasts on a biodegradable polyglycolic acid or polyglactin mesh	Advanced Tissue Sciences (LaJolla, CA)
Epicel™	Epidermal skin substitute	Cultured autologous human keratinocytes	Genzyme Biosurgery (Cambridge, MA)
Myskin™	Epidermal skin substitute	Cultured autologous human keratinocytes on medical grade silicone polymer substrate	Celltran Limited (University of Sheffield, Sheffield, UK)
TranCyte™	Human fibroblast derived skin substitute (synthetic epidermis)	Polyglycolic acid/polylactic acid, extracellular matrix proteins derived from allogenic human fibroblasts and collagen	Advanced Tissue Sciences
Apligraf™	Epidermal and dermal skin substitutes	Bovine type I collagen mixed with a suspension of dermal fibroblasts	Organogenesis (Canton, MA)
Hyalograft 3-D™	Epidermal skin substitute	Human fibroblasts on a laser-microperforated membrane of benzyl hyaluronate	Fidia Advanced Biopolymers (Padua, Italy)
Laserskin™	Epidermal skin substitute	Human keratinocytes on a laser-microperforated membrane of benzyl hyaluronate	Fidia Advanced Biopolymers
Bioseed™	Epidermal skin substitute	Fibrin sealant and cultured autologous human keratinocytes	BioTissue Technologies (Freiburg, Germany)

Most commercially available skin substitutes contain many biological components (Table 8). Concerns with biological scaffolds are their poor biostability, low mechanical properties, high cost, low shelf-life, risks of immunological rejection and lot-to-lot variability [116]. Organogenesis Inc. and Advanced Tissue Sciences Inc. suffered financially as a result of their overestimating the number of chronic wounds cases that were best solved by high-tech, tissue engineering skin substitutes as opposed to simpler, cheaper synthetic solutions that aid regeneration. As such there is now a philosophy emerging in tissue engineering to eschew biological materials and recreate the biomimetic solutions with synthetic materials that are more commercially viable [28].

Song *et al* [116] developed a synthetic cell-adhesive polypeptide hydrogel with inherent antibacterial activity. The lysine and arginine polypeptides were used to both crosslink and impart hydrophobic and cationic properties to a Polyethylene glycol (PEG) based hydrogel resulting in both cell adhesive and antibacterial properties. However, the polypeptides could not be terminally sterilized and the cell-

adhesion was still 10-fold less than collagen sponges. The non-adherence of hydrogels is a problem with true synthetic skin grafts and may be overcome by forming composites with more adherent polymers.

2.2.3 Biofilm Forming Bacteria

Biofilms are a collection of bacterial colonies that are tightly adhered to a surface within a polymer matrix created by those bacteria [120-123]. This behaviour has evolved as biofilms give the bacteria the best chance of survival by being able to shelter from harsh environments.

Pathogens exist in the wound environment as biofilms. This enables the pathogens to persist in the wound for an extended period defending them from the host immune system and protecting them against other interventions such as cleaning and antibiotics. The biofilm chronically maintains the wound in the inflammatory phase, preventing it from healing [117].

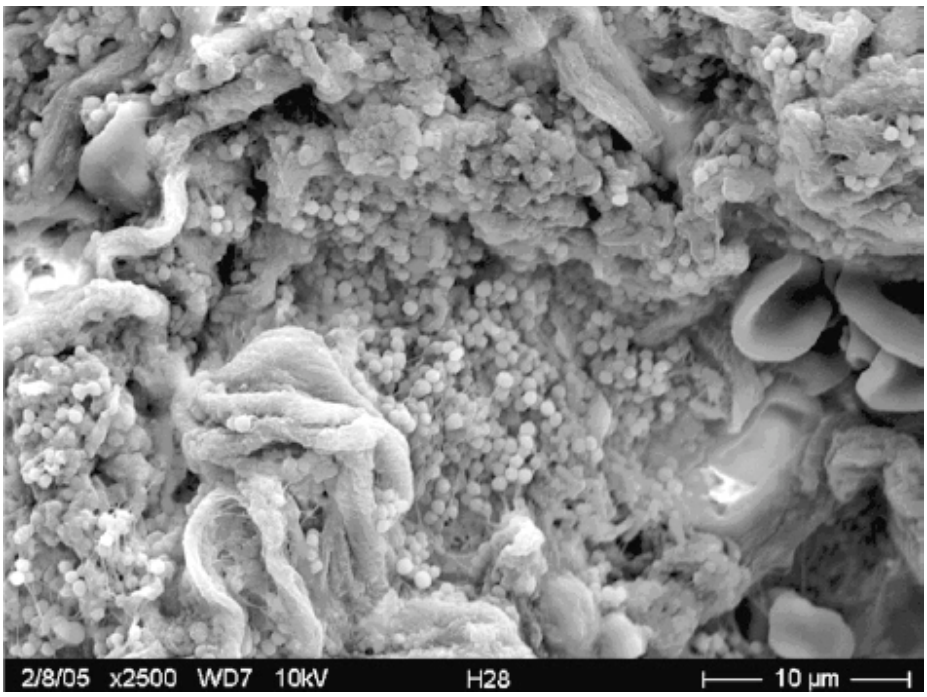

Figure 13. Biofilm community of bacteria living within a chronic wound [117].

2.2.3.1 Formation

The establishment of biofilms is a two part process: 1. Physical, reversible adhesion and; 2. Biological, irreversible adhesion [123-124].

The first involves the bacteria coming into close contact with a surface; this is influenced by a number of physical interactions between bacteria, surface and solution. These include surface charge, ionic strength, pH, hydrophobicity, surface roughness, Brownian motion, Van der Waals forces, etc [123-128]. A number of theories try to explain this initial adhesion in terms of these physical forces but in reality all bacteria are different and certain biological features of the cell surface (e.g. pilli, fimbrae, slime layers, etc) are known to also play a crucial role in this initial adhesion [121, 123-124]. Common physical and biological factors affecting adhesion have been summarised by Pavithra *et al* [124]. (Figure 14)

Once the cells are adhered to the surface certain genes are up-regulated and they begin to produce exopolymeric substances (EPS). These form a matrix around the cells that accounts for the vast majority of the biofilm. The EPS matrix can be made of proteins, polysaccharides, DNA, lipids, etc. They attach to the surface using rather weak H-bonds or electrostatic bonds but the long polymer chains means more binding points which actually make the adhesion of biofilms to the surface very strong and irreversible.

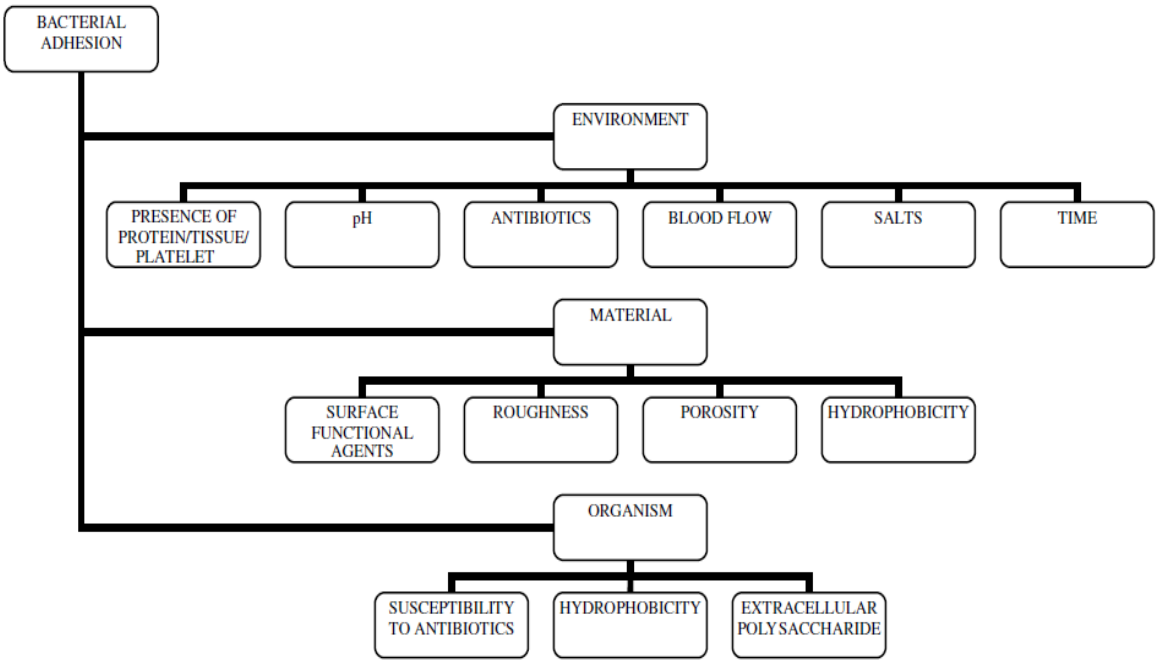

Figure 14. Parameters that determine bacterial adhesion [124].

Oxygen has been shown to be an important factor in biofilm growth. Colon-Gonzalez [129] correlated a decrease in *E. coli* biofilm formation after 24 hours incubation in LB broth with oxygen deficiency rather than nutrient depletion and claimed biofilms could not form in anaerobic conditions. A more extensive

study by Bjergbaek *et al* [130] tested several clinical *E. coli* strains and proved that biofilms could form in anaerobic conditions but that this attribute is heavily variable between strains.

2.2.3.2 Properties

2.2.3.2.1 Architecture

Biofilm structure is the spatial arrangement of cells in an EPS matrix. Biofilms are highly hydrated structures with interconnected pores and channels creating a network of nutrients for the bacterial community within. Recently it has been shown that biofilms are heterogeneous structures and have flowing water channels linking the non-uniform clusters of cells to the bulk liquid phase. Biofilm thickness is dependent on growth conditions, bacterial strains and time, but generally ranges from a few micrometres to a centimetre [121].

The EPS layer composes 50-80% of the biofilm. It serves as a protective barrier and determines most of the biofilm chemical and physical properties such as resistance to antibiotics and mechanical stability [121]. The composition of the EPS layer determines its function and is differs between bacterial species.

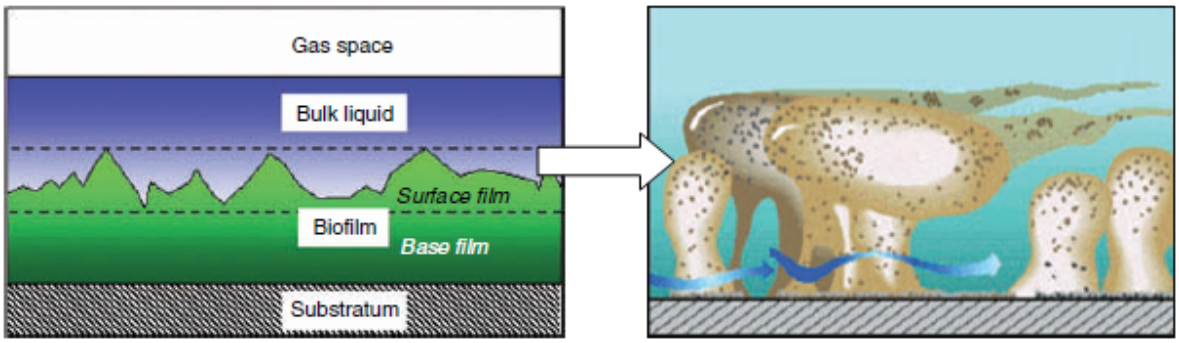

Figure 15. Change of thinking on Biofilm structure: From rough planar structure to complex heterogeneous architecture with water channels connecting microbial clusters.

2.2.3.2.2 Resistance

Microbes in biofilms are more resilient than planktonic (free-floating) cells. They establish a network and share nutrients extending their survivability [131]. The EPS matrix and production of slime also protects them from antimicrobial agents, greatly reducing effects of common antimicrobials such as antibiotics. This layer importantly also protects the community from phagocytosis allowing the bacteria within to elude the immune system [124]. In clinical setting bacteria will often form biofilms in wounds, teeth, implants and the gastrointestinal tract which can lead to long-term infections [121, 123, 131].

Biofilm cultures have been shown to be far less susceptible to antibiotics than planktonic cells, with MIC/MBC measurements of a range of antibiotics being higher for biofilms by orders of magnitude [76, 124, 132-133]. Diffusion of antibiotic molecules are slowed or unable to enter the EPS matrix due to size restrictions, EPS viscosity and EPS chemical interactions [131]. Due to high resilience and the formation of drug resistant strains [133], the prospect of using antibiotics in biofilm treatment in a traditional sense is minimal [132].

Heavy metal resistance of biofilms is a contentious field. It has been found that the EPS layer is capable of binding heavy metals [134]. Teitzel and Parsek [134] showed that *P. aeruginosa* biofilms were more resistant than planktonic cells through MIC/MBC assays. However, Harrison *et al* [76] later showed that metal-toxicity of biofilms was time-dependent and after long culture periods biofilms were just as susceptible to heavy metals as free cells.

2.2.3.3 Biofilm-forming Bacteria Types

2.2.3.3.1 Staphylococcus aureus

Many different types of bacteria can become pathogenic within a wound, but it has been shown that 94% of slow healing or recurring ulcers contained *Staphylococcus aureus* [101].

Polysaccharide intercellular adhesin (PIA), composed of poly-β-1,6-linked-N-acetylglucosamine, is the main constituent of *S. aureus* biofilm matrix [135]. PIA is produced by the intercellular adhesion operon present in nearly all *S. aureus* strains. Many *S. aureus* strains were seen to be biofilm negative in standard biofilm assays despite being PIA positive. It was later found that PIA was highly regulated and that anaerobic conditions up-regulated ica transcription resulting in PIA production and biofilm formation [136].

The way bacterial cells “talk to one another” is referred to as quorum sensing and is vital for biofilm formation. The *S. aureus* quorum-sensing system is encoded by the accessory gene regulator (*agr*) locus, which has been show to influence the antibiotic resistyance of the biofilm [137].

2.2.3.3.2 Pseudomonas aeruginosa

P. aeruginosa biofilm phenotype is dependent on the nutritional environment. With glucose as the carbon source *P. aeruginosa* biofilms formed as large mushroom shaped communities. With citrate as the carbon source the biofilms were flat, uniform structures [138].

Genetic factors also have a great impact on *P. aeruginosa* biofilm formation. *P. aeruginosa* is able to swim in liquid by means of flagella and to move on surfaces by means of type IV pilli. This results in colony aggregation on surfaces explaining the mushroom-shaped colonies described above [138].

P. aeruginosa use Acyl-Homoserine lactone (AHL) pathways for quorum sensing to coordinate biofilm formation. Quorum sensing pathway inhibitors are being developed and are shown to prevent biofilm formation [117].

2.2.3.3.3 Escherichia coli

E. coli are a native gut flora in most warm-blooded animals. When *E. coli* are released into a non-host environment they can exist as biofilm communities and cause pathogenesis. A large number of cell surface components have been found to influence biofilm formation such as, flagella, type I fimbrae, conjugative pilli and extracellular polymeric substances [130].

Both laboratory and clinical strains have been shown to form biofilm in vitro on abiotic surfaces. This growth is dependent on the strain and the nutritional environment and subject to great variation given different combinations of the two [129]. Bjergbaek *et al* [130] tested the biofilm formation of thirteen clinical strains and concluded that TSB media in the presence of oxygen provided the best biofilm-forming conditions.

E. coli quorum sensing occurs by cell-cell signalling thorugh the autoinducer-2 (AI-2). *E. coli* quorum sensing has been linked to virulence-associated factors, such as genes encoding the expression and assembly of flagella, motility and chemotaxis, were also activated by quorum sensing [139].

2.2.3.4 Interaction with Biomaterials

Biomaterial-associated infection poses a serious complication due to the increased used of biomaterial implants in modern medicine. These infections occur in 0.5 – 6% of all cases, strongly dependent on the implant site. Biomaterial associated infections are difficult to treat as the implant creates a favourable niche for biofilm communities [140-141].

Targeting the EPS would be the obvious way to break up biofilms so the underlying bacteria can be targeted, but this is difficult due to the complex nature of the EPS and its variability in different bacterial communities. Thus focus is often on the prevention of biofilms using antimicrobial and non-adhesive surfaces. Al-ahmad *et al* [142] introduced tri-calcium phosphate (TCP) to PLLA scaffolds to decrease the

hydrophobicity and consequently decrease the adherence of common plaque bacteria. Wang *et al* [143] coated the surface of scaffolds with microgels impregnated with antibacterial peptides. This system took advantage of the non-adhesive properties of the hydrogel with the static antimicrobial nature of the peptides to prevent adhesion of *Staphylococcus epidermidis.* The microgels were spotted onto the surface of the base PCL-chitosan scaffold, leaving much of the tissue adherent surface exposed. The problem with antibacterial surface design is the initial layer of bacteria that die on contact with the biomaterial then condition the surface for biofilm colonisation by the next layer of bacteria. Thus far there is no ideal solution for dealing with biofilms on biomaterial.

When a medical device is implanted, there is a "race for the surface", between host cells and opportunistic pathogens [141, 144]. Encouraging rapid host cell migration and adhesion to the implant surface may simultaneously decrease the likelihood of biofilm formation.

2.2.3.5 Measurement and Analysis

2.2.3.5.1 Assays

Firstly it needs to be made clear that adhesion is not necessarily biofilm formation. Many studies in the literature will make claims about biofilm formation but really what was being tested was bacterial adhesion. Biofilm formation as previously mentioned is not only adhesion it is also the following production and growth of EPS. A method for distinguishing biofilm studies from adhesion studies is examining growth conditions used. Adhesion studies are usually performed in buffer (transport media) and for a short time period (< 1 day). Biofilm assays are performed in growth media so cells have vital energy and nutrients to produce EPS. These studies typically run longer than adhesion studies (> 1 day) so cells have sufficient time to produce the biofilm matrix [133, 141, 145]. For Goa *et al* [133] *Pseudomonas aeruginosa* incubated from 10^8CFU/ml at 37C took 7 days to form a significant biofilm (Figure 16).

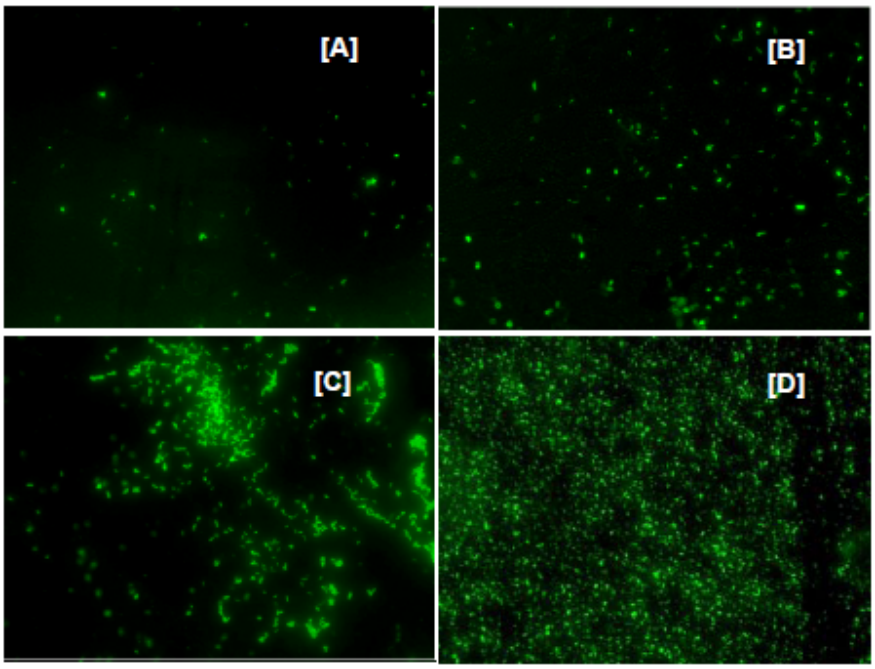

Figure 16. Bare titanium slide surfaces after incubation with *Pseudomonas aeruginosa* in ¼ BHI, magnification 1:600. Bacteria are stained using SYTO 9 (Invitrogen). [A] 1 day. [B] 2 days. [C] 3 days. [D] 7 days. [133]

Biofilm growth can be quantified through a number of different assays. These are usually carried out in two distinct parts: 1) disruption of the biofilm and; 2) quantification of cells, proteins or DNA. Harrison *et al* [76] and others [142, 146] used sonication as the biofilm disruption technique followed by turbidity measurements in a plate reader or viable counts. Biofilm disruption followed by cell counts has been used by many others as a means of biofilm quantification. It has been claimed that sonication disrupts biofilms while having no impact on cell viability [76, 134, 147].

Characteristic stains are also in common use. Patel *et al* [148] soaked dried biofilms in crystal violet (CV), washed off the excess and re-solubilised the stain in ethanol. Absorbance at 600nm was then measured using a plate reader. This method was only used to quantify the biofilm matrix formation. Tote *et al* [132, 135] used CV for *Pseudomonas aeruginosa* and dimethyl methylene blue (DMMB) for *S. aureus* biofilm matrix quantification claiming DMMB was a more specific indicator binding only to glycosaminoglycans (GAGs), the major constituent of S. aureus biofilms. To get a sense of viable cells, Tote [132] used resazurin, a commonly used redox indicator that gives a fluorescent signal proportional to metabolic activity. A period of 30min incubation time in resazurin was used.

2.2.3.5.2 Microscopy

Since biofilm bacteria are encased in EPS, assays may not accurately enumerate a given biofilm. Biofilms containing numerous bacterial species further complicates assay type analysis. Microscopy techniques allow characterisation of the biofilm and microbial community with minimal disruption to the biofilm. Specialised stains and microscopy coupled with appropriate software are used to count biofilm cells.

Scanning electron microscopy (SEM), transmission electron microscopy (TEM), normal light microscopy (LM), fluorescence microscopy (FM) and confocal scanning laser microscopy (CSLM) all have been used to study biofilms. Most of these methods include sample preparation such as sectioning, staining, dehydration, freezing and many more [121].SEM can be used to view biofilms, providing a depth a view making it easy to identify different bacterial cells and extracellular structures. However, the dehydration required for SEM sample preparation affects the morphology of the highly hydrated biofilm EPS which experiences deformation and shrinkage [121].

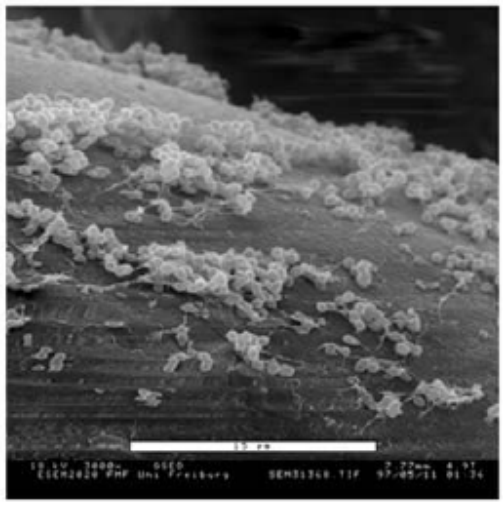

Figure 17. SEM image of *Enterococcus faecalis* biofilm on PLLA scaffold [142].

Stains are particularly useful for illuminating different components in the biofilm. Gao *et al* [133] used the fluorescent stain SYTO 9 (Invitrogen) to examine *Pseudomonas aeruginosa* on silicon wafers (Figure 16).

2.2.4 Novel Tissue Engineered Graft

2.2.4.1 Antibiotic Delivery

2.2.4.1.1 Antibiotics

2.2.4.1.1.1 Chloramphenicol

Chloramphenicol is a bacteriostatic (bacterial growth-inhibiting) antibiotic [149-150]. Its antibacterial mechanism is the inhibition of protein synthesis by altering the 50S ribosomal unit in the bacterial ribosome, thus preventing bacterial growth and proliferation [151]. The drug has a half life of 1.5 to 4 hours. In the body and chloramphenicol is hydrophobic which increases its binding affinity to biopolymeric scaffolds [152]. The antibiotic has a absorbs strongly in the UV spectrum primarily due to the aromatic ring present in the molecular structure as seen in Figure 18 [152-153].

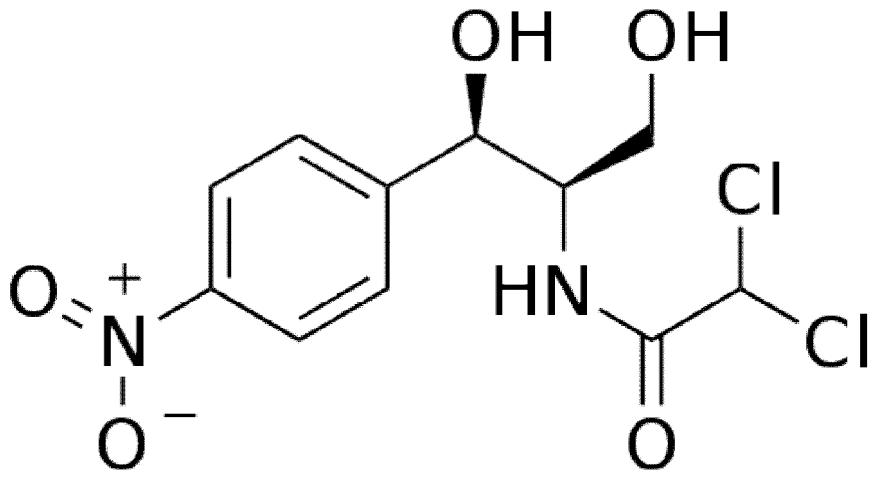

Figure 18.Chemical structure of Chloramphenicol.

2.2.4.1.1.2 Erythromycin

Erythromycin is a macrolide antibiotic. Macrolides have a common macrocyclic lactone ring to which one or more deoxy sugar groups are attached. They are weak bases and only slightly soluble in water (2 mg/ml) compared with ethanol (50 mg/ml) [154]. They are bacteriostatic and bactericidal (bacteria killing) depending on concentration; interfering with bacterial protein synthesis. Macrolides have low cytotoxicity, making them ideal antibiotics [155-156].

Erythromycin was the first macrolide to be discovered and marketed. It has a similar antibacterial spectrum as penicillin. Erythromycin is generally thought to be bacteriostatic [150], however time-dependent killing of *S. aureus* has been reported [149]. Erythromycin concentrations of 0.5μg/ml and 8μg/ml was found to be the MIC (minimum inhibitory concentration) of 86% and 99% (60 strains studied) of methicillin-resistant *S. aureus* as oppose to chloramphenicol for which the same concentrations only inhibited 4% and 91% of strains [157]. It occurs as a white/yellow powder. It exhibits characteristic UV absorption maxima when dissolved in water (pH 6.3) at 280nm (ε = 50). The pKa value is 8.8. Erythromycin is non-polar and has poor solubility in water. The chemical structure of erythromycin can be seen below [156].

Erythromycin has been reported to have relatively high toxicity to human skin fibroblasts compared to other well known antibiotics. The minimum concentration which caused no change in fibroblast viability was 300μg/ml compared with Gentamycin at 1000 μg/ml [158]. The mechanism of cytotoxicity of fibroblasts is not well documented but Zimmerman *et al* reported leakage of enzymes from Chang liver cells [159], suggesting modifications to the cell membrane.

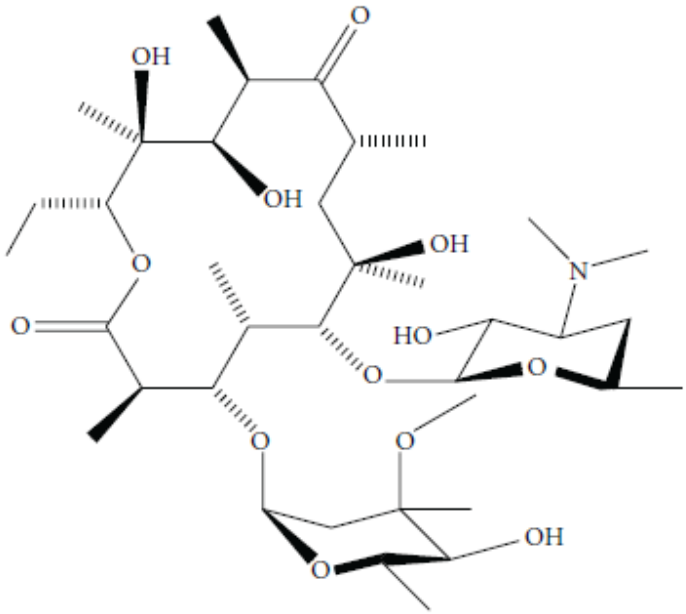

Figure 19. Chemical structure of erythromycin.

Detection of macrolides is more complex then other antibiotics. They do not have sufficient chromophore groups to be detected by simple spectrophotometry and thus many standards still suggest

tedious microbial assays for low concentration determination. Recently, new methods have been developed to quantify macrolides. The most widely used method of detection is high performance liquid chromatography (HPLC). This technique uses low wavelength UV. The method is requires precolumn extraction and is thus time consuming [156]. However by reacting erythromycin with other chemicals such as acidic dyes, concentrated sulphuric acid, and ferric ions, erythromycin can then be measured by spectrophotometry.

Macrolide antibiotics react with eosin Y dye in acetate buffer to instantaneously form a stable binary complex which can then be easily detected by spectrophotometry. The binary complex showed absorption maxima at 542–544 nm. The absorbance of the binary complexes obeyed Beer's law over the concentration range of 2–20 μgmL^{-1} for erythromycin [155-156, 160].

Danielson *et al* [161] used 14-16N H_2SO_4 to react with the sugars in erythromycin. The resulting yellow product could be analysed by spectrophotometry at 470nm. However the reaction time needed for the product to reach its maximum absorption was 350min, somewhat mitigating the simplicity of this procedure.

Erythromycin can be gamma sterilized in powder form up to 50kGy with no change in activity. In aqueous solution Erythromycin is 90% inactivated at 5kGy [162] which is much lower than the standard sterilizing dose of 25kGy [94-95].

2.2.4.1.2 Drug delivery systems

2.2.4.1.2.1 Function

Drug delivery systems (DDS) have been used for decades in the pharmaceutical industry and are becoming increasingly popular in tissue engineering systems. DDS are designed to suit the physiochemical and pharmacokinetic properties of the drug as well as its application [21]. DDS aim to control the rate of drug released to achieve a therapeutically effective dosage of the drug.

DDS can be used to improve the delivery of a drug in a number of ways. Capsules and pills are commonly used to protect unstable drugs from early degradation allowing these compounds to be administered orally. These devices are made of gelling agents that protect the drugs until they are ready to be eluted.

More recently DDS have are being incorporated into tissue engineered medical devices and scaffolds [21]. Very often the purpose of DDS in these devices is either delivering growth factors to up-regulate

the growth and differentiation of the tissues that need healing; or delivering antibiotics to inhibit infections. Bourke *et al*. [35] investigated photo-cross linked hydrogels for delivering platelet derived growth factor (PDGF) to chronic wounds to accelerate the growth of human dermal fibroblasts. Hwang *et al*, [29] impregnated PVA/Dextran wound dressings with gentamicin to improve wound healing in a rat animal model.

2.2.4.1.2.2 Parameters

The gel fraction is often measured when characterising a hydrogel DDS. The gel fraction is the amount of insoluble hydrogel compared with the amount of hydrogel after fabrication. This is commonly tested by gravimetric analysis of the hydrogel before and after long soaking in water. This is meant to remove any soluble polymers from the hydrogel, before drying and re-weighing. The gel fraction is directly proportional to the level of crosslinking, which locks polymers within the hydrogel. The gel fraction is inversely proportional to swelling ratio, because the less densely crosslinked hydrogel can better absorb water and swell [29].

The swelling of a hydrogel is a key parameter in its effectiveness as a DDS. The swelling kinetics will determine the onset of drug delivery. Generally swelling will occur at a linear rate before reaching a plateau when the hydrogel is saturated with fluid. The relative amount of swelling is also important as this partly controls the permeability and thus the diffusion through the hydrogel [21].

2.2.4.1.2.3 Kinetics

The drug release mechanism is a crucial property of the DDS as this controls the timing of drug delivery – one of the primary functions of DDS. Different mechanics can be utilised to attain the drug release profile that is most suitable for the intended medical application.

In most hydrogel drug carriers the release of the drug is governed largely by diffusion through the hydrophilic network as well as the T_g. The rate-controlling factor is the resistance of the polymer network to an increase in volume and change in shape [21], that is reaching the T_g and swelling. But once this occurs diffusional parameters such as network pore size and drug-solvent solubility mediate release [22]. This results in a phenomenon whereby two interfaces are controlling drug release: The interface between the glassy polymer core and the rubbery hydrated polymer; and the interface between the exterior hydrated polymer and the dissolution media [22]. Depending on the interaction occurring at these interfaces, Fickian or non-Fickian drug transport may be observed. Fickian drug transport results from one of the interfaces having a large effect on the delivery of the drug relative to

the other. That is, relaxation of the polymer is dramatically faster than diffusion or vice versa. Non-Fickian drug transport results from these two mechanisms having a virtually equal effect. The drug released through a thin polymer slab (Mt) proportional to the total drug released (M_∞) is expressed as follows:

$$\frac{M_t}{M_\infty} = kt^n \qquad (3)$$

The value of *n* determines the dependence of the release rate on time. The relationship between *n* and the drug transport mechanism through a polymer slab is shown below in Table 9. Time-independent drug release is described by values of n = 1.00. The constant k incorporates characteristics of the macromolecular network/drug system and the dissolution medium [22].

Table 9. Transport Mechanisms of a diffusible substance through a polymer slab [22]

Exponent *n*	Type of transport	Time dependence
0.5	Fickian diffusion	$f(t^{-0.5})$
$0.5 < n < 1.0$	non-Fickian (anomalous)	$f(t^{n-1})$
1.0	Case II transport	time-independent
$n > 1.0$	super Case II transport	$f(t^{n-1})$

From analysis of drug release kinetics above it becomes obvious that the selection of the hydrogel/drug combination is crucial as the physical-chemical interactions in this system will determine the release rate of the drug.

2.2.4.1.2.4 Sterilization

Many DDS systems are classed as medical devices and must undergo terminal sterilization to ensure safe use for patients and physicians. However, many sterilization methods use high energy levels with altering effects on DDS systems.

Gamma radiation is a common method for sterilizing medical devices and it is also known to crosslink hydrogels [22]. Thus, gamma irradiation may offer a way to simultaneously sterilize and crosslink hydrogel DDS. However, this needs to be carefully designed as many drugs that are gamma-stable in powder form are easily inactivated by gamma when in solution [162-163].

2.2.4.1.3 PVA hydrogels for drug delivery

Poly vinyl alcohol (PVA) is a highly hydrophilic, biocompatible, bioabsorbable material that has excellent film-forming properties making it suitable for use in pharmaceutical and medical devices [15, 38-39]. Crosslinked PVA has a high swelling ratio and good in situ stability making it useful for sustained release applications in particular [35, 38]. The properties of slow releasing PVA hydrogels can be tailored by controlling crosslinking density [35].

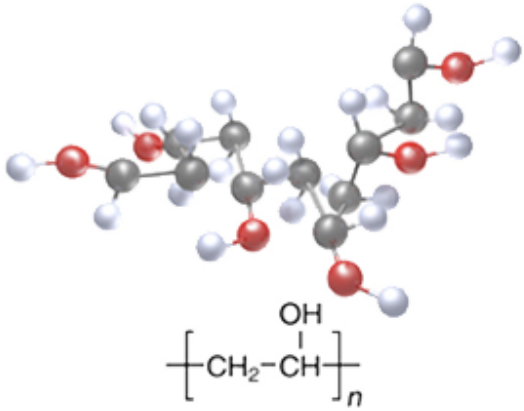

Figure 20. Chemical formula and structure of PVA.

2.2.4.1.3.1 Crosslinking PVA

Crosslinking can be achieved by many physical or chemical methods. For the purpose of drug delivery devices, the interaction between the crosslinker, the drug and the host must be taken into account.

Protein adverse affects from chemicals like glutaraldehyde and protein denaturation affects from freeze-thawing forced Bourke *et al* to employ UV photo-crosslinking to form controlled release PVA devices for delivery of platelet-derived growth factor (PDGF) [35]. Hassan and Peppas point out the disadvantage of using chemical crosslinkers and catalysts in biomedical hydrogels: Residues in the resulting PVA hydrogel may have negative effects in patients and removing the residues is time-consuming and often not possible [26].

Gamma irradiation can be used to crosslink PVA hydrogel. This method can only be used to crosslink hydrated PVA, as water is needed to both generate free radicals and allow for polymer chains to move freely. When solid PVA was gamma irradiated the resulting material dissolved in water rather than swelling, showing no crosslinks had formed [164]. Gamma irradiation addresses the toxic residue problem by introducing no chemicals or catalysts. However, gamma irradiation is a high energy method

that may damage the drug being carried. Drug inactivation is very likely to occur particularly if in aqueous solution, where the drug acts as a scavenger for oxidising and reducing radicals [162-163]. Effectively, gamma irradiation crosslinking of DDS (which must be hydrated) cannot contain the drug, which would be inactivated in the hydrated state. The drug phase would need to be incorporated into the DDS afterward, preventing simultaneous terminal sterilization and crosslinking. This design catch-22 is, to my knowledge, not identified in the literature. Another problem encountered in this method is bubble formation in hydrogel films [26].

PVA has a crystalline structure. When polymer chains become folded small ordered regions are formed (crystallites) within the otherwise amorphous PVA matrix. Inducing this crystallite formation physically crosslinks the PVA matrix. Cyclic freeze/thawing is a commonly used method to produce PVA hydrogels by crystallite formation. This method also leaves no toxic residues because no chemicals are used in the process. Aqueous solutions of PVA are frozen to typically -20C and thawed back to room temperature. The level of crystallisation can be easily controlled by the number of freeze/thaw (F-T) cycles [22, 25-26] and hence control crosslinking and hydrogel properties. F-T formation of PVA hydrogels can be performed in the presence of organic solvents and has been used to create transparent hydrogel for lens biomaterials [26]. Hyon *et al* formed transparent PVA hydrogels using the F-T method with solvent-polymer solutions that were up to 100% solvent. The decreased freezing temperatures (Figure 21) affected the F-T process. Crystallisation of the PVA network still took place. In the case of 50:50 ethanol-water PVA solution (15% w/v) the optimal crystallisation settings were 3 hours maturation at -20C. The hydrogels became transparent due to crystallisation at lower temperatures resulting in smaller crystals and thus smaller pore size. This impacted mechanical properties with tensile strength increasing with higher solvent concentrations [165]. The decreased porosity may also be an advantage for slow drug release devices this was not discussed in the patent by Hyon *et al*. Nor was the opportunity for using the method for increasing the drug-loading efficiency of water-insoluble drugs such as erythromycin and chloramphenicol.

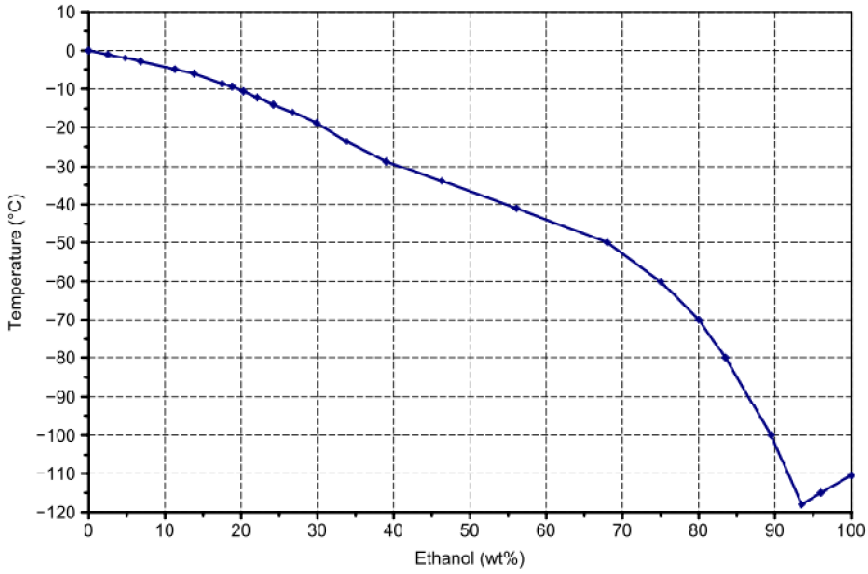

Figure 21. Melting point of water-ethanol mixtures [166].

The F-T method and gamma irradiation methods have been combined to examine the effects on PVA/chitosan hydrogels for wound dressings. Yang *et al* [167] performed F-T and gamma in that order and visa versa. It was found that F-T produced more desirable properties than gamma alone. Further the addition of gamma irradiation after F-T had little effect on the mechanical properties or swelling behaviour of the hydrogel.

More recently, PVA cast gels have been developed that are also crosslinked from crystallite formation. These form transparent and more elastic hydrogels than those formed by freeze/thaw cycles. However, crack formation in PVA cast gels may affect their viability [168].

2.2.4.1.3.2 Slow release from PVA

Due to its favourable properties, PVA has been extensively studied for many slow release applications.

Adi *et al* [169] manufactured PVA microspheres by a spray drying technique for a respiratory spray treatment. These microspheres (2um diameter) were made using 90% w/w PVA solution. In a previous study this stock concentration produced the slowest drug release. Microspheres contained 10% w/w antibiotics (ciprofloxacin or doxycycline). During in vitro release testing < 50% of the drugs were released over a 6 hour period. A previous ovine model showed that these could continue to elute

antibiotics up to 6 days. Ciprofloxacin released slower than doxycycline apparently due to their relative aqueous solubilities (30 and 50 mg/ml respectively).

Basak *et al* [38] manufactured pH-sensitive PVA hydrogels films by cross-linking with maleic acid for controlled drug release to improve the efficiency of oral drug administration. 10% w/v PVA films containing a higher concentration of maleic acid became more crosslinked. Crosslinking was found to have an inversely proportionate relationship to drug permeability and a proportionate relation ship to drug release time.

Bourke *et al* [35] tested PVA hydrogels for delivery of bioactive proteins in wound healing. The study used 15% solid content PVA hydrogels containing uncrosslinked PVA fillers. The study concluded: "the release profiles of proteins from PVA hydrogels can be tailored by modifying 3 major parameters: solid content, initial protein loading and incorporation of hydrophilic fillers." The last two parameters are especially relevant for protein delivery but the solid content parameter is applicable for other drug classes. In fact many studies perform a solid content (whether this be the PVA itself or another crosslinker) optimization experiment when testing PVA DDS. However, Sung *et al* [33] reported that in PVA/chitosan hydrogels the total solid content had little effect on release kinetics of minocycline, despite gel fraction and swelling ratios obviously being affected. This may be due to chitosan greatly increasing the porosity of PVA hydrogels such that all samples tested were eluting the antibiotic at the maximal rate.

2.2.4.2 Wound modelling

There have been a number of wound models developed to test the efficacy and safety of wound care devices. A wound model aims to represent features of a real clinical wound while simplifying the complexity of the wound healing interactions to provide insights [170]. Wound models can be split into two broad categories: In vitro and in vivo. The different type of models in these two broad categories have been reviewed by Gottrup *et al* [170]. I will summarise this and include more recent models. In addition I will focus on septic wound models – an under-researched area.

2.2.4.2.1 In vitro models

Table 10. Summary of in vitro wound and infection models

Cultured Cell diversity	Culture Architecture	Infection level	References
Single cell type	2D	Aseptic	[171-172]
Single cell type	3D	Aseptic	[171, 173]
Single cell type	2D	Septic	[104, 174]
Single cell type	3D	Septic	[175]
Multi-cellular*	2D	Aseptic	[176]
Multi-cellular*	3D	Aseptic	[177-178]
Multi-cellular*	2D	Septic	[140-141, 179-180]
Multi-cellular*	3D	Septic	none

* 'Multi-cellular' systems are classified as allowing direct contact between 2 or more different cell types

In vitro models, apart from their simplicity of set up and lower cost, have a number of other benefits over their *in vivo* counterparts. In vitro models have virtually no ethical considerations compared with in vivo (this is particularly true in septic wound models). They are more controlled as they lack the inherent heterogeneity of in vivo models. Further, mechanisms are easier to study due to the decreased biological interaction and complexity [170].

Most *in vitro* wound models involve growing a monolayer of cells on tissue culture plastic. These cells are either healthy cells that were grown *in vitro* or explanted cells from subcutaneous wounds. Monolayer (2D) cultures are useful for characterising the phenotype of cells as well as for easy processing, however they lack the tissue architecture and the spatial and mechanical cues associated [171]. Fibroblasts, keratinocytes, macrophages and endothelial cells are the most commonly used cells in these wound models [170].

The scratch assay is a common 2D wound healing model [170, 178]. Skin cells, either fibroblasts or keratinocytes are grown in a monolayer. Then a section of the monolayer is scraped off and washed leaving a standard area devoid of any cells. Scratch area closure can then be measured microscopically to model wound closure. There is no extracellular matrix or inflammatory system in this simple model but it does allow direct observation of how cells are affected by external agents [104, 174].

In vitro co-culture of critical wound healing cells has been performed. Oberringer *et al* [176] designed a wound model co-culturing fibroblasts and endothelial cells then performed scratch assays. The cells were co-cultured on glass slides (2D) and were pooled together before seeding the slides resulting in random dispersion of the cells on the slide. The different cells were distinguished for analysis by immunocytochemical staining. This method would likely not be possible in 3D wound models as visualisation becomes too difficult.

Two-chamber co-culture models have been used to study wound healing processes. Loo *et al* [172] used such a system to study wound epithelialisation in the presence of H_2O_2, co-culturing fibroblasts and keratinocytes. The model in essentially comprised of mono-layers of each cell type cultured in the same medium. This does not allow for direct cell-cell contact and interactions but the 2D nature and separation of the cells allows simple and direct analysis of each cell type.

Gottrup *et al* [170] discusses 3D *in vitro* cultures briefly and concludes that most measurement techniques for migration, proliferation and other important wound healing metrics can be determined in the same ways as 2D culture. Gottrup cited Schor's [173] work as an example, which used light microscopy to determine the migration of fibroblasts on collagen gels. However, important physical characteristics of the gels were not defined such as thickness and porosity. The processing method suggested the gels were thin films – similar to 2D. Further the microscopy method used data obtained by counting cells on the scaffold surface in a given area and calculating to find the percentage of cells inside the gel. This is 2D data obtained and converted into 3D and may not be representative of the culture condition. In our experience, light microscopy of 3D cultures yields qualitative results as cells are difficult to visualise and count with lacking depth of field. Removal of cells from the 3D matrix is also difficult due to entrapment in the porous matrix [181].

Recently more complex "skin equivalents" have been developed to model wound healing. These models involve multiple wound tissue cell types cultured on a 3D matrix. Defects are induced in these skin equivalents to model the wound. Herman *et al* [177] produced such a model growing microvascular

endothelial cells and human keratinocytes in a Matrigel/collagen matrix (BD Biosciences) to study wound angiogenesis in vitro. Xie *et al* designed and manufactured human skin equivalents by culturing keratinocytes and fibroblasts on decellularised de-epidermised matrix. A punch biopsy was used to simulate a wound in these standardised skin samples. The morphology of the skin equivalents had a similar morphology to native skin when compared with multiphoton microscopy. Further, histological analysis wound area measurements allowed visualisation of wound healing [178].

2.2.4.2.2 In vivo models

The advantage of *in vivo* wound models is they closely mimic the wound environment in clinical practice. The disadvantages are that analysis of a single cell type becomes difficult and that ethical issues arise when inducing wounds in animal models [170].

The most common *in vivo* skin wound model uses an excision of a full thickness piece of tissue from an animal. This represents the actual loss of tissue seen in many acute and chronic wounds in the clinic. This model is mainly used in mouse, rat, rabbit and pig. The superficial wound allows analysis of different types of dressing, grafts and locally applied therapeutics. Wound healing can be visualised by biopsies and histology. Wound contraction and epithelialisation can also be measured although not easily independently from one another [170].

Li *et al* [182] tested the bioactivity and degradation characteristics of PDGF (a co-factor with vascular endothelial growth factor [VEGF]) eluting polyurethane scaffolds in rat models. Scaffolds were implanted into excisional wounds made in the backs of male rats. The rats were then sacrificed at different time point. The scaffolds were harvested from the wounds and analysed using histological imaging. In this way the scaffold-granulation tissue ratio could be calculated and inflammatory cells could be observed.

Recently a review paper was written assessing in vivo septic wound models. The author stressed the importance of modelling the interplay between bacteria and host cells in understanding wounds. Animal models included mouse, rat, rabbit and pig. The vast majority of the models were murine and the author emphasised that mouse skin wounds contract mediated by myofibroblast migration whereas human skin wounds contract by new tissue ingrowth. Yet most rodent wound healing studies ignore this variable. Either splinted wounds or wounds induced around cartilage can provide mechanical strength against contraction making the model more applicable to humans. The importance of modelling a biofilm-planktonic phase rather than one or the other was also mentioned [183].

It was stated that this interplay between host cells and bacteria cannot be evaluated in vitro. This is true to some degree: The complexity of the immune system and the interaction with microbes is virtually impossible to model outside of an organism, however, specific cells and tissues can be tested in the presence of bacteria and insights can be gained as showcased above (2.2.4.2.1).

2.2.4.2.2.1 Clinical models

Clinical models are the most meaningful as they test the therapeutic in the situation for which it is proposed to be used for. Since patients partaking in these studies are at risk, ethical and safety considerations are numerous. Finding patients that fit the appropriate demographics and have the appropriate pathology must be controlled for a meaningful study. This can mean these studies take a long time while appropriate patient participants are located.

Dermagraft, a commercially available tissue engineered scaffold, was tested in a pilot study to treat 18 patients with chronic venous leg ulcers. Patients were selected that had ulcers for at least 12 weeks without healing. Treatment with Dermagraft over a further 12 week period was compared to a control treatment which was a non-adherent dressing (Dermanet, Smith and Nephew Plc). Both treatments were used in combination with existing wound care standards: regular debridement, compression bandaging, etc. The healing rates were compared by measuring the change in wound area at defined time points [111].

In terms of studying wound regeneration, clinical models can be unsuitable as human biopsies are difficult to acquire. This is because it is not advised to remove some of the tissue that needs to do the healing. Here especially *in vitro* models are preferable [176].

2.2.4.2.3 In vitro septic wound models

Most septic wound models are performed using a single bacterial species. *S. aureus* is often the chosen pathogen as it is the most common in clinical septic wounds [104, 141, 174]. In reality, wound biofilms contain a number of diverse species: *Staphylococcus*, *Pseudomonas*, *Peptoniphilus*, *Enterobacter*, *Stenotrophomonas, Finegoldia*, and *Serratia* species [174]. Bacteria exist predominantly in biofilms as this is what protects the pathogens from the host immune system. Planktonic bacteria are also present during initial infection and subsequent shedding from biofilms. Wound models often will limit bacterial state to planktonic or biofilm, rarely both.

An invasion model was designed by Mempel [179] and colleagues testing the virulence of different *S. aureus* strains on keratinocytes. Planktonic *S. aureus* cells were added directly to keratinocytes grown to confluence in 24-well plates. After 2 hours gentamicin and lysostaphin were added to the media to kill any bacteria that had not invaded the cell cytoplasm. The media was changed and the cells were cultured for varying times up to 24 hours. Cells were then detached, collected and analysed morphologically by trypan blue dye exclusion and TEM. The results showed dose dependent internalisation and time dependent cell death when invaded by all strains. This is not a wound model, but does illustrate the effects of direct contact between *S. aureus* and epidermal cells which is relevant to wounds. The removal of *S. aureus* after 2 hours of culture prevents the effect of other toxins and cytotoxic enzymes that are produced by the bacteria and would be present in septic wounds.

A similar invasion model of *S. aureus* on keratinocytes was performed by Nuzzo *et al* [180] to study *S. aureus* intracellular survival and virulence. After antibiotic destruction of non-internalized S. aureus, further culture proceeded in media containing gentamicin to prevent further growth of bacteria and controlling the experiment. This limited the model to only intracellular effects. The authors mention that *S. aureus* is "primarily known as an extracellular pathogen". The extracellular virulence factors may have an important synergistic effect. I suspect though that the extracellular factors were removed to simplify the method as these factors would rapidly kill keratinocytes in static cell culture.

Kirker *et al* [104] tested the affects of *S. aureus* biofilms products on keratinocytes. Biofilms were grown in diluted trytone soya broth (TSB) on tissue culture inserts (10mm diameter plastic discs) for 3 days. These were then co-cultured with keratinocytes in scratch assays, however the biofilm was isolated from the cells. Biofilm culture media was also created by culturing the 3-day biofilms in the keratinocyte cell culture media. This too was used in scratch assays and compared to the biofilm co-culture and another altered culture media made with planktonic *S. aureus*. The 2D assay allowed visualisation of cell phenotype using brightfield and confocal microscopy. In summary, all cases prevented closure on the scratch in the keratinocyte monolayer. An XTT viability assay was also performed and revealed that there was significantly more apoptosis seen in keratinocytes cultured in the presence of biofilm altered media compared with planktonic media, but both bacterial media greatly reduced viability compared to the healthy cell controls. The authors conclude toxins are the cause of the cell death and hint at *S. aureus* biofilms producing increasing amounts of α-toxins which had previously been reported to be very cytotoxic to keratinocytes.

The same group carried out a similar study but tested *S. aureus*-toxified media on dermal fibroblasts. Enzyme-linked immunosorbent assay (ELISA) was used to test treated fibroblasts production of wound-healing cytokines, growth factors, and proteases. There was no significant difference between the planktonic and biofilm toxified media in terms of scratch area reduction or fibroblast viability – the scratch could not be bridged and apoptosis was seen. ELISA showed, for most wound healing factors tested, a larger divergence from the healthy state when subjected to planktonic MRSA media over biofilm media. The authors reasoned this could demonstrate a bacterial strategy to decrease virulence when already infiltrated into the dermis (mainly consisting of fibroblasts) to in turn better evade the host immune system. The differing effects between fibroblasts and keratinocytes in the presence of *S. aureus* are difficult to explain but these cell types have been known to respond differently to other same bacteria (e.g. *Peptostreptococcus* spp.) before [174].

Werthen *et al* [175] grew biofilms of *S. aureus* and *P. aeruginosa* on separate collagen matrices to produce an infected chronic wound model. Biofilms were quantified by break down of the collagen matrix with collagenase followed by spread plating. Visualisation was conducted by laser confocal microscopy and histology. The model was developed for simulating the morphology of bioiflms in chronic wounds in vitro and testing therapeutics that may prevent wound infection. The obvious shortcoming of this model is no human cell type was used, so the interaction between cell-biofilm and cell-therapeutic cannot be tested.

Subbiahdoss *et al* [140-141] designed and tested a model for the "race for the biomaterial surface" between osteoblasts and *S. epidermidis*. A modified culture medium was optimized for co-culture of bacteria and cells. Absolute numbers of each cell type attached to a glass slide was determined by counts with a light microscope. Both static and flowing cultures were tested. In static culture the S. epidermidis secreted toxins killing osteoblasts independent of the bacterial numbers. This was attributed to the build up of the toxins in static culture. In flowing culture conditions the bacterial-dependent killing of osteoblasts was seen allowing the competitive testing of the biomaterial colonisation. This is one of the few bacteria-cell co-cultures that physically put cells and bacteria together in the same culture media. However, the model is only 2D, with species competing for the surfaces of a flat glass slide. Most implanted biomaterials are 3D and have complex porous geometries. This would make the visualisation of cells impossible and thus a new measurement method would be needed to update this method to a 3D model.

To my knowledge an *in vitro* experiment does not exist that combines the ideas of 3D culture on biomaterials and biofilm infection.

2.2.4.2.4 RT-qPCR

Reverse transcription quantitative polymerase chain reaction (RT-qPCR) is a method of detection and quantification of RNA. Conventional PCR, which has become the corner stone method of molecular biology, is only possible with DNA. Thus to quantify RNA it is first converted to cDNA by a reaction with the enzyme reverse transcriptase. The cDNA can then undergo PCR or qPCR allowing the quantification of the initial RNA.

Recently, RT-qPCR has been used to quantify bacteria by targeting the highly conserved 16s ribosomal RNA (rRNA) [184-185]. 16s rRNA contains both highly conserved and highly variable regions in the sequence allowing design of taxa specific and prokaryote universal primers as the study requires[185]. This method has the advantages over conventional plating methods of sensitivity, specificity and convenience; that is primers can be designed to target bacteria in a multi-cellular population and the process is high-throughput and scalable. rRNA has a high copy number per cell which makes RT-qPCR more sensitive than PCR [184]. Although, rRNA expression is more constant than other genes (and as a result it has been used as a reference housekeeper gene in many quantitative studies) [186], levels have been known to fluctuate depending on cellular growth rates. This may preclude its use for quantifying cells in studies where growth rate of cells changes dramatically, e.g. under stressed state, exposed to antibacterial, starvation, etc. rRNA is a convenient marker for viability as it degrades more rapidly than DNA [184]. It may be the viability marker of choice in situations where viable counts are impractical.

Matsuda *et al* [184] designed different primers for 16s rRNA sequences in a number of bacteria. RT-qPCR was used to quantify numbers of bacterial species including *S. aureus* and *P. aeruginosa* in blood and faecal samples by formation of standard curves relating cycle threshold (C_t) to bacterial samples of known number. A linear relationship was seen between C_t and bacterial numbers.

As far as I know, 18s rRNA targeted qPCR has not been used to quantify eukaryotic cell types. However, 18s is the most common housekeeper gene for relative qPCR analysis of eukaryotes [187-189] and is presumed to be essential for cell viability [190]. Therefore, utilising 18s rRNA as a marker for viable cells in co-culture may represent a convenient and relevant procedure.

2.2.4.2.4.1 RNA extraction from Staphylococci

The septic wound model designed in this study uses *S. aureus*. Staphylococci species have a particularly tough cell wall making many standard RNA isolation techniques unreliable [191]. Enzymatic treatments (by enzymes such as lysostaphin) break down the cell wall but require extended amounts of time resulting in RNA degradation and low yields. This problem has been largely solved by using disruption by ceramic beads and vigorous shaking to mechanically break open the Staphylococcal cell wall in a chaotropic agent followed by phase separation and precipitation in isopropanol [184, 186, 191].

Dobinsky *et al* [191] tested RNA extraction methods on *S. eppidermidis* biofilms. It was found that after biofilm formation bacterial cells were much more resistant to RNA extraction even after mechanical disruption with sonication followed by shaking with silica beads. Dobinsky introduced a very short (2 minute) lysostaphin treatment before disruption which greatly increased the RNA yields.

2.3 Ethylene Biofilters

2.3.1 Ethylene

Ethylene or ethylene (C_2H_4) is an alkene hydrocarbon compound with two double-bonded carbon atoms each with two hydrogen atoms (Figure 22). Ethylene is a gas at room temperature and is both naturally occurring and a by-product of industrial operations, largely related to petrochemicals and vehicle exhaust [192]. Ethylene is detected easily using a gas chromatographer equipped with a flame ionization detector [192-197].

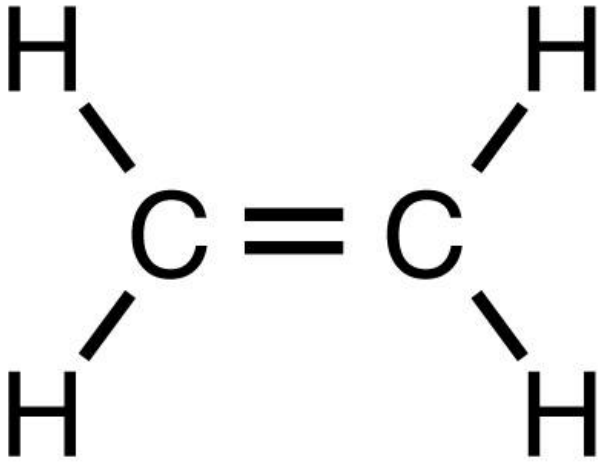

Figure 22. The molecular structure of ethylene

2.3.1.1 Plant Hormone

Ethylene is a plant hormone regulating a large number of physiological processes. As a hormone ethylene binds the ethylene receptor and a signal is transduced which elicits a biological response [198]. Ethylene confers both negative and positive effects on produce depending on storage time, concentration and dosage. Initially ripening increases flavour and colour, but later it promotes rotting, senescence and physiological disorders [198-199]. Ethylene is also a stress hormone and its release is upregulated from both abiotic and biotic stresses [199].

Ethylene is biosynthesised by *climacteric* fruits (bananas, apples, mangos, tomatoes) in response to ethylene in a positive feedback mechanism – a trait in nature used to coordinate ripening. Thus these fruits are generally the most susceptible to ethylene effects [199-200]. However, in non-climacteric produce (citrus, strawberries, grapes), ethylene is not important for ripening, but still increases susceptibility to disorders and pathogens [198]. Table 11 below shows the relative ethylene production and sensitivity of fruits.

Table 11. Ethylene production and sensitivity of several commodities [198].

Commodity	Ethylene production	Ethylene sensitivity
Climacteric fruit		
Apple, Kiwifruit, Pear, Cherimoya	***	*** (0.03–0.1 μl l^{-1})
Avocado, Cantataloupe melon, Passion fruit	***	** (>0.4 μl l^{-1})
Apricot, Banana, Mango	**	*** (0.03–0.1 μl l^{-1})
Nectarine, Papaya, Peach, Plum, Tomato	**	** (>0.4 μl l^{-1})
Vegetables and non-climacteric fruit		
Broccoli, Brussels sprouts, Cabbage, Carrot,	*	*** (0.01–0.02 μl l^{-1})
Cauliflower,Cucumber, Lettuce, Persimmon.	*	***
Potato, Spinach, Strawberry	*	***
Asparagus, Bean, Celery, Citrus, Eggplant	*	** (0.04–0.2 μl l^{-1})
Artichoke, Berries, Cherry, Grape, Pineapple,	*	* (>0.2 μl l^{-1})
Pepper	*	*

* low, ** medium and *** high ethylene production or sensitivity.

In nature ethylene synthesis by plants ensures their seed dispersal by animals that eat their fruits, but in agriculture ethylene is a problem as it accelerates ripening and causes fruits to spoil before reaching consumers [199]. A relationship between storage life for fruit and ethylene concentration has been found which states that levels greater than 0.1 ppmV causes distinguishable quality loss [198]

Prices of fresh fruit are increasing. Factors like a growing population, climate change, growing incomes and health awareness are greatly increasing demand of fresh produce ensuring that price rises continue [201]. Food spoilage is a key inefficiency in the fresh produce value chain. Food growers, transporters, distributers and consumers all have an interest to decrease wastage. The current estimate is that 'as much as half of all food grown is lost or wasted before and after it reaches the consumer'[202]. 'Spoilage' specifically refers to wastage attributed to post-harvest stages of the value chain. Economically viable methods for ethylene removal are required to minimise this spoilage.

2.3.1.2 Pollutant

Ethylene is produced synthetically as a by product of hydrocarbon pyrolysis which is released as air pollution [198]. Ethylene is a pollutant and a suspected carcinogen. Even sustained dosages at the parts per billion (ppb) level have been shown to increase the risk of mutagenic effects [192]. It also causes air pollution problems like the production of carbon monoxide and ozone as well as preventing removal of chlorine from the stratosphere [203]. Ethylene pollution may also have an effect on plants in urban centres where concentrations consistently reach high levels. Control of ethylene emissions is therefore a priority for public health.

2.3.2 Current Ethylene Removal Systems

2.3.2.1 Chemical Filters

Only two types of ethylene removal systems have found success on a commercial scale. The first is using potassium permanganate to absorb and to oxidise gaseous ethylene giving off carbon dioxide and water. However this method can only be applied to small storage rooms as the potassium permanganate is quickly consumed and must be replaced [196, 200, 203]. It has been reported that even its use in packaging may be limited due to the high accumulation of ethylene which would require a large amount of the oxidiser [198]. Potassium permanganate is highly toxic such that special packaging in required so it cannot contact food. Scott *et al* [195] showed that potassium permanganate preserved the firmness of Australian banana fruits stored in polyethylene bags for an extra two weeks compared to the control.

Bananas are known to produce an increasing amount of ethylene after harvest during which time the fruit becomes more sensitive to the gas [193].

The second system involves catalytic oxidation of ethylene at high temperatures (~ 200°C). Despite the need for expensive catalysts like platinum, copper and zinc, this method is thought to be more economical than potassium permanganate and more adaptable to large volume rooms. This method still has substantial costs primarily associated with energy usage. Blidi *et al* [200] trialled a low temperature (100-130°C) system using a catalyst which was a mixture of oxides of manganese and copper. The system successfully conserved Granny Smith apples for 134 days after harvest.

Chemical scrubbers and filters are commercially used in agriculture and industry for removing ethylene in large volumes, but they have more recently been introduced into the home in the form of the Ethylene Gas Guardian (EGG). EGG comprises small sachets of potassium permanganate coated zeolite enveloped in a hard plastic slitted egg for protection. This is left in a refrigerator vegetable draw and prevents produce from spoiling as quickly. The potassium permanganate is either in pellet form or coated onto a high-surface area substrate, commonly zeolite – a natural volcanic rock. The sachets need to be replaced every 3 months to replenish the potassium permanganate, however the sachets are very cheap – $10 for eight sachets [204].

Figure 23. Ethylene Gas Guardian. Blue hard plastic perforated containers for sachets of potassium permanganate [204].

2.3.2.2 Biofilters

Biofiltration is the removal of pollutants from a fluid (gas or liquid) by microorganisms that are separated from the treated waste. This often involves immobilization of the microbes of porous supports which the waste flows through – like a filter [205]. The waste is broken down by the microbes by biodegradation performed by natural metabolic enzymes, which also serves as an energy source for the bacteria. Biofilters have proved useful on an industrial level for the treatment of hazardous air pollutants from gas streams [206].

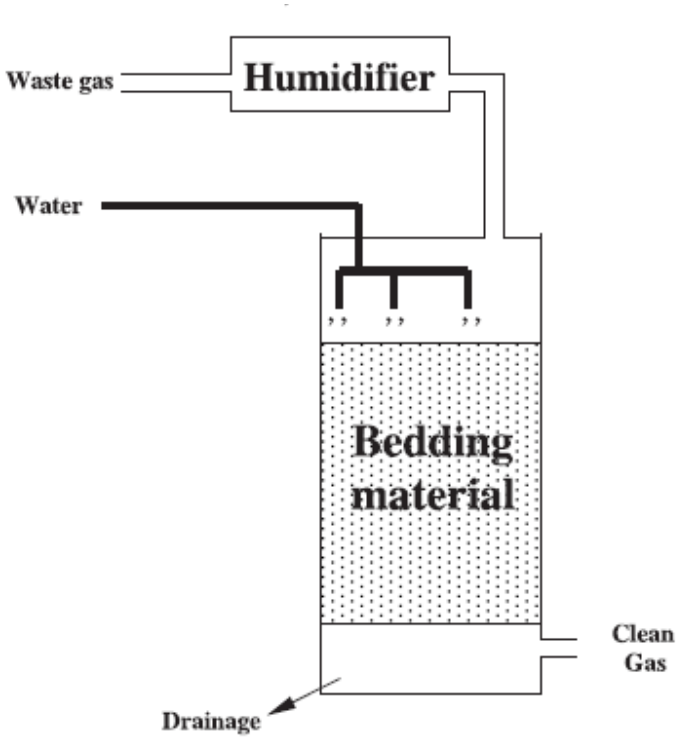

Figure 24.Schematic of a typical biofilter system. The bedding material contains waste-degrading microbes immobilized to support material [205].

Biofiltration is a method of ethylene removal with great potential. Biological agents immobilized on a filter consume the ethylene, simultaneously sustaining the biological agents and removing ethylene from surrounds. Theoretically biofilters can operate far longer than chemical oxidising agents such as potassium permanganate which need to be constantly replaced. Further, they can operate at ambient temperatures and require no energy to breakdown ethylene unlike chemical catalysts. This in turn makes biofiltration a less costly solution [196, 198, 207].

Biofiltration of ethylene has been documented by Elsgaard *et al* [196-197]. The biofilter used live whole bacterial cells (strain RD-4) immobilized to peat soil in a hard plastic casing to form a column (678 cm^3). Other favourable characteristics of the biofilter were that the operational stability extended for more than 75 day; the biofilter was able to remove ethylene at 5°C with 98% removal efficiency; and storage of the inoculated peat-soil for 2 weeks at 20°C caused only a halving of the ethylene removal efficiency.

Kim *et al* [208] made a biofilter using *Pseudomonas sp* isolated from wastewater and immobilized to activated carbon. The biofilter exhibited an operational stability of 90 days and a removal efficiency of 34g of ethylene m^{-3} day^{-1}. De Heyder [209] had previously constructed a biofilter containing biofilms of *Mycobacterium* strain E3 on active carbon granules. It was found that moisture was essential to maintain the biological activity of the biofilter but that too much water decreased activity due to increased mass transfer resistance.

Fu *et al* [203] isolated microbial populations from activated sludge and constructed a biotrickling filter system by immobilizing the bacteria in biofilms on natural zeolite. The mixed microbial community contained *Betaproteobacteria*, *Gammaproteobacteria*, *Bacilli*, and *Actinobacteria*. Liquid mineral salts medium was continuously fed through the biofilter to deliver nutrients and moisture to the cells. The biofilter was run for 110 days over which time the inlet ethylene concentration was stepped up from 50ppm to 1000ppm. Up to 600ppm the biofilter demonstrated 100% removal efficiency but at 1000ppm this dropped off to <83% suggesting restriction of microbial activity or capability limitation of ethylene-degrading bacteria at high ethylene concentrations. It was observed that the majority of bacteria settled at the bottom of the biofilter column near the gas inlet. The author suggested this is a result of adaptation as the ethylene concentration drops as it moves up through the biofilter. However, I suggest that the cells delivered in liquid biofilm may not have been adequately immobilized and settled and the majority of cells were pulled to the bottom by gravity. It is probable that a more even distribution of bacteria would have an impact on the removal efficiency as the ethylene removal capacity of cells would less likely be exceeded.

Lee *et al* [210] tested a number of different biofilter and biotrickling system designs for removing a mixture of pollutants including ethylene, acetone, butanol and ammonia. Activated sludge containing a mixed community of microbes was circulated through the biofilters containing different packing media: polyurethane foam, perlite granules and a mixture of compost and wood chips. Biofilters were still soaked in mineral salts medium at regular intervals to preserve a moist environment. After 145 days of operation it was shown that biofilters had a higher elimination capacity compared to biotricklers due to

the poor water solubility of ethylene. The perlite biofilter had the highest elimination efficiency followed by the polyurethane biofilter, this is reportedly due to the high surface area of perlite despite it having less porosity (65% compared to 93%).

Most biofilters described above are concerned with larger systems where gas streams are pumped through large columns containing biofiltering media. No studies so far investigate biofiltration on a smaller scale for stationary non-flowing filters or active packaging which remain key ethylene removal technologies [198].

2.3.3 Biofilter Design

2.3.3.1 Bacterial Immobilization

2.3.3.1.1 Immobilization of Biocatalysts

Biocatalysis is the use of enzymes to catalyse useful reactions for industrial and environmental applications. In conventional biocatalysis, enzymes become deactivated on the completion of the batch reaction [211].

In recent years, wide attention has been directed towards exploring the use of immobilized enzymes as biocatalysts [125]. Immobilization is the isolation of enzymes on a substrate preventing its movement to other parts of an aqueous system [212], allowing the enzymes to be re-used and enabling the continual large-scale biocatalysis of reactions [126, 211, 213]. In addition, immobilization seems to increase enzymatic stability and activity [125-126, 211-213] as well as ease of handling; separation of cells from products, smaller bioreactor sizes and reduced risk of contamination [125, 213-214].

The immobilization of viable bacterial cells has received particular attention due to a number of key advantages compared with immobilized enzymes [102, 125-126, 212-213]:

- Increased enzymatic stability due to the protection of enzymes by a bacterial cell membrane.
- Potential of catalysing more complex multi-enzymatic reactions compared.
- No need to extract and purify enzymes prior to immobilization. This is saves time and avoids the inactivation of enzymes during this process.

Immobilized cells can be dead or resting while preserving enzymatic activity. However, immobilized living cells are the most promising due to their ability to grow and regenerate, thereby retaining enzymatic activity long term [213, 215].

2.3.3.1.2 Immobilization Methods

The immobilization of cells can be carried out using a number of different methods (Figure 25) [126, 128, 215]:

1. Adhesion to a surface
2. Entrapment within a porous matrix
3. Containment behind a barrier
4. Self aggregation

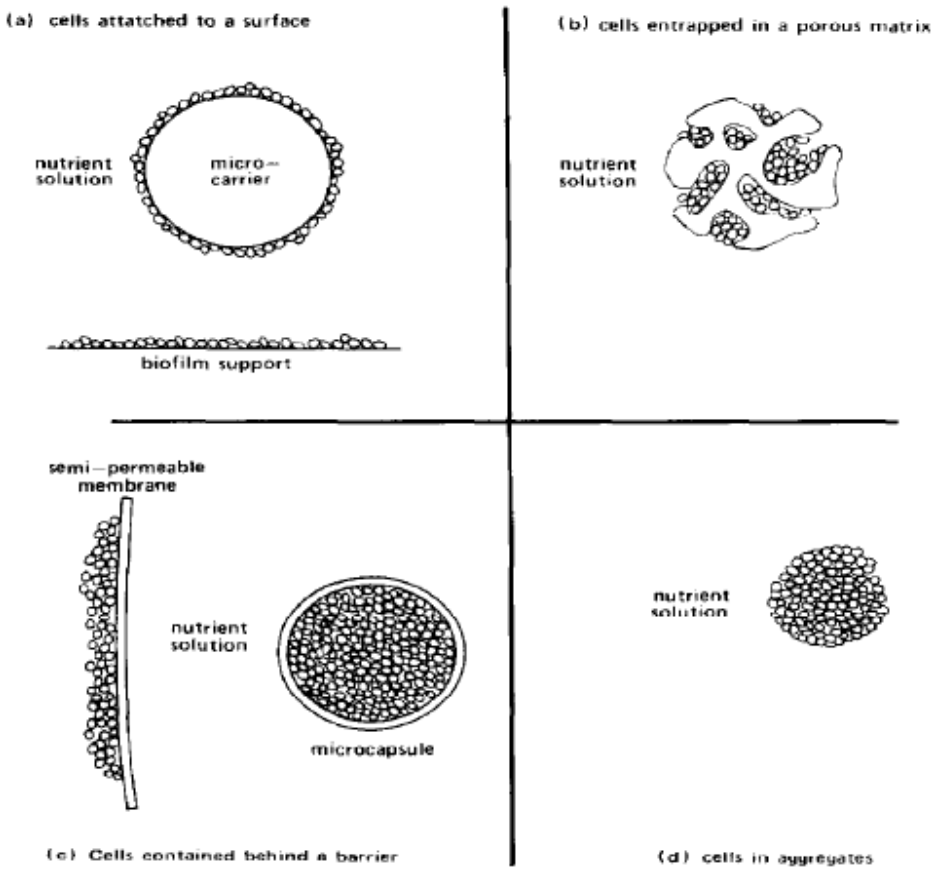

Figure 25. The four methods of immobilizing whole cells [215].

2.3.3.1.2.1 Adhesion to a surface

Adhesion is the adsorption and immobilization of cells directly onto the surface of a supporting matrix. This immobilization technique requires less processing than the entrapment methods and is less likely to damage cells [126], meaning cell viability and enzymatic stability can be more holistically preserved. Adhesion is initially a weak reversible, physical attachment, the strength of which is governed by physiochemical interaction between the cells, matrix and surrounding liquid phase. Properties influencing these interactions include hydrophobicity, surface Free Energy, pH, surface charge, ionic strength and temperature [120, 126, 128]. Thus, certain combinations of matrices and bacterial strains will be more suited toward this technique than others [215]. This is followed by a strong irreversible attachment when the cells biosynthesise a polymer layer, fixing themselves to the surface and forming a biofilm [121, 126].

Attachment of cells to a surface can also be achieved through covalent coupling. It involves covalent bonding between cells and support, allowing a stable and often permanent adhesion. However, due to the toxic nature of the coupling chemicals used in this method, it tends to be toxic resulting in a loss of viability and biocatalytic activity of the cells [128, 215].

A number of different supports can be used for this immobilization method. Natural fibres such as wood chips have been used to adsorb bacteria which were used in fixed bed reactors to produce acetic acid [215]. The other benefit of using natural fibres is that these supports are very cheap, often left over off-cuts from some organic raw materials. This presents an extra environmental benefit by recycling these waste materials. Robeldo-Ortiz *et al* [128] used agave fibres, waste products from *Agave Tequilana*, the plant used to make Tequila, to immobilise *Pseudomonas* whole cells. Mixed culture biofilms are grown on sand or rock in fixed bed reactors for wastewater treatment [215].

Natural adhesion gives the maximum cell viability and bioactivity due to the formation of biofilms. Generally bacteria prefer the community-based, sedentary lifestyle experienced in biofilms [128]. In addition, Biofilms offer excellent protection to the bacteria within, even in environments where free cells and entrapped cells would perish [128]. This immobilization is also very simple, requiring minimal processing under very gentle conditions ensuring maximum cell viability.

As there is no barrier between the cells and the solution in these systems, there will be fewer problems with diffusion of substrates, nutrients and wastes to and from cells. However, it also means that this method cannot be used when a cell-free effluent is desired as some cell leakage is likely to occur [215].

2.3.3.1.2.2 Entrapment within a porous matrix

There are two types of entrapment [215]:

1. Cells diffuse into performed porous matrix, grow and become entrapped by mutual presence of other cells.
2. Porous matrix is formed in situ around cells.

Entrapment in preformed porous matrices is fast becoming a widespread immobilization technique. Porous materials used for this method include; cordierite, bricks, volcanic rock and various types of ceramics including glass. Surface attachment plays a minor role in these systems due to the small surface area of these supports. Self-flocculation on the other hand can be utilised in systems when using supports with large pores (> 100µm). High degrees of cell viability are maintained in these systems making them suitable for growing cells, however high cell densities are difficult to achieve. This method, like adsorption, has the problems associated with not being separate from the reaction effluent [215].

Entrapment of cells in an in situ formed porous polymer gel matrix is the most common immobilization technique [213-215]. The entrapment can be physical or chemical depending on whether there is cross-linking with the polymer matrix and is usually achieved by mixing cells into a polymer solution which then is hardened into a gel, trapping the bacteria within its pores.

Polyacrylamide gel was the most widely used gel matrix for this technique, but was replaced due to reactive cross-linking agents damaging cells [213]. The interaction between the cells and the matrix should be favourable and improve cell stability. Further, the immobilization condition should be mild enough to preserve cell viability [213, 215]. Carrageenan is a polysaccharide that can be used as an entrapment gel. The advantage of carrageenan is the immobilization method is carried out under very mild conditions; 10-37°C - This ensures a high survival ratio after immobilization [213]. Anisha *et al* [214] effectively immobilized *S. griseoloalbus* by entrapment in non-toxic sodium alginate beads. However testing was needed to optimize the concentration of matrix in relation to diffusional limitations and cell leakage. In general, cross-linking and physical entrapment allow stable immobilization of cells in high

concentrations, but the entrapment media used such as gel networks often limit diffusion rates [128]. The most common confirmation of these systems is many small beads which can be used in fixed bed or fluidized bed reactors.

Because of the emphasis on physical imprisonment of cells from their surroundings, diffusional limitations can be problematic in these systems. Although, highly hydrated gel matrices have been used allowing almost un-hindered diffusion [215]. These systems have the highest cell densities; up to 700 mg per gram of support material – much higher than adsorptive immobilization. Also unlike adsorption, this form of entrapment is indiscriminate of cell surface characteristics, making it simpler from a design point-of-view [126].

2.3.3.1.2.2.1 Gel Entrapment with Agar

Agar is a natural polysaccharide gel that is commonly used in microbiological research and has been used to immobilize cells for bioreactor applications [215-216]. Cell leakage is a common shortcoming for immobilized cell systems using polysaccharide gels as the gel entrapment matrix in liquid phase bioreactors [217].

Jouenne *et al* [217] entrapped bacteria in agar disc composites comprising cells inside agar discs and coated in a microporous membrane filter. This significantly decreased cell leakage compared to agar discs alone. Cell leakage is a common issue in liquid-media bioreactors. A later study showed *E. coli* entrapped in agar discs exhibited biofilm-like properties including resistance to antibiotics [218].

Zhu *et al* [219] immobilized *Rhodobacter sphaeroides* by gel entrapment in agar for hydrogen production. The cell suspension was added to the agar solution at 45°C as to keep the cells viable while maintaining the agar in a liquid state.

Chen *et al* [220] found *Methylibium petroleiphilum* PM1 entrapped in agar cubes were able to degrade methyl tert-butyl ether more rapidly than when entrapped in other synthetic polymers such as PVA and polyacrylamide. This phenomenon was attributed to natural polymers better preserving the activity of microbial enzymes.

2.3.3.1.2.3 Containment behind a Barrier

This method involves immobilizing cells behind a semi-permeable membrane. Just like with entrapment, this barrier can be preformed or formed around the cells. Nutrients are delivered and products removed from the cells by diffusion [215].

Preformed semi-permeable membranes have been used for the immobilization of live and resting cells. Both ultrafiltration and microfiltration membranes have been used for this purpose. Microencapsulation has been employed with a permeable barrier of polylysine being formed around microbes [215].

These systems are particularly useful when complete cell separation from the effluent is required. The disadvantages of these systems are that sampling cells for testing is difficult and delivery of nutrients to the cell mass can be problematic [215].

2.3.3.1.2.4 Self Aggregation

Some cells will form aggregates naturally. This is considered a form of immobilization. Artificial flocculating agents can also be added to enhance this effect [215]. This method is particularly prone to biomass losses.

2.3.3.1.3 Biofilter Characterisation

Independent of the method chosen, the characterization of the immobilization procedure should be conducted using the following criteria [126]:

1. Biomass loading; concentration of cells on the support
2. Retention of biomass/strength of the adhesion; assessment of cell leakage under flow conditions
3. Retention of the enzymatic activity of the biocatalyst; short-term stability - activity may be lost due to the immobilization process.
4. Effectiveness/mass transfer/engineering; biocatalytic efficiency of the immobilization construct as a whole and determination of optimal operating conditions.
5. Operational stability; determines life time of immobilized biocatalysts.

2.3.3.1.3.1 Biomass Loading

This is simply the amount of cells which can be packed into the immobilization support. The biomass loading is directly proportional to reaction efficiency, as more cells will be available to catalyse reactions. Using the gel entrapment method of immobilization, the highest biomass loading concentrations can be achieved, indiscriminate of cell taxonomy and physiology [126, 205]. In this method biomass loading is easily controlled and diffusional limitations resulting from high packing concentrations become the limiting factor.

In contrast, for entrapment and adsorption in preformed matrices, achieving high levels of biomass loading is a challenge and is dependent on a number of variables. Physical and chemical interactions between microorganisms, support matrix and liquid phase are vitally important. There are two theoretical approaches to describe the adsorption of a particle to a surface. The first is the DLVO-theory based on Van der Waals forces and electrostatic interactions. The second is based on Gibbs Free Energy equation which takes into account the interfacial tension between different elements in the system [123]. Hydrophobicity can be correlated with Free Energy and it has been shown experimentally that the biomass loading of bacteria on porous glass was higher using more hydrophobic microbes [126].

The physical conformation of the support matrix also plays a vital role in biomass loading. For the most efficient immobilization of microorganisms into porous support material the smallest available pore diameter must be larger than the largest dimension of the microorganism. The optimum pore diameter of the support was determined using different kinds of bacteria immobilized on porous glass and should be in the range of the 4-5-fold length of the microorganism [221]. It is important to note that Messing *et al* could not use conventional plating methods to count the cells bonded within pores. Instead, the amount of ATP was monitored to derive the number of viable microbes.

2.3.3.1.3.2 Retention of Biomass

This refers to the assessment of cell leakage under flow conditions. For entrapment, retention of biomass is not a particularly big concern as the microorganisms are often completely protected from shear forces developed in reactors and thus have very high or sometimes complete retention. The exception is when using natural polymers that have significant biodegradability [218]. On the other hand, for immobilized cells that are attached to surfaces, this is a very important design parameter.

For immobilized cells attached to a surface, retention of biomass is directly related to the strength of adhesion. Some suggest this can be determined by calculating the free energy of both support and cell, but this method does not take into account the adhesion strength added by the formation of biofilms, only initial physiochemical interactions. Biofilms do however shed bacterial cells either by exposure to shear forces or as an active process [131] which is in a sense cell leakage even though there may not be a net-change in the biomass.

The strength of cell adhesion can easily be monitored macroscopically by determination of the maximum flow rate (MFR) which leads to a shear enforced detachment of the cells: The immobilized cells are on a fixed bed under defined fluid conditions. Then the flow rate is increased continuously. The MFR leads to detachment of the cells from the support material and can be measured by a rapid increase of the turbidity of the surrounding liquid phase [126]. This can in turn be quantified by recording the liquid phase optical density at 600nm [214].

2.3.3.1.3.3 Enzymatic Activity

This refers to the specific activity of the bacterial enzymes once the cells have been immobilized. Adsorption is a very gentle immobilization technique so it can be assumed that the specific activity of the enzymes will not be reduced by this method. On the contrary, there are many studies which show that immobilization has imposed some change on the microbe's physiological state and actually increased the catalytic efficiency [126, 222]. A possible mechanism for this is a chromosomal change; Doran *et al* reported a higher ploidy of *S. cerevisiae* immobilized in gelatin-coated glass beads [223].

To determine the true enzymatic activity of immobilized cells, catalytic efficiency must be calculated by running transformation experiments and measuring products. However, secondary experiments must also be run to rule out changes in catalytic efficiency brought about by cell leakage, diffusional limitations and cell growth. This is not often easy and probably accounts for the controversy over the physiological behaviour of immobilized cells [126, 222].

2.3.3.1.3.4 Effectiveness – Reaction Engineering

Klein *et al* [126] makes the statement that no biocatalytic system has failed due to low efficiency of the biocatalyst. This is logical as up-scaling the reactor by the addition of more biocatalysts is relatively simple. An instance where this statement does not hold is, when there is a profound loss of enzymatic activity. An example of this would be running a reaction at low temperatures or in other environments that are unfavourable to microbial biocatalysts [197] or deactivating the microorganisms during immobilization [224].

Klein [126] suggests that efficiency problems are usually a result of mass transfer resistance of which there are two types:

a) External mass transfer resistance based on film diffusion;

b) Internal mass transfer resistance caused by the pore diffusion within the catalyst matrix.

Pore diffusion is much more limiting and plays a major role in mass transfer problems of polymer entrapped biocatalysts. Pore diffusion is dependent on the internal architecture of the immobilization matrix. In contrast, internal mass transfer does not limit efficiency as much in absorptive immobilized biocatalysts. Instead film diffusion is the main limiter of mass transfer and is solely based on the fluid dynamics of the reactor [126]. This is of course a generalisation; the type of mass transfer resistance at work and the effect on efficiency is very much dependent on the immobilization construct's conformation and the nature of the fluid phase [224]. Another possible effect of mass transfer resistance is the inhomogeneity of cell distribution as cells flock to available nutrients and growth changes [126].

The mechanical stability of the matrix must also be taken into account. Fragility and compressibility are both important mechanical properties [126] that will affect the stability and efficiency of the reactor.

2.3.3.1.3.5 Operational Stability

Operational Stability refers to the life-time a biocatalyst reactor can operate efficiently. This can only really be determined by long-term monitoring of the reaction yields [196, 200]. Whether a single enzyme or whole cell multi-enzymatic reactions are taking place, the reactor will have a 'half-life' of efficiency [126].

It has been widely documented that operational stability can be vastly increased by feeding the immobilized cells with nutrients, vitamins and trace elements [205]. The use of viable growing cells is the logical way to greatly extend operational stability. This is likely the future of absorption immobilization [126].

2.3.3.1.4 Immobilization Supports

More efficient, easier to handle and low-cost immobilization supports are continuously sought as a result of the advantages of immobilized cells previously discussed [128].

Firstly immobilization supports must be insoluble in reaction substrates or products. Immobilization supports must be porous to allow efficient diffusion of fluid substrates [126]. They must provide a strong irreversible bond (either by entrapment or adsorption) between the cells and the supporting surface. They should be non-toxic to the cells and provide a favourable environment for cell growth [128, 213].

This may be in the form of surface pores which act as perfect niches for bacterial colonies or even essential nutrients in the support's chemical composition.

Entrapment immobilization supports are generally either natural or synthetic polymer gels [213], where as supports used for adhesion immobilization are many and varied. Degiorgi *et al* [225] immobilized a number of different types of bacteria onto acrylic-based hydrogels by the adhesion method. Dias *et al* [224] tested the adhesion of Mycobacterium sp to a number of different support materials by quantifying the biofilm by dry weight. The support materials tested were: glass beads, pumice stone, alumina, Celite, silica gel, polyurethane and titanium oxide. The supports allowed varying of adhesion including no adhesion at all in the case of polyurethane foam. This illustrates the variety of possible adhesion supports and the variability and unpredictability of biomass loading obtained.

In biofiltration, supports are often chosen for their adsorbing abilities. Adsorption is a surface phenomenon in which particles (gas or solid in solution) are held on the surface of solid material, thereby attracting waste particles toward the biocatalysts. Adsorbing materials such as activated carbon [208] and zeolite [203] which is an volcanic aluminosilicate crystalline material have been commonly used for as supports in both chemical filter and biofilter systems [198].

Polymeric tissue engineering scaffolds are interesting and novel candidates for immobilization supports. They are highly porous and biocompatible with customisable surface properties. Tissue scaffolds are suggested to be suitable immobilization supports using either the adsorption or entrapment method.

2.3.3.1.5 Immobilization of Mycobacterium sp.

2.3.3.1.5.1 By Adhesion

Mycobacterium has a highly hydrophobic cell wall. The *Mycobacterium* cell wall consists of a peptidoglycan layer covalently attached to a thicker layer of mycolic acid–arabinogalactan complex [120]. Therefore, initial adhesion to immobilization substrates is largely governed by hydrophobic interactions [123]. There is substantial literature providing examples of mycobacterium and other microbes with similar cell wall characteristics (e.g. *Rhodococcus*), binding to hydrophobic surfaces [127, 222, 226-228]. Mazumder *et al* [127] clearly showed that *M. smegmatis* adhered and formed biofilms more readily on highly hydrophobic materials. The hydrophobicity was a result of both chemical characteristics of the material as well as physical properties namely surface roughness. Further, more hydrophobic mutants with rough colony morphology exhibited slightly enhanced adherence and greatly

enhanced biofilm formation. This last point of colony phenotype correlation with hydrophobic adherence is contentious as previous studies claim that rough mutants have an absence of glycopeptidolipids (GPLs) resulting in decreased membrane hydrophobicity and surface attachment [145].

As *Mycobacterium* grows, they begin to develop a capsule around the cell wall containing outward-facing hydrophobic moieties. These have been reported to interfere with hydrophobic interactions and thus greatly decrease the surface attachment of the bacterium. The capsular material seems to form in late exponential phase and thickens in late stationary phase. Alavi *et al* [120] related the harvest OD_{600} of *Mycobacterium marinum* to its attachment to polypropylene. It was found the most binding occurred in early to mid exponential phase (Figure 26). This was correlated to the amount of capsular material found in different growth phases; low amounts in exponential phase and high amount in stationary phase.

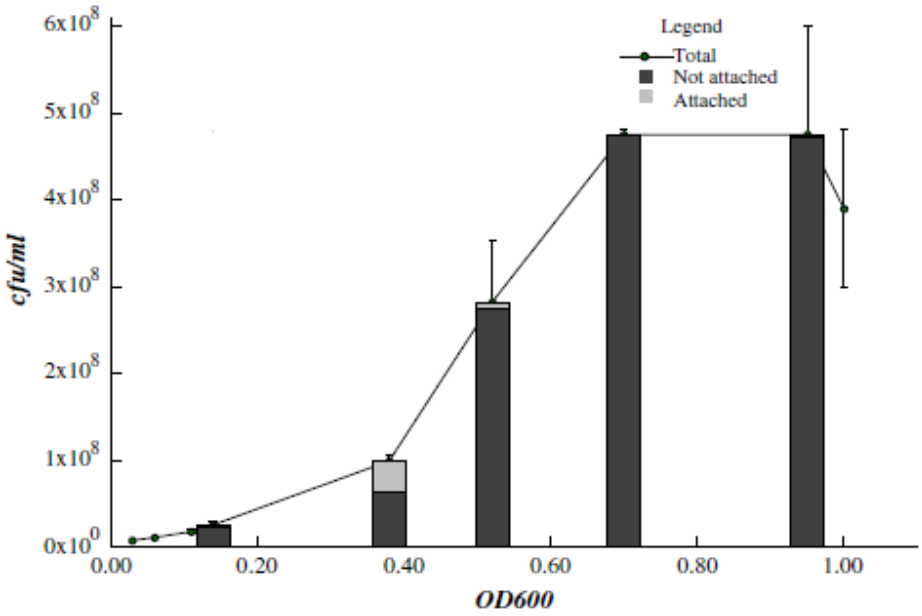

Figure 26. Growth Curve of Mycobacterium marinum and proportional attachment to polypropylene at different stages of growth [120]. OD600 is the turbidity of the culture measured at 600nm.

It is important to note that in documented adhesion assays only a proportion of microbes are seen to adhere onto the target immobilization surface. This is most likely due to two factors: 1) The competition for binding sites on the surface and; 2) That cell suspensions have mixed morphologies, with only a fraction of cells being attracted to surface [120, 227].

The hydrophobicity of the *Mycobacterium* cell wall can also be influenced by the growth substrate used to culture the cells. Lyew *et al* [228] reported a change in hydrophobicity when *Mycobacterium austroafricanum* was grown up in the presence of different carbon sources. This is due to changes in cell wall fatty acid composition [229].

2.3.3.1.5.2 By Entrapment

Dias *et al* [224] tested entrapment based immobilization of *Mycobacterium* sp. NRRL B-3805 using polyurethane foam and carrageenan beads. Bacteria entrapped in polyurethane showed no activity and were believed deactivated from the foaming process. However, *Mycobacterium* trapped in carrageenan beads were active but produced less reaction product than adhesion immobilization systems due to diffusion limitations and hydrophobic interactions with organic wastes.

An early bioreactor for the production of ethylene oxide reported *Mycobacterium* strain Py1 immobilized in sodium alginate beads to form the bedding material. This bioreactor had stable activity but suffered from mass transfer resistance problems [230].

Li *et al* [231] immobilized *Mycobacterium goodie* X7B by gel entrapment within a number of different polymers including: calcium alginate, carrageenan, agar, polyvinyl alcohol, polyacrylamide, and gelatin-glutaraldehyde. They earlier determined immobilization in calcium alginate yielded the greatest dibenzothiophene desulfurization activity. Thus it was used to form gel beads of immobilized bacteria for a liquid phase bioreactor to remove sulphur sources from gasoline.

2.3.3.2 NBB4 ethylene-degrading bacteria

NBB4 is a strain of *Mycobacterium chubuense*, a fast growing *Mycobacterium* species. Like all Mycobacteria, NBB4 is aerobic, acid-fast actinomycetes that usually forms short Gram-positive non-motile rods. NBB4 colonies appear a very bright yellow, characteristic of rapidly growing Mycobacterium [232].

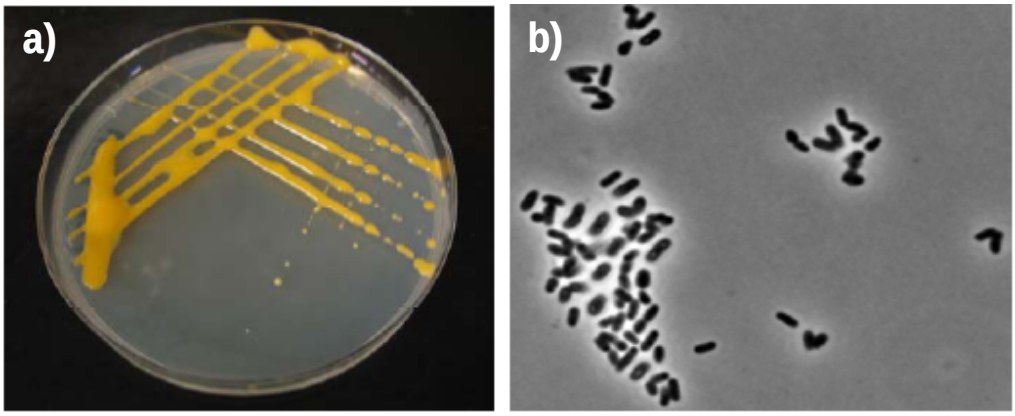

Figure 27. Morphology of NBB4 a) Slimy bright yellow-orange colonies when plated; b) Phase contrast light microscopy image of bacterial cell with short rods (x1000).

2.3.3.2.1 Ethylene Assimilation Pathway of NBB4

Mycobacterium strain NBB4 was isolated by ethylene enrichment of estuarine sediments and is able to grow on a wide range of hydrocarbons including ethane, ethylene, propane, butane, pentane, hexane, octane and hexadecane. Its versatility is likely due to it possessing an unprecedented six different types of Soluble Di-Iron Monooxygenase (SDIMO) enzymes [233-234]. NBB4 has also been affirmed for its ability to remove harmful pollutants (vinyl chloride, cis-dichloroethylene and 1,2-dichloroethane) from wastewater [235].

NBB4 possess the ethylene SDIMO allowing it to subsist solely on ethylene as a carbon and energy source. The first step of ethylene assimilation is the conversion to ethylene oxide by the ethylene SDIMO followed by transformation into an open ringed epoxide by coenzyme M transferase. The final product is thought to be acetyl- CoA formed by oxidation. Acetyl-CoA is a central metabolic intermediate of the energy-generating tricarboxylic acid cycle [233]. Other products are carbon dioxide and water.

Mycobacterium rhodesiae strain NBB3 was isolated the same way as NBB4. It too contains the SDIMO necessary for ethylene degradation. NBB3 is morphologically different to NBB4: It clumps in self aggregates during bacterial culture and when plated exhibits a roughened morphology. This is because it is missing the slimy cell wall envelope which may increase its adhesion due to hydrophobic interactions [120].

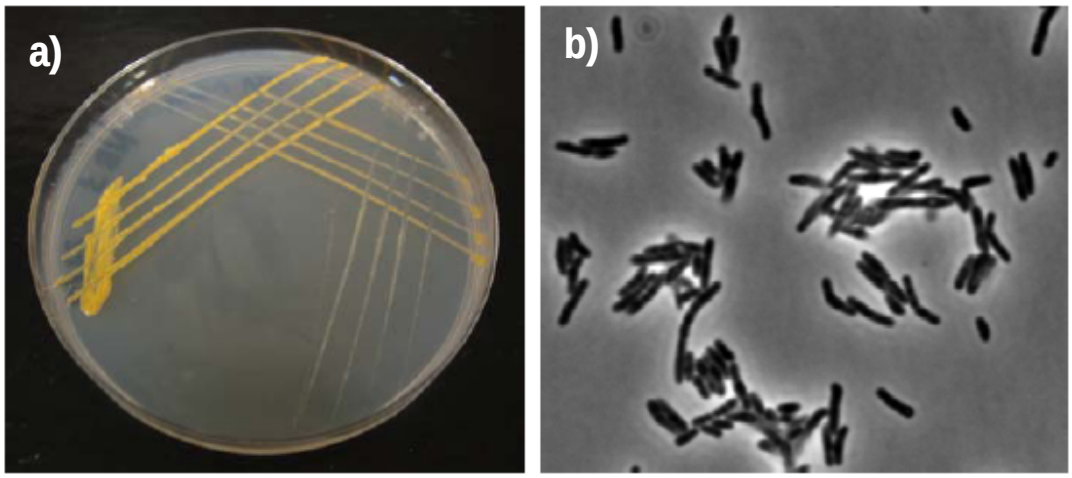

Figure 28. Morphology of NBB3 a) Rough dull yellow small colonies when plated; b) Phase contrast light microscopy image of bacterial cells with short rods clustered in lines (x1000).

2.3.3.2.2 Safety of NBB4

The virulence factors for pathogenic *Mycobacterium* are generally thought to be associated with survival in the hostile macrophage environment. This is mediated by the expression of Protein Kinase G (PknG) which blocks macrophage lysosomal delivery. Non-pathogenic strains such as *Mycobacterium smegmatis* are known to posses the gene for PknG but the expression remains very low due to elements interfering with translation [236].

NBB4 is thought to be a non-pathogenic strain of *Mycobacterium*. This is because it is an environmental strain, being isolated from soil samples and probably has not evolved the virulence factors required for pathogenesis. NBB4 being a fast growing Mycobacterium is further evidence of its non-pathogenic classification [232]. Houber *et al* [236] tested a number of Mycobacterium strains and found that only slow growing strains were able to express PknG.

The literature analysis along with a safe working history of over 10 years in physical containment level 2 (PC2) conditions ensures that NBB4 is a safe candidate for biofiltration bacteria.

3 Methodology

3.1 Composite and Material Fabrication

3.1.1 Agar Composite Scaffolds

3.1.1.1 Scaffold Manufacture

Scaffolds were fabricated using methods developed by Elizabeth Boughton [237]. High molecular weight PCL (80,000 mw, Sigma) was dissolved in a solvent and the polymer solution was allowed to leach into a porogen, the porogen was then removed simultaneous to polymer-solvent solution coagulation to leave an interconnected high porosity (>95%) PCL matrix. These scaffolds were washed in purified water and dried by centrifugation. The scaffolds produced were rectangular prisms in shape (l=16mm; w=15mm; h=11mm). There is a summary of the scaffold's properties in Table 12.

Table 12. Properties of the PCL Scaffold.

Dimensions (l x w x h mm)	Porosity (%)	Compressive Modulus* (MPa)[181]	Tensile Modulus* (MPa)[181]
16 x 15 x 11	> 95	0.02-0.06 MPa	0.04-0.08 MPa

* Mechanical testing performed on gamma sterilized scaffolds at 20% strain.

3.1.1.2 Gel Scaffold Porosity Control

The appropriate amount of agar was weighed, placed in Schott bottle and added to minimal salt media (MSM) [238] to make up to 0.1, 0.2, 0.4 and 0.6% w/v. Agars were sterilised by autoclaving. Before use agars were liquefied and homogenised using a microwave then kept in a 65°C water bath. 30 minutes before contacting scaffolds, Agars were transferred to a sterile 250ml beaker and placed in a 42°C water bath. Using a sterile tea-strainer scaffolds were submerged into MSM-agar mixture one at a time for 1 minute. The excess was allowed to drip off for 10 seconds before placing on sterile 4-layer-thick absorbent paper. Scaffold was flipped once after 3 seconds and then left to sit for 10 minutes. Scaffolds were then placed on a sterile tray and left to air-dry for 24 hours. Ten MSM-agar scaffolds were made per different agar concentration. Scaffolds were weighed before and after gel coating to determine the resulting biofilter porosity. A light microscope was used to observe the resulting scaffold structure.

3.1.1.2.1 SEM Imaging of non-biological samples

Agar composite scaffolds were prepared for SEM imaging: Samples were adhered to aluminium stubs using carbon paint. Care was taken to paint the sides of the scaffolds to ensure good conduction. Samples were then sputtered with 10nm gold (25mA, 2 minutes, argon atmosphere) and examined using SEM (EVO Ultra, Zeiss). SEM parameters were: acceleration voltage 10kV, spot size 300, and working distance 10 - 30 mm.

3.1.2 Antibiotic Loading

3.1.2.1 Soak-in Method

3.1.2.1.1 Stock solution

A stock solution of chloramphenicol (Sigma Aldrich) was created with a concentration of 100mg/ml. chloramphenicol powder was dissolved in pure ethanol (Sigma Aldrich), filter sterilised and stored in a cold room. New stock solutions of chloramphenicol were made every month.

3.1.2.1.2 UV Spectrophotometry - Standard Curve

Serial dilutions of chloramphenicol (100, 50, 20, 10, 5ug/ml) were prepared in chloroform to generate a standard curve. 1ml of each solution was pipetted into a quartz cuvette and the absorbance was measured using a spectrophotometer (BisPhotometer, Eppendorf) at wavelength 280nm.

3.1.2.1.3 Disc Manufacture

PCL pellets (80,000 mw, Sigma) were heated in a microwave for 60 seconds on a piece of Teflon. Then molten PCL was rolled into a tube and compressed to a thickness of 1 mm in a Teflon-lined vice. The PCL was allowed to rest for 1 minute before being removed from the vice and cooled at 4°C for 5 minutes. Discs were then punched from the PCL sheet using a 6 mm Hole Punch.

3.1.2.1.4 Chloramphenicol Soak-in

Soaking solutions containing 10mg/ml chloramphenicol were produced by transferring 200µl of chloramphenicol stock solution to sterile 1.8ml of pure water in Mini-McCartney bottles. Discs were weighed, UV sterilised, then soaked in separate bottles for 48 hours whilst being agitated on an orbital shaker operating at 120rpm at room temperature (20°C). After the soaking period, the discs were

removed from solution and dried on a sterilized Kim Wipe (Kim Wipe, Kimberly-Clark) in a Class 2 biological safety cabinet (BH-EN, Gelaire). To ensure that all the solvent had evaporated, the discs were placed in a desiccator overnight. chloramphenicol-discs were stored in separate sterile Eppendorf tubes.

3.1.2.1.5 Determination of Antibiotic Loading

Chloramphenicol-soaked discs were dissolved, by leaving in 2ml of chloroform in mini-McCartney bottles (very tightly-screwed chloramphenicol) overnight at lab temperature (20°C). Using a 1ml syringe (Terumino), a 200µl aliquot was then transferred to 10ml of chloroform. 1ml samples from each diluted solution was then transferred to a quartz cuvette and placed in a spectrophotometer (BisPhotometer, Eppendorf) and the absorbance at 280nm was recorded. A control set of PCL discs that were not soaked in chloramphenicol were used as controls. Triplicates were performed for each sample type.

3.1.2.2 Hydrogel Method

3.1.2.2.1 Characterisation of PVA-PCL scaffold morphology

3.1.2.2.1.1 Scaffold 'Plunger' device

A scaffold plunging device was designed and manufactured for submerging and coating scaffolds in hydrophilic gels. The initial idea for the plunger came from the tea strainer used in Method 3.1.1.2.The plunger had a number of design input requirements that needed to be accounted for (Table 13).

Table 13. Plunger design inputs and outputs

Design input	Design Outputs
Allow flow of gel through scaffolds	Porous containment cages positioned over inlet holes
Symmetric flow of gel through scaffolds	Symmetrical design and cage positioning
Allow easy access and manipulation of scaffolds	Fit-lock system and sheath
Allow submerging of plunger	Inlet holes
Tracking of individual scaffold samples	Individual mini-cages, colour-fast numbering

Two equal discs (diameter = 100 mm, thickness = 3mm) were cut from polycarbonate sheets. Small pieces of stainless steel gauze were cut then bent to form mini-cages with dimensions: 13 x 13 x 5 and 10 x 10 x 5 (l x w x h; mm). 10 mm from the disc circumference and at 60deg intervals, 6 inlet holes (diameter = 5 mm) were drilled into each disc. In one disc a larger hole (diameter = 7 mm) was drilled through the centre point. A polycarbonate shaft was attached to the centre of the disc without the centre-hole. A hollow polycarbonate sheath was attached to the centre of the disc with the centre-hole, such that the disc-sheath would stack directly on top of the disc-shaft. The mini-cages were attached to the discs over the inlet holes, with the larger cages on the top. All attachment was performed using superglue.

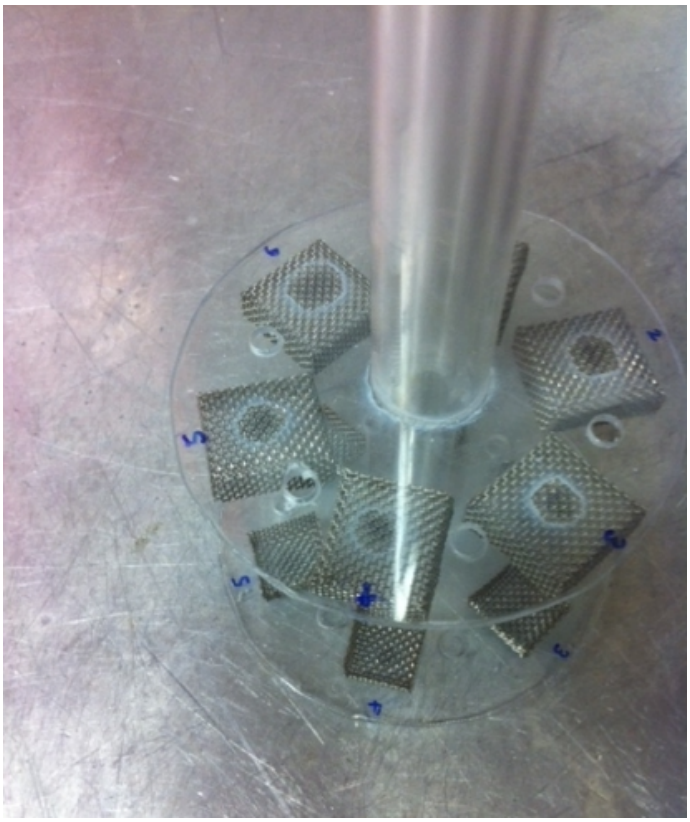

Figure 29. Scaffold plunger device. Stainless steel cages for holding scaffolds are mounted on polycarbonate.

3.1.2.2.1.2 Manufacturing PVA-PCL scaffolds

PVA (99+% hydrolysed, Sigma Aldrich) was added to 200ml of distilled water in a 500ml beaker to make solutions of various concentrations: 5, 8, 10, 12 and 15%w/v. These were heated on a hotplate to 80°C and stirred until the solution was homogenous. The solution was then left to cool (while stirring) to 40°C

(approximately 1 hour). Scaffold slices (7 x 6 x 2 mm) were weighed then loaded into the plunging device. The scaffolds were plunged using an up and down motion repeatedly for 2 minutes in the PVA solution. The scaffolds were then put on absorbent paper to remove the excess PVA solution, and then transferred to a sample holder to dry for one hour. The scaffolds were re-weighed. A calculation was made based on weight change to determine the theoretical swollen porosity of the scaffolds. After 24 hours of drying in air, scaffolds were prepared for SEM as described in Methods 3.1.1.2.1.

3.1.2.2.2 Spectrophotometry - Standard Curve and Validation

An Erythromycin (Sigma) stock solution of 200ug/ml was made in RO water. The stock solution was vortexed and left overnight to become fully homogenous. Differing volumes of the stock solution were added to 1 ml Eppendorf tubes and diluted to 700ul with RO water. 70ul of 4mM eosin Y (Sigma) was added and tubes were vortexed. 100ul of 0.4M Acetate buffer (made by combining 0.4M acetic acid and 0.4M sodium acetate and bring to pH=3) was added then tubes were topped up to 1ml with RO water and vortexed again. The final erythromycin concentration in tubes was: 20, 10, 5, 2 and 1ug/ml. The absorbance was tested at 543nm with plastic cuvettes and with use of an appropriate blank. Tubes were prepared and tested in triplicate.

To test the stability of the eosin Y-erythromycin complex formed, 3 solutions were prepared as described above: 1) Water only; 2) Buffered eosin Y with 700ul water (no erythromycin); 3) Buffered eosin Y with 20ug/ml erythromycin. Solutions were transferred to plastic cuvettes and the absorbencies were tested at 543nm, blanking with the Water only sample. The absorbencies were tested again after an hour.

3.1.2.2.3 Microbial Assay – Standard Curve and Validation

A stock of erythromycin in water was prepared (1000ug/ml). Solutions of varying concentration of the stock were prepared in PBS.

An overnight suspension of *Staphylococcus aureus* (strain: ATCC 29213, see Appendix A.1) was diluted to OD600 = 0.1 in PBS. 100ul of this suspension was inoculated onto TSA plates and spread ensuring the plates were uniformly covered. Filter paper discs were soaked in 500ul of diluted erythromycin-PBS solutions of known concentration. The excess liquid was removed before placing discs on the pre-inoculated TSA plates. Plates were incubated at 37C for 18 hours at which point the zone of inhibition

(ZoI) was measured using Vernier calibres. Triplicates of each concentration were tested. A filter paper disc soaked in PBS only and water containing soluble PVA was also tested.

3.1.2.2.4 PVA Hydrogels in Ethanol-Water mixtures

10% w/v PVA solutions were prepared in different water-ethanol mixtures: 85:15, 75:25, 50:50 and 35:65 (water:ethanol). Each solution was formed by addition of 12g of PVA into the appropriate volume of water. Continual stirring and heating to 80°C for 1 hour completely dissolved and homogenised the gel. The solution was then allowed to cool to 40°C. The appropriate volume of ethanol was added to bring the solution up to 120ml. The solution was stirred for 1 hour to completely dissolve and homogenise the gel once again.

Gels were either poured into petri dishes to form films or scaffolds were coated in the gel following the Method 3.1.2.2.1.2 described above. Gels and gel-scaffolds were immediately vacuum packaged. Packages were placed in a -20°C freezer for 16 hours, then left to thaw at room temperature for 8 hours. Samples were removed from their vacuum packages and allowed to dehydrate in a laminar flow hood for 24 hours. Samples were then stored at room temperature until ready for use.

PVA hydrogel film and PVA-PCL scaffold samples were weighed in the dehydrated state then transferred to McCartney bottles and submerged in 50ml of distilled water. Samples were soaked for 72 hours refreshing the water every 24 hours. Hydrated samples were superficially dried with absorbent paper towel for 10 minutes and weighed. Samples were then re-dehydrated in air and weighed once more. 10 film samples and 12 scaffold samples were tested per water-ethanol mixture.

3.1.2.2.5 DSC Analysis of PVA Hydrogels in Ethanol Mixtures

Hydrogel samples of 5-10mg were weighed into aluminium sample pans and crimp sealed. Differential Scanning Calorimetry (DSC) was performed (DSC 2920 Modulated DSC, TA Instruments) with the assistance of Trevor Shearing (University of Sydney). Dried samples of PVA and cross linked PVA weighing 5-10 mg, were put into aluminium sample pans, crimp sealed then placed in the DSC instrument. Samples were first heated from 35°C to 150°C (first heating cycle); then cooled to 35°C followed by heating up to 250°C (second heating cycle), all at a heating rate of 10°C min^{-1} under nitrogen. Results were taken from the second heating runs of the experiments in order to avoid experimental effects arising from the previous thermal history, structural relaxation and incomplete chemical reactions [38].

3.1.3 Bioglass Manufacturing

3.1.3.1 Precursor Preparation

The following materials were weighed into a 300ml glass beaker:

Table 14. Bioglass raw materials for precursor pellet formation

Material	Chemical Symbol	Weigh Percentage w/w%	Weight (g)
Hydrophobic fumed Silica (HDK H17, Wacker)	SiO_2	34.67%	14.40
Soda Ash (>99%, Redox)	Na_2CO_3	31.30%	13.00
Lime Stone (T-Grade, Omya)	$CaCO_3$	23.93%	9.94
Tricalcium Phosphate (Food Grade, Redox)	$Ca_3(PO4)_2$	10.10%	4.19
TOTAL		**100%**	**41.53**

30ml of acetone was added to the beaker and then mixed in gently for approximately 3 minutes until the powder reduced in volume forming a 'bread crumb' consistency. The mixture was then loaded into a hardened steel die (Inner Diameter = 42mm) and compressed at 1000psi for 6 minutes. The pellet that formed was reverse-pressed out of the die and stored in an air-tight container.

Precursor pellets were weighed and their height measured using vernier calibres. The pellets were transferred to either a Pt-Au crucible or an alumina tray. These were positioned side-by-side in a furnace (Tetlow Pty Ltd) and heated up at 300°C/hour to 800°C, 100°C/hour to 1000°C and 50°C/hour above 1000°C. When the target furnace temperature was reached it was held for 1 hour before turning off and cooling naturally. A number of heating cycles were tested as seen in Figure 30. The resulting calcined

pellets were removed the next day when fully cooled. They were weighed, height measured and examined.

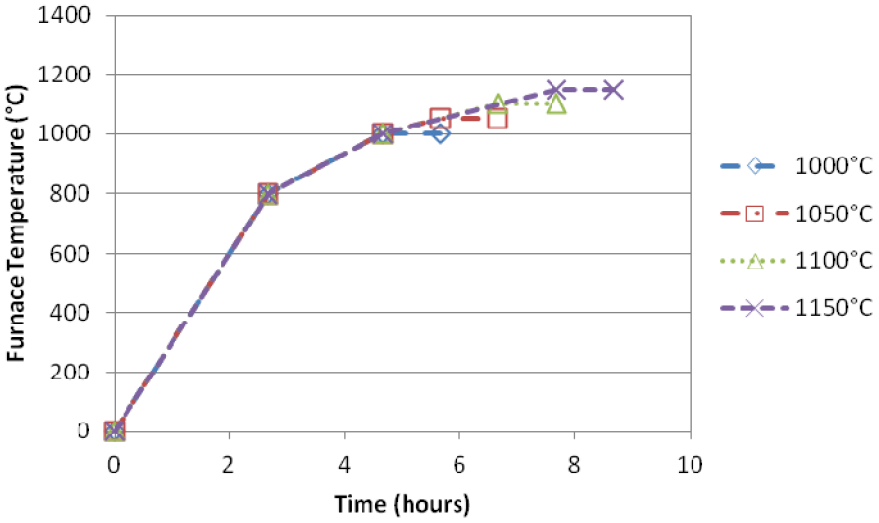

Figure 30. Heating cycles for optimising calcination. Temperature rates for natural cooling were not determined.

3.1.3.2 Melting

Melting was performed with the assistance of Rahmat Kartono (Univeristy of New South Wales). Calcined pellets were loaded into a crucible. Crucible types used were: Slip-cast Alumina (3.1.3.2.1) , Platinum-sputter-coated slip-cast Alumina (3.1.3.2.2), Platinum foil (custom folded, American Elements, 4" x 4", thickness: 0.001") and Platinum-Gold crucible (Pt 95/Au5, APS Labware). Crucibles were then loaded into a furnace with a hydraulic drop-down door and heated up at 300°C/hour to 900°C, 100°C/hour to 1350°C and held at this temperature for 2 hours. The hot crucible was removed from the oven and the molten glass was poured into a stainless steel bowl with distilled water or empty to form either frit or marbles respectively as depicted in Figure 31. The resulting frit glass was observed along with the crucible used. The composition of the Bioglass was analysed using Energy-dispersive X-ray spectroscopy (EDS) on frit granules obtained from each melt.

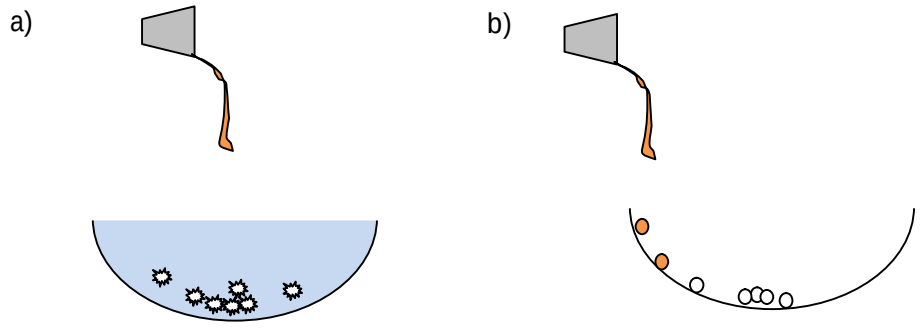

Figure 31. Molten bioglass is poured from platinum crucible: a) Pouring into distilled water to form frit; b) Pouring intermittently while rotating empty bowl to form marbles.

3.1.3.2.1 Slip Cast Crucibles

A mix of pottery plaster and water was formed as per the manufacturer's instructions. The plaster mix was poured into a plastic container which served as the outer mould. An aluminium tube lubricated with petroleum jelly was partially submerged in the plaster acting as the inner mould. The plaster was dried for 48 hours at 50°C after which the inner mould was removed leaving a plaster mould to form a crucible.

A 0.6 wt% Sodium Carboxylmethyl-cellulose (NaCMC) solution was formed and left to stir overnight. Alumina powder and magnesia were added in the proportion: 500 g NaCMC solution to 611 g alumina and 0.37 g magnesia; and mixed in a ball mill with 2 kg of 1 cm diameter alumina balls. This alumina slurry was poured into plaster moulds and allowed to dry for 40 minutes. Alumina slurry was topped up 3 times to ensure an even wall thickness. The mould was placed upside down for a couple of minutes to pour off excess slurry then the edges of the cast were finished with a sharp tool and paint brush.

Casts were further dried at 120°C until they were fully dried and separated from the plaster mould. Then casts were sintered at 1400°C for 2 hours to form the finished crucibles.

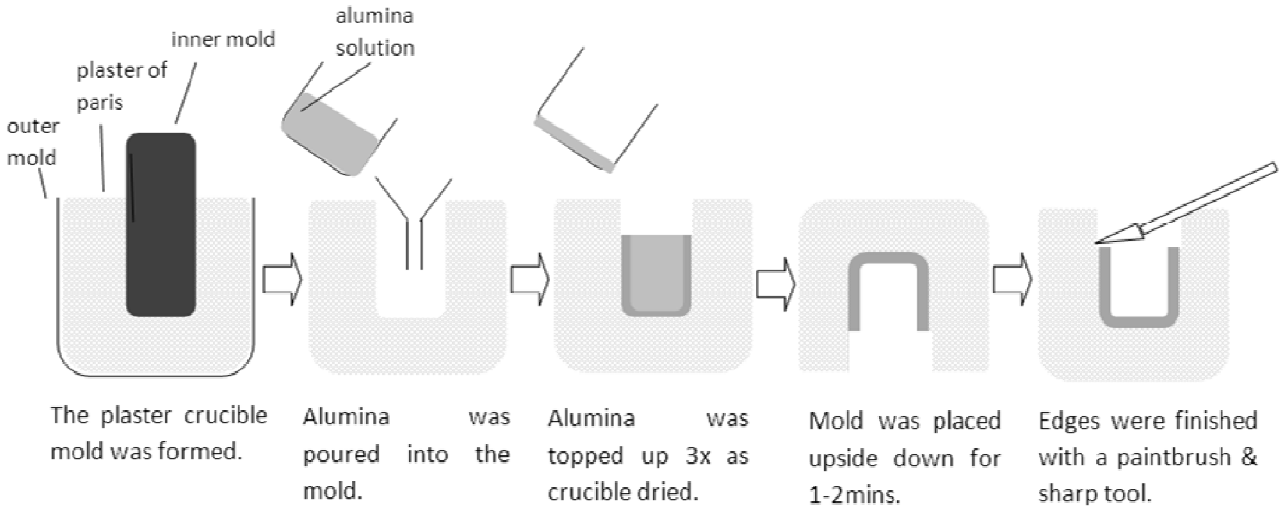

Figure 32. Slip-casting of alumina crucibles.

3.1.3.2.2 Platinum Sputter Coated Crucible

An alumina slip cast crucible was placed in the magnetron sputter coater. Platinum foil (American Elements, 4" x 4", thickness: 0.001") was used as the target. Sputtering took place in an argon atmosphere for 3 x 5 minute periods. A rotating stage was used to move the alumina crucible inside the plasma field during sputtering. The clearance between the target and the crucible was 5cm.

3.1.3.2.3 Bioglass EDS Sample Preparation

An epoxy cylinder was first cast (ClaroFast, Parameters: 80C 3min, 180C 3min, cooling 6min, "sensitive") then a 5mm diameter longitudinal hole was drilled through the centre. A diamond cutter was used (Wheel 330CA, Parameters: 2800 rpm, 0.050mm/s, High-force) to make 3mm thick slices then the edges were ground down (SiC[220] paper) so they no longer were flush with the piston. These were used as templates to hold bioglass granules and prevent them from being pushed to the sides during hot epoxy pressing.

Granules were mounted in the hole of the template and loaded into the piston. 7ml of Epoxy was added, followed by a paper label (pencil, face-up) then topped up with 7ml more. Hot epoxy pressing was carried out (Struers, CitoPress10).

Samples were ground down on the granule-side to remove excess epoxy so the granule could be polished (SiC [500] paper, Parameters; 300 rpm, 25 N, 30 seconds). Sample polishing was a 3 step process with each step using a different suspension; 9um diamond (DiaPro Largo), 3um diamond

(DiaDuo) and 0.4um silica. Before each step the samples were washed in water and dried with an air-blower.

Samples were mounted on aluminium stubs using carbon tape and carbon coated to 20nm.

3.1.3.2.4 SEM EDS of Bioglass Samples

EDS spectra were generated on the EVO SEM (Settings: EHT = 20kV; WD = 20mm, Zeiss). Note: WD (working distance) should be at least double of highest expected X-ray energy. Robostage was used to automatically gather spectra from several different positions on the surface of each grain. Magnification was set to 800x. Spectra were collected for 150,000 counts at 30% countables.

X-ray peaks for signature elements were converted to oxides to calculate the chemical composition. A minimum of two granules were analysed on from each batch with at least three spectra gathered from each granule.

3.1.3.3 Post-processing

Two different grinding methods were tried and compared:

1. Bioglass frit was ground using an agate mortar and pestle followed by sieving.
2. Bioglass frit was ground using a ball milling apparatus containing bioglass frit to bioglass marble volume fraction of 2:1. Milling duration was 150 hours.

Microscopic analysis (DM Microscope, Leica) was used to determine the particle size distribution of the bioglass powders.

3.1.3.4 Bioglass Coating

Scaffolds or disc samples were loaded into a Medipack package (3M). A small amount of bioglass powder was added into the package: 1g/10 scaffolds or 1g/20 discs. The package was heat sealed then vigorously shaken for 5 minutes to evenly disperse the bioglass powder. The package was secured in a rotisserie oven at 50℃ for 1 hour. The rotating motion allowed the bioglass to contact the PCL surfaces while the gentle heat made the PCL sticky so the bioglass became attached. The package was removed from the oven and the excess bioglass was removed. Coated samples were stored in the packages until ready to use.

Coated scaffolds were used to qualitatively test the adhesion strength and homogeneity of the coating process. Coated scaffolds were submerged in DMEM media for a 14 day period after which they were dried in air. Samples were prepared and examined by SEM (see Methods 3.1.1.2.1)

3.1.4 Bulk Metallic Glass Sputtering

The BMG alloy material ($Mg_{60}Zn_{35}Ca_5$) was synthesised by Jake Cao (School of Materials Science and Engineering, UNSW). The material was carefully ground into a circular disc so as to be fitted as the sputter target. Scaffold slices were placed in a magnetron sputter coater (custom setup, Prof. Nick Savvides, UNSW, Australia) and the machine was vacuumed pumped. Once the vacuum has been achieved, the chamber pumped with argon gas (2 Pa). The scaffolds were coated at 50W with 500nm of BMG on both sides.

3.2 Biofilm Formation

3.2.1 Biofilm Inhibition on Disc Composites

Bacteria (*E. coli*, *S. aureus* and *P. aeruginosa*) were grown up overnight in 5ml broth cultures (Appendix A.1). A PCL disc (Method 3.1.2.1.3) with biomaterial surface coating (Table 15) was put in the bottom of wide-mouth McCartney 15ml Bottles. 2ml of bacteria specific biofilm media (

Table 16) was brought to OD600 = 0.1 and transferred to bottles. Stoppers were left loose to ensure good aeration. Bottles were incubated shaken at 100rpm for 24 hours at 37°C. Discs were removed with sterile tweezers and transferred to a petri dish filled with sterile PBS for to wash of excess media. Discs were gently washed two times in sterile PBS, transferred to Eppendorf tubes containing 1ml of PBS and sonicated at maximal frequency for 5 minutes. 100 µl of the sonicated PBS was used for serial dilutions of which 50ul were drop plated on appropriate plate media (see

Table 16). Drop plates were incubated for 18 hours (to ensure small colonies) and counted to determine the viable number of cells in the biofilm recovered. SEM analysis was also performed to characterise biofilm formation. Triplicates were used for each sample/pathogen combination.

Table 15. Coated disc sample sets

Sample Coatings:	**Coating Method Section:**
Un-coated PCL control	-
PVA-hydrogel coated	3.1.2.2.1
PVA-hydrogel coated, gamma sterilized	3.1.2.2.1
45S5 bioglass coated, PVA-hydrogel coated, gamma sterilized	3.1.2.2.1; 3.1.3.4

Table 16. Biofilm culture media for different pathogens

	E. coli (strain: ATCC 11775)	***P. aeruginosa (strain: NCTC 7244)***	***S. aureus (strain: ATCC 29213)***
Overnight Growth Media	LB	LB	TSB
Biofilm Media	10% LB	10% LB	10% TSB
Plate Media	LB Agar	LB Agar	TSA

3.2.1.1 SEM Imaging of biological samples

Biological samples were prepared for SEM: Primary fixation was achieved by immersion in 2% glutaraldehyde (in 0.1M Na-PBS) overnight at 4°C. Glutaraldehyde was removed by washing in 0.1M PBS (3 x 5min). Post-fixation was achieved with 1% osmium (OsO_4) in 0.1M PBS for 1 hour. OsO_4 was then

removed by washing in Milli-Q water (3 x 5min). Samples were dehydrated in ethanol solutions at 50%, 70% and 95% (2 x 5min each), then at 100% (2 x 10min). Chemical drying was used by immersion for 3min in 100% hexamethyldilazane (HMDS). This was then quickly removed and samples were then placed in a dessicator and left overnight for HDMS fumes to evaporate. Specimens were mounted on aluminium stubs with carbon paint and sputter coated with 10nm gold (25mA, 2 minutes, argon atmosphere) and examined using SEM (EVO Ultra, Zeiss). SEM parameters were: acceleration voltage 10kV, spot size 300, and working distance 27-30 mm.

3.2.2 Adhesion of NBB4

3.2.2.1 Effect of Time on NBB4 Adhesion

3.2.2.1.1 Ethylene-Active NBB4 Growth Protocol

A sterile loop-full of plated healthy NBB4 (Appendix A.1) was deposited in a sterile 1.5ml ependorf tube and suspended in 1ml of MSM. The turbidity of this suspension was measured and based on this the suspension was diluted to give an OD600 of 0.1 in 30ml of MSM. 300ul of Tween 80 (0.02%) and 60ul of Trace Element Solution were added to the NBB4 suspension. The container was crimp sealed with a butyl gas top and aluminium sheath. Using a sterile syringe with filter 9ml ethylene gas (10% of head space) was injected into the culture vessel. NBB4 was incubated in a shaker for 48 hours at 30°C or until the desired growth phase was reached.

The ethylene gas was vented and the bottle's contents were poured into a 50ml Falcon tube. This was centrifuged at 4000rpm for 15min and the supernatant removed. The pellet was resuspended in 3ml PBS/Tween (0.02%) and washed twice by further centrifugation. The OD600 of suspension was measured (blanking with PBS/Tween).

3.2.2.1.2 NBB4 Freezer Stocks

2 x 500ml TSG (Triptic Soya Both (Oxoid) with 10% glucose (Sigma)) were made up Erlenmyer flasks, corked with cotton bung and wrapped with Aluminium foil and autoclaved.

All colonies from a streaked plate of NBB4 were harvested with a sterile loop and deposited into 5ml of sterile LB. A volume of this suspension was added to bring each Erlenmyer flask to OD of 0.1 and Flasks were incubated at 30°C with shaking for 48 hours.

The flasks were harvested at OD600 = 0.8. The contents of flasks were poured into 4 x 500ml centrifuge containers. Containers were centrifuged for 10min at 6000rpm (Sorvall Evolution VC, SLC 3000) and the supernatant was disposed of. The pellet was washed twice in PBS then combined in 1ml of PBS to form a very cell-dense suspension.

The OD600 of this suspension was measured and specific volumes aliquotted into mini-Eppendorf tubes to bring 300ml of liquid to an OD600 of 0.1 (for processing ease in future experiments). These tubes were stored in a -80°C freezer.

NOTE: This protocol is prone to contamination and only filter-tips should be used when pipetting.

3.2.2.1.3 Adhesion Time Course

Sterilised ¼ scaffolds were added into a 3ml active NBB4 suspension. Bottles were given a single hard shake to fully submerge the scaffold. Table shaking proceeded (100rpm) at room temperature, measuring OD600 (100ul into 900ul PBS/Tween) at time intervals: 1, 2, 5, 10, 20, and 30 minutes, 1 and 2 hours, 1 and 2 days. The change in OD600 in the media was used to quantify adhesion.

3.2.2.2 Effect of Growth Phase

Ethylene active NBB4 suspensions were harvested at different growth phases based on optical densities; OD600 = 0.1, 0.2, 0.3, 0.4, and 0.8. An adhesion assay was performed similar to described above in Methods 3.2.2.1.3, except OD600 measurements were performed only initially and at 24 hours. Triplicate samples were performed for each growth phase.

3.2.2.3 Alteration of Scaffold Surface

Scaffolds were coated using Method 3.1.3.4 but substituting bioglass for E-glass and Hydrophobic Fumed Silica (Wacker). Ethylene active NBB4 suspensions were harvested at OD600 = 0.4. E-glass, Silica and Uncoated scaffolds were used in an adhesion assay, performed similar to described above in Methods 3.2.2.1.3, with OD600 measurements performed after 0, 1, 2 and 24 hours. Triplicate samples were performed for each scaffold type.

3.2.2.4 Alteration of Cell Surface

Ethylene active NBB4 suspensions were harvested at OD600 = 0.4. Ethylene active NBB3 cells (Appendix A.1) were also prepared using the same method as for NBB4 (Method 3.2.2.1.1). A proportion of NBB4 cells were treated with solvents to modify their cell wall: NBB4 suspensions were pelletted in Eppendorf

tubes and resuspended in acetone or methanol for 5 minutes after which the cells were washed 3 times with MSM. An adhesion assay was performed on NBB3 and solvent-treated NBB4 similar to described above in Methods 3.2.2.1.3, except OD600 measurements were performed only initially and at 24 hours. Duplicate samples were performed for each cell type.

3.2.3 Gel Entrapment of NBB4

300ml cultures of NBB4 were grown in presence of 10% ethylene for 40 hours to late exponential phase (OD600 = 0.8). Cells were harvested by centrifugation and resuspended in 3ml MSM. To liquid MSM agar (42°C) was added: sterile Metal-ion solution (0.2% v/v) and concentrated suspension of NBB4 (maximum 2% v/v as not to alter gel viscosity; final OD600 = 0.5). Scaffolds were then treated using the above Method 3.1.1. Ten NBB4-MSMagar scaffolds were made per different agar concentration. Microscopic characterisation of the resulting biofilm was performed using SEM using the preparation protocol outlined in Method 3.2.1.1.

3.3 Antibacterial/Probacterial Activity

3.3.1 Activity of Antibiotic Eluting Scaffolds

3.3.1.1 Effect of Ethanol Content on Erythromycin Release

3.3.1.1.1 Erythromycin Infused Scaffolds

PVA hydrogels were prepared in water-ethanol mixtures as described in Methods 3.1.2.2.4, but with the following addition to the method: After homogenous water-ethanol PVA gel was formed an amount of erythromycin (Sigma) was added to form a super saturated solution. (This was typical around 20mg/ml). The solution was stirred at 40°C for 2 hours to allow the erythromycin time to dissolve. The solution was then transferred to a falcon tube and centrifuged at 4000rpm for 5 minutes to separate the undissolved erythromycin. The supernatant was retained for preparing scaffolds as described above.

3.3.1.1.2 Erythromycin Slow Release

The *in vitro* elution of the drug was examined by placing dehydrated, erythromycin infused PVA-PCL scaffolds in a well containing 500µl of PBS. At certain time intervals a filter paper disc was placed in the well to soak and scaffolds were removed and placed in a new well containing 500µl of fresh PBS. The

filter paper disc was then used to perform a Microbial assay (Method 3.1.2.2.3) to determine the concentration of erythromycin in the well. Triplicates of each sample type were tested.

3.3.1.2 Effect of Gamma Sterilization on Erythromycin Release

Erythromycin-PVA scaffolds were prepared as detailed above (Methods 3.1.2.2.1.2 and 3.3.1.1.1) using a PVA concentration of 10% w/v and an ethanol concentration of 50%v/v. After crosslinking and dehydrating the Erythromycin-PVA scaffolds they were packaged and gamma sterilised at 25kGy using a Cobalt-60 source (Steritech). The slow release of erythromycin was tested as previously described using the bioassay for measuring erythromycin concentration (Method 3.1.2.2.3). Gamma sterilised scaffolds were compared to a control-set of unsterilized scaffolds that were from the same production batch. Tests were performed in triplicate.

3.3.1.3 Cytotoxicity of Erythromycin

Human dermal fibroblasts CRL-2097 (HFb) were grown to confluence, harvested and counted as described in detail in Method 3.4.1.1.1. 90μl of cells in DMEM 10% FCS containing ~25,000 cells were added into a 96 well plate. Cells were then cultured for 24 hours under normal culture conditions. The media was replaced with media that contained varying concentrations of erythromycin (0, 25, 50, 100, 250, 500, 750, 1000μg/ml) and cells were cultured for a further 24 hours. 20μl of MTS reagent (CellTiter 96 AQueous One Solution Cell Proliferation Assay, Promega) was added to each well and cultured for 1 hour after which a colour change could be seen. The absorbance of the solutions was measured at 490nm. A sample set of media containing erythromycin but no cells was used to account for the drug interfering with the MTS reagent and any change in background absorbance. Triplicates were performed for all tests.

3.3.1.4 Erythromycin Soak-off

Erythromycin-PVA scaffolds were fabricated using 50% ethanol and gamma sterilised in preparation for erythromycin release measurements as detailed above (Method 3.3.1.2) but with the following difference: Before placing scaffolds in well plates, scaffolds were soaked in bottles containing 1 ml of PBS for 15, 30 or 60 minutes to soak off superficial erythromycin and reduce the initial burst release. Afterwards erythromycin slow release testing proceeded as normal. Triplicates samples were performed for each soak-off time.

3.3.2 Antibacterial Biomaterials

3.3.2.1 Zone of Inhibition

E. coli, *S. aureus 'Oxford'* and *P. aeruginosa* (Appendix A.1) were grown up overnight (37°C, 200rpm). 100 µl aliquots of bacterial broths were spread onto LB or TSA agar plates. The following biomaterials were sterilised under UV for 1 hour:

1. PCL disks
2. Chloramphenicol powder
3. Hydroxyapatite powder
4. 45S5 bioglass powder
5. MgZnCa bulk metallic glass strips

Uniform pellets of biomaterials were then positioned the centre of spread-plates. The surface area of contact between biomaterial and plate was kept constant and confined to a 5mm diameter circle. Plates were incubated for 24 hours at 37°C after which the zone of inhibition was measured. The antibacterial effect biomaterial was tested on each bacterium in triplicate.

3.3.2.2 MIC/MLC Protocol

One colony of each bacterium (*E. coli*, *S. aureus 'Oxford'* and *P. aeruginosa*) from storage plates was used to inoculate a 5ml broth cultures (Appendix A.1) and grown up overnight at 37°C and 200rpm. The OD600 of this culture was measured and diluted to OD = 0.1 with sterile LB (approximately 10^8 cells/ml). In mini-McCartney bottles samples of biomaterial (Hydroxyapatite, 45S5 Bioglass and MgZnCa BMG) or antibiotic (Chloramphenicol) were made up in 500ul LB and 500ul of diluted culture in concentrations of 2.5, 5, 7.5, 10, 12.5 µg/ml for antibiotics; 20, 40, 60, 80, 100 mg/ml for HA and 45S5; and 5, 10, 15, 20, 25 mg/ml for BMG. Negative controls with cells only were included for each bacterium. Chloramphenicol has been tested previously on these bacteria and represents the positive control. After culturing at 37C and 200rpm for 22 hours, 50ul of 0.2% nitrotetrazolium chloride was added to each aliquot. Incubation continued for no more than 2 hours after which aliquots were observed for a blue colour change indicating cell metabolism. The lowest concentration which resulted in no colour change was defined as the MIC. All conditions were tested in triplicate.

3.3.3 Bacterial Ethylene Degradation

3.3.3.1 Optimisation of Agar Concentration

NBB4 was immobilized in agar composite scaffolds as described in Methods 3.2.3. Agar concentration of 0.1, 0.2, 0.4 and 0.6 %w/v were used to make separate batches of 10 NBB4-scaffolds. Control sets were fabricated: 0.2%w/v agar scaffolds containing no NBB4 cells and; 0.4%w/v agar cubes containing NBB4 cells by casting inoculated agar gel into petri dishes.

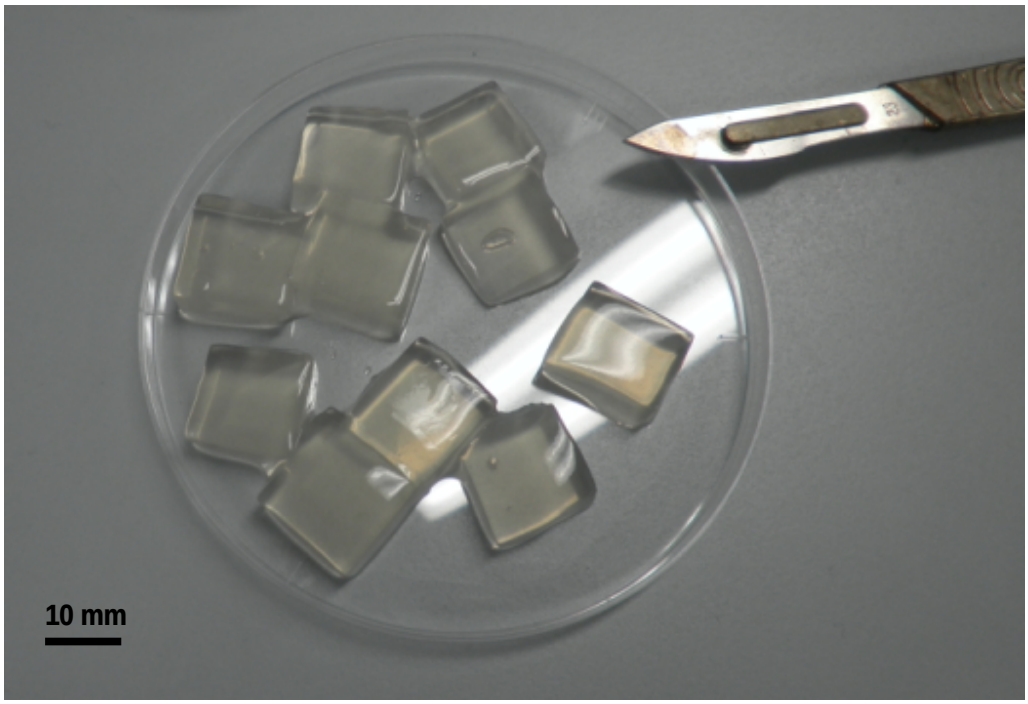

Figure 33. Agar cubes cut with scalpel to scaffold dimensions

Scaffolds were cut carefully with sterile scissors along their long axis and entire batches (20 half-scaffolds) were placed 120ml serum bottles and crimp sealed with butyl septa. Gel cubes were cuts to the same dimensions as scaffolds and also added to serum bottles (Figure 33). 500ppmV of ethylene was added to bottles and Gas Chromatography (GC) readings were taken after: 0, 4, 8, 12 , 16, 20 and 24 hours. Triplicate batches of each sample set were tested.

3.3.3.2 Effect of Altered Cell Surface

NBB3 and solvent-treated NBB4 scaffolds tested for adhesion efficiency in Method 3.2.2.3, were tested for their ethylene degrading abilities as described above (Method 3.3.3.1), but with the following

exceptions: Scaffolds were already in quarters and thus added directly to serum bottles and; GC readings were taken at: 0, 24 and 120 hours.

3.4 Device Pilot Studies

3.4.1 *In vitro* wound modelling of Synthetic Skin Graft

3.4.1.1 Validation of PCR and qPCR standards

3.4.1.1.1 Fibroblast and bacterial culture

Human dermal fibroblasts CRL-2097 (HFb) was cultured at 37°C and 5% CO_2 in a cell media of DMEM with 10%v/v Fetal Calf Serum (FCS, Sigma). Media was changed every 3-4 days and fibroblasts were sub-cultured weekly. Cells of passage 2-6 were used for experiments. *Staphylococcus aureus* ATCC29213 (Appendix A.1) was grown up overnight at 37°C and 200rpm in Tryptic soya both (TSB). *S. aureus* was maintained on TSB agar (TSA) plates at 4°C.

3.4.1.1.2 RNA extraction from cells

Confluent HFb were washed, trypsinised to detach from cell culture flasks, washed with PBS and resuspended in fresh cell media. HFb were counted using a hemocytometer and light microscope. HFb were then pelletted in Eppendorf tubes. 1ml of Tri-reagent (Sigma) was added followed by 200 µl of 1-bromo-3-chloropropane (Sigma) to induce phase separation. Tubes were then centrifuges for 10s.

S. aureus cells were washed in PBS and collected by centrifugation (10,000rpm, 1 min), resuspended in 1ml Tri-reagent (Sigma) and then transferred to bead beater tubes: 2ml Screw chloramphenicol tubes (Astral Scientific), Standard crew caps (black, Astral Scientific) with 110mg of 150-212um diameter glass beads (G1145, Sigma), 110mg of Glass beads (G8772-100g, Sigma) and 1 Solid-glass bead 5mm (Z265942-1EA, Sigma). 200ul of 1-bromo-3-chloropropane was added. Bead beating proceeded at 6 m/s for 40 seconds and was repeated once to break up the bacterial cell wall.

All tubes were rested on ice for 10 minutes then centrifuged at 13000rpm for 15 minutes at 4°C. 500µl of the clear supernatant containing the RNA was carefully removed and added to separate tubes containing 500µl of isopropanol (2-propanol, Sigma). Tubes were stored overnight at -20°C. RNA was pelletted by centrifugation (13000rpm for 10minutes) and washed twice with 70% ethanol then air dried

before resuspending in 23ul water. RNA amount was quantified spectrophotometrically (NanoDrop), and the purity was determined from the A_{260}/A_{280} ratio (1.80 - 2.00).

3.4.1.1.3 RNA to cDNA

1000ng of RNA in 8µl was treated with DNase I (Invitrogen) to remove any contaminants before being reverse transcribed to complementary DNA (cDNA) using Random Hexamer Primer (Invitrogen, CA, USA) and SuperScript™ III Reverse Transcriptase (Invitrogen) [188]. Briefly, 1µl of DNase and 1µl 10x Reaction buffer was added to each tube and incubated at room temperature for 15 minutes. A master mix of 0.5ul Oligo DT, 0.5ul RH and 1.5ul water was added to each tube then brought to 70°C for 10 minutes in a thermocycler (BioRad). A second master mix of 4µl 5x Buffer, 2µl DTT, 1µl dNTPs and 0.5µl Superscript was added to each tube. Tubes were subjected to 25°C for 10 minutes, 42°C for 60 minutes and 70°C for 10 minutes for reverse transcription to take place. cDNA samples were stored at -20°C until ready for PCR.

3.4.1.1.4 Primer Design

16s rRNA sequence was obtained from the GenBank database for *Staphylococcus aureus*. Primers were generated using Primer Blast. Primer specificity was tested by qPCR and gel electrophoresis was used to quantify the product size.

Target	Primer	Sequence	Product size (bp)	Reference
Fibroblast 18s RNA	18Sf	5'-CGGCTACCACATCCAAGGAA-3'	187	[189]
	18Sr	5'-GCTGGAATTACCGCGGCT-3'		
Staphylococcus aureus 16s RNA	ASB1	5'-GCCACACTGGAACTGAGACA-3'	247	This study
	ASB2	5'-GGATAACGCTTGCCACCTAC-3'		

3.4.1.1.5 Conventional PCR amplification

To create internal qPCR standards, cDNA was amplified using conventional PCR with the following reaction mastermix: 1µl dNTPs, 2µl forward primer, 2µl reverse primer, 5µl Buffer, 5µl MgCl2, 27.5µl

water and 2.5µl 1U/µl Taq DNA Polymerase (AmpliTaq Gold, Applied Biosystems). 5µl of cDNA template was added to bring the reaction to 50µl. The cDNA template was replaced with 5µl of water for the no-template (NT) controls. Reactions took place using a thermocycler (DNA Engine, BioRad) with the following program: 92°C for 10 minutes, then 35 cycles of 92°C for 20s → 57°C for 20s → 75°C for 50s. Afterwards the amplified cDNA was stored at -20°C until ready for use.

3.4.1.1.6 Gel Electrophoresis

Gel electrophoresis was performed on cDNA PCR products and NT controls for 18s and 16s samples. Samples mixed with DNA loading dye (Gel Pilot, Qiagen) and were run for 1h at 90V and 37°C on 2% agarose gels containing 1x Gel Red (Biotium). HyperladderV (Bioline) was also run as the reference. Gels were observed under UV light to identify band locations. Products were tested in triplicate.

3.4.1.1.7 Purifying and aliquoting Standards

cDNA product was purified using the UltraClean GelSpin kit (MO BIO) and stored in 10mM Tris at -20°C. Quantification of cDNA concentration (in ng/µl) was performed using a spectrophotometer (Nanodrop) and blanking with 10mM Tris Buffer. Ten-fold serial dilutions were made in water to form standard solutions of DNA with known concentration.

3.4.1.1.8 Quantitative PCR

cDNA was amplified using quantitative PCR (qPCR). qPCR was carried out in microtubes with following mastermix added to each: 0.5ul of forward primer, 0.5ul of reverse primer, 7.5ul of SensiMix (Contains: Heat-activated DNA polymerase, Ultra-pure dNTPs, MgCl2 (6mM), SYBR® Green I, Bioline), 1.5ul pure water and 5ul of 1/5-diluted sample cDNA (final cDNA concentration 1ul/15ul reaction). Thermocycling was performed using a Rotor-Gene™ 3000 (Corbett). The PCR conditions were: 50°C for 2min and 95°C for 5min, followed by 40 cycles of 95°C for 10s, 60°C for 20s, and 72°C for 20s [187-188]. Duplicate qPCR reactions were run samples for each sample.

qPCR was carried out on standard solutions as described above along with a melt analysis obtained by slow heating from 70 – 95°C at 0.2°C/s.

3.4.1.2 Addition of Fibroblasts to the Scaffold

HFb were cultured as described in 3.4.1.1.1, harvested and counted. Four methods of adding the HFbs to scaffolds (Method 3.1.1.1) of dimensions 6x5x2mm were tested:

1. *Normal method.* Scaffolds were soaked in sterile media (DMEM + 10% FCS) for 10min and transferred to a 24 well-plate. 400µl of media was added to the well. ~60,000 HFbs in 100µl of media were carefully pipetted onto the scaffold.
2. *New method 1.* Scaffolds were soaked in sterile media (DMEM + 10% FCS) for 10min, dried on sterile filter paper and transferred to a 24 well-plate. ~60,000 HFbs in 100µl of media were carefully pipetted onto the scaffold. The scaffold was incubated under normal culture conditions for 12 hours to allow cell attachment. 400µl of media was added to the well.
3. *New method 2.* Dry scaffolds were transferred to a 24 well-plate. ~60,000 HFbs in 100µl of media were carefully pipetted onto the scaffold, forming a droplet on top. The scaffold was incubated under normal culture conditions for 12 hours to allow cell attachment. 400µl of media was added to the well.
4. *New method 3.* Dry scaffolds were transferred to a 24 well-plate. ~60,000 HFbs in 50µl of media were carefully pipetted onto the scaffold, forming a droplet on top. The scaffold was incubated under normal culture conditions for 12 hours to allow cell attachment. 400µl of media was added to the well.

Scaffolds were removed and put in a new well containing fresh media. Triplicates were used for each HFb addition method. Incubation was under normal HFb cell culture conditions (3.4.1.1.1) and scaffolds were harvested at 14 days. The old wells were then observed using a light microscope to visualise the amount of cells that did not adhere to the scaffolds.

Scaffolds were gently washed with PBS and transferred to Eppendorf tubes. 200 µl of 1-bromo-3-chloropropane was added first followed by 1ml of Tri-reagent (Sigma). The 1-bromo-3-chloropropane dissolved the scaffold fully allowing all the RNA to be reliably recovered (See Appendix A.3). Tubes were then centrifuges for 10s. RNA extraction then proceeded as described in 3.4.1.1.2.

3.4.1.3 Bacterial Growth in DMEM and Toxic Media

S. aureus cultures were grown up overnight in TSB. The cells were pelletted, washed and resuspended in DMEM with 10% FCS to a turbidity of OD_{600} = 0.1. These cultures were incubated for 24 hours at 37°C

with 200rpm shaking. The colour of the cultures was observed and the turbidity was measured. The cultures were streaked onto TSA plates, which were incubated overnight at 37°C. The colonies that formed were characterised.

The cultures were filter sterilised and the resulting *S. aureus*-filtered media was collected. The *S. aureus*-filtered media was mixed with fresh DMEM + 10% FCS in a ratio of 1:1 and 500ul was added to confluent fibroblasts in 24 well plates. These were then cultured for 24 hours as described above (3.4.1.1.1). The phenotype of the fibroblasts was examined using a light microscope.

3.4.1.4 Cell and Bacterial Growth on bi-Phasic Scaffold

HFb and *S. aureus* were grown up as described in 3.4.1.1.1. 100,000 HFb were added to PVA-PCL-γ scaffolds by the Normal Method (3.4.1.2). 100,000 *S. aureus* were added to separate PVA-PCL-γ scaffolds by the Normal Method except the cells were delivered in a 10µl droplet of PBS pipetted to the bottom edge of the well. Cells were cultured up at 37℃ with 5% CO_2 on a shaking table at 55rpm (Model HJ III, Pacific Rim Bio Tech Inc.) for up to 5 days, refreshing media daily. Different cell-scaffold samples were in duplicate.

Scaffolds were removed and washed in sterile PBS to flush out non-adherent cells. To remove HFb, scaffolds were submerged in 500ul of trypsin and incubated for 5 minutes at 37℃. This was followed by addition of 500ul FCS, vortexing, removal of the scaffold to a separate tube and centrifugation at 2000rpm for 5 minutes. The pellet was resuspended in TriReagent. The scaffold with then sonicated for 5 minutes in PBS to remove any biofilms. This is followed by vortexing, disposal of the scaffold and centrifugation at 2000rpm for 5 minutes. The two tubes are combined in 500ul of TriReagent and stored at -80C until ready to extract RNA. NOTE: The bi-Phasic scaffold could not be fully dissolved in 1-bromo-3-chloropropane as described in 3.4.1.2, as the PVA hydrophilic phase was extracted along with aqueous nucleic acid phase hence contaminating the RNA (See Appendix A.3.2).

Tubes were thawed and RNA was extracted as if all tubes contained S. aureus cells (3.4.1.1.2). This was to prepare for the co-culture and process both cell types the same way. 8µl of RNA was not standardised to 1000ng but otherwise converted to cDNA as above in 3.4.1.1.3.

Samples were quantified by qPCR as described in 3.4.1.1.8. 18s and 16s primer sets were tested on HFb and S. aureus samples respectively. Internal controls containing a standard curve of the purified 18s and

16s gene of interest of known gene copy concentration (dilutions: 10^{-1}, 10^{-4}, 10^{-7}) were run in each qPCR. This was used to calculate the gene concentration of each sample. All reactions were run in duplicates.

3.4.1.5 Final Co-culture

Scaffold samples were soaked in PBS for 15 minutes to bring down erythromycin concentration to less than 500ug/ml. Scaffolds were placed on sterile filter paper to remove excess PBS, and then placed in tissue culture wells (24 well-plate, Dolphin).

Table 17. Sample names and description of scaffolds used in final co-culture experiment.

Sample Name	Scaffold Description
PCL	Normal PCL scaffold, UV sterilised
PCL-PVA	PVA coated PCL scaffold, UV sterilised
PCL-PVA-Gamma	PVA coated PCL scaffold, Gamma sterilised
PCL-PVA-BG-Gamma	PVA coated, 45S5 bioglass coated PCL scaffold, Gamma sterilised
PCL-PVA-Ery-Gamma	Erythromycin loaded PVA coated PCL scaffold, Gamma sterilised
PCL-PVA-Ery-BG-Gamma	Erythromycin loaded PVA coated, 45S5 bioglass coated PCL scaffold, Gamma sterilised

S. aureus and HFbs grown and prepared as previously mentioned in Methods 3.4.1.1.1. 100,000 *S. aureus* was pipetted into each well in a volume of 10ul PBS. 100,000 HFb were added to each well in 500ul of culture media. A set of scaffolds were not inoculated with *S. aureus* and served as the HFb-only control set.

Scaffolds were cultured, the cells harvested after 1 and 5 days; the RNA extracted and converted to cDNA all exactly as described in 3.4.1.4. All cell-scaffold combinations were grown in quadruplicate. 1 sample would be harvested and prepared for SEM imaging. The remaining triplicate was used for qPCR.

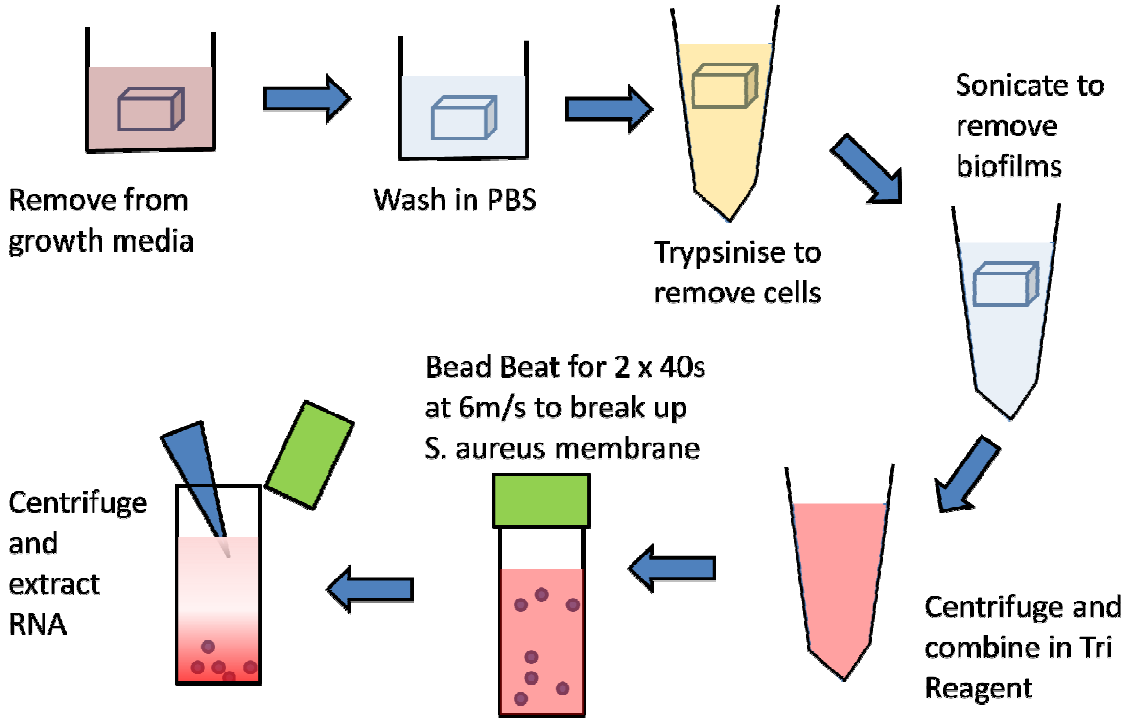

Figure 34. RNA extraction process for co-cultured scaffolds.

The sample reserved for SEM was treated differently. The adhered wells were not removed. Instead the Scaffolds were washed in PBS and then stored in 2.5% Glutaraldehyde in PBS. SEM sample preparation and SEM imaging was carried out as outlined elsewhere (Method 3.2.1.1).

qPCR was carried out in the same way as above with 18s and 16s primer sets were tested on each sample, including the HFb-only control set. Internal controls containing a standard curve of the purified gene of interest of known gene copy concentration (dilutions: 10^{-1}, 10^{-4}, 10^{-7}) were run in each PCR. This was used to calculate the gene concentration of each sample. All reactions were run in duplicates.

3.4.2 Mechanical Properties of Synthetic Skin Graft

Scaffolds were manufactured as discussed in Method 3.1.2.2.1. Scaffolds were soaked in distilled water for at least one hour so gel phases would become fully hydrated. Excess water was removed using absorbent paper. Samples were weighed and there dimensions measured with a ruler (accurate to 0.5 mm). Scaffolds were tested by DMA (DMA Dynamic Mechanical Analyzer, TA Instruments) in compression: The compression plate was lowered onto the sample until a force registered in order to locate the height of the sample. Compression proceeded at 5N/minute until a maximal force of 15N. The

resultant stress-strain curve produced by the computer program was analysed to quantify the mechanical properties for the scaffold.

Samples tested were: PCL, PCL-PVA, PCL-PVA-Gamma, PCL-PVA-BG, PCL-PVA-BG-Gamma, PCL-PVA-Ery-BG-Gamma and PCL-PVA-Dry. PCL-PVA-Dry is a non-hydrated PCL-PVA sample used to showcase the difference in the mechanical properties of hydrogel scaffold in the dry and hydrated states.

3.4.3 Long-term degradation of Ethylene

Batches of NBB4-scaffolds were prepared using the gel entrapment method described in Method 3.2.3. Batches were then prepared for ethylene degradation measurements according to Method 3.3.3 with the following changes: 200-300ppmv of ethylene was injected into the bottles. Bottles were monitored daily with a Gas Chromatographer using an injection volume of 250ul, until the ethylene was depleted. The ethylene was replenished each week and monitoring continued for 3 months. Triplicate NBB4-scaffold batches were used. An empty bottle that was initially injected with 200ppmv served as the control.

3.4.4 Storage Life of Biofilter

3.4.4.1 Starvation Conditions and Activity

Six batches of 5 NBB4-scaffolds were prepared (with 0.4%w/v agar, Method 3.2.3)and stored in a Parafilm-sealed Schott Bottle for different starvation periods of 0, 2, 5, 12, 20, and 30 days. Three more batches of scaffolds were made to investigate the effect of starvation combined with desiccation. These were stored in sterile petri dishes.

On completion of the starvation period, four NBB4-scaffolds from each batch were transferred into a 120ml serum bottle with aluminium crimp-sealed PTFE-faced butyl rubber stoppers. 100ppm of ethylene gas (99% commercial purity), obtained from BOC Gases Australia, was filtered first and injected into the headspace of the sterile sealed serum bottle. GC sampling was conducted 3 hours after the injection to allow gas to equilibrate and then on a daily basis.

3.4.4.2 Viable Cell Recovery

From each batch in Method 3.4.4.1, the one left-over, pre-weighed scaffold was immersed in 5ml of MSM (0.02% Tween 80), followed by sonication and vortex mixing which were performed for 5 minutes and 1 minute respectively. A ten-fold dilution series with MSM buffer was performed, and 100ul plated

on TSG plates. All cultures were grown aerobically at 30°C for two weeks, and viable cell counts within the range of 30-300 were recorded.

3.4.5 Fruit Preservation

Banana fruits were brought at more green than yellow stage (Indicated from the banana colour chart from Soltani, *et al*., 2011), they were detached from three bunches, mixed and distributed evenly into four sealed desiccators with no desiccants presence. Each desiccator contained ten NBB4-scaffolds randomly dispersed throughout. Fruits were stored at 25°C, and the deterioration condition was monitored by observing the skin colour change weekly.

3.5 Statistical Analyses

Microsoft Excel was used to perform T-tests to demonstrate statistical difference within the results. Log-transforms to Ct were used to account for logarithmic variability where appropriate. A p-value < 0.05 was considered significant.

4 Results & Discussion

4.1 Composite and Material Fabrication

4.1.1 Agar Composite Scaffolds

The porosity of agar-scaffolds was determined by weighing before and after coating. The porosity of the base PCL scaffold has been vigorously tested previously [181] and is 95% with little variation. This was validated by weighing scaffolds and calculating volumes (data not included). The volume of the pores, V_0 (ml) for each scaffold before coating was calculated:

$$V_0 = \frac{p_0 \times m_0}{\rho_{scaf} \times (1 - p_0)} \quad (4)$$

Where p_0 is the constant porosity of 95%, m_0 is the dry weight of the scaffold and ρ_{scaf} is the density of the scaffold biopolymer, PCL (g/ml). The volume of agar was calculated using the following equation:

$$V_{agar} = \frac{m_1 - m_0}{\rho_{agar}} \quad (5)$$

where m_1-m_0 is the mass change (g) after coating and drying. The density of agar, ρ_{agar} (g/ml), was assumed as being the density of the solvent [239], in this case water. Finally, the new porosity of the coated scaffold, p_1, was calculated, by subtracting the pore saturation from the initial porosity:

$$p_1 = p_0 \times (1 - \frac{V_{agar}}{V_0}) \quad (6)$$

Agar concentrations of 0.1, 0.2, 0.4 and 0.6% were used because they could be maintained as liquid and homogenous at temperatures that would not affect NBB4 cell viability. The emulsion coating technique could be used to make biofilters with consistent porosity. Further, varying the agar concentration of the emulsion produced varying porosities in a predictable way. The increased agar concentration lead to a more viscous emulsion which set faster and faced more resistance when being removed from the scaffold pores. This resulted in biofilters of lower porosity. The agar concentrations selected were able to produce a range of porosities: 88, 81, 70 and 67% respectively (Figure 35). Only a small difference in porosity was seen between 0.4% and 0.6% agar biofilters. This is likely due to the more viscous agar having poorer penetration of the scaffold as well as removal during the emulsion coating.

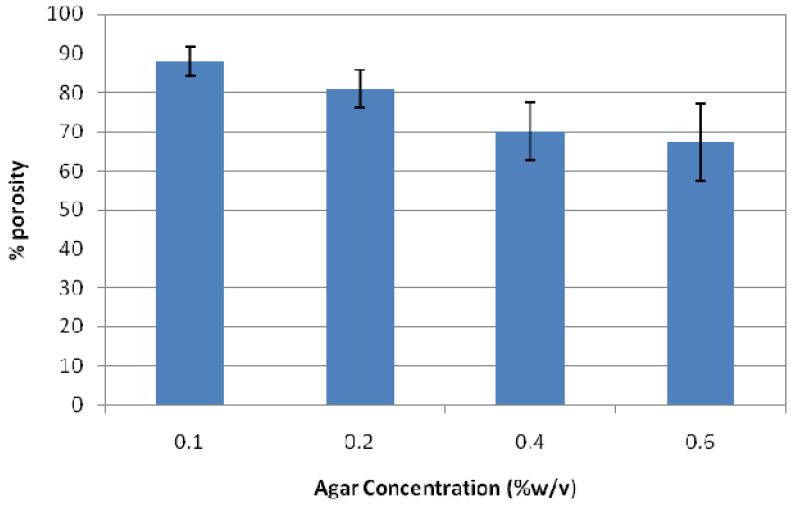

Figure 35. Porosity of scaffolds after treatment with differing agar concentrations. Increased agar concentration resulted in a decreased porosity (Error bars = SD).

It should be noted that even the least porous biofilter manufactured here, is substantially more porous than previous natural support materials such as natural zeolite (Porosity = 43.83%) [203] and peat soil [196]. Furthermore we have demonstrated that the porosity can be controlled unlike the aforementioned systems.

Light microscopy was used to characterise the agar coated scaffolds after 24 hours of drying in air at ambient temperature (Figure 36). The 3D geometry of the scaffold makes it difficult to focus clearly. Nevertheless, translucent areas distinct from the darker opaque areas of the scaffold were identified as agar hydrogel. These areas had the geometry one would expect for a hydrogel: Cohesive and adhesive forces creating meniscus-like shapes inside pores. The full coating of struts was also observed.

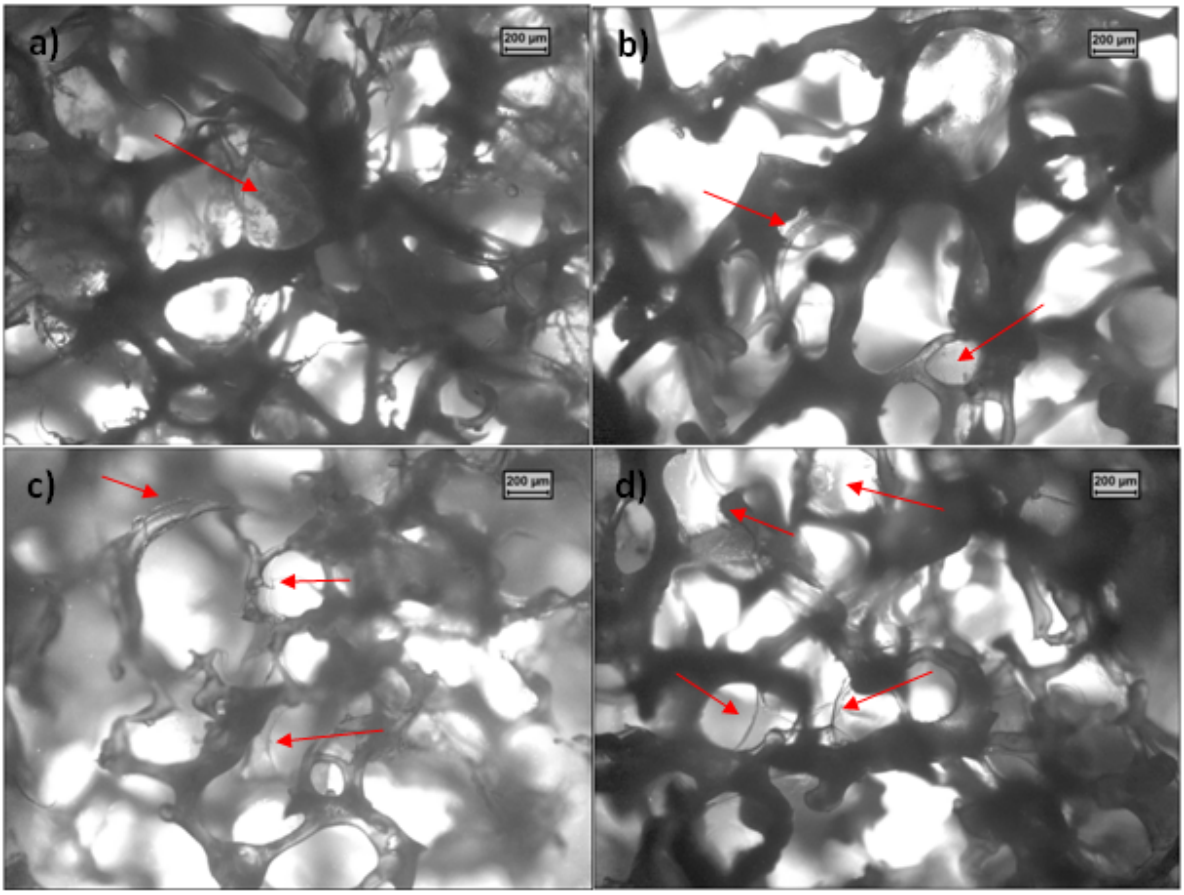

Figure 36. Light microscope images of gel-coated scaffolds. a) 0.1% agar; b) 0.2% agar; c) 0.4% agar; d) 0.6% agar. Arrows indicate areas coated with agar.

A concern with the gel entrapment method was that pores would become occluded by the hydrogel resulting in poor diffusion. This was not seen in the above images. In fact, while imaging was being conducted some areas of hydrogel were seen to collapse coating the inner surface of pores. This was likely due to the accelerated drying imposed by the heat generated from the light microscope. Still, this phenomenon may also occur during natural air drying which would lead to the thin surface coating required.

SEM imaging of MSM agar coated scaffolds provided a clearer view of the scaffold surface (Figure 37). These images confirmed the formation of a very thin agar coating covering some of the struts of the scaffold. The agar coating can be easily distinguished due to their web-like appearance. This dehydrated polymeric coating is approximately 1-4 µm in thickness, which is desirable for entrapping bacteria while allowing for gas exchange and not inhibiting the diffusional capacity of the scaffold. In practice the agar

gel would be maintained as hydrated and thus would swell [21]. However, the coating is thin enough for this swelling to have little effect on mass transfer resistance.

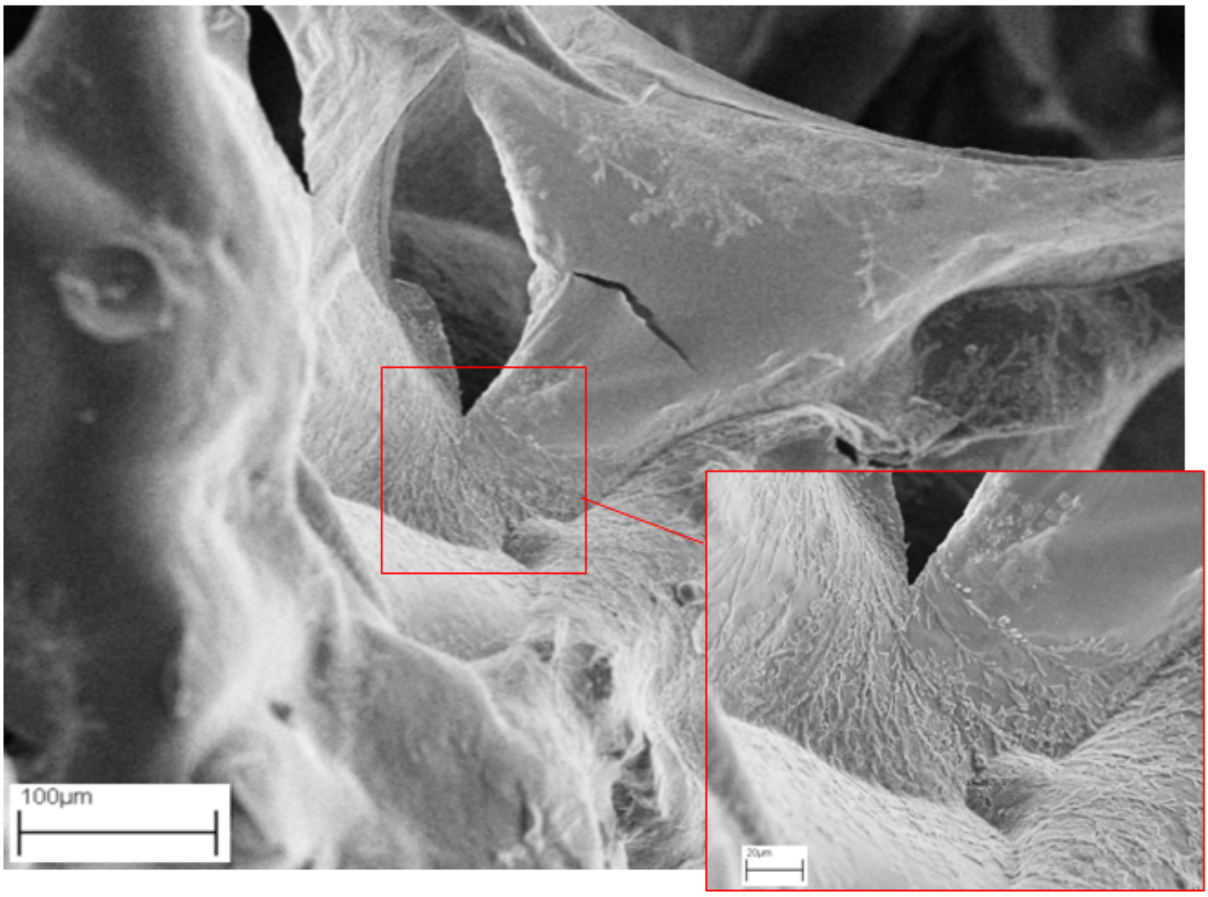

Figure 37. Agar Coating. SEM images of MSM-agar coated scaffold. Magnified view of rough textured area: Likely semi-crystalline dendritic formations of dried agar are observed; only a few micron thickness.

4.1.2 Antibiotic Loading

4.1.2.1 Soak-in Method

Chloroform was known to fully digest chloramphenicol as well as the PCL scaffold as demonstrated by Chow *et al* [240]. While the chloramphenicol stocks were best prepared in ethanol the standard curve (Figure 38) relating chloramphenicol concentration to absorbance was performed in chloroform to

conform to the test solvent. The linear relation had a good correlation and agreed with previous standard curves obtained using ethanol as the solvent.

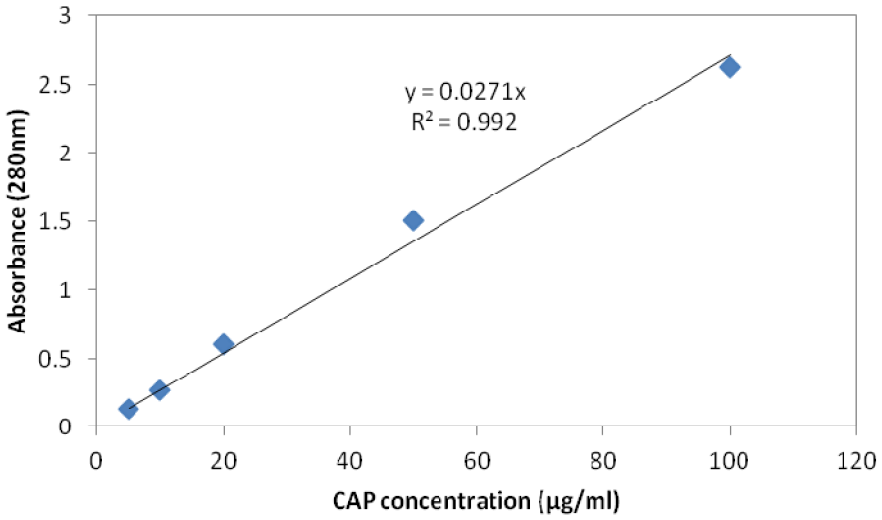

Figure 38. Chloramphenicol Standard Curve: Linear trend of chloramphenicol concentration in chloroform and absorbance at 280nm. Equation and correlation co-efficient are shown on chart.

The soak-in procedure produced discs that appeared to have formed crystals on their surfaces. This was the chloramphenicol precipitating out of solution and forming on the more hydrophobic PCL discs. The hydrophobic interactions that govern adhesion may be the mechanism for antibiotic loading in the soak-in method, that is: hydrophobic surfaces attract hydrophobic particles [123]. The crystals of chloramphenicol were very brittle and care was taken when handling the chloramphenicol-soaked discs. When these discs were stored in tubes, one could see numerous crystals and white particles fall to the bottom reflecting chloramphenicol detaching from the disc surface.

The discs fully dissolved in chloroform overnight along with all chloramphenicol attached to the disc. In this way the drug loading could be very accurately determined due to the lack of losses inherent in this method. The absorbance was measured at 280nm. The blanking solution was a mixture of chloroform and PCL made by dissolving a disc. This was used as the blank because dissolved PCL is known to absorb light in the UV range [240]. To account for this the weight of each disc selected for this experiment were controlled to be very close in weight.

The mass of chloramphenicol loaded onto each disc ($Mass_{CAP}$) and the percentage of chloramphenicol loaded by weight (CAP %w/w) were calculated using the following equations:

$$Mass_{CAP}(mg) = \frac{100 \times A}{K} \quad (7)$$

$$CAP\ \%w/w = \frac{Mass_{CAP}}{Mass_{CAP} + Mass_{DISC}} \quad (8)$$

Where *A* is the absorbance at 280nm and *K* is the linear constant obtained by the standard curve (0.0271). $Mass_{DISC}$ was the weight measured of each disc before chloramphenicol soak-in.

Table 18. Chloramphenicol Loading of PCL Discs. Results are given as mean ± std; n = 3.

Sample	Mass of chloramphenicol (μg)	Mass chloramphenicol/Mass PCL Disc (%w/w)
Control Disc	1.23 ± 2.13	0.002 ± 0.004
Chloramphenicol Disc	323.49 ± 39.11	0.580 ± 0.063

The results of the chloramphenicol soak-in method can be seen in Table 18 above. The control discs were not soaked in chloramphenicol and were included to check for errors occurring from absorbance of varying amounts of PCL. The low antibiotic loading found for the controls verifies that the method was closely controlled and that the absorbance readings related to chloramphenicol and not PCL. The chloramphenicol-soaked disks carried 323.49 ± 39.11 μg of chloramphenicol antibiotic which correlated to 0.580 ± 0.063 %w/w. Given the scaffold has a much higher surface than the disc we would expect these values to increase dramatically if scaffolds were used for the same experiment. Our group has previously shown a 10.16 %w/w loading into scaffolds using the same soak-in method [240]. This is comparable with other drug delivery devices [241] and may allow sustained release.

The advantage of performing this experiment using discs instead of scaffolds is that the results are easier to analyse when the complex architecture and porosity of the scaffold are eliminated. The disc showed the formation of the superficial chloramphenicol crystals which were previously hidden inside the scaffold pores. The brittleness and superficial nature of these precipitates suggests weak binding of chloramphenicol to the PCL surface which precludes slow release. Indeed we showed that scaffolds released all their chloramphenicol after approximately 2 hours [240]. The brittleness of the adhered

chloramphenicol means losses to antibiotic loading would likely be sustained due to further processing steps.

The results are somewhat deceptive: A method is presented that can load a comparable amount of antibiotic onto a PCL structure. However, visual analysis of discs revealed a brittle and superficial attachment that it probably not suitable for sustained drug delivery.

4.1.2.2 Hydrogel Method

4.1.2.2.1 Characterisation of PVA-PCL scaffold morphology

PVA solutions of higher concentration had visibly more viscosity (seen by the wake of the magnetic stirrer). By plunging the Plunger device up and down, the PVA solution is forced through the scaffolds and air bubbles were seen coming to the surface. Placing the soaked scaffolds on absorbent paper removes the excess, leaving only a thin coating on the scaffold surface.

The gel volume, pore saturation and PVA-PCL scaffold porosity was calculated in the same way as in the agar gel entrapment experiments (Results & Discussion 4.1.1); using gravimetric analysis while assuming the porosity of the scaffold is constant and the density of the PVA solution was close to water. One difference was dramatically decreased drying time before the second weight measurement was collected. This was to attempt to model the porosity of the of the PVA-PCL scaffold in its swollen state (which is its working state). The numerical results can be seen in Table 19 and graphically in Figure 39 and Figure 40.

Table 19. Porosity of PVA-PCL scaffolds of varied PVA concentration.

	PVA concentration (%w/v)				
	5	8	10	12	15
Porosity of Scaffold (%)	84.51±7.50	81.64±8.16	81.63±7.21	76.98±5.21	71.85±4.61
Pore saturation (%)	11.05±7.90	14.07±8.59	14.08±7.59	18.97±5.49	24.37±4.86
Volume of PVA gel (µl)	21.20±16.13	31.17±18.44	33.67±21.02	40.79±14.96	52.98±17.56

Increased PVA concentration resulted in decreased porosity ($r = -0.959$, $P < 0.05$), while volume of PVA coating increased ($r = 0.989$, $P < 0.05$). This was expected as the mechanism of coating depended on the higher concentration PVA solutions becoming more viscous and thus more resistant to being leached-

out of the scaffold by the absorbent paper. The large error bars seen in Figure 40 are due to the very small volumes being measured which are prone to mass distortion due to incomplete drying.

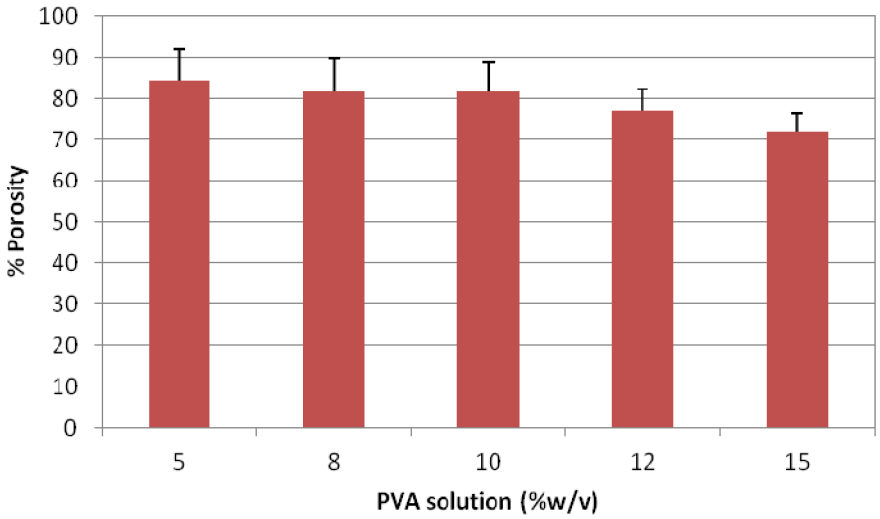

Figure 39. Scaffold porosities coated with PVA gels of varied concentration. Errors bars = std; n=12.

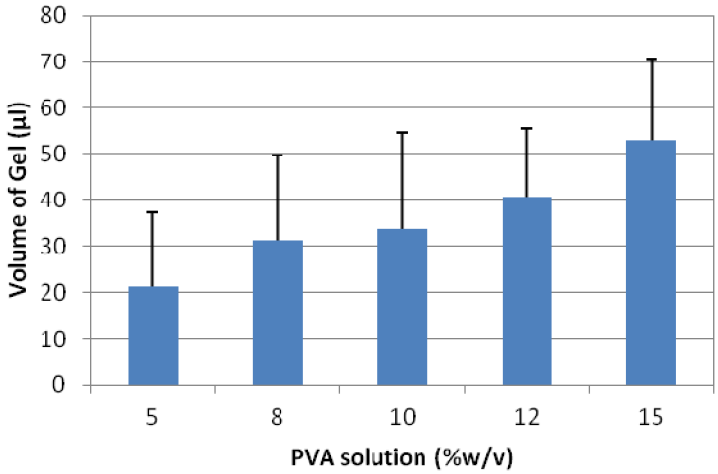

Figure 40.Volume of PVA gel coated onto PCL scaffolds depending on PVA solution. Error bars = Standard deviation; n=12.

The gravimetric results have been validated by SEM micrographs of the macro-scaffold architecture (Figure 41). The figure clearly shows that as PVA solution concentration is increased the scaffold appears denser and porosity decreases. The SEM micrographs also prove that this is due to the thickness of the PVA coating. The base PCL scaffold has very large macropores (>500um). The optimum pore size range for skin tissue engineering is thought to be around 100-200um for migration and adhesion of fibroblasts

[6, 10, 147]. In previous studies, there have been difficulties growing cells on the scaffold largely due to its very large pore size. The PVA coating can be seen to decrease the pore size closer to this optimum without fully occluding pores.

The PVA gel-layer can be easily distinguished from the PCL scaffold: The PCL appears as a rougher surface while the PVA is smooth (Figure 42). Both PCL and PVA surfaces are visible in all scaffold iterations. This is the desired morphology as hydrogel scaffolds alone have been shown to have poor tissue adherence [27] which the hydrophobic PCL will dramatically improve. There were signs of brittle fracture and delamination of the PVA coating from the PCL scaffold. This is due to the glass-like properties of PVA hydrogels when dehydrated. The surface interactions of the polymers PVA being hydrophilic and PCL, hydrophobic) may also have worked to cause the delamination. This may be prevented by copolymerisation to instil more elastic mechanical properties in the gel coating. Lian *et al*, found that the addition of PEO to PVA hydrogel films dramatically increased the elongation at break[32]. It is also probable that crosslinking before dehydration may provide more order to the system and prevent cracking.

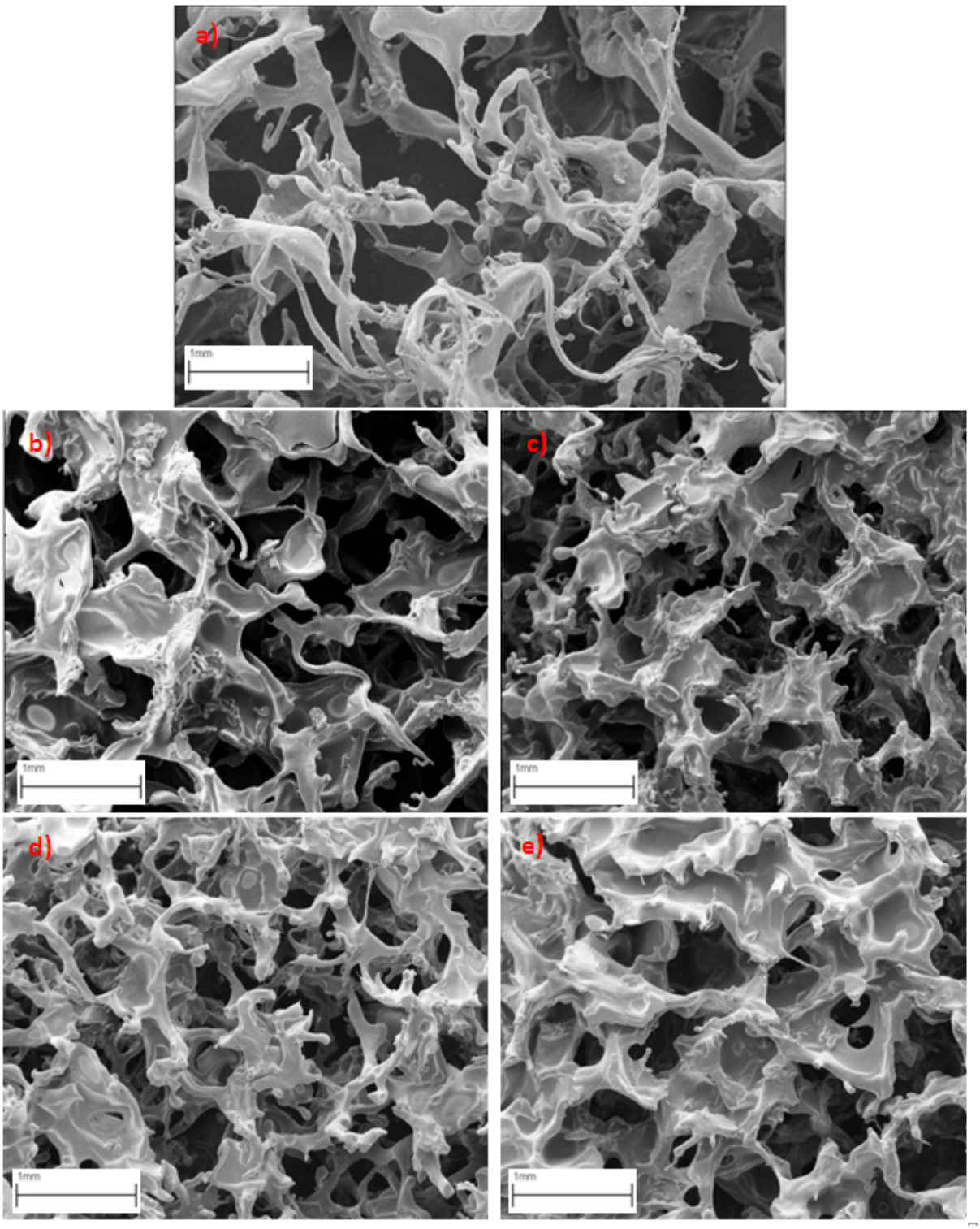

Figure 41. SEM images of PVA-PCL scaffolds of various concentrations: a) 0% PVA – control; b) 8% w/v PVA; c) 10% w/v PVA; d) 12% w/v PVA and; e) 15% w/v PVA. SEM conditions: Magnification 20x; Accelerating Voltage 10kV.

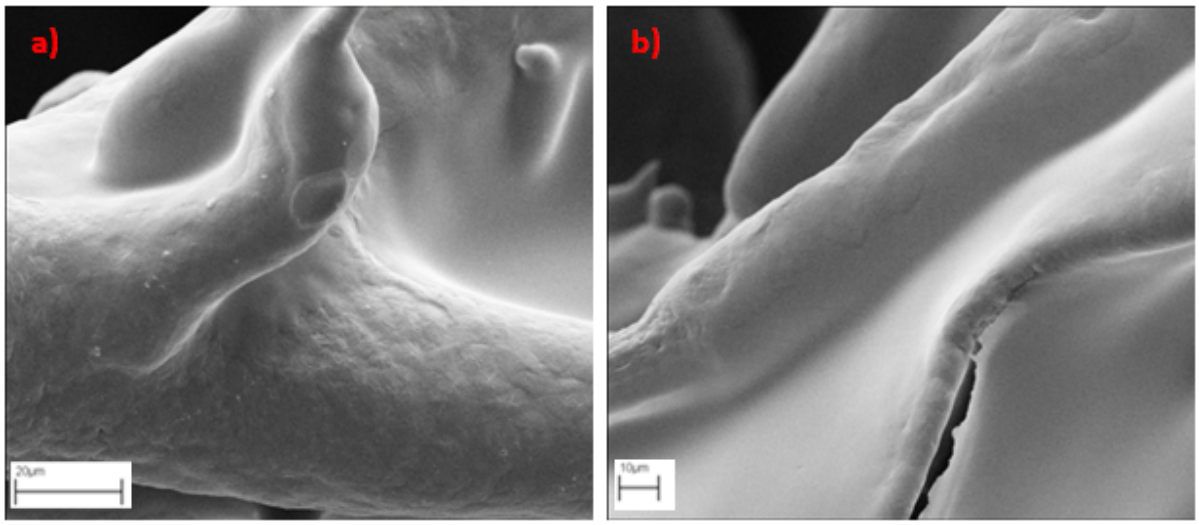

Figure 42. SEM images of 10% w/v PVA-PCL scaffolds. a) 800x magnification; b) 600x magnification.

The optimal porosity for tissue engineered skin is thought to be around 90% [10]. All of the PVA-PCL theoretical swollen porosities lie below this. High porosity is essential for tissue ingrowth and pore size has been shown to be a determinant of cell migration in vivo with absence of pores relating to earlier formation of a fibrous capsule [242]. The theoretical porosity calculated in this experiment assumes that the PVA coating will swell to 100% of its post manufacturing size after crosslinking, dehydration and re-swelling. This assumption will be validated and the actually swollen porosity determined later in this study.

Porosity is not the only important parameter in designing the proposed scaffold. Both the volume of gel and the level of crosslinking will determine the drug release profile of the device. It is accepted that the PVA solution concentration is directly related to cross-linking [26, 30, 35]. Therefore increasing PVA concentration is likely to slow down drug delivery, which is the desired outcome for treating chronic wounds. Volume of gel will determine the amount of antibiotic entrapped into each scaffold. Obviously a higher antibiotic load is preferential for long-term slow releasing DDS.

To address these related and conflicting design parameters a PVA concentration was chosen in the middle of the range; 10% w/v. This will be used for following characterisation of the PVA-PCL device. It is interesting to note that this concentration is used in many other studies for PVA DDS [29, 35, 38]. It is important to note that we have proved that these key parameters: porosity and volume of gel can be controlled simply by altering the PVA concentration.

4.1.2.2.2 Spectrophotometry - Standard Curve

The absorbance at 543nm for solutions containing various concentrations of erythromycin was tested to assemble a standard curve which could be used in future experiments to determine and quantify erythromycin. This experiment also served to validate the method that would be used in drug elution experiments using erythromycin.

As expected the absorbance increased as the concentration of erythromycin increased in a linear fashion. The equation derived from the linear relationship is:

$$A = 0.0394c + 0.0287 \quad (9)$$

Where A is the absorbance at 543nm and c is the concentration of erythromycin (µg/ml).

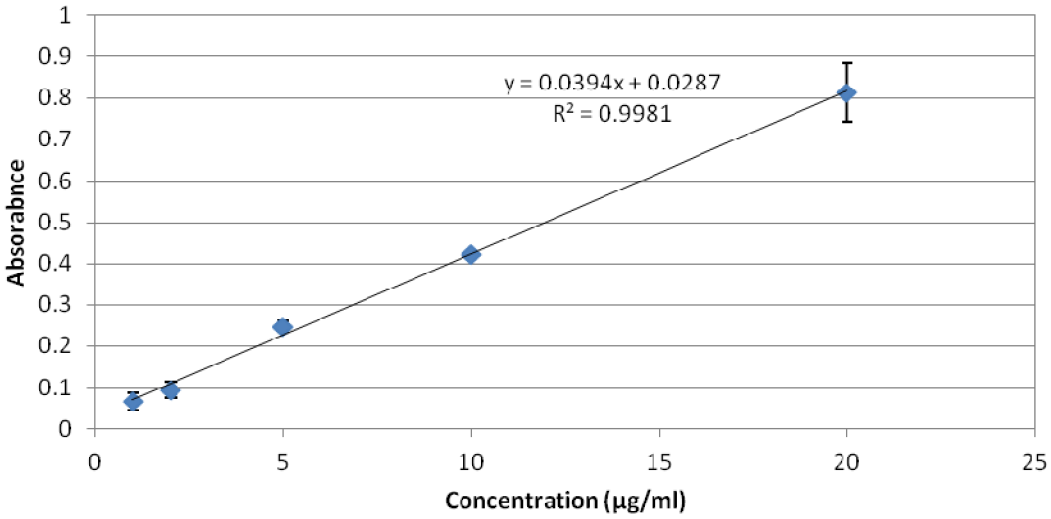

Figure 43. Erythromycin standard curve. Mean absorbance of solutions containing various concentrations of erythromycin was plotted. Equation and regression coefficient are shown on figure; Error bars = Std; n=3.

The stability of the eosin Y buffered solution and the eosin Y-erythromycin complex was tested by measuring the change in absorbance (ΔAbs) over the course of one hour. Solutions were kept in the same cuvettes and at laboratory conditions. Pure water was tested to determine the absorbance drift due to the spectrophotometer itself. This was found to be a decrease of 0.01 absorbance units. The Buffered eosin Y solution containing no erythromycin decreased 0.066 units, almost a 700% decrease compared to the pure water sample. This suggests instability of the dye solution itself. The 20ug/ml erythromycin sample decreased 0.083 units after 1 hour. This decrease is 25% greater than the solution

containing no erythromycin and may suggest instability of the complex, but it is minor compared to the instability of the die solution alone. There is also a possibility that absorbance drift due to the spectrophotometer may be accentuated at higher absorbencies and that that instability is not causing the decrease.

Either way if the buffered eosin Y was used as the blank the absorbance of the erythromycin at time 0 and 1 hour would have been: 0.893 and 0.876 respectively. This minor decrease of 1.9% is only a fraction of the standard deviation found when performing the standard curve (8.7% for 20ug/ml erythromycin). Further, when performing experiments, solutions will sit for less than one hour before spectrophotometry is performed, limiting the decreased absorbance.

The minor absorbance decrease found here validates the use of this very rapid method for assaying erythromycin and other macrolides using eosin Y.

Table 20. Validation of eosin Y-erythromycin complex stability over time.

Sample	Abs t=0	Abs t=1 hour	ΔAbs
Water	0*	-0.01	**-0.01**
Buffered Eosin Y; Water	0.687	0.621	**-0.066**
Buffered Eosin Y; 20ug/ml Erythromycin	1.58	1.497	**-0.083**

*Used to blank spectrophotometer at time=0

Unfortunately preliminary testing using Erythromycin infused PVA-PCL scaffolds produced unquantifiable results. There was a marked difference in the concentration of erythromycin calculated when different sample volumes were tested using the eosin Y assay. Further testing showed that PVA had some effect on the eosin Y assay. Table 21 shows that when water was used as the blank PVA had a produced an absorbance between 0.5 and 0.7 absorbance unit. Uncrosslinked PVA became soluble in water and produced a significant absorbance. When the eosin Y reactants were used as the blank, PVA

again produced a significant absorbance. However when erythromycin was added, the absorbencies of erythromycin-eosin Y complex and the PVA do not follow the principle of superposition. This suggests that the PVA may interfere with the erythromycin-eosin Y complex. Whatever the mechanism of this interference the variability in the amount of soluble PVA eluting from different scaffolds makes the spectrophotometric method of macrolide detection unviable in this instance.

Table 21. Detection of spectrophotmetric assay contamination

Sample	Concentration of Erythromycin (µg/ml)	Contaminated water sample volume (µl)	Absorbance (λ = 543 nm)
EosinY Blank*	0	0	0
EosinY PVAscaf 100*	0	100	0.434
EosinY PVAscaf 600*	0	600	0.53
EosinY Ery*	20	0	0.749
EosinY Ery PVAscaf*	20	600	0.813
Water Blank†	0	0	0
Well Water†	0	700	0.098
PVAscaf Water 200†	0	200	0.504
PVAscaf Water 400†	0	400	0.589
Scaf Water†	0	700	0.07
PVA Water†	0	700	0.685

* 1ml samples contain 70ul eosinY, 150ul Acetate buffer and water
†1ml samples contain water

4.1.2.2.3 Microbial Assay – Standard Curve

A microbial disc diffusion assay, similar to that described in the British Pharamacopoeia [243] was used to determine concentrations of erythromycin. *Staphylococcus aureus* was used as the test organism so a calibration curve was set-up relating the zone of inhibition (ZoI) of the microbe growing on TSA plates to the concentration of antibiotics in a soaked filter paper disc.

A clear measurable ZoI could be seen after 18 hours culture time in the presence of erythromycin soaked discs (Figure 44). The ZoI diameter increased as the concentration of antibiotic in the discs increased. Below 10ug/ml no ZoI could be seen. The ZoIs appeared very consistent. A disc soaked in water containing soluble PVA was tested to determine whether PVA was antibacterial to *S. aureus* and would interfere with the assay. Fortunately the PVA control did not cause any ZoI to appear.

The relationship followed a logarithmic trend seen in Figure 45 below. The equation of this trend can be re-arranged to calculate an unknown concentration of erythromycin c (ug/ml) from a ZoI, Z (mm):

$$c = e^{\frac{Z+0.1263}{3.0449}} \quad (10)$$

The observation of consistent ZoIs is reinforced by the small error bars in figure. This suggests that the assay is reliable. Because interfering molecules such as PVA do not produce a false positive result the method is valid for specific detection of erythromycin eluting from PVA-PCL scaffolds.

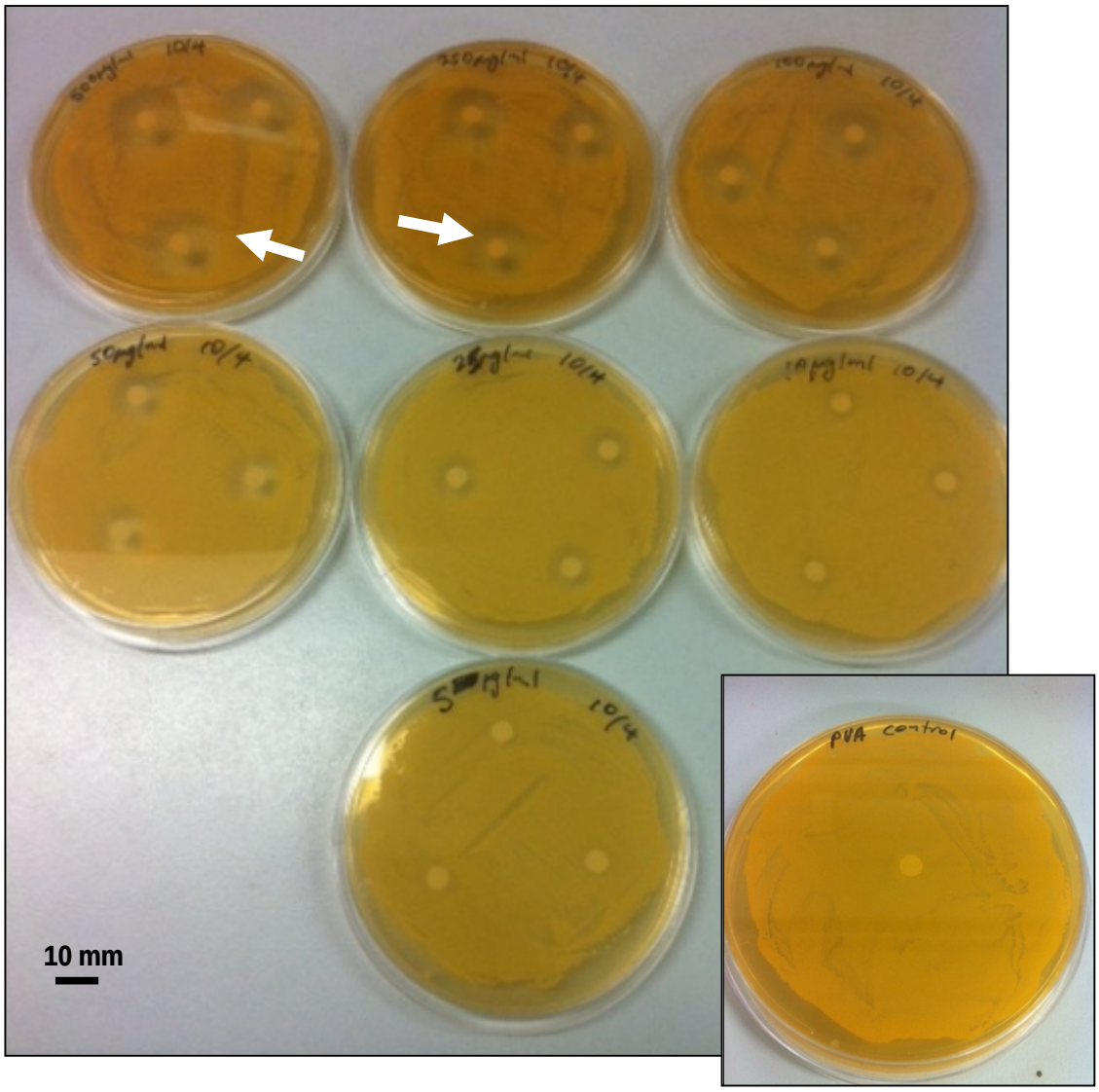

Figure 44. Disc diffusion assay. Clear ZoIs (indicated examples shown by white arrows) can be seen around discs containing >10ug/ml erythromycin. PVA control did not produce a ZoI.

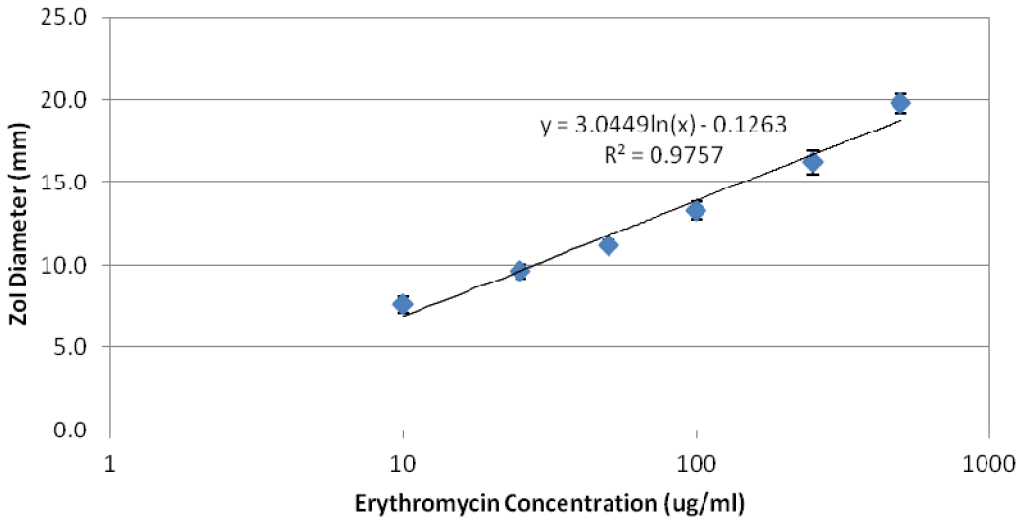

Figure 45. Standard curve relating zone of inhibition (ZoI) of *S. aureus* to concentration of erythromycin. Error bars = Std; n = 3.

4.1.2.2.4 PVA Hydrogels in Ethanol-Water mixtures

The PVA dissolved readily in water with application of heat and remained dissolved in solution when the temperature was lowered to 40°C, despite the high initial PVA concentration (20% w/v). On addition of the ethanol, the PVA came out of solutions, forming stringy white threads of solid polymer. However these dissolved back into solution after 1 hour. This shows that PVA is insoluble in absolute ethanol. The formation of the strings formed in areas of higher ethanol (EtOH) concentration as it was added to the water. When the EtOH concentrations equilibrated the PVA slowly re-dissolved. A portion of the resulting PVA-ethanol-water solution was poured into Petri dishes to form cast PVA hydrogels. Scaffolds were also plunged in solution to coat scaffolds in PVA as previously described.

An attempt to make a 35:65 solution resulted in a lump of undissolved PVA, showing that the PVA concentration of 10% PVA exceeded the solubility limit for this ethanol-water mix (Figure 46). This observation speaks to the patent by Hyon *et al* [165]. The patent presented hydrogels formed in a number of organic solvents with water. The highest ethanol concentration that formed a hydrogel as presented by Hyon was 50:50 whereas in hydrogels were made in pure DMSO. This suggests that Hyon may have been unable to form hydrogels using more than 50% ethanol and corresponds with our observation.

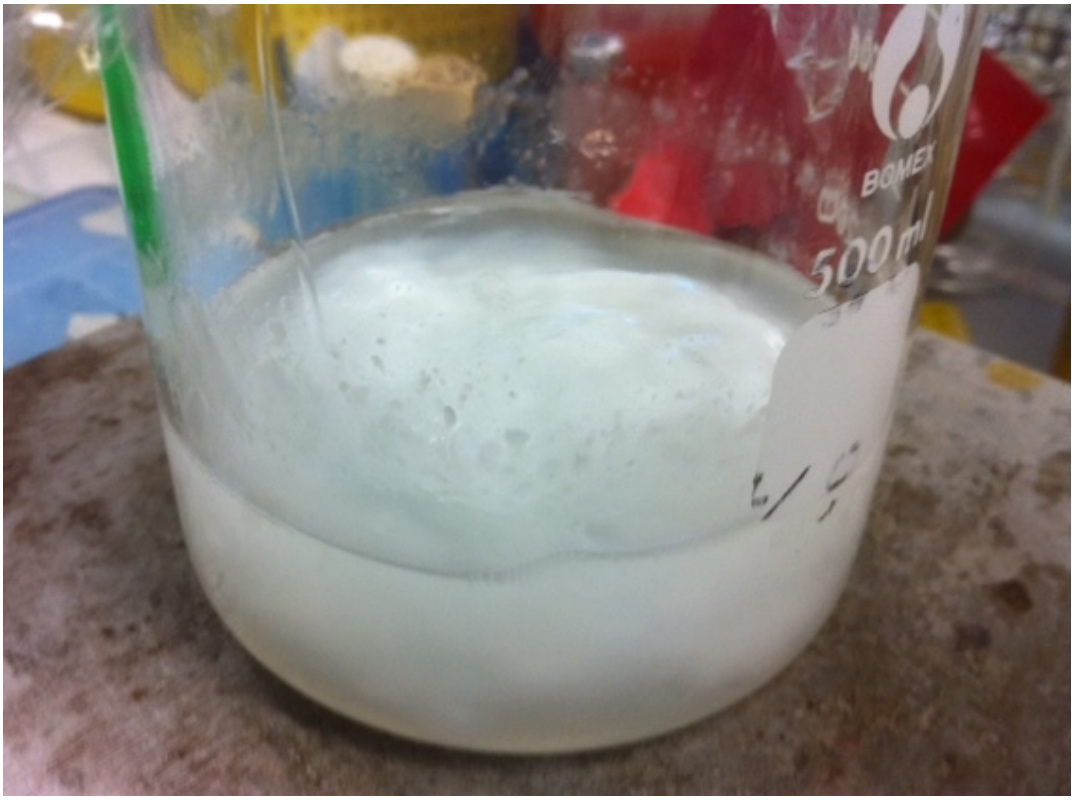

Figure 46. Failed attempt to dissolve a 65% v/v EtOH solution containing 10% w/v PVA.

When the hydrogels were vacuum packaged they were viscous gel liquids. After the freeze-thaw cycle they were hydrated solids. These were then dehydrated and stored before use. On dehydration, PVA gels lost significant volume. The 50% ethanol gels became contorted while hydrogels containing lesser ethanol amounts remained flat. No significant change could be seen in PVA-PCL scaffolds due to the small volumes of PVA used.

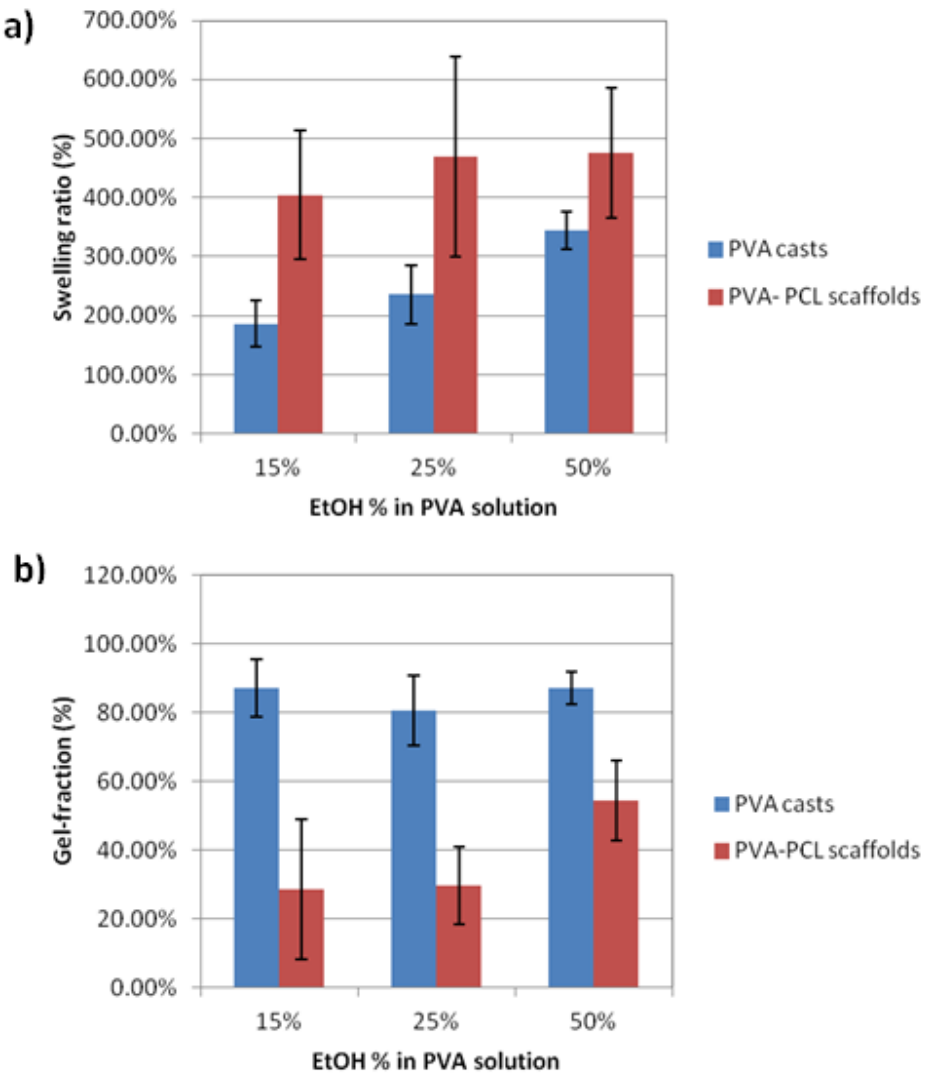

Figure 47 Hydrogel properties of PVA cast hydrogels and PVA-PCL scaffolds made using varying amounts of ethanol (EtOH) in the polymer solution. a) Swelling ratio (%) and; b) Gel fraction (%). Error bars = Standard deviation; n = 10 for PVA casts; n = 12 for scaffolds.

To calculate swelling, gel fraction, porosity and gel volume of cast PVA hydrogels and scaffolds, samples were weighed before coating, after coating once dried, after 72 hours soaking time with only excess water removed and after re-dehydration. Then Equations 1 and 2 were applied (see Background 2.1.3.6)

In the case of cast gels, swelling ratio was shown to increase when increasing amounts of ethanol were used in the polymer mixture. The swelling ratios of PVA casts manufactured with 15, 25 and 50% v/v ethanol were 186.6, 235.35 and 344.89% respectively. The swelling ratio for the PVA phase coated onto

scaffolds also showed a trend of increasing with ethanol concentration but this did not appear significant. Further the swelling ratios found for scaffold samples were substantially higher than those found for cast gels. Scaffolds coated in PVA solutions containing 15, 25 and 50% v/v ethanol were 404.58, 469.44 and 475.93% respectively.

When gel fraction was calculated, cast PVA hydrogels showed little to no change with increasing ethanol content. The exact gel fractions for 15, 25 and 50% v/v ethanol were 87.22, 80.54 and 87.01% respectively. For scaffolds the PVA gel fraction was seen to increase with increasing ethanol content. Gel fractions for 15, 25 and 50% v/v ethanol were 28.70, 29.77 and 54.53% respectively. These values are also notably much smaller than that of the cast PVA gels.

As expected the results for hydrogel characteristics on scaffold samples were difficult to determine. Compared to PVA cast hydrogels, results were approximately 50% lower for swelling ratio and almost 300% greater for gel fraction. This is due to the very small sample weight with only 20-50ul of polymer solution coating each scaffold which exacerbates any weighing errors due to losses or gains. Losses occurred from material sticking to glass sample holders during dehydration which would then become detached from the scaffold during removal for weighing. This created results for gel fraction that were much lower than expected. Conversely, weight gains occurred due to poor water removal from the porous scaffold architecture creating swelling ratio results much higher than for PVA cast hydrogels. These types of errors would suggest less consistent results, which can be seen by the large standard deviation for scaffold samples (Figure 47). Therefore, for the purpose of further design work the results from PVA casts were assumed as the hydrogel properties of scaffold-coated PVA.

The results for swelling were not expected. Hyon *et al* showed that increasing EtOH content in the polymer solution decreased water content [165], which is directly proportional to swelling percentage. The results presented here show a clear increase in swelling ratio with EtOH content. The freezing period of cross-linking in Hyon's work was substantially shorter than the majority of studies on freeze-thaw PVA hydrogels. The method used in this thesis has a number of differences:

1. The freezing time to induce crystallisation of PVA was notably longer at 18 hours as opposed to 3 hours.
2. Ethanol was not removed by soaking in water but instead air dried leading to a varied shrivelling effect due to the rapid evaporation of ethanol.

These manufacturing differences may explain the trend in swelling ratio. Particularly the rapid drying in hydrogels made with high EtOH content may create polymer chain entanglements.

The gel fraction results were more predictable. Gel fraction is related to cross-linking such that the gel fraction is the proportion of PVA molecules that are cross-linked and remain insoluble after long-term soaking [21, 27, 30]. Considering there was no change in crosslinking method or the concentration of PVA in the polymer solution no appreciable change in gel fraction was expected.

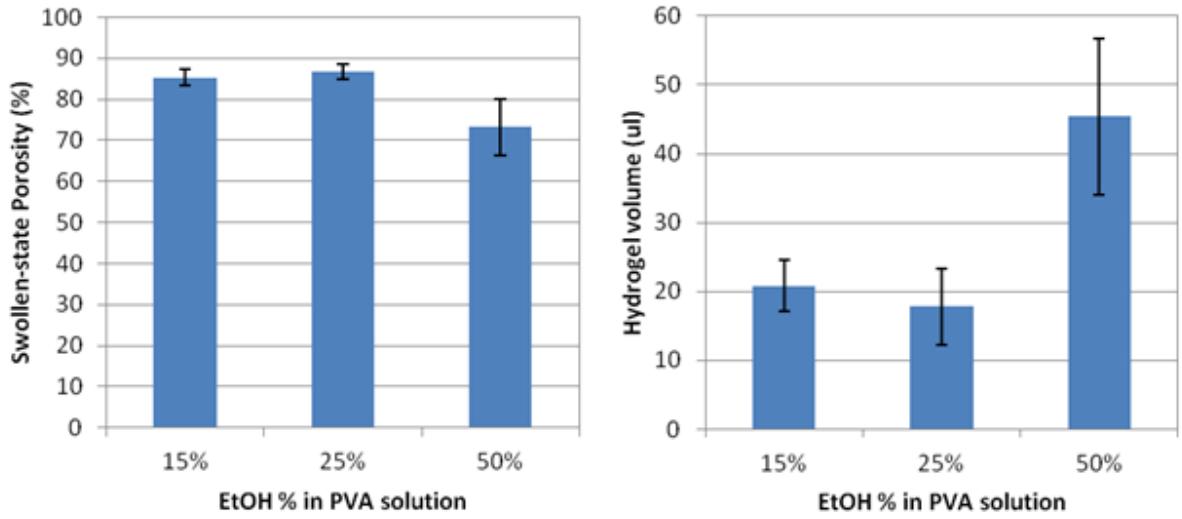

Figure 48. Porosity and hydrogel volume of scaffolds coated in PVA solution containing varied concentration of ethanol (EtOH). EtOH concentration given as % v/v. Error bars = std; n = 12.

The volume of hydrogel is directly related to the porosity in an inversely proportional manner as can be seen in the charts above (Figure 48). There was a stark difference seen between the 15 and 25% samples and the 50% sample which had a hydrogel volume of more than double (45.4 µl) forcing down the porosity of the scaffold. Scaffold porosities for 15, 25 and 50% ethanol samples are 85.32, 86.73 and 73.18% respectively.

4.1.2.2.5 DSC Analysis of PVA Hydrogels in Ethanol Mixtures

There was very little change in the thermo graphs obtained from un-crosslinked PVA samples to crosslinked PVA sample made with varying amounts of ethanol (Figure 49). The exothermic peak indicates the melting temperature. There is a very minor shift towards a lower temperature in the crosslinked samples. This can be attributed to crosslinking attenuating the hydrogen bonding capacity of

the polymer network [38]. What looks like a step-down feature just before the exothermic peak is probably a chain relaxation related to the melt and not a separate thermal property.

Attempts were made to extract the T_g from the data. This is characterised as a 'step-down' feature on the thermo gram. Unfortunately a significant step-down was not observed. Modulating DSC was used to amplify the feature, but it was still not significant enough to calculate a T_g for the samples (Appendix B.1). T_g is a crucial characteristic in hydrogel design [21]. Despite this, many studies that perform DSC analysis do not mention the T_g [38]. This may be that the step-down feature is difficult to detect for PVA. Lian *et al* reported the Tg of Freeze-Thaw crosslinked PVA as 19.2°C [32]. This result is spurious as the T_g of pure PVA is commonly known as 85°C. Further if the T_g of pure, dried, crosslinked PVA was 19.2°C, this would mean that sample would have rubbery mechanical properties at room temperature. Mechanical testing in later samples will show that this is not the case.

DSC analysis showed that there was no change in the thermal properties between crosslinked and non-crosslinked PVA or between samples fabricated with varied levels of ethanol.

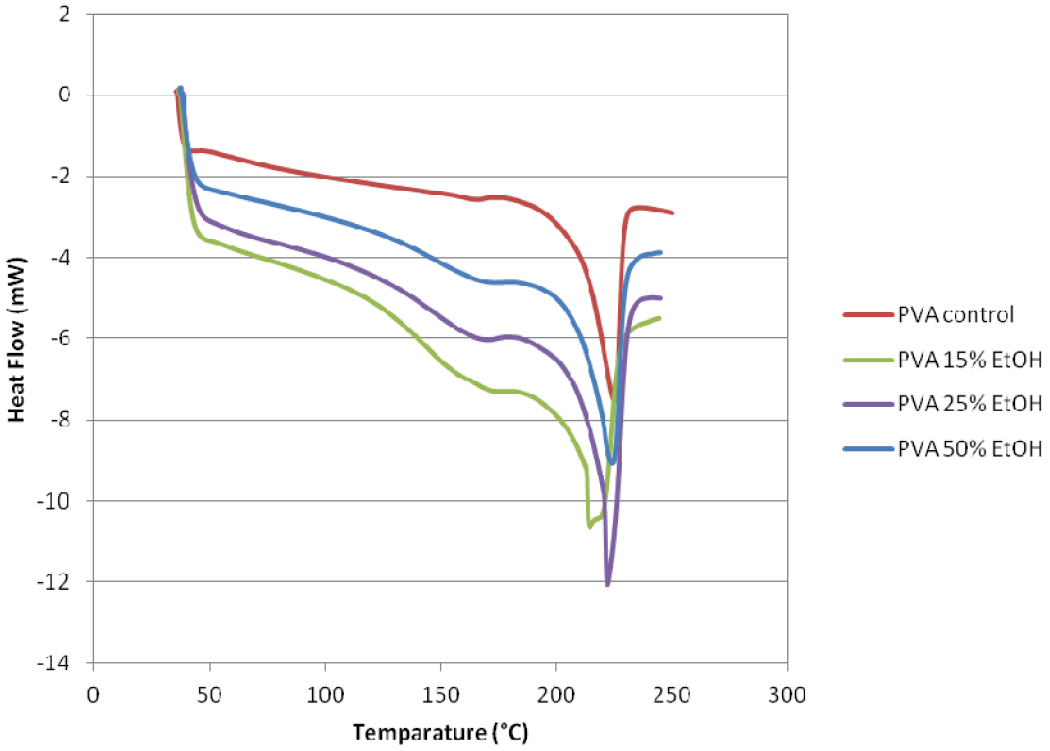

Figure 49. DSC heat flow analysis of PVA hydrogels fabricated using varied ethanol (EtOH) concentration (%v/v).

4.1.3 Bioglass Manufacturing

4.1.3.1 Precursor Preparation

The precursor was weighed out precisely based on stoichiometry calculations performed with the help of Dr Michael la Robina. Mixing the raw materials together is necessary to ensure homogeneity when making pellets and later for melting. This is essential for controlling the composition.

A homogenous powder suspension was difficult to achieve using conventional mixing techniques. This is due to the relative densities of the raw materials: The fumed silica is so light that the other precursor powders simply fall through it unable to form a suspension. The heavier grains would fall through the smaller, lighter silica particles to rest at the bottom of the mixing vessel. The result was inhomogeneous pellets.

It is known that acetone can produce strong sol-gel networks with fumed silica [244]. Thus acetone was added to the mixture as a particle binder. The acetone served to agglomerate the fumed silica into sol gel globules that could entrap other larger precursor particles resulting in a homogenous mixer of the precursors. This also decreased the volume of the mixture and produced less airborne particles improving handling and safety respectively.

After undergoing compression in the hardened steel die the resulting pellet was a hard white cylinder of compressed powder (dimensions: ~ 35mm x 37mm [h x d]). The diameter of the pellet is determined by the die dimensions. The diameter of 37mm was chosen to fit tightly in the platinum crucible allowing the highest possible yields per melt cycle. There was an odour of acetone coming off the pellet.

Calcination is a term used in the glass industry for an early stage of the melt phase used to eliminate any unwanted reactant volatiles and impurities from the precursor prior to fusing. To ensure bioglass purity, the precursor was calcined. Pellets were placed in their calcination vessels and underwent the different heating cycles. Afterwards pellets were observed and changes in height and weight were measured. The results are summarised in Table 22.

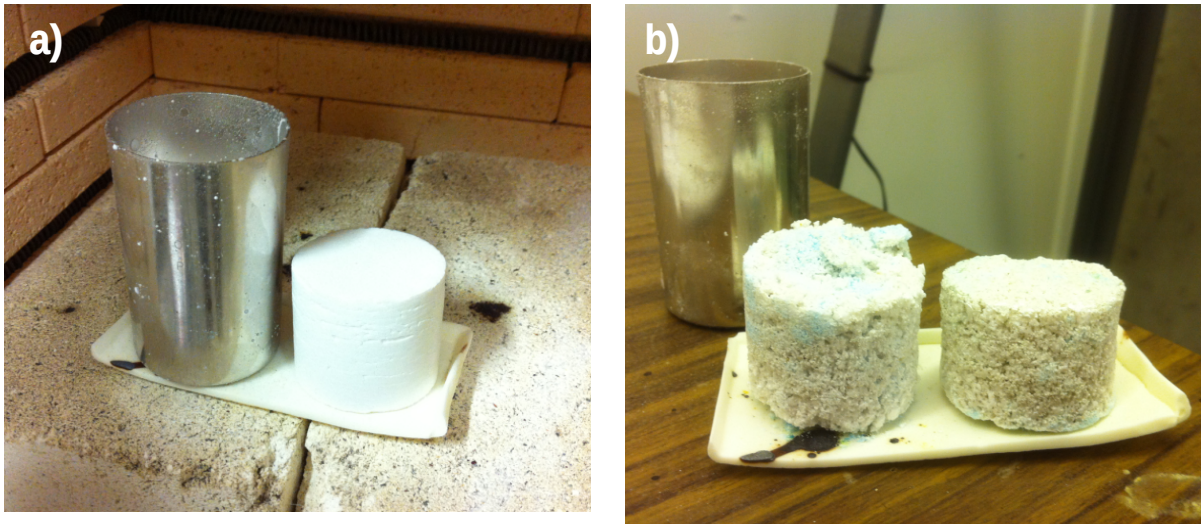

Figure 50. Calcination of bioglass precursor pellets. a) Uncalcined pellets loaded in oven in Pt-crucible and on alumina tray (left to right). b) Pellets after calcination become porous and have different colour depending on vessel (Pt-crucible or alumina tray; left to right).

In comparison to the un-calcined pellet, calcined pellets were more porous and lighter; patches of colour could be seen on areas of the calcined pellets; the odour of acetone was absent (Figure 50). A very minor shrinkage was also detected however this may not be significant as the porous structure made these height measurements un-reliable. Further the maximum decrease in height detected (3mm) would make little difference to production. Pellet shrinkage or increase in pellet density would have been favourable as this would have increased bioglass melt yields. Despite the porous nature of the pellets they maintained their stability and could be picked up by hand with minimal crumbling. The blue colour change is likely due to the photoluminescence from the thermally oxidised silica [245] and is not a contaminant. The different containers produced only slightly varying effects on calcined pellets. In general, the crucible produced whiter pellets that stuck slightly less to the container minimising losses. The consistent grey colour of pellets calcined on the alumina tray was attributed to airborne carbon particles in the furnace that contaminate the more exposed pellets. Carbon is the best possible contaminant in glass making as it is unreactive at fusion temperatures and doesn't interfere with the chemical structure. Carbon particle are also bioinert. It was concluded that the grey colouring was caused by the contaminants of the oven and would not happen in a clean oven. During the 1050°C calcination the pellet that contacted the alumina tray showed a severe colour change at the interface with the container. This may be a sign of alumina contaminating the pellet which is known to occur during glass melting in alumina vessels.

Table 22. Resulting precursor pellets calcined at different temperatures and on different containers.

Temp (°C)	Furnace Container	Weight (g)				Height (mm)			Notes	
		initial	final	Δ	Δ%	initial	final	Δ	Appearance	Handling
1000	Pt-Au Crucible	41.496	29.791	11.705	28.208%	36.0	36.0	0.0	patchy blue and white, hardened, porous	not too brittle to pick up, no sticking to crucible
	Alumina Tray	40.215	28.778	11.437	28.440%	32.0	31.5	0.5	patchy aqua and grey, hardened, porous	not too brittle to pick up, minimal sticking to tray
1050	Pt-Au Crucible	39.408	28.157	11.251	28.550%	34.0	32.0	2.0	patchy blue and white, hardened, porous	not too brittle to pick up, no sticking to crucible
	Alumina Tray	36.448	26.188	10.260	28.150%	30.0	27.0	3.0	patchy aqua and grey, some yellow hardened, porous, blue at interface with container	not too brittle to pick up, minor sticking to tray
1100	Pt-Au Crucible	40.222	28.794	11.428	28.412%	32.0	31.0	1.0	patchy blue and white, hardened, porous	not too brittle to pick up, minor sticking to crucible
	Alumina Tray	38.311	27.553	10.758	28.081%	31.0	30.0	1.0	patchy aqua and grey, hardened, porous	not too brittle to pick up, minimal sticking to tray
1150	Pt-Au Crucible	42.457	29.869	12.588	29.648%	37.0	35.5	1.5	patchy blue and white, hardened, porous, some glassy formation	not too brittle to pick up, some sticking to crucible
	Alumina Tray	42.283	29.442	12.841	30.369%	35.5	34.5	1.0	patchy aqua and grey, hardened, porous, some glassy formation	not too brittle to pick up, some sticking to tray

Increasing the calcination maximum temperature caused little change to the calcined pellets for the temperature range examined. A fairly constant weight loss of around 28% suggests all volatile reactants were removed even at 1000°C. When precursor materials are heated the carbonates undergo decomposition at around 1000°C and are released from the pellet in the form of carbon dioxide. Stoichiometric calculations determine a mass loss of 22.89% from the raw materials. From the results, larger losses were measured: between 28-30%. This accounts for the acetone in the pellet that would quickly gas-off during the calcination heating. At 1150°C some opaque glassy formation could be seen on the pellet (Figure 51). Despite this negligible shrinkage was observed. Further, this glassy formation may account for the increased sticking to the containers at this temperature which is undesirable for easy handling.

Figure 51. Pellet calcined at 1150°C. Glassy formation is indicated by arrows.

For the calcination heating cycles tested the max temperature of 1000°C was selected for further bioglass manufacturing as all unwanted reactants were expelled while the least amount of energy was used. The alumina tray was chosen as the calcination container because colour changes that may indicate trace contaminants do not justify the expense of purchasing numerous platinum-gold crucibles for this application. For quality manufacturing a new furnace may need to be purchased to decrease

contaminants, however the protocols used here were deemed suitable for research-only bioglass production.

4.1.3.2 Melting

After the sample was soaked at 1350°C for the indicated time and fusion was allowed to take place the drop-down furnace was opened. The drop-down design minimised heat loss and heat-shock to the furnace. The red-hot crucible was carefully picked up with platinum-tipped steel pincers and the molten glass was poured as seen in Figure 52. The resulting glass was clear and colourless. Granules from each batch were mounted in epoxy and polished for SEM-EDS analysis. This allowed determination of the composition of each batch.

Alumina crucibles often fractured during the melt (Table 23). Although these crucibles were made in-house from very cheap ingredients, a lot of time and energy was spent just to have them break after two melts. Given that sintering the alumina slip-casts yields only around half that amount of useable crucibles, this is not a sustainable practice. Substantial bioglass losses were also experienced due to sticking to the alumina crucible. Five batches of bioglass were made using platinum crucibles. The chemical composition of these batches was very close to the true composition of 45S5 bioglass (see Table 24 and Table 25). However every batch produced with an alumina crucible had substantial alumina contamination of between 1.03 – 3.84%wt. Alumina in the bioglass composition has been shown to prevent bone bonding [42] and is thus very likely to effect bonding to soft tissue. This contamination also affects the validity of the relative composition of the other compounds in the bioglass.

Table 23. Crucibles used, bioglass appearance and production notes of different experimental batches

Batch	Crucible Used	Glass Appearance	Notes
1	Alumina	Clear glass	Crucible cracked, significant losses in stuck glass
2	Alumina	Purple and blue glass with some white	Significant losses in stuck glass
3	Alumina	Clear glass	Significant losses in stuck glass
4	Alumina	Clear glass	Crucible cracked, significant losses in stuck glass
5	Alumina	Clear Glass	Significant losses in stuck glass
7	Pt foil	White opaque glass	Incomplete melting, significant losses in stuck glass, Crucible cracked.
8	Pt sputtered Alumina	White opaque glass	Incomplete melting, significant losses in stuck glass, Pt coat sloughed-off
9	Pt/Au	Clear glass	Non-stick, no losses

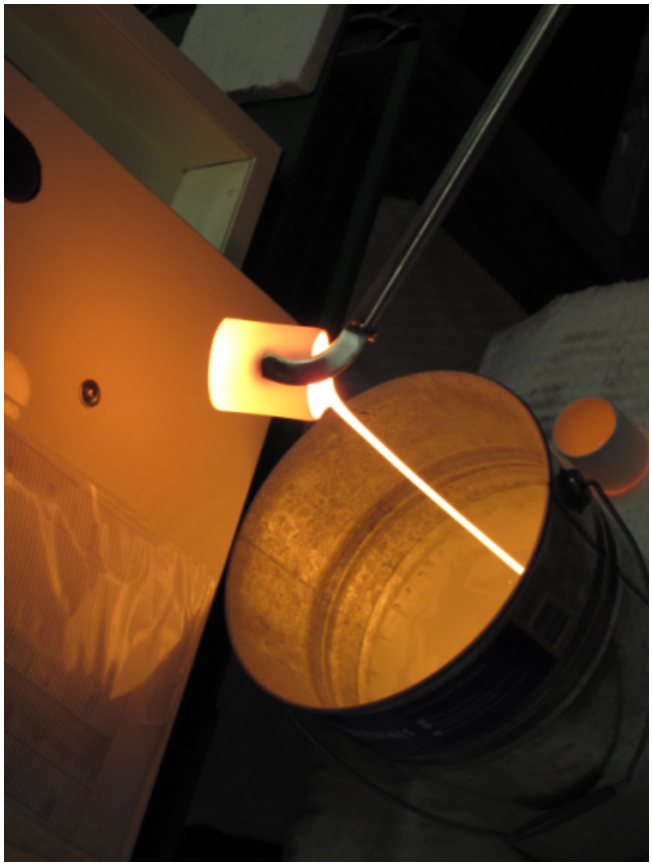

Figure 52. Pouring molten glass from an alumina crucible.

A crucible constructed of thin platinum foil (25μm thickness) was used to make a batch of glass. The results were poor with white opaque glass being produced containing un-melted precursor powder. The crucible itself was warped and damaged from the pouring and the majority of the glass stuck to the crucible. EDS showed that the bioglass contained no traces of alumina which was further evidence that the source of the alumina contamination was the alumina crucible and not contaminants in the raw materials. However, the amount of SiO and Na_2O were both far off the true bioactive composition (Table 24 and Table 25). This may be due to the shape of the crucible which required pellets to be crushed before loading. This in turn may have resulted in poor flux between reagents leading to the incomplete melting and wrong composition.

An alumina crucible was sputter-coated in platinum to attempt to stabilise the crucible against cracking and prevent alumina contamination of the bioglass. During sputter coating a plasma was seen around the platinum target indicating charged argon particles were accelerated toward the target (Figure 53). Afterwards the alumina crucible had turned metallic grey on most surfaces. The sputter coating was not

particularly successful as only a superficial coating could be seen on the inside of the crucible. Sputter coating is a physical deposition technique and atoms released from the platinum target follow a direct path to coat the crucible. The high walls of the crucible caused incomplete coating on regions as released atoms were blocked and less likely to reach some surfaces, in particular the curved edges at the crucible's base (Figure 54). A cylindrical target would be needed to properly coat the crucible [246] and this was not feasible. A batch of bioglass was melted in the Pt-sputtered alumina crucible. Incomplete melting was seen with white opaque glass produced and a substantial amounts was stuck to the crucible and could not be recovered. Inspecting the crucible revealed that the platinum coating had been sloughed off during melting, and the platinum may have contaminated the glass. EDS analysis showed that the platinum coating did not prevent alumina contamination of the bioglass produced (Table 25).

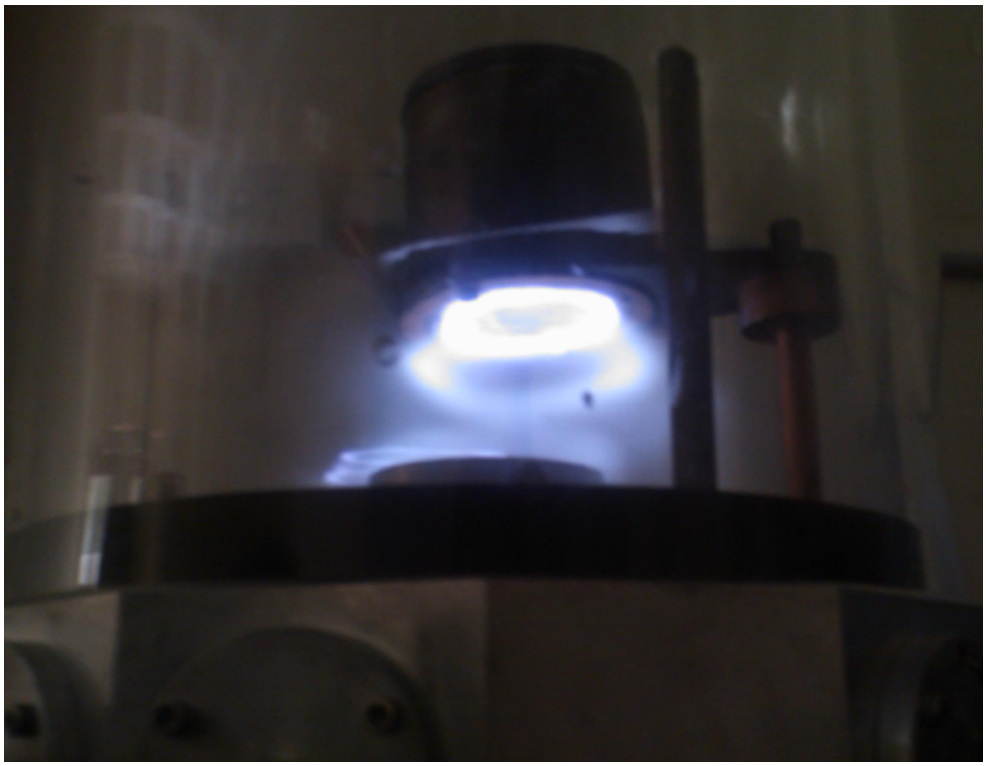

Figure 53. Plasma ring around platinum target in magnetron sputter coater

A Pt-Au crucible was used to make a batch of bioglass. The crucible performed very well producing clear homogenous glass that did not stick to the crucible – After cooling; shards of glass could easily be removed. Predictably no alumina contamination was detected in the resulting bioglass and the composition measured by EDS was very close to the 45S5 composition (Table 24 and Table 25). Platinum

crucibles are the industry standard for high temperature reactions. Platinum has high strength and low chemical reactivity even at very high temperatures. The addition of gold to the platinum crucible creates a non-wetting surface making it the perfect material of glass formation [247]. The notable down-side of using this crucible is its significant expense. However, the main cost is the rare metals used which do not depreciate and can be easily sold.

Figure 54. Platinum sputter-coated alumina crucible. Left: An un-coated alumina crucible. Right: A platinum coated crucible – incomplete coating can be seen on the edges on the base.

Table 24. Composition of 45S5 Bioglass [248]

Compound	wt%
Silica, SiO_2	45
Sodium Oxide, Na_2O	24.5
Calcium Oxide, CaO	24.5
Phosphorous pentoxide, P_2O_5	6

Table 25. Chemical composition of bioglass batches by EDS analysis. Weight percentages (%wt) given as mean±std. Batch 6 was not analysed.

	Batch Composition %wt							
Species	1	2	3	4	5	7	8	9
Na_2O	20.61±0.14	23.19±0.13	19.88±0.24	18.02±0.56	19.56±0.42	13.50±0.77	24.02±0.20	21.20±0.30
Al_2O_3	1.03±0.20	2.86±0.09	3.69±0.32	3.84±0.07	2.29±0.79	0±0	4.66±0.12	0±0
SiO_2	49.80±0.62	45.29±0.53	49.78±0.29	51.41±0.38	51.18±0.66	61.89±2.13	43.09±0.23	47.92±0.49
P_2O_5	5.28±0.09	5.53±0.17	4.20±0.17	4.57±0.05	4.96±0.22	5.44±0.16	4.26±0.17	4.64±0.14
CaO	23.07±0.64	23.13±0.39	22.44±0.13	21.91±0.24	22.02±0.33	19.17±1.53	23.97±0.36	25.54±0.36

Calcined bioglass precursor compounds undergo fusion at around 1300°C creating the covalent bonds between species and forming the amorphous glass chemical structure. EDS proved an effective method of determining the chemical composition of the glass and detecting any contaminants. Under estimations of volatile elements such as Na have been seen due to these species migrating away from the electron beam [249]. Later it was found that the Soda Ash raw material was prone to absorbing humidity compared with the other reactants thus leading to weighing errors and the consistent deficit in Na_2O in the bioglass composition.

It was found that the use of alumina crucibles were unsuitable for Bioglass manufacturing due to the alumina contamination which renders the glass bio-inert. The platinum-gold crucible performed the best in terms of both manufacturing efficiency and glass composition. This crucible was used to produce Bioglass for all further experiments. The composition was not exactly that of 45S5, however according to Hench *et al*, "when the glass composition exceeds 52% by weight of SiO_2 the glass will bond to bone but not to soft tissues" [248]. Therefore the Bioglass produced by this process should be bioactive for soft tissue cells such as fibroblasts.

4.1.3.3 Post processing

Bioglass frit was dried in a 60°C oven for 24 hours before milling. Milling was performed using an agate mortar and pestle, sieving regularly. Two sieves were used, a coarse sieve and a finer one, with pore sizes 300μm and 120μm respectively. A sample of milled and sieved bioglass was suspended in a droplet of distilled water on a glass slide to disperse the particles. Then the sample was observed under the microscope and analysed with a computer program to calculate the particle distribution of the milled glass.

The results show that >40% of particles were < 10μm with approximately 75% of particles < 20μm in length (Figure 55). This shows that the mortar and pestle were able to reduce the bioglass particle size to < 20μm making it a reasonable method to produce bioglass particles for coating scaffolds. Interestingly the sieve pore sizes were far greater than the largest bioglass particles found – 120 μm pore size compared with 60μm particle length. This suggests considerable and rapid agglomeration of particles into larger ones that are unable to pass through the sieve. Agglomeration is common in dry-sieving of ceramics. However, wet sieving may cause the bioglass to react and diminish its bioactivity.

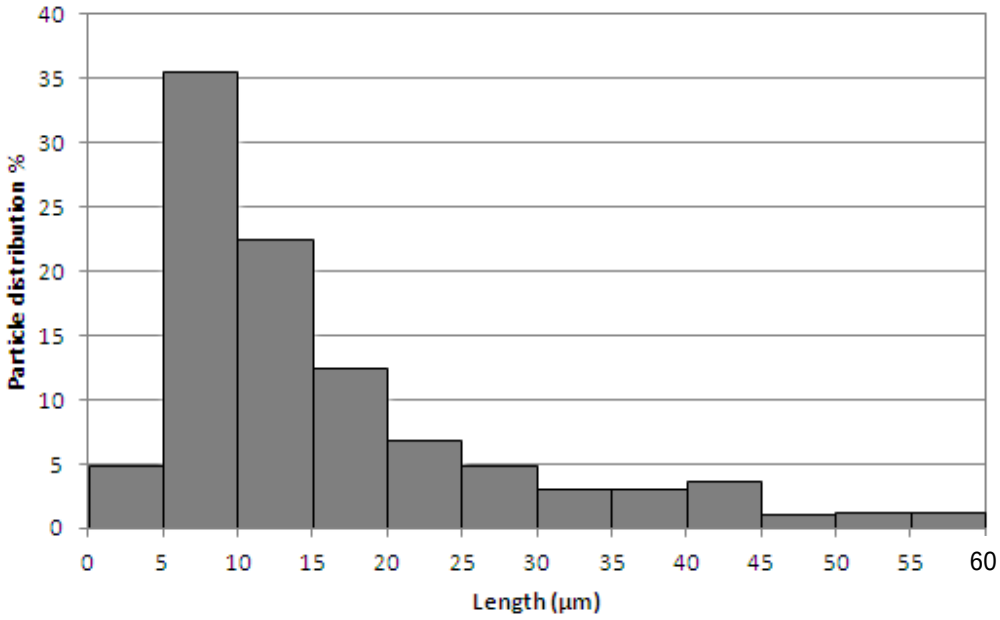

Figure 55. Particle size distribution of Bioglass particles milled in an agate mortar and pestle.

Bioglass frit and bioglass marbles were added to a PCL-lined ball milling container and milled for 150 hours. A sample of the milled powder and granules was not sieved but directly analysed under the light microscope. The particle size distribution chart (Figure 56) shows a graph with two distinct regions: One region of very small particles (0 - 30μm) and another representing larger particles (60 - 200μm). In the ball mill larger granules of bioglass experience both normal and shear impacts causing the steady breakdown of the granules and creation of smaller bioglass wear particles.

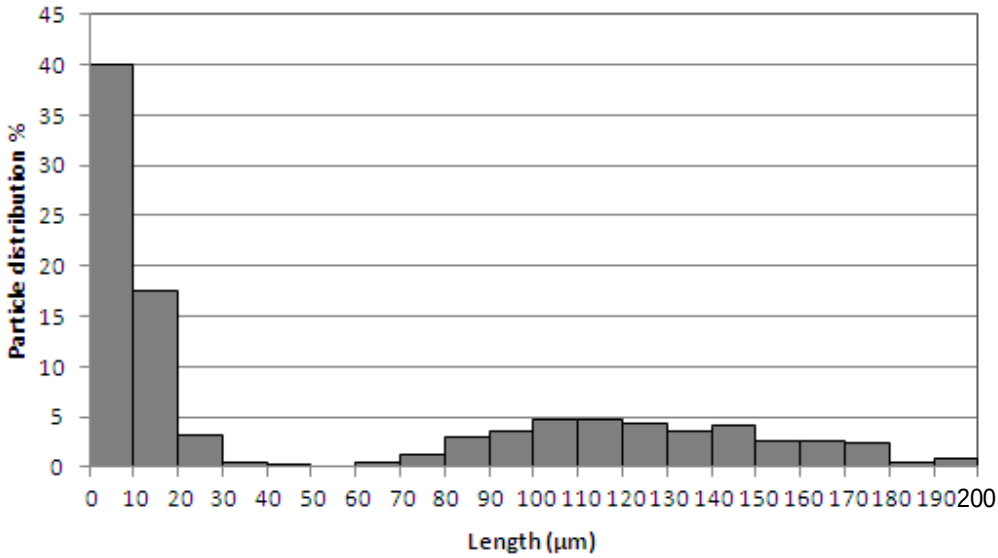

Figure 56. Particle size distribution of Bioglass particles milled in a Ball mill for 150 hours.

Samples from the ball mill were removed at different times to determine whether ball milling for extended periods would produce more small particles. The results in Figure 57 show that over time the proportion of particles < 30µm in size increases from 18% after 50 hours of milling to 60% at 150 hours. This was an expected result as more time allows more collisions between particles and hence the breakdown of larger granules and the creation of smaller bioglass wear particles.

Amongst the bioglass powder small stringy fibrous white particles were discovered. These particles are most likely from wearing of the PCL lining. The PCL is a polymer and a much softer material than bioglass. During mall milling collisions between these two materials causes abrasion of the PCL surfaces and creation of small PCL wear particles. These contaminate the bioglass powder and this decreases the utility of the ball milling method. However, for the purpose of coating PCL scaffolds the PCL traces in the bioglass are not contaminants thus the method is suitable for this application. The stringy PCL contamination could easily be discriminated from the jagged bioglass particles under the microscope.

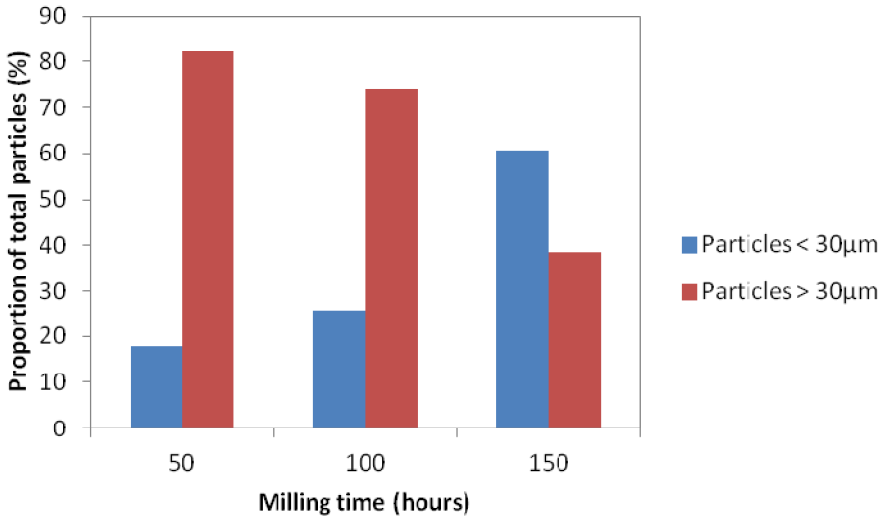

Figure 57. Ball milling products sampled over time.

The milling methods tested both produced bioglass particles < 30µm that could be used for biomedical and tissue engineering applications. Mortar and pestle produced bioglass with no signs of contamination; however the process was very laborious. In contrast the ball milled bioglass contained small amounts of PCL contamination that would be acceptable for coating PCL scaffolds. Further, the ball mill could be left running indefinitely and required far less labour than the mortar and pestle. For further experiments it was decided that mortar and pestle would be used to generate bioglass that would be tested on its own; and ball milled bioglass would be used when in conjunction with PCL.

There may be ways to remove or prevent the formation of PCL contamination: Organic solvents such as acetone could be used to dissolved and remove the PCL contaminants, while not reacting with the bioglass [250]. Alternatively a ball milling vessel completely made of bioglass could be fabricated which would wear to produce more bioglass, free of contamination. However bioglass is more brittle then regular glass and such a vessel would be prone to cracking.

4.1.3.4 Bioglass Coating

Differences in bioglass-coated scaffolds could not be seen with the naked eye, however containers for these samples would begin to build up small amounts of fine white powder which is the bioglass that detached from the scaffolds.

SEM analysis showed the struts of the scaffold coated with jagged particles typically around 5µm in size (Figure 58). The coating was more or less homogenous over the scaffold surface. These particles are

adhered bioglass. It is important to note that the presence of the bioglass shows that it is strongly adhered and did not wash off in the liquid media. The particle size of the bioglass is smaller than indicated by particle size distribution studies conducted above (see Results and Discussion 4.1.3.3). The reasons for this are degradation of the bioglass over the 14 day period and the increased mobility of smaller particles leading to better penetration of the scaffold. 45S5 bioglass is a bioresorbable compound and breaks down in aqueous media [42, 248, 251]. Therefore the smaller particle sizes seen here may indicate that the bioglass produce by the manufacturing process we designed is indeed bioresorbable.

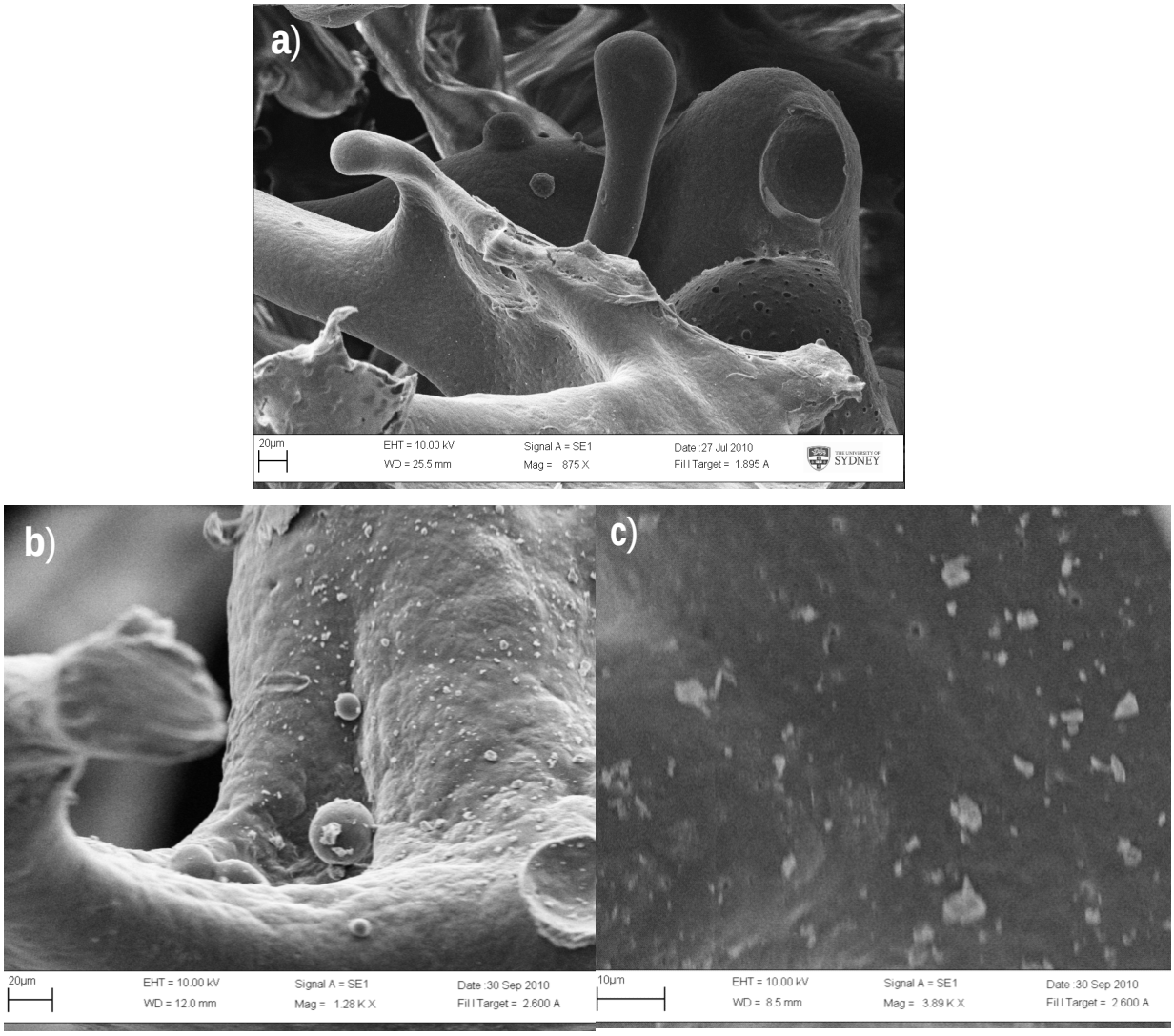

Figure 58. SEM images of bioglass coating PCL scaffold. a) Control uncoated PCL scaffold with smooth surface (x875); b) Bioglass specs seen evenly dispersed over scaffold strut (x1280); c) Shard-like bioglass micro and nano specs (x3890)

The bioglass coating technique used here has been validated for initial coating efficacy by our group in previous studies [252]. Rezwan *et al* mentions the disadvantages of scaffold coating in composite formation are the coating adhesion may be too weak and organic solvents are often used [2]. This study tested the coating *in vitro* and showed strong adhesion of bioglass particles for an extended period in liquid media. Further, the coating mechanisms involved heating the PCL to entrap the bioglass particles in the PCL surface without ruining the scaffold's interconnected architecture and without the use of solvents. The coating method is simple to perform and effective, ensuring the scaffold surface remains bioactive long enough for cellular adhesion to occur.

4.1.4 Bulk Metallic Glass Sputtering

Purple plasma was formed around the BMG target suggesting sputtering was occurring. To achieve a 500nm thickness the process took around 15 minutes, this does not include the 40 minutes combined time to pump up and pump down the chamber. Due to the small area inside the chamber the sputter coating was a slow process to mass-produce BMG-coated scaffolds.

Figure 59. Left: Un-coated scaffold slice. Right: BMG sputter coated scaffold slice.

BMG coated scaffolds appeared a metallic grey, although some small patches of white remained (Figure 59). This is likely due to incomplete coating and results from the nature of this deposition method and the porous structure of the substrate. The BMG particles ejected travel in straight lines making the probability of particles penetrating the scaffold's pores low [77, 246]. The phenomenon is similar to that discussed earlier with the platinum target and crucible cup-shaped target (Results and Discussion 4.1.3.2). Essentially the sputtering set-up is not optimised for the substrate's geometry. For the scaffold a 3D rotation mechanism to constantly rotate the scaffold may allow the multitude of differently oriented surfaces to be sputtered. A chemical method, such as electroless plating could be used to apply a homogenous BMG coating [103], but this method has thus far been unexplored for MgZnCa alloys.

4.2 Biofilm Formation

4.2.1 Biofilm Inhibition on Disc Composites

The biofilm growth of common wound bacteria on discs was tested to determine whether the scaffold surface could inhibit biofilm formation – a favourable property for wound healing. After 24 hours of incubation the biofilm culture of all samples increased in turbidity and thick mucus-like biofilm formed on discs (Figure 60). This indicates growth of biofilm and no major antibacterial effects from the discs.

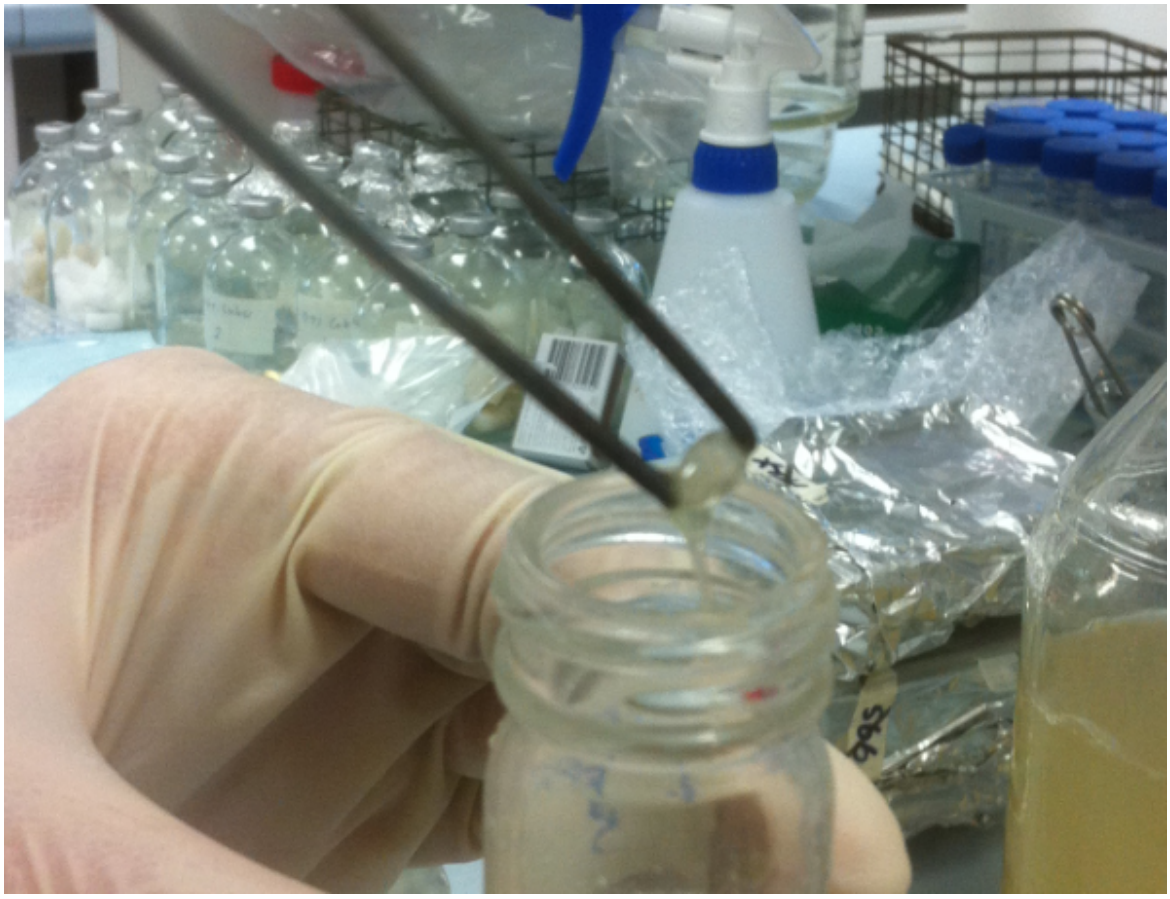

Figure 60. *S. aureus* biofilm cultured on PCL disc. Mucus like biofilm can be seen trailing off the disc.

Biofilm discs were removed from cultures and washed in sterile PBS twice to remove any non-adhered bacterial cells. The washing and sonication processes were both validated for adequate removal of non adherent and biofilm bacteria respectively (Appendix A.1).

Serial dilutions and drop plating were used to quantify the biofilm cell number. A 50ul drop of each dilution was used allowing small cells to be counted accurately in drops below 150 colonies. Anything below 15 colonies was rejected. The method was very similar to that performed by Al-Ahmad *et al* [142].

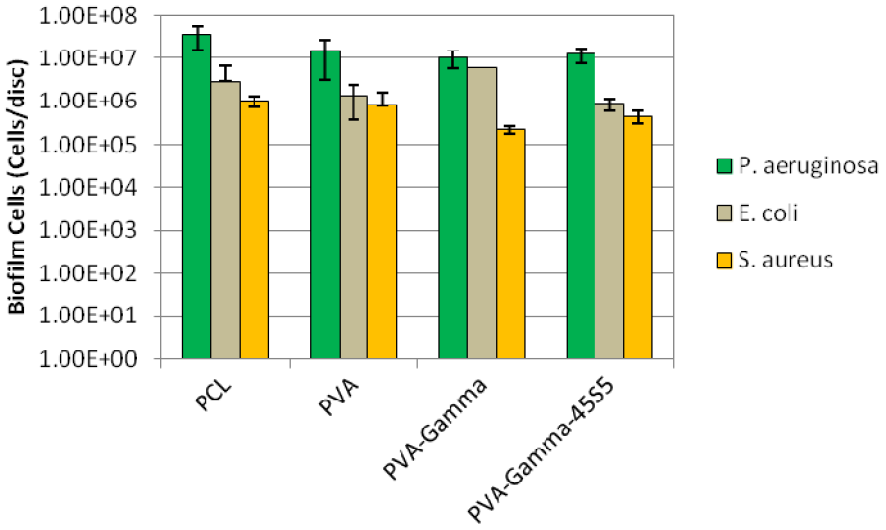

Figure 61. Biofilm formation on biomaterial discs. Biofilm formation is measured as cells recovered per disc sample. The horizontal axis represents the different biomaterial surfaces exposed to the biofilm culture. Three bacterial strains were used: *Pseudomonas aeruginosa*, *Escherichia coli* and *Staphylococcus aureus*. Error bars indicate ± Standard Deviation; n = 3.

P. aeruginosa formed the largest biofilms, followed by *E. coli* and *S. aureus*. *P. aeruginosa* is well known for forming thick biofilms causing complications in cystic fibrosis, so this result is consistent with expectations [138].

The different biomaterial discs had no significant ($p > 0.05$) effect on the biofilm formed. There is a minor decrease in biofilm formation between the PCL and PVA coated discs, with more biofilm cells collected from PCL samples than others. This trend was consistent across all bacterial strains. However, the decrease in biofilm with respect to PCL was only significant in the case of *S. aureus* grown on PVA-Gamma discs ($p < 0.05$). The hydrophobic surface of the PCL versus the hydrophilic surface of the PVA may account for this trend, as surface hydrophobicity is generally related to increased bacterial adhesion – a key step in biofilm formation [120, 127]. The trend may instead be due to the experimental method. All biofilm samples were removed simultaneously by sonication, but serial dilution drop-plating was done in order (PCL, PVA, PVA-Gamma, PVA-Gamma-45S5) and took around 5 minutes per sample. This meant that there was considerable time between the biofilm removal and the plating. This may have allowed planktonic bacteria to re-adhere with the disc surface; driving down counts in the later-tested PVA samples. Vortexing before each serial dilution was performed in attempt to mitigate the re-adhesion effect on results, but it cannot be ruled out.

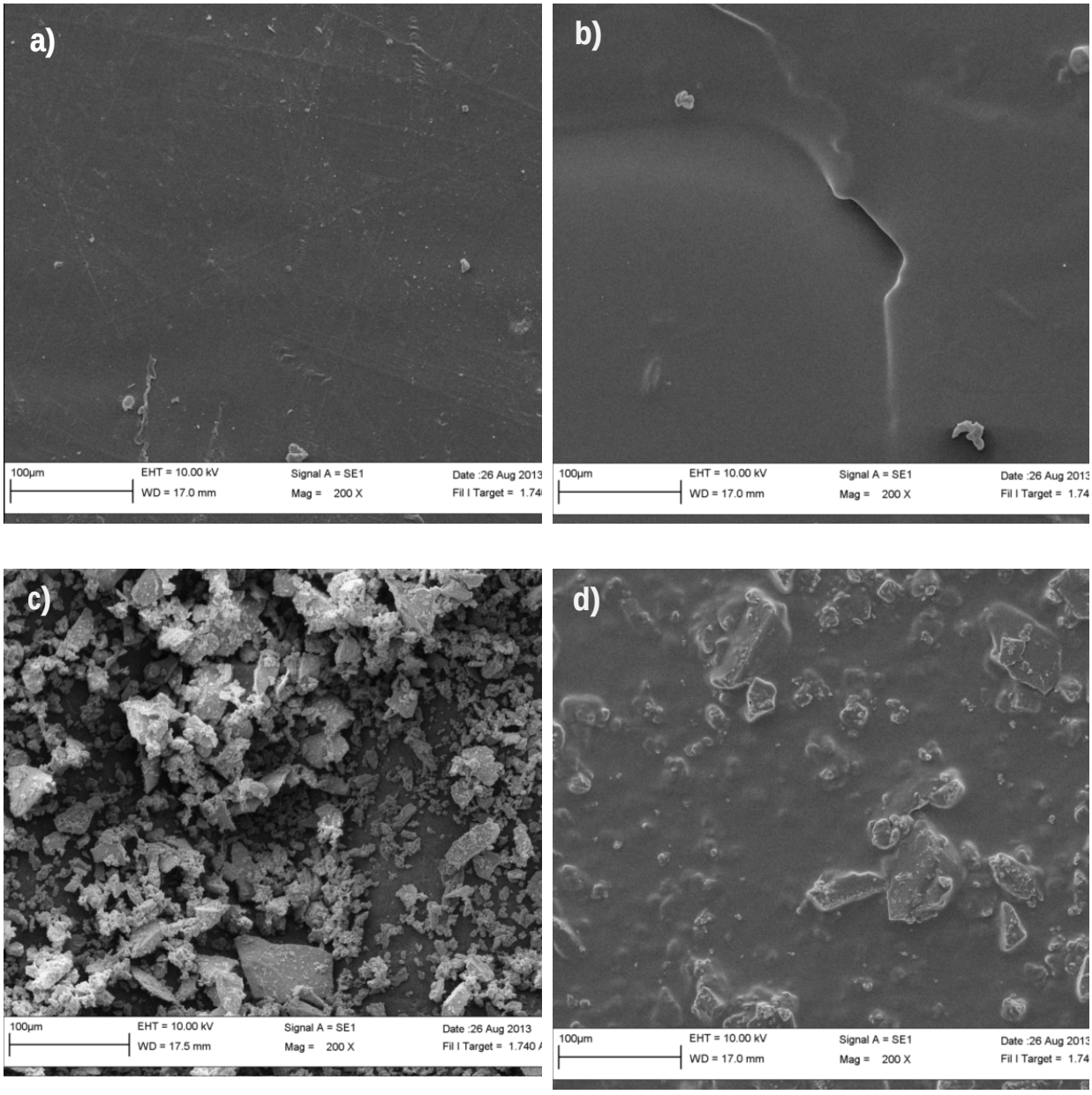

Figure 62. Un-cultured control samples of biofilm assay discs with different surface coatings: a) PCL; b) PCL-PVA/Gamma; c) PCL-BG; d) PCL-PVA-BG-Gamma. Magnification 200x, accelerating voltage = 10kV.

Gamma irradiated PVA and 45S5 bioglass looked to also have minimal effect on biofilm formation. The biofilm cell count decreased slightly in the in the *S. aureus* and *P. aeruginosa* samples but increased in the case of *E. coli*. Again, none of these changes are particularly significant. Further, in the Bioglass samples which are also gamma irradiated the biofilm cell count is very similar to the non-Gamma-irradiated PVA sample. Gamma irradiation was not expected to effect biofilm formation as PVA is relatively stable when gamma-irradiated while dehydrated [253]. The Bioglass was also expected to

have minimal effect as it is underneath the PVA coating, thus not increasing surface roughness or being directly involved in interfacial adhesion with bacteria.

There is possibly a minor decrease in biofilm adhesion on PVA surfaces compared to PCL surfaces which may be attributed to the relative hydrophobicity of these surfaces. This may be an added benefit of designing tissue scaffolds with hydrophilic hydrogel surfaces.

SEM was used to characterise the different scaffold surfaces and observe biofilm formation. To characterise the scaffold surface, normal sample preparation was performed to protect manufactured features on the scaffold from washing off during bio-specimen preparation. To observe biofilm formation bio-specimen preparation was required to fix biological features adhered to the surfaces during the biofilm assay.

Figure 62 shows some of the different tests surfaces used in the biofilm assay. Figure 62a shows a PCL disc: The surface is relatively smooth with some sharp lines running across the surface which may be scratches or stretch lines from the disc-pressing manufacturing process. In Figure 62b the surface of a PVA coated scaffold can be seen. The surfaces of the PCL-PVA and PCL-PVA-Gamma discs appeared identical and thus only one image was used here. The surface is smoother than the PCL, however zooming in on some of the lighter patches showed the existence of very small pores which can be seen in some of the images below. Figure 62c and d show Bioglass coated discs that have been left as is and PVA-coated respectively. These images show how rough the surface becomes when the particles of Bioglass are added. The PCL-PVA-BG-Gamma sample has immobilised Bioglass penetrating through the dehydrated PVA coating. It is possible that cells may still be able to interact directly with the Bioglass surface, although the hydrogel will swell when hydrated and probably engulf the Bioglass particles. Importantly, this proves that the hydrogel coating process is not too vigorous such that all the Bioglass is removed from the surface.

Pseudomonas aeruginosa showed the most biofilm growth (Figure 61) and this was verified by SEM. The white rods seen in Figure 63 are *P. aeruginosa* cells; they were abundant on all disc samples. Figure 63a shows *P. aeruginosa* forming thick biofilm on the PCL surface. These structures were seen more frequently on the PCL surface than the PVA surfaces. As mentioned above some sections of PVA had very fine pores (< 1µm) which bacteria cells tended to flock toward; the extra surface roughness may assist in adhesion (Figure 63b). However, *P. aeruginosa* cells still happily attached to smooth PVA surfaces (Figure 63c). In Figure 63d *P. aeruginosa* cells are seen forming colonies on top of a piece of

Bioglass coming through the PVA. This validates the quantitative results which showed no decrease in biofilm formation on bioglass coated discs.

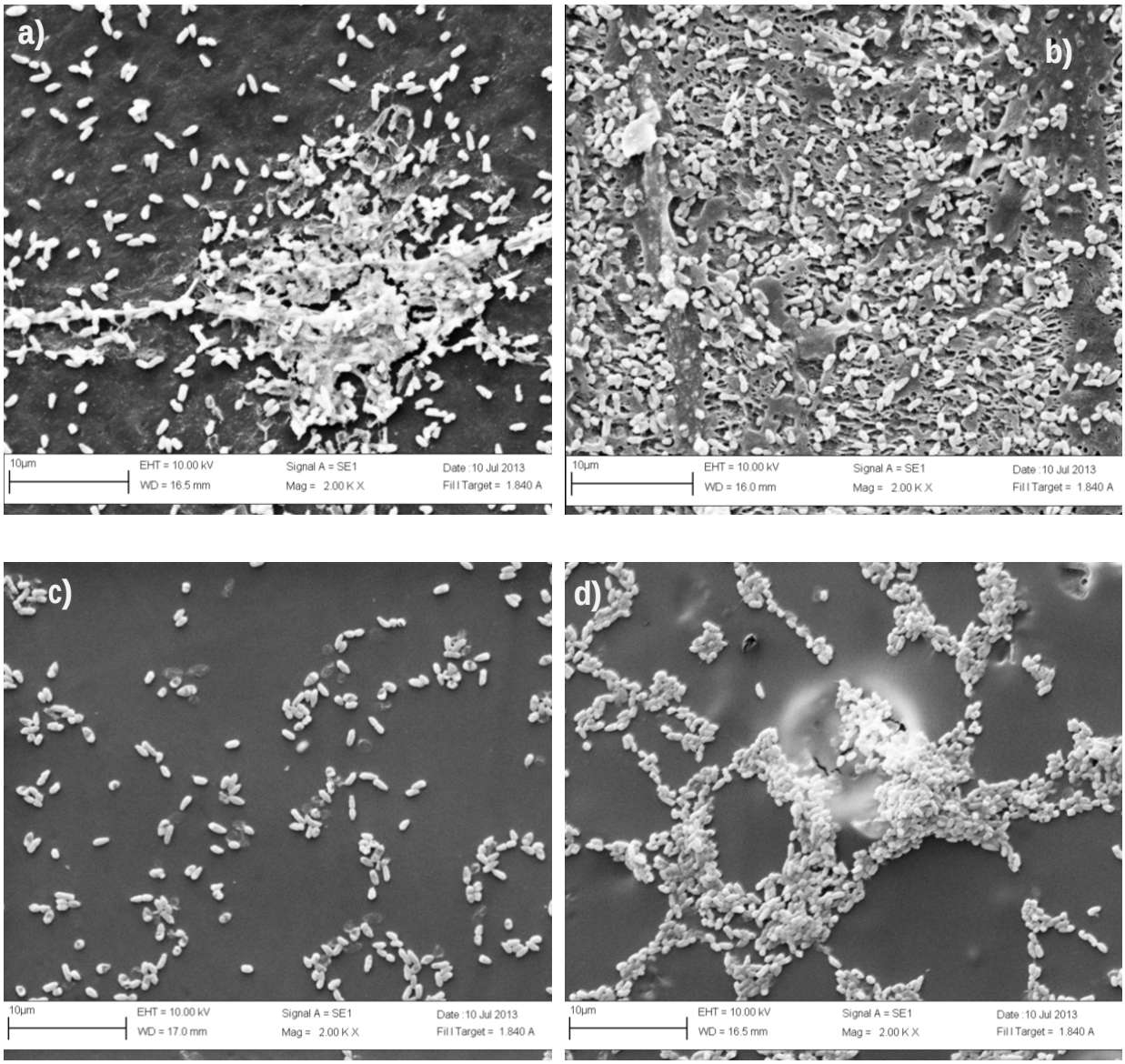

Figure 63. Biofilm assay: *P. aeruginosa* culture of discs with different surface coatings: a) PCL; b) PCL-PVA/Gamma; c)PCL-BG; d) PCL-PVA-BG-Gamma. Magnification 2000x, accelerating voltage = 10kV.

Staphylococcus aureus were much sparser than *P. aeruginosa*. The cocci were seen under SEM as 1um spheres making them easy to identify. *S. aureus* cells were seen on all surfaces including Bioglass-coated (Figure 64). In Figure 64b a colony of *S. aureus* can be seen forming a biofilm next to some dehydrated PVA. These biofilms were much thinner compared with biofilms seen in *P. aeruginosa* samples.

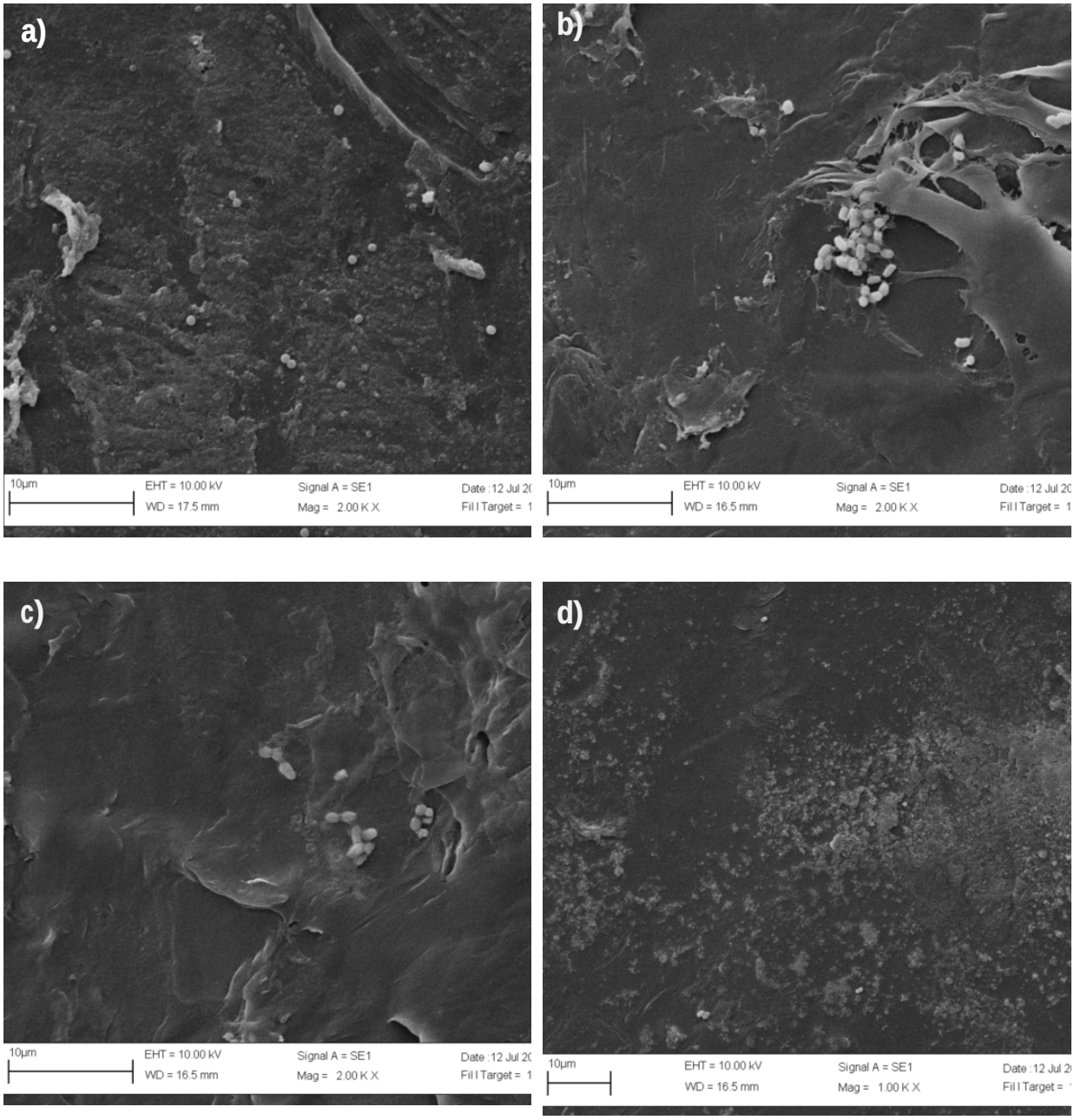

Figure 64. Biofilm assay: *S. aureus* culture of discs with different surface coatings: a) PCL; b) PCL-PVA/Gamma; c)PCL-BG; d) PCL-PVA-BG-Gamma (1000x). Magnification 2000x unless noted, accelerating voltage = 10kV.

E. coli were seen as short rods in SEM images. Biofilm formation was seen in all disc samples. *E. coli* cells had no trouble growing in close proximity to Bioglass (Figure 65d). In Figure 65b and c, the *E. coli* biofilms looked to almost fuse with the PVA coating – it is not obvious where one starts and the other begins. It is possible that the *E. coli* fall inside the PVA hydrogel pores during culture and are then

trapped when the hydrogel is dehydrated. Although this may just be one large biofilm as the polysaccharide biofilm will likely closely resemble dehydrated PVA. This issue of distinguishing hydrogel from biological features after dehydration is a limitation of SEM analysis [121].

From Figure 61 there was approximately ten-fold more biofilm formation measured in *P. aeruginosa* cultures than *E. coli* and *S. aureus* across all surfaces. SEM analysis revealed that there were indeed far more *P. aeruginosa* cells but the difference was even starker – at least a hundred fold difference by eye (Figure 66). This may be due to biofilm-surface attachment of *P. aeruginosa* being stronger compared with *E. coli* and *S. aureus*. *P. aeruginosa* produces biofilm alginates that 'cement' the bacterial cells to surfaces [131].This may have the effect of decreasing the removal of biofilm by sonication and thereby decreasing the number of viable counts in Figure 61. The thicker biofilm may also resist wash-off from the numerous washing steps in bio-specimen preparation, which would also account for this result.

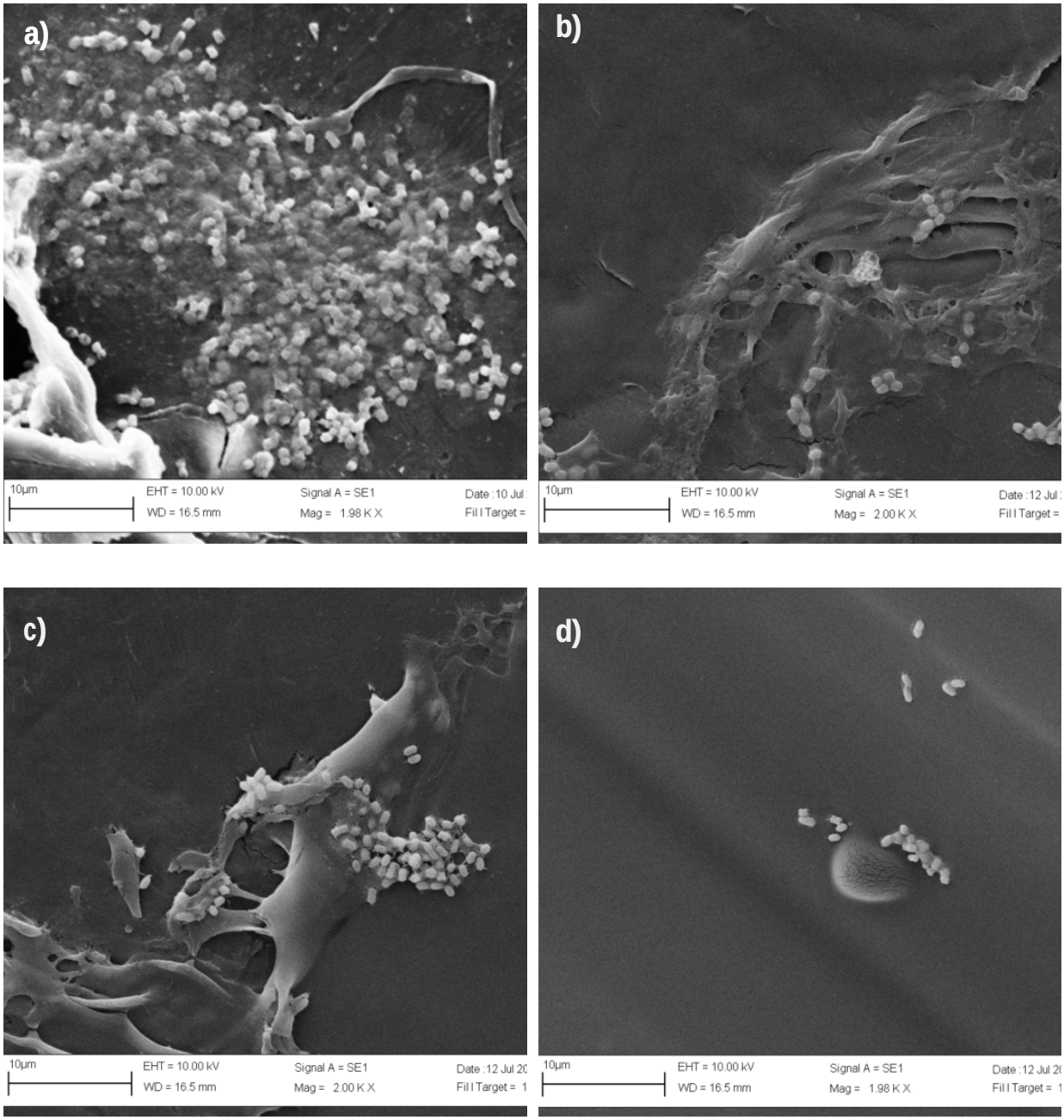

Figure 65. Biofilm assay: *E. coli* culture of discs with different surface coatings: a) PCL; b) PCL-PVA/Gamma; c)PCL-BG; d) PCL-PVA-BG-Gamma. Magnification 2000x, accelerating voltage = 10kV.

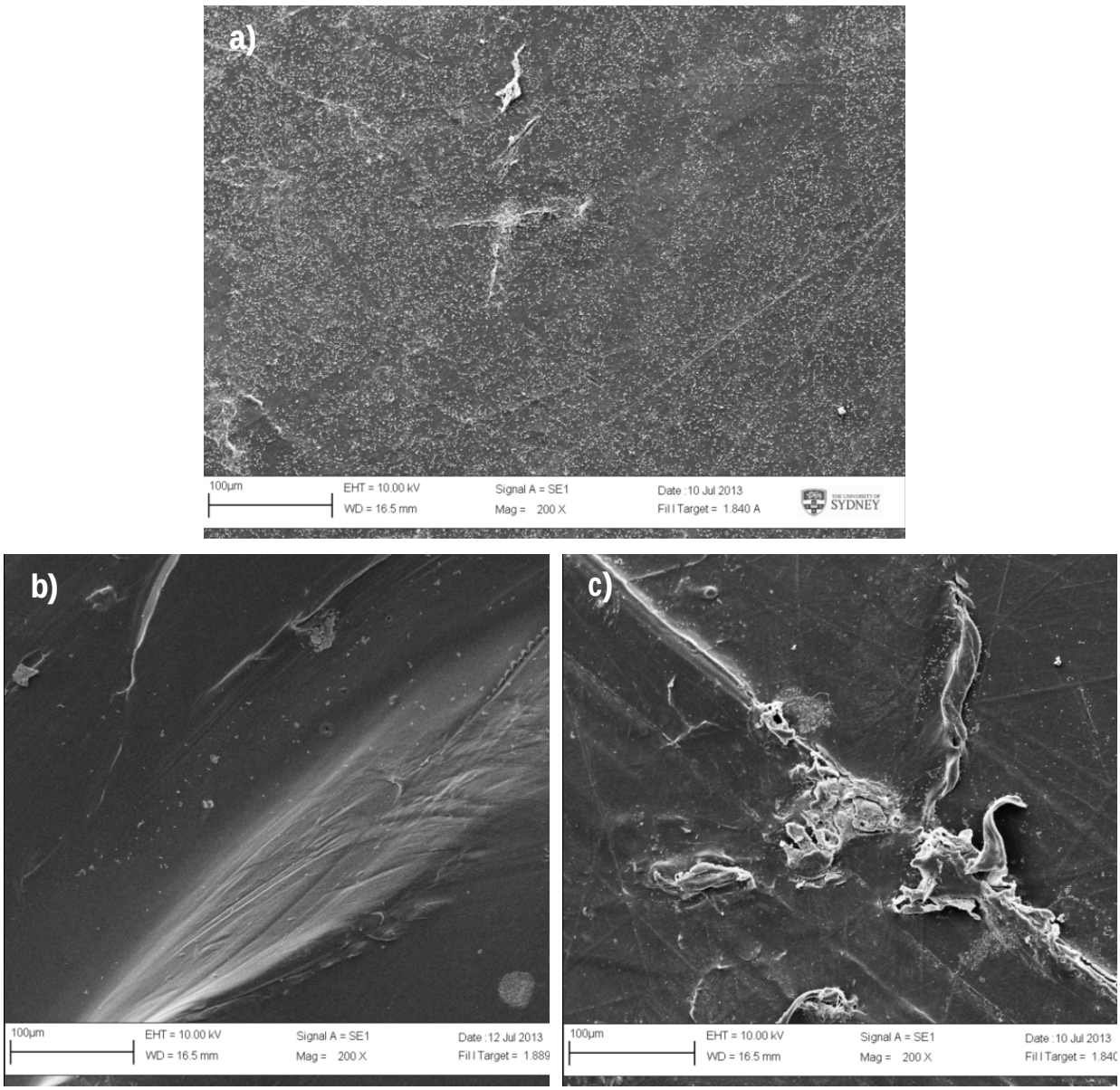

Figure 66. . Biofilm assay: Culture of PCL discs. The white specs on the surfaces are bacterial cells of: a) *P. aeruginosa* b) *S. aureus* c) *E. coli*; Magnification 200x, accelerating voltage = 10kV.

4.2.2 Adhesion of NBB4

4.2.2.1 Effect of Time on NBB4 Adhesion

PCL scaffold quarters that initially appeared white, were shaken in a suspension of NBB4 cells. After around 24 hours the scaffolds appeared yellow and the suspension looked clearer (Figure 67). This was

evidence that NBB4 cells had come out of suspension and were adhering to the scaffold accounting for the colour change.

Figure 67. Scaffold turned yellow after 24 hours in the presence of NBB4. This is due to NBB4 adhering to the scaffold.

The extent of NBB4 adhesion was quantitatively determined by measuring the turbidity (absorbance at OD600) of the cell suspension around the scaffold. The assumption was a decrease in OD600 relates to cells coming out of suspension by adhering to the scaffold. Considering that the suspension started at a high OD600 the greater the change in OD600 the more cells were adhering to the scaffold. This method for determination of adhesion is the same as the principle used by Kuyukina *et al* [227].

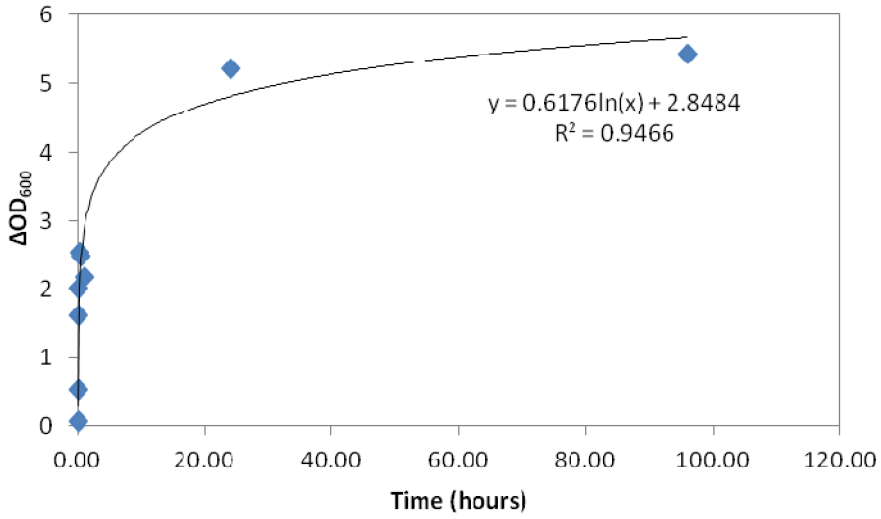

Figure 68 Adhesion Time course: The change in OD600 is measured over time.

The OD600 of the suspension decreased with time. The graph above (Figure 68) shows a rapid drop in OD600 in the first hour. The OD600 levels out and is near its lowest after 24 hours. This indicates near complete adhesion of the NBB4 cells to the scaffold surface such that there is no free scaffold surface area for more cells to attach. Growth of NBB4 is not affectiong the results of this assay. If growth were occurring the surrounding PBS would become more turbid and thus the ΔOD600 would decrease again with increased time. This does not occur - A logarithmic relation ship describes this phenomenon. From this experiment on, 24 hours would be used as the time for adhesion assays as extra cells ceased to attach beyond this time point.

4.2.2.2 Effect of Growth Phase

NBB4 was cultured in the presence of ethylene and harvested at different OD600 absorbencies: 0.1, 0.2, 0.3, 0.4, and 0.8. Lower OD600 absorbencies correlate to earlier stages of growth. The adhesion assay described earlier was performed, but measuring absorbance of only the initial suspension and after 24 hours. The change in OD600 over this time was calculated and divided by the initial OD600 reading to determine the proportion of adhesion or the adhesion efficiency:

$$\%\text{adhesion} = (OD_1 - OD_0)/OD_0 \times 100 \qquad (11)$$

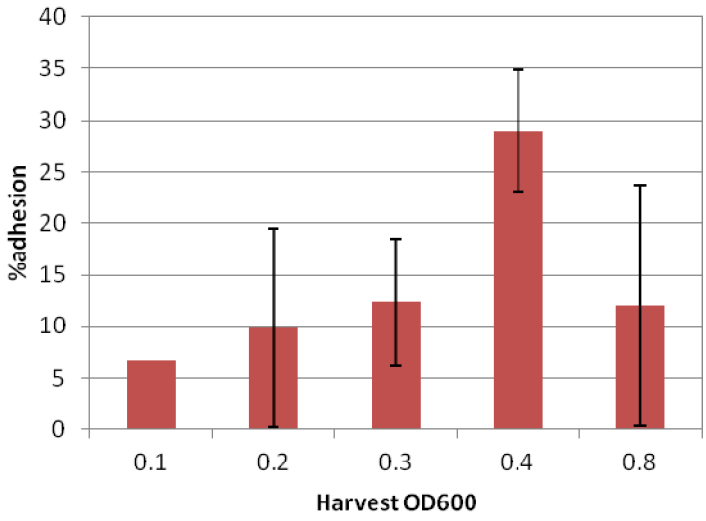

Figure 69. Effect of Growth Stage on Adhesion. The chart indicates the mean percent adhesion of NBB4 cells harvested at differing OD600 values to scaffolds. Error bars indicate ± Standard Deviation. Tests were carried out in triplicate.

Growth phase seemed to have an effect on the proportion of adhesion (Figure 69). There was little difference in the adhesion of NBB4 cells harvested at 0.1, 0.2 and 0.3 with adhesion efficiencies of less than 15%. NBB4 cells harvested at OD600 = 0.4 adhered to the scaffolds far more effectively with 28.97% of cells binding to the scaffold. NBB4 cells harvested at OD600 = 0.8 had a lower adhesion efficiency of only 12.03%.

The adhesion assay proved very inconsistent indicated by the large error bars on the chart. During the experiment, yellow slime build up was seen on the walls and bottom of glass McCartney bottles (Figure 70). This indicates preferential adhesion to the glass bottle as oppose to the scaffold and may explain the variability in the results. The NBB4 falling out of suspension and aggregating on the glass bottle is a symptom of the method and therefore uniform, thus the results still are valid for showing the trend of adhesion to the scaffold with varying growth phase in a semi-quantitative manner.

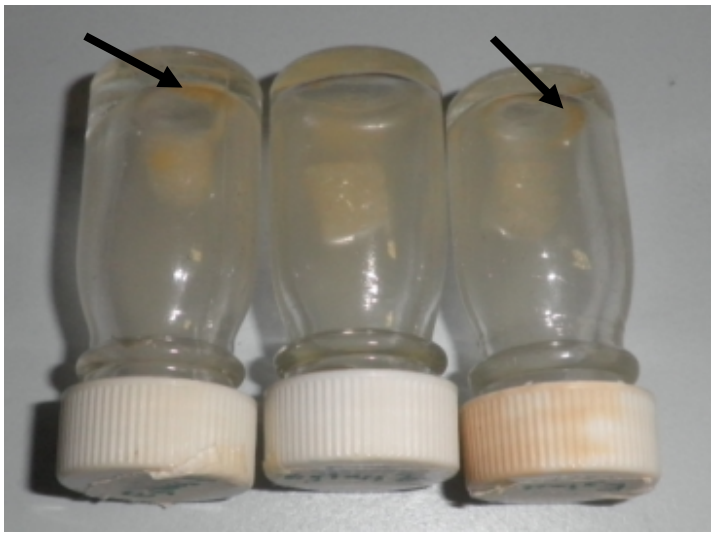

Figure 70.NBB4 cell aggregates on glass bottles during adhesion assay. Arrows point out yellow cell aggregates.

A trend was seen whereby an optimum growth phase for adhesion was found at OD600 of 0.4. This agrees well with a study by Alavi *et al* [120] that found *Mycobacterium marinum* adhered most efficiently to polypropylene supports at a growth phase OD600 = 0.4. The suggested mechanism for this result is *Mycobacterium sp.* develop a thicker capsule in late stationary growth-phase that envelopes the cell wall components and inhibits adhesion to hydrophobic surfaces [120, 123]. Our results suggest a similar mechanism exists: NBB4 (which is a *Mycobacterium sp.*) develops a thicker capsule at later

growth stages which inhibits its adhesion to the hydrophobic PCL surface of the scaffold. As such NBB4 would be grown to OD600 = 0.4 for future adhesion assays.

4.2.2.3 Alteration of Scaffold Surface

In attempt to improve the hydrophobicity and surface area of the scaffold to increase the adhesion of NBB4, the scaffold was coated with ceramic powders. Particles E-glass and Hydrophobic Silica were coated and adhered onto the scaffold, which was validated by macroscopic examination. The adhesion assay was performed on these scaffolds to see if NBB4 could be adhered more efficiently and more reliably. Adhesion efficiency was calculated using the Equation (9) above.

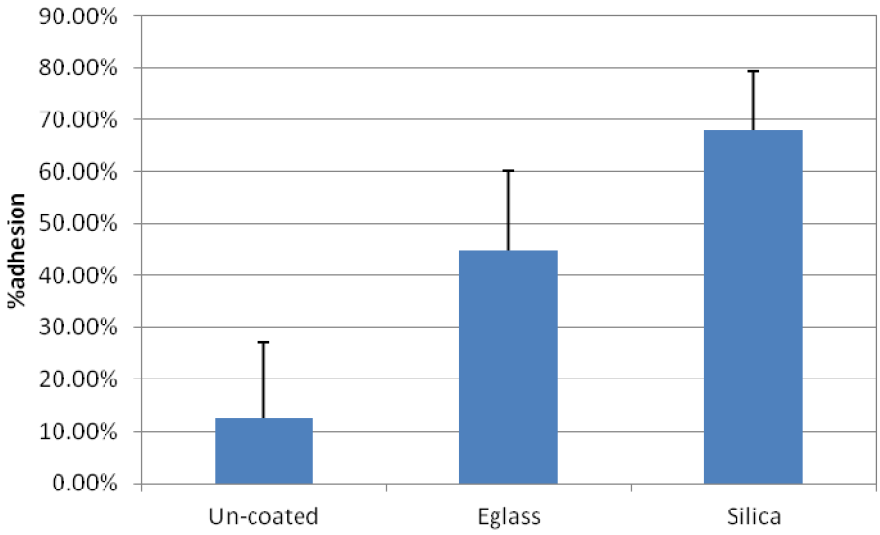

Figure 71. Effect of Scaffold Coatings on Adhesion of NBB4. The chart indicates the mean percent adhesion of NBB4 cells to scaffolds with different coating: Un-coated (control), E-glass, Hydrophobic Silica. Error bars indicate ± Standard Deviation. Tests were carried out in triplicate.

Un-coated scaffold control showed a low adhesion efficiency and low reliability as seen by the large standard deviation compared with the mean (Figure 71). Coating with E-glass and Silica increased the adhesion efficiency dramatically, to 45% and 68% respectively. The standard deviation was much smaller compared to the mean in these samples as seen by the error bars in the chart. This indicates higher reliability using these coatings.

From previous results (Results & Discussion 4.2.1) the attachment of glass particles greatly increases the surface area of scaffold allowing more room for initial adhesion onto the scaffold. This may account for the increased adhesion efficiency seen in coated scaffolds. The silica has a particularly high surface area

at ~120m^2/g possibly accounting for the further increase in adhesion. Hydrophobicity is known to be important in bacterial adhesion [123]. Changes in the surface hydrophobicity due to the coatings may also account for the increased adhesion of NBB4, as Mycobacterium are more likely to adsorb to hydrophobic surfaces [226]. The silica coating was extremely hydrophobic to the extent that the silica is barely miscible in aqueous solution.

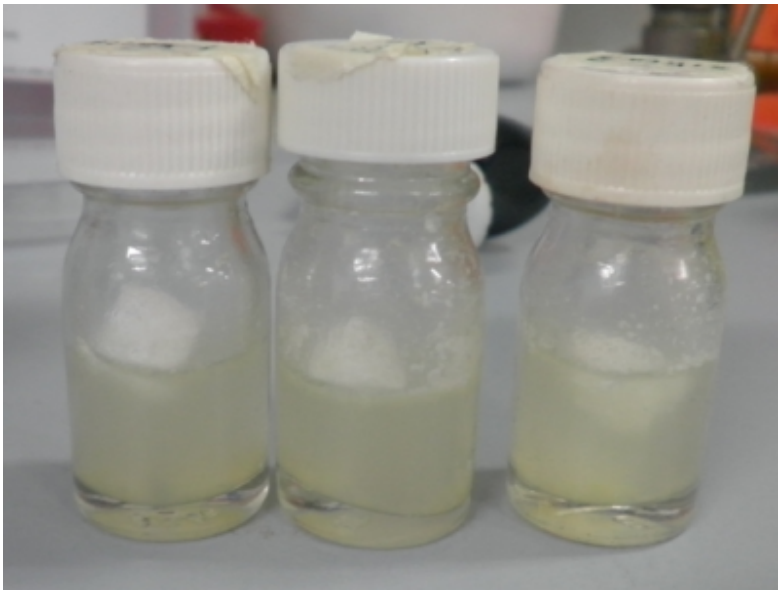

Figure 72.Silica coated scaffolds were so hydrophobic they were difficult to submerge and floated above the cell suspension.

However, as seen in previous experiments clumping of NBB4 cells was observed and much of the drop in OD600 was due to adhesion to the bottle as oppose to the scaffold. With the coated scaffolds in particular this was true, as loosely coated particulates fell into solution and attracted adhesion making the results seem somewhat invalid. Further problems resulted from failure to submerge the hydrophobic silica-coated scaffolds properly (Figure 72). Excess shaking in attempt to submerge the scaffolds in the NBB4-suspension resulted in a large proportion of the coating being dislodged. The impractical nature of this coating due to its ultra-hydrophobicity makes it unsuitable for adhering bacteria for biofiltration.

It was concluded that due to experimental problems the adhesion efficiency of coated scaffolds was not certain and given the extra manufacturing time required and characterisation difficulties that this was not a practical strategy to produce NBB4-adhered biofilters.

4.2.2.4 Alteration of Cell Surface

From the growth phase results obtained above (Results & Discussion 4.2.2.2), it was suspected that NBB4's slimy cell envelope was decreasing the hydrophobic interaction with the scaffold and preventing adhesion. NBB4 cells were washed in solvents to strip away this envelope and increase adhesion with the scaffold. Another strain, NBB3, also containing the SDMO for degrading ethylene was tested for its adhesive abilities. NBB3 does not have the slimy cell envelope like NBB4 and thus may have a stronger hydrophobic interaction with the scaffold.

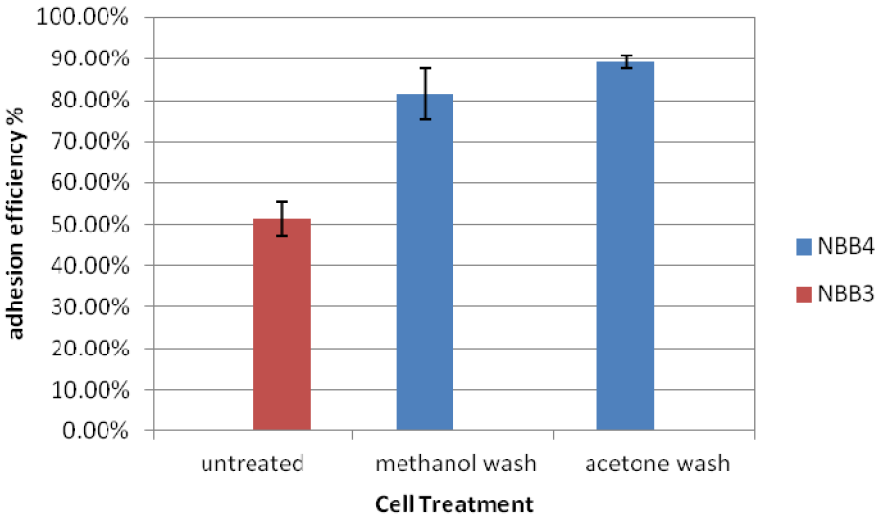

Figure 73. Affect of altered cell surface on bacterial adhesion to scaffold. NBB3 cells were left untreated whereas NBB4 cells were treated with the solvents specified. Error bars indicate ± Standard Deviation. Tests were carried out in duplicate.

NBB3 cells had an adhesion efficiency of 51.32%. This is much higher than previous NBB4 adhesion efficiencies. NBB4 cells treated with washing in methanol and acetone, recorded adhesion efficiencies of 81.47% and 89.17% respectively. However, once again and in this assay in particular cell clumping and adhesion to the glass bottle will have accounted for the majority of the adhesion. The distinct yellowing of NBB4 and NBB3 was seen in these scaffolds [233, 235], but only superficially and in a patchy rather than homogenous manner, suggesting cell-to-cell adhesion was being increased rather than cell-to-scaffold. The results confirm the importance of hydrophobic interactions for *Mycobacterium* adhesion [120, 123, 226].

Despite the encouraging adhesion efficiencies after altering the cell surface, there was concern that:

a) the adhesion seen was superficial – cells were not immobilised and would be sloughed off by physical contact
b) the washing in solvents left the cells unviable and deactivated the cell's ability to degrade ethylene

The ethylene degradation of NBB3 and solvent treated NBB4-scaffolds was tested and the results are shown below (Results and Discussion 4.3.3.2).

4.2.3 Gel Entrapment of NBB4

SEM images were taken of NBB4 biofilter scaffolds of varying agar concentrations. An image at minimal magnification was captured to exhibit the porous architecture of the scaffolds. The increased occlusion of pores can be seen in scaffolds with higher agar concentrations. This correlates with the data presented in Results & Discussion 4.1.1 where a similar coating method was used. The 0.6% agar NBB4 biofilter looks particularly clogged (Figure 76a). However this may be because that surface of the scaffold was toward the bottom during the drying step. During this period molten agar may have continued to migrate to the bottom of the scaffold due to gravity.

The lower SEM image in each figure is a higher magnification micrograph focussing on the NBB4 cells adhered to the scaffold. The NBB4 can easily be distinguished: The cells appear brighter due to absorption of the osmium stain; they are the right shape – short rods approximately 2μm x 1μm [233, 235]; and they are behaving like bacteria forming biofilm communities [121]. NBB4 were seen on the surface of all agar coated scaffolds which means all iterations may be able to degrade ethylene.

These images may also provide insight into how these biofilms formed. In Figure 75, some NBB4 cells are seen partially covered by the agar coating. This suggests that NBB4 entrapped within the gel as been allowed to come to the surface as the gel coating dehydrated. In Figure 78 imprinted of NBB4 rods in the agar coating are further evidence for entrapment in the agar hydrogel. The imprints are probably a result of cells being washed off during the dehydration with ethanol in biological sample preparation, which contains repeated washing steps. In all cases the agar coating appeared very thin which is important as to not inhibit diffusion of ethylene to NBB4 cells [126].

NBB4 is able to form natural biofilm on the scaffold or agar surface. Evidence of this is seen in the high magnification images in Figure 78: NBB4 cells can be seen anchoring themselves to the surface utilising pilli-like extensions of their membranes. This biological attachment by the cells reflects the initial stages

of biofilm formation [121, 124]. Further evidence can be seen in Figure 74b, where NBB4 is forming biofilm on PCL characterised by its uniform bevelled appearance rather than the smooth agar. It is probable that the gel entrapment method facilitates immobilization by adhesion by forcing close contact between the cells and the scaffold. This phenomenon of enforced adhesion is not documented in gel entrapment immobilization literature. Although gel entrapment in agar had been documented to impart biofilm qualities to the entrapped bacteria [218].

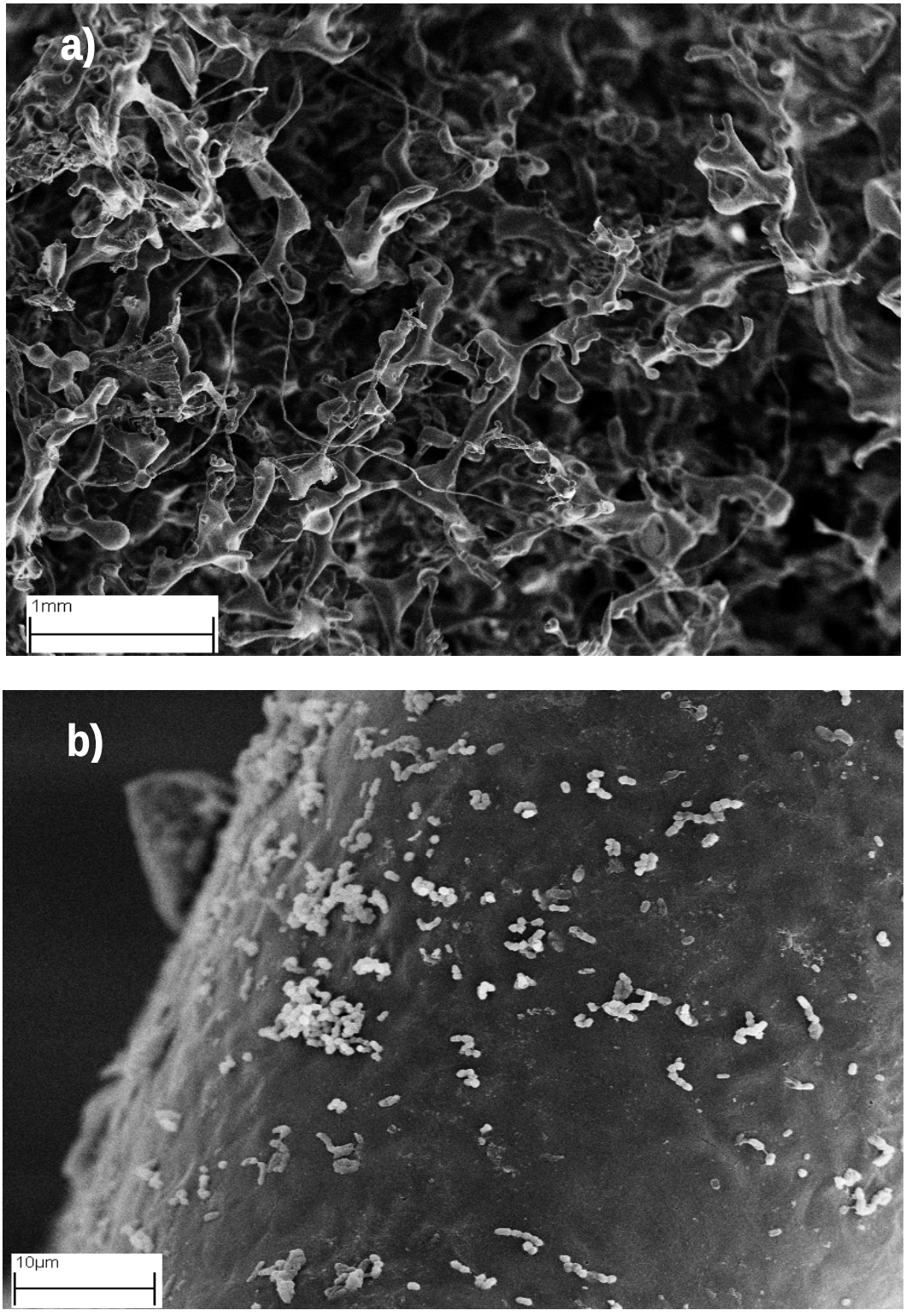

Figure 74. 0.2% w/v agar NBB4-agar-scaffold: a) porous architecture (x50); b) NBB4 biofilms (x5000).

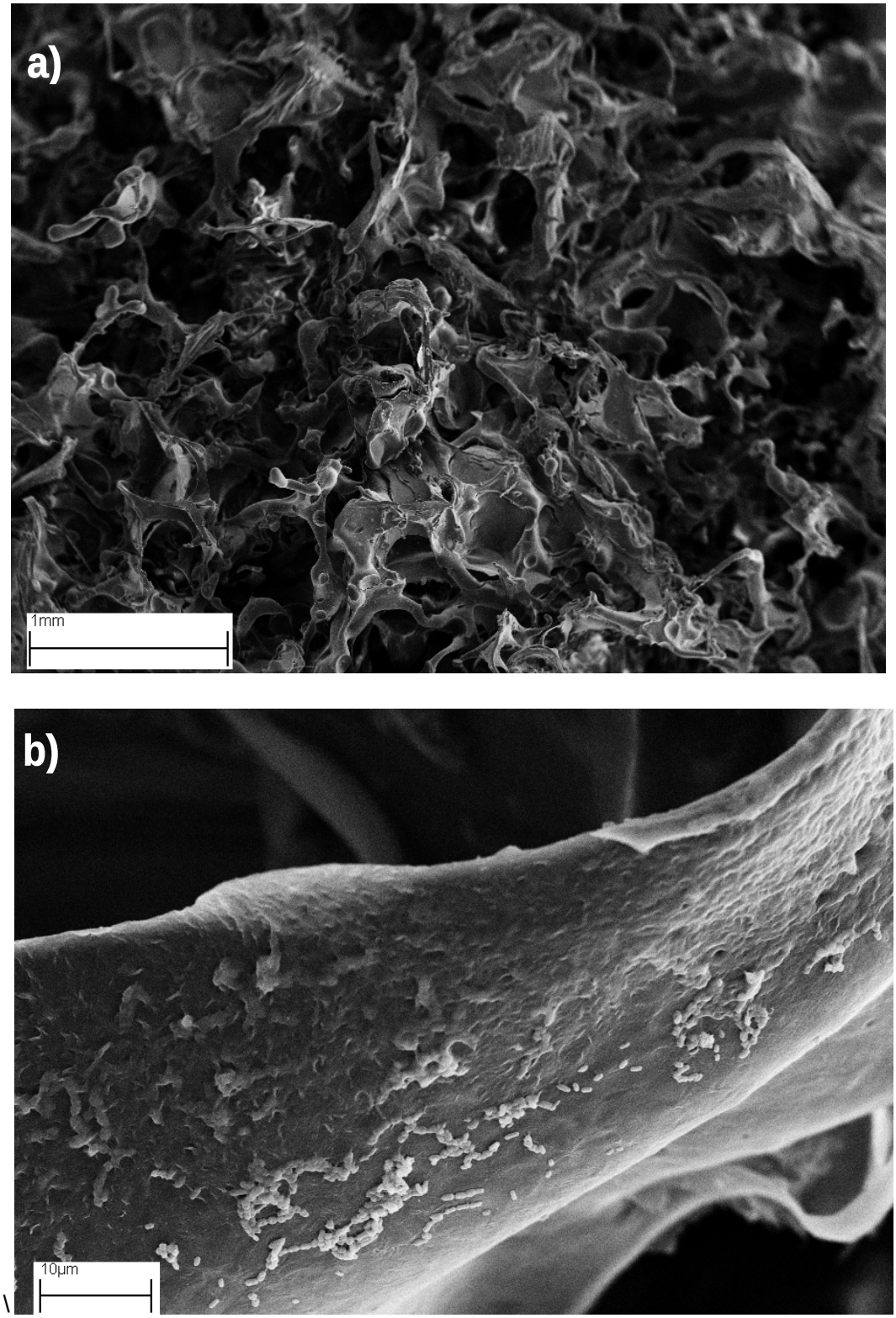

Figure 75. 0.4% w/v agar NBB4-agar-scaffold: a) porous architecture (x50); b) NBB4 biofilms (x5000).

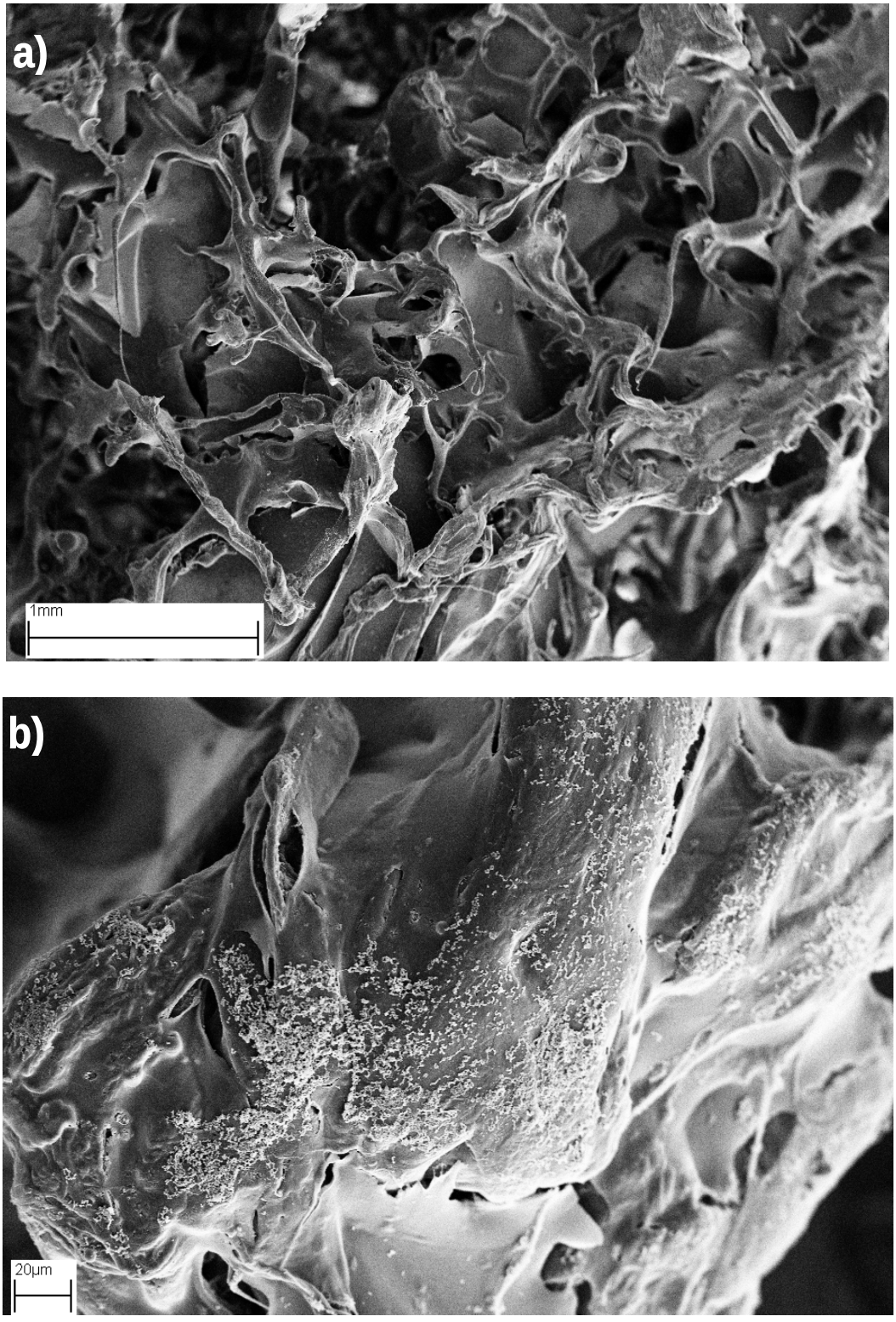

Figure 76. 0.6% w/v agar NBB4-agar-scaffold: a) porous architecture (x50); b) NBB4 biofilms (x5000).

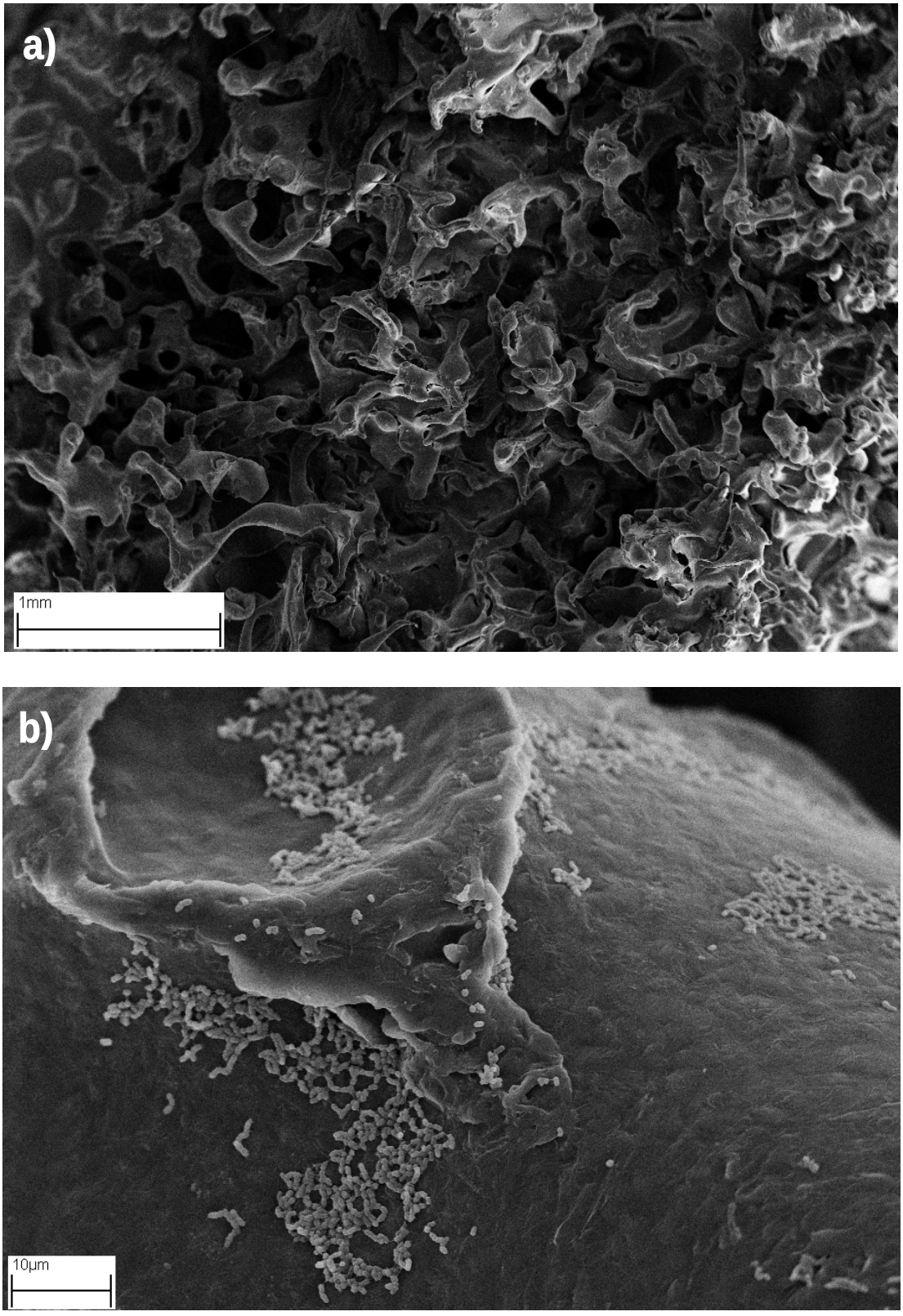

Figure 77. 0.8% w/v agar NBB4-agar-scaffold: a) porous architecture (x50); b) NBB4 biofilms (x5000).

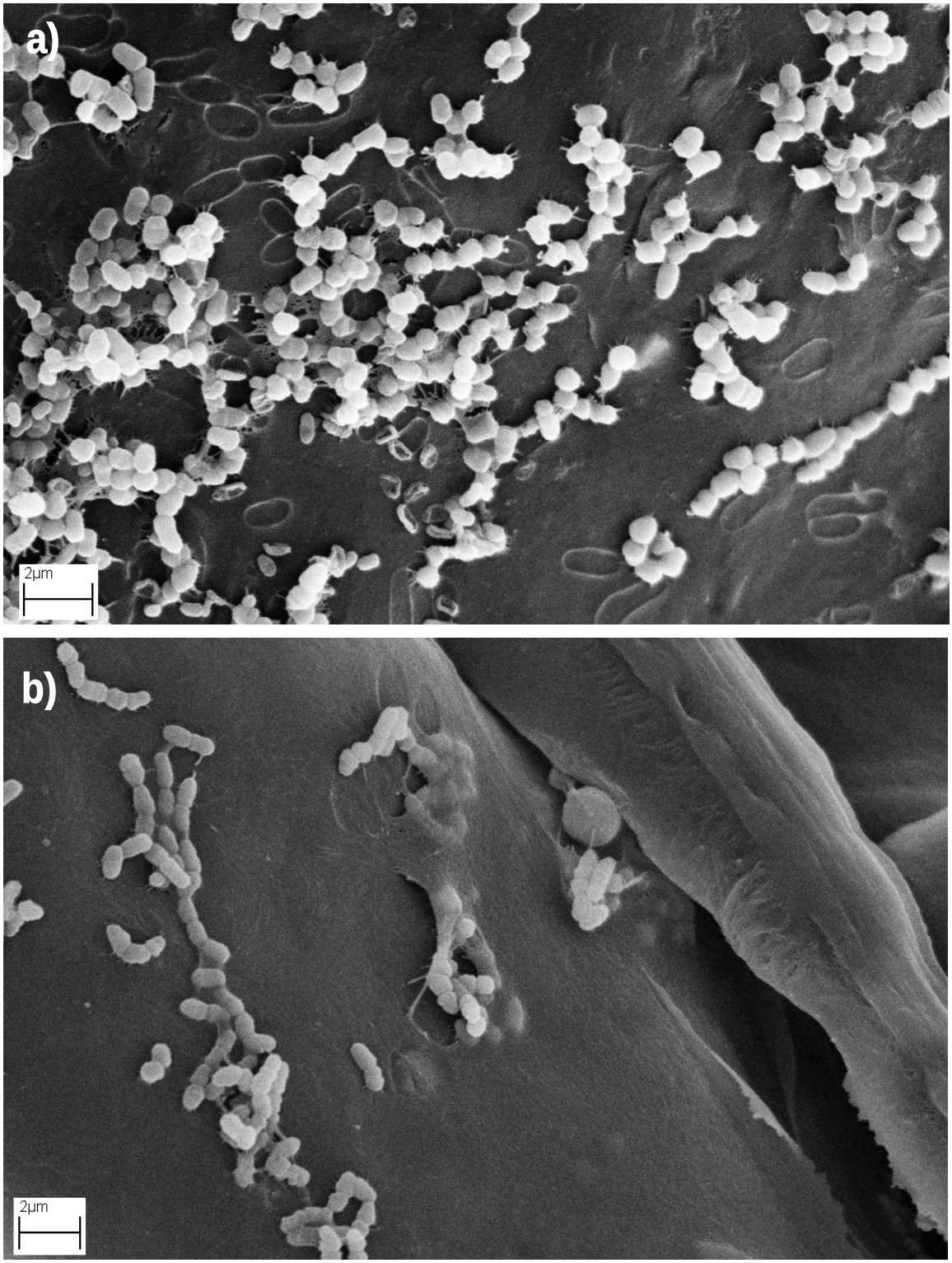

Figure 78. High magnification SEM images of NBB4 biofilms on NBB4-agar-scaffold: a) Imprints of NBB4 cells in thin agar coating (x12000); b) NBB4 biofilms partially entrapped in agar, with visible pilli (x13000).

4.3 Antibacterial/Pro-bacterial Activity

4.3.1 Antibiotic Elution

4.3.1.1 Effect of Ethanol Content on Erythromycin Release

Antibiotic eluting scaffolds were placed in wells of PBS and transferred to a fresh well at set time points. A microbial assay was performed by submerging sterile filter paper discs into these wells then placing them on an inoculated plate of the test organism, *S. aureus*. As explained earlier, the resulting zone of inhibition is proportional to the concentration of antibiotics eluted. A standard curve relating zone of inhibition diameter to erythromycin concentration was plotted and the resulting logarithm (Equation 10, Results & Discussion 4.1.2.2.3) was used to extrapolate results in the following experiments.

Scaffolds manufactured with varying concentrations of ethanol (EtOH) in the PVA solution were tested in this way. Measurements were taken until they fell below the detectable limit, at which point there was no observable zone of inhibition. Erythromycin concentration decreased over time in all samples meaning scaffold were releasing erythromycin at a decreasing rate (Figure 79). The elution profiles followed a text-book two part pattern, with a burst release of erythromycin followed by a prolonged slower release. The burst release is due to erythromycin on the periphery of the hydrogel coating rapidly dissolving. The slower release is controlled by hydrogel kinetics with PVA relaxation and hydrogel channel diffusion affecting erythromycin release. In particular, this phenomenon can be seen around the 6-24 hour mark where erythromycin concentration stayed constant or even was seen to increase. This highlights the time dependence of the elution is owed to hydrogel kinetics rather than simple diffusion which would result in continually decreasing concentrations over time [21-22].

A relationship between the ethanol concentration (%w/v) and the elution profile can be seen: The higher concentration of ethanol that was used, the higher the concentration at a given time and the longer the elution of erythromycin above the detection limit. In Figure 35 the 50% EtOH samples produced by far the greatest burst concentrations of erythromycin with 1478ug/ml recorded after 1 hour of elution compared to 58ug/ml and 47ug/ml for the 25% and 15% EtOH samples respectively. Based on the similar gel properties of these scaffolds determined earlier, it is safe to conclude that this is not due to lower %EtOH scaffolds having vastly slowed release kinetics. It is much more likely due to a much greater erythromycin loading. Erythromycin is 25 times more soluble in ethanol than water [154]. Solubility in mixes is said to follow a logarithmic relationship [254] meaning erythromycin was much

more soluble in the 50% EtOH PVA mixture enabling much more erythromycin to become entrapped in these scaffolds. The increased hydrogel coating thickness (see Results & Discussion 4.1.2.2.1) also played a smaller but not insignificant role in the higher erythromycin loading.

The 50% EtOH scaffold maintained an erythromycin concentration above the detectable limit for 5 days. It should be noted that here the 'detectable limit' is directly related to the MIC for *S. aureus*. This was significantly longer than for the 25% sample (48 hours).The 50% EtOH scaffold exhibits slow delivery of antibiotic that will protect skin wounds from *S. aureus* bacteria over the 5 day period. Therefore this scaffold was chosen for use in future experiments and device pilot studies.

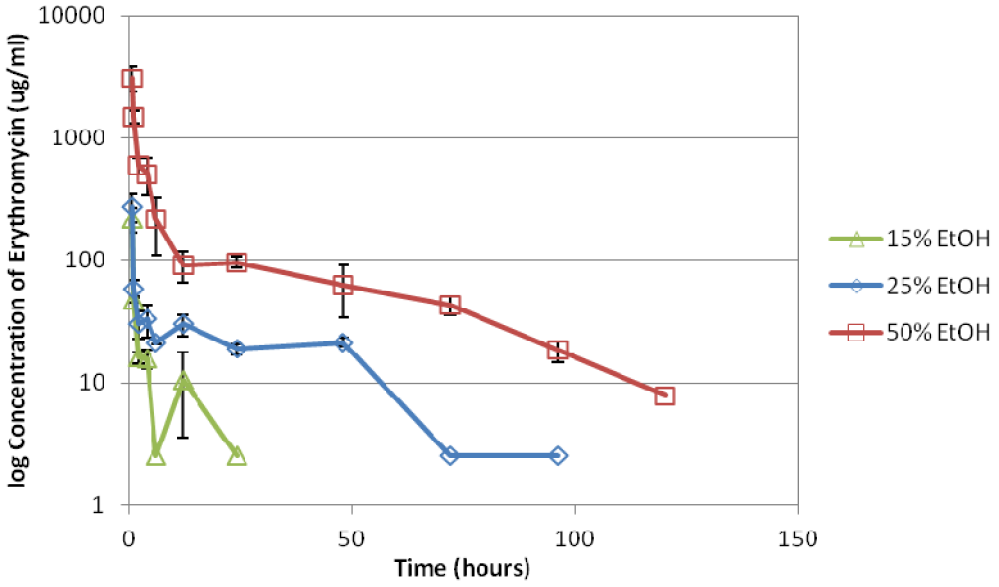

Figure 79. Drug delivery of erythromycin from scaffolds manufactured with varying amounts of ethanol (EtOH). Error bars = Std; n = 3.

4.3.1.2 Effect of Gamma Sterilization on Erythromycin Release

Gamma irradiation at sterilization doses are known to cause alterations in many polymers which may affect the performance of sterilised devices and therapeutics [8, 17, 82, 91]. Further, Gamma irradiation has been known to inactivate drugs [163]. The following investigation was performed to identify changes in the elution profile of the PVA-erythromycin scaffold following gamma sterilization at 25kGy.

A batch of erythromycin scaffolds were manufactured with 50% EtOH PVA as described above. A proportion of these scaffolds were Gamma sterilised at 25kGy and their elution profiles were compared

to the un-sterilised controls. Testing was conducted in the same manner as in 4.3.1.1. Scaffolds tested were of the same batch to account for natural time-dependent drug degradation.

In Figure 80, the two elution profiles are virtually superimposed indicating that there was no difference in the elution or activity cause by Gamma sterilization. Both sterilised and unsterilized scaffolds maintained erythromycin concentrations above the detectable limit for 96 hours. This elution time is slightly less than seen in 4.3.1.1, probably due to variations in the erythromycin loading from batch to batch. The burst release does not reach as high concentrations suggesting loading is likely the case.

The results validate gamma irradiation at 25kGy as a viable sterilization method for this device, as neither the activity nor the elution kinetics of the drug seems to be compromised. Toward the end of the drug delivery period (between 48 and 96 hours), the Gamma sterilised scaffold registered higher erythromycin concentrations. This may reflect slower elution kinetics which may be beneficial if a relevant erythromycin concentration can be maintained for a longer period and would offer greater protection from wound infection. Increasing Gamma irradiation dosage may cause slower kinetics due to PVA crosslinking and should be investigated in the future. Improvements caused by sterilization are sought after as they add favourable properties at no added manufacturing cost [17, 181].

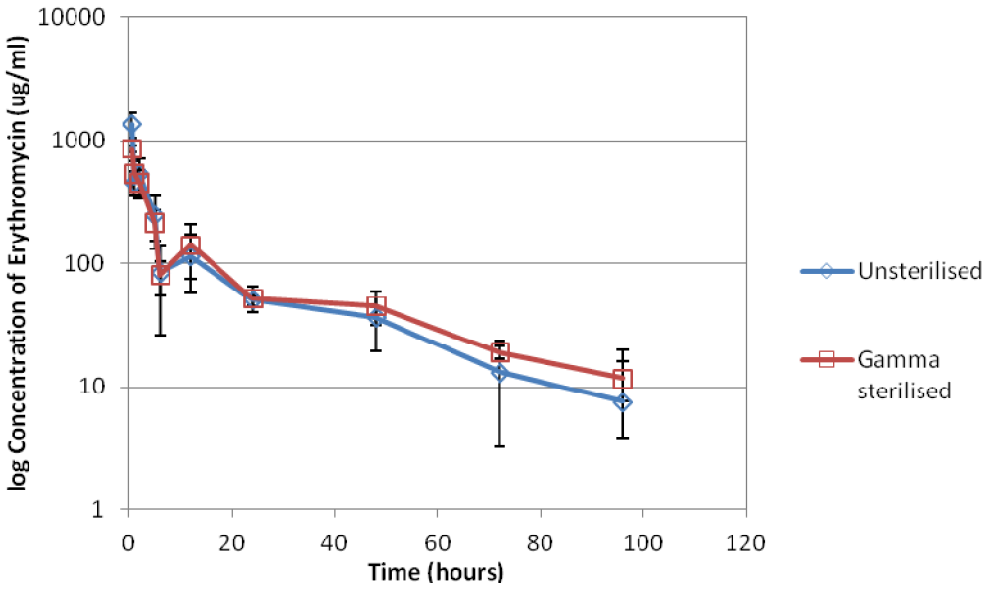

Figure 80. Drug delivery of erythromycin from scaffolds after gamma sterilization at 25kGy. Error bars = Std; n = 3.

4.3.1.3 Cytotoxicity of Erythromycin

The burst release of erythromycin seen in the release profiles (Results & Discussion 4.3.1.1) may represent cytotoxic concentrations that would impact the bioactive efficacy of the wound healing graft. As such, a dose-response experiment was setup to measure the cytotoxicity of erythromycin on human fibroblasts (HFb).

The MTS reagent contains tetrazolium and phenazine ethosulfate as an electron transfer reagent that facilitates cellular reduction into a coloured soluble formazan [255]. In this way essential metabolic activity can be measured colorimetrically and related to cell viability: Increased cellular metabolism brings about an increased colour change and an increased absorbance at 490nm.

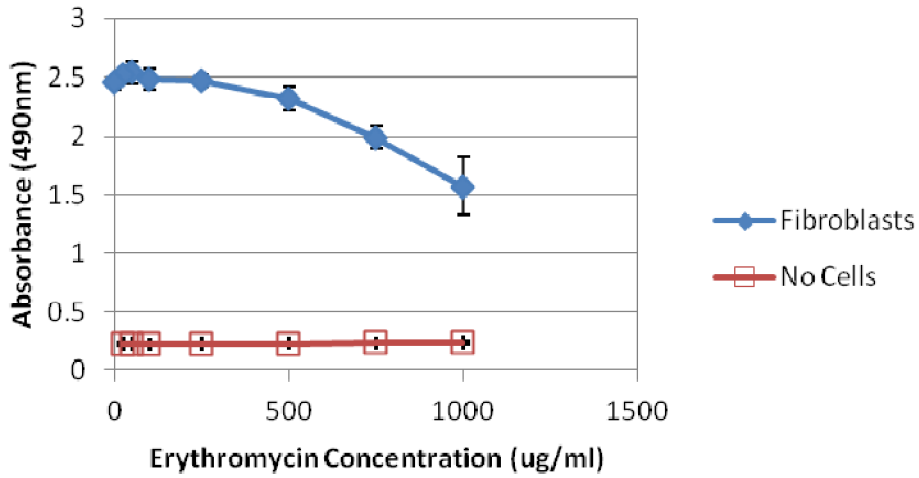

Figure 81. MTS assay: dose-response of Human Fibroblasts (HFb) treated with erythromycin. Error bars = std; n = 3.

The results show that erythromycin in the media had no effect on the assay at the concentrations tested. All concentrations (0 - 1000μg/ml) produced an absorbance of ~0.23. The addition of fibroblasts elicited a strong absorbance at 490nm, reflecting the active metabolism of the cells. Figure 81 shows a trend: Increasing concentrations of erythromycin caused a decrease in absorbance. The dose response curve shows a plateau in absorbance from erythromycin concentrations of 0 - 500 μg/ml, then drops quite steeply between 500 - 1000 μg/ml. In the graph it appears that the absorbance has already started to drop between 250-500 μg/ml but the difference in absorbance between the 0 μg/ml and 500 μg/ml samples was not statistically significant ($p > 0.05$, Student's T-test).

The decreased absorbance seen at erythromycin concentrations of 750 μg/ml and 1000 μg/ml represent a loss in HFb viability. This loss of viability is due to cytotoxic effects from the high concentrations of erythromycin. The mechanism of cytotoxicity is not well documented but could be due to leakage of enzymes [159]. 500 μg/ml was found to be the maximal concentration that caused no significant loss of viability to HFbs. This result is little higher than found by Byarugaba *et al* - 300 μg/ml, although this difference could be due to a number of factors such as differences in erythromycin drug potency and cell lines [158]. Some have remarked that macrolides, such as erythromycin have low cytotoxicity [155-156] and this is true in the sense that the MIC for most pathogens is significantly lower [157]. However, compared with other antibiotic candidates, such as gentamycin, it is significantly higher [158]. The cytotoxicity of an antibiotic is especially important in drug delivery devices as this has an impact on drug loading limits and therefore sustained drug release. This also has a significant negative impact on bioactivity.

For future experiments and design, 500 μg/ml was considered the maximum concentration of erythromycin that would not elicit a cytotoxic response from HFb.

4.3.1.4 Erythromycin Soak-off

Scaffolds were immersed in sterile PBS to remove burst release of erythromycin. This was designed to prevent erythromycin concentrations from reaching the cytotoxic level for fibroblasts found earlier to be approximately 500ug/ml (Results & Discussion 4.3.1.3). Scaffolds were immersed in the PBS for varying times in order to control the amount of erythromycin soaked off. Then scaffolds were blotted dry on sterile filter paper and transferred to the test wells where erythromycin elution was measured using the microbial assay described above.

Even the shortest soak-off time (15 minutes) did not produce an erythromycin concentration higher than the 500ug/ml cytotoxic level after a 24 hour elution time (Figure 82). The 15 minute soaked scaffolds registered the highest concentrations at each time point. This was followed by the 60 minute and 30 minutes soaked samples respectively. One would expect that a shorter soaking time would result in less erythromycin being soaked off and consequently an elution profile of higher concentrations, as was the case with the 15 minute sample. However this was not the case with the 30 minute-soaked samples producing lower concentrations than 60 minute soaked samples. The differences in these concentrations were not particularly significant ($p > 0.05$) as can be seen from the overlapping error

bars. Despite the soak-off procedure, all samples maintained detectable concentrations of erythromycin for up to 5 days which is similar to other reported DDS using PVA hydrogels [169].

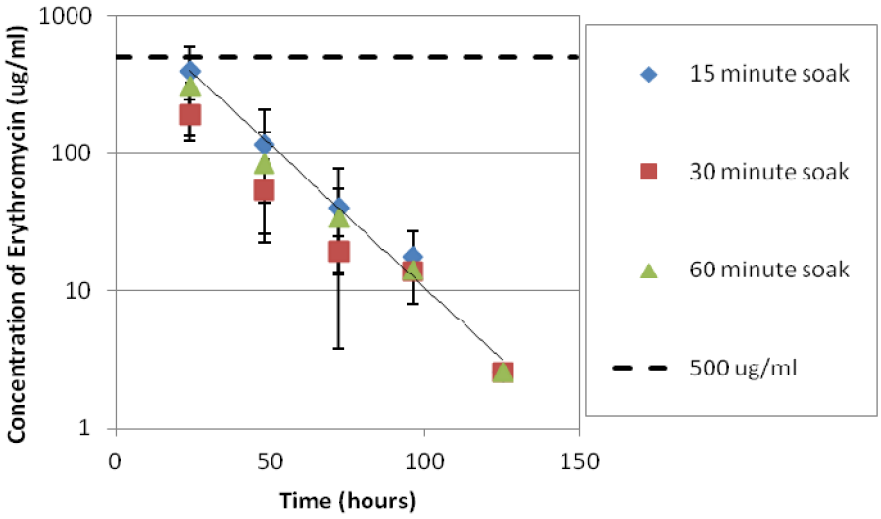

Figure 82.Drug delivery of erythromycin from scaffolds that were soaked in PBS for varied amounts of time. Error bars = Std; n = 3.

When the cumulative release of these scaffolds was plotted for the 24 hour time point, there was no difference seen in the cumulative release of erythromycin, with all scaffolds having lost around 70% of their erythromycin since the soak-off (Figure 83). If less erythromycin was removed in the 15 minute soak compared to the 60 minute soaked scaffold, the cumulative release would be expected to be greater as more of the burst release was maintained. This could indicate that the soak off could be even shorter and any variation in the elution profiles was due to minor differences in scaffold size (which cumulative release measurements account for).

The results from this experiment show that a quick soak-off in PBS can prevent the scaffold erythromycin concentration from reaching cytotoxic levels. Since the 15 minute soak is the most time efficient method to achieve sub-cytotoxic levels, it was chosen as the protocol for further *in vitro* testing.

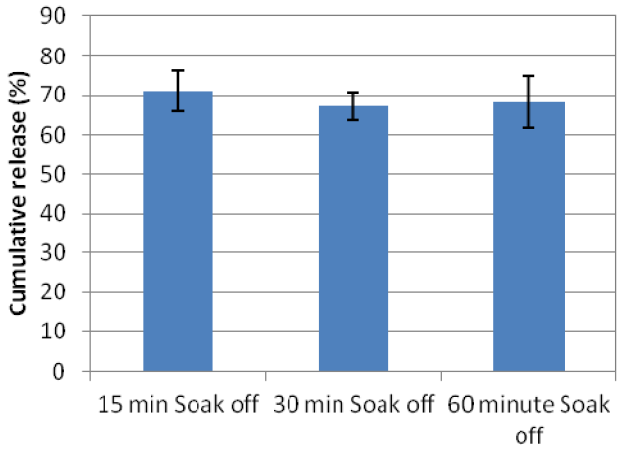

Figure 83. Cumulative release of erythromycin 24 hours post-soak from scaffolds that were soaked in PBS for varied amounts of time. . Error bars = Std; n = 3.

4.3.2 Antibacterial Biomaterials

4.3.2.1 Zone of Inhibition

A pellet or disc of biomaterial was placed at the centre of an inoculated spread plate. The contacting area of the biomaterials was kept constant to limit diffusional variability. Antibacterial activity was quantified by measuring the Zone of Inhibition (ZoI). This was the clear circular region where no bacterial colonies formed on a spread plate after a sufficient period of incubation for colony formation. The size of the ZoI is proportional to antibacterial effect. The results can be seen in Figure 84.

PCL and HA did not elicit a ZoI in any of the test pathogens, suggesting they have no antibacterial activity. There is no evidence of either of these materials being antibacterial in the literature. They are both widely recognised has biocompatible materials [1, 6].

Chloramphenicol is a well-known broad spectrum antibiotic and was used as the positive control for this experiment. chloramphenicol produced a large ZoI in all pathogens tested. The ZoI in P. aeruginosa was significantly less than for *E.coli* and *S. aureus*. This shows that *P. aeruginosa* is comparatively more resistant to chloramphenicol.

Bioglass (BG) produced a ZoI for *S. aureus* and a small ZoI for *E. coli* but none for *P. aeruginosa*. These ZoIs were significantly smaller than for chloramphenicol showing it as a weaker antibacterial material. The antibacterial mechanism for BG is the elution of positive metal ions causing an increase in pH [47,

54]. Based on these results, resistance toward this pH change for these pathogens is: *P. aeruginosa* > *E. coli* > *S. aureus.*

Bulk metallic glass (BMG) caused a ZoI only in *S. aureus*. This ZoI was smaller than both those cause by chloramphenicol and BG for the same organism. The antibacterial mechanism for BMG is likely to be related to elution of the toxic metal ions zinc and magnesium [57, 76]. The results show that *E. coli* and *P. aeruginosa* are more resistant than *S. aureus* toward these ions.

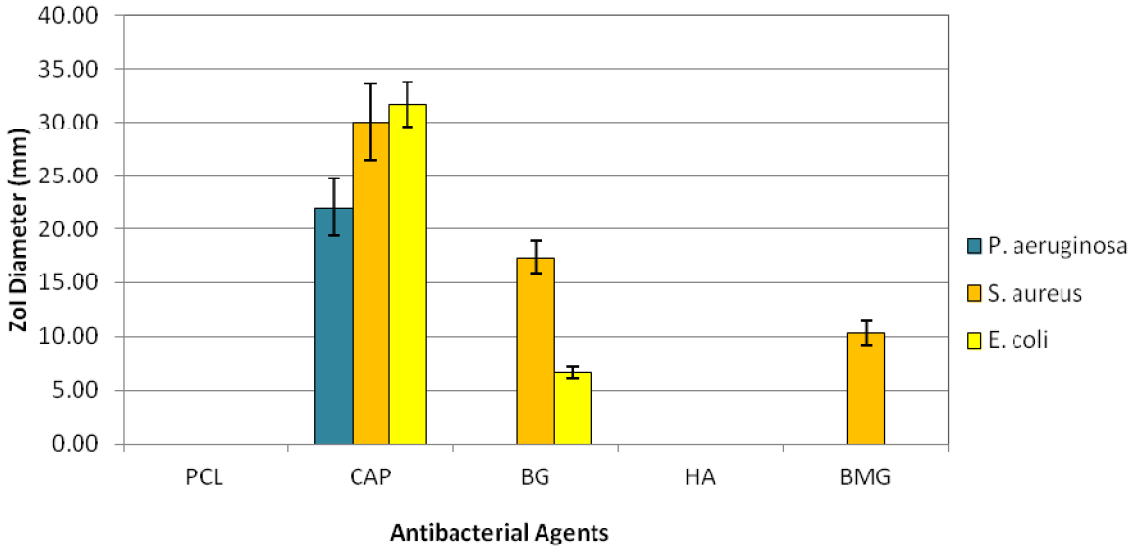

Figure 84. Antibacterial activity of biomaterials. Quantified by a biological Zone of Inhibition (ZoI) assay on three common wound pathogens. Materials tested were: Polycaprolactone (PCL), Chloramphenicol (chloramphenicol), 45S5 bioglass (BG), hydroxy apatite (HA) and Bulk metallic glass (BMG). Error bars = Std; n=3.

4.3.2.2 MIC/MLC Assay

A minimum inhibitory concentration/minimum lethal concentration (MIC/MLC) assay was used to quantify the antibacterial activity of biomaterials found to have some antibacterial effect in the Zone of inhibition (ZoI) study. The MIC is the minimum concentration of the material to inhibit growth in a liquid culture. Growth inhibition was identified by a colorimetric indicator. MLC is the minimum concentration at which no viable cells were left after the incubation period in liquid culture. Viable cells were detected by subsequent culture of growth-inhibited samples on solid media. No colony formation was said to

mean no viable cells. The MIC/MLC is inversely proportional to antibacterial effect of a biomaterial to a pathogen.

It is important to note that for the BMG and the 45S5 the results here are understated; that is the bacteria are subject to lower concentrations than the numerical results. This is because these materials were weighed into a given volume to calculate the concentrations, but the materials did not fully dissolve in volume. It is these dissolution/degradation products that have the antibacterial effect. More experiments would be needed to properly establish the antibacterial mechanism of these biomaterials and quantify them directly if the MIC/MLC are to be accurately determined. This experiment gives insights into scaffold design and antibacterial loading rather than precision antibacterial data. Unfortunately the differences in particle sizes and therefore diffusion between samples was a source of error.

Table 26. MIC/MLC measurements for biomaterials on common wound pathogen.

	P. aeruginosa		S. aureus		E. coli	
	MIC	**MLC**	**MIC**	**MLC**	**MIC**	**MLC**
BMG (mg/ml)	9±1	> 10*	< 2~	< 2~	5±1	3±1
45S5 (mg/ml)	47±12	100±0	47±12	47±12	73±12	100±0
chloramphenicol (µg/ml)	> 10*	> 10*	7±1	> 10*	6±0	> 10*

*** = The maximum concentration tested. ~ = The minimum concentration tested.**

BMG was found to inhibit growth of *P. aeruginosa* at 9 mg/ml. The MLC was above the maximum concentration tested (10 mg/ml). For S. aureus, both the MIC and MLC were below the minimum concentration tested (2 mg/ml). The MIC and MLC for E. coli was 5 and 3 mg/ml respectively. These results agreed well with the ZoI results which revealed S. aureus as the most susceptible to BMG. No inhibition was seen for *E. coli* and P. *aeruginosa* in the ZoI experiment and this illustrates the increased sensitivity of the MIC assay. Poor diffusion of BMG degradation products through solid media may be the reason why the ZoI assay did not result in growth inhibition. The results show that BMG is an effective antibacterial agent for wound scaffold development, as all three pathogens' growth was inhibited at BMG concentrations below 10mg/ml. These concentrations would be possible to achieve using a scaffold to deliver the BMG.

For 45S5 the MIC for *P. aeruginosa* was 47 mg/ml and the MLC was 100mg/ml. The MIC and MLC for *S. aureus* was 47 mg/ml and 33 mg/ml respectively. For *E.coli* the MIC and MLC were 73 mg/ml and 100mg/ml respectively. The results for 45S5 were inconsistent with those found in the ZoI experiment. Bioglass produced no ZoI for *P. aeruginosa* and a considerable one for *S. aureus*, but here the MIC for these pathogens was identical. It is possible that *P. aeruginosa* is more susceptible in liquid culture, as it is known to be a strong biofilm former [121]. Otherwise the *E. coli* was found to be less susceptible than *S. aureus* here, as it was through the ZoI assay. Bioglass elicited a bactericidal effect in all pathogens tested. *S. aureus* was found to have the lowest MLC which was equivalent to its MIC. This shows a very low tolerance and survival rate past a certain concentration of bioglass degradation particles, which is linked to pH [47, 54]. Concentrations required for an inhibitory effect were greater than 45 mg/ml. These are likely not achievable for a skin wound healing scaffold where only a coating is required. As such the bioglass will probably not assert an antibacterial effect when employed as a scaffold.

Chloramphenicol is a potent antibiotic drug and thus was tested at a much lower concentration range. The MIC and MLC for *P. aeruginosa* were above the maximum tested (10 µg/ml). The MIC for *S. aureus* was 7 µg/ml and the MIC was above the maximum. For E.coli the MIC was 6 µg/ml and the MLC was above the maximum. *S. aureus* and *E. coli* were far more susceptible to chloramphenicol than *P. aeruginosa* which matches the ZoI results. No MLC result was found for any pathogen. This is because chloramphenicol is generally a bacteriostatic drug [150], and after re-inoculation on fresh media inhibited cells can grow once more.

From the results BMG may be suitable as an antibacterial scaffold coating as it has a bactericidal effect at low enough concentrations that can be achieved by loading onto the scaffold. In contrast, bioglass as a scaffold coating will not be present in large enough amounts to reach inhibitory concentrations. Antibiotics such as chloramphenicol have an antibacterial effect at much lower concentrations and given the limited space on the scaffold, this positions antibiotics best as providing sustained protection from bacteria. Alternate antibiotics such as erythromycin may be better for wound healing then chloramphenicol due to their greater antibacterial effect against common wound bacteria such as MRSA [157].

4.3.3 Bacterial Ethylene Degradation

4.3.3.1 Optimisation of Agar Concentration

Batches of NBB4-agar scaffolds were manufactured with varying agar concentrations. Batches of 0.2% agar scaffolds with no NBB4 cells and batches of 0.4% agar cubes were tested as controls. The scaffolds were placed in gas-tight bottles and injected with ethylene. Whole batched were used to decrease variance in the results due to structural variation from scaffold to scaffold. This is also more relevant as the final device would likely be a filter system containing many packed scaffolds. Bottles were injected with ethylene which was periodically measured by GC.

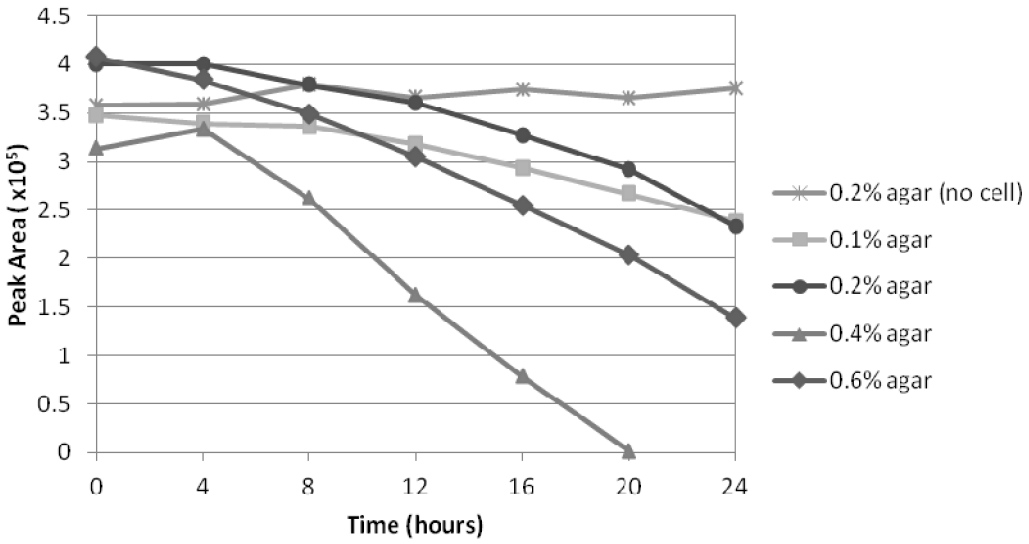

Figure 85. Degradation of ethylene by NBB4 coated scaffolds of varying agar concentration over 24 hours. Ethylene is represented by GC Peak area which decreases over time in a linear fashion. The no-cell control scaffolds show no change in Peak Area.

Ethylene produced a characteristic peak after approximately 1.1 minutes. GC readings given in peak area were plotted against time from which linear relations were found from the Excel software (Figure 85). Generally linear relations were calculated from the 4 hour time point as the NBB4 cells seemed to not degrade ethylene for the first 4 hours. The gradient of the line was the change in GC peak area over time. These were converted to ethylene degradation rate, in parts per million per hour (ppmV/h) by applying the formula obtained by running a standard curve of ethylene concentrations through the GC.

The combined results from the ethylene degradation tests of all scaffold batches is summarised in Figure 86. The agar-scaffold composites with no NBB4 cells did not degrade ethylene. This proves that the

NBB4 is solely responsible for ethylene degradation and no ethylene is removed via physical or chemical interactions with the scaffold or agar gel. They NBB4 gel entrapped scaffolds as well as the NBB4-agar cubes were able to degrade ethylene at variable rates. Of these the 0.4% scaffold was the most effective with a mean ethylene degradation rate of 21ppmV/h. This was significantly greater than the 0.1% and 0.2% agar scaffolds but not the 0.6% scaffolds. However, it was found that the difference between the 0.6% scaffold's degradation rate of 16ppmV/h and the 0.1% and 0.2% scaffolds was not statistically significant. The 0.4% scaffolds degraded ethylene at a significantly faster rate than the agar cubes of the same agar concentration.

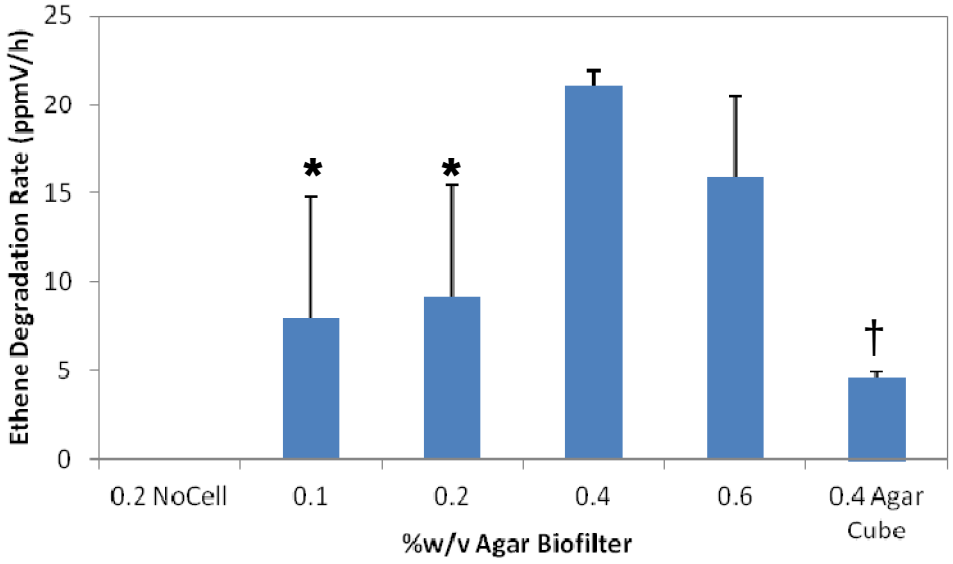

Figure 86. Identification of optimal agar concentration of scaffold coating based on ethylene degradation rate. Error bars = Standard deviation; n=3. Significant difference compared with 0.4%w/v biofilter using Student's t-test: *($p \leq 0.05$); †($p \leq 0.001$).

The agar concentration has already been shown to be inversely proportionate to the composite porosity (4.1.1). However the agar concentration was also shown to be proportionate to the gel volume and thus the number of entrapped NBB4 cells if one assumed the bacteria is evenly suspended in the liquid gel. Furthermore, porosity is known to promote diffusion of ethylene through the composite. Therefore, it was hypothesised that there would an optimal agar concentration that produced a biofilter which balanced porosity and NBB4 numbers for a maximum ethylene degradation rate. From the results the 0.4% is thought to be the optimal agar concentration.

The fact that cubes of agar containing NBB4 showed a much decreased degradation rate speaks to the importance of porosity in a biofilter design. These agar cubes had a much higher gel volume than the

scaffolds and consequently many more NBB4 cells – the active ethylene degraders. The lacking porosity meant that the NBB4 mediated ethylene degradation took place on a dramatically decreased surface area compared to the composite scaffolds. They also likely suffered from mass transfer resistance which is a commonly related issue to gel entrapment systems [126, 217, 224, 230]. The 0.4% agar scaffolds retain 70% porosity which allows ethylene gas to perfuse easily through the scaffold and provides a larger surface area for NBB4 to access the ethylene and perform gas-exchange. Porosity rather than pore size is the key parameter here influencing ethylene degradation rate. This is because the ethylene particles (molecular scale) are of negligible size compared to the biofilter pores (micrometer scale).

NBB4-agar-PCL composites were shown to degrade ethylene in a static system. Composite support materials have only been used once previously for biofiltration in an attempt to reduce cell leakage [217]. These can be classified as biofilters as the active ethylene-degrading agent is viable NBB4 bacteria. Biofilters fabricated using 0.4%w/v agar was found as the optimum concentration to maximise ethylene removal efficiency. This would be the concentration used for future work and Device Pilot studies.

4.3.3.2 Effect of Altered Cell Surface

The ethylene degradation ability of each scaffold was determined by injecting serum bottles with 350ppm of ethylene and monitoring its degradation over time. Ethylene concentration was quantified in the same way as described above (Results & Discussion 4.3.3.1).

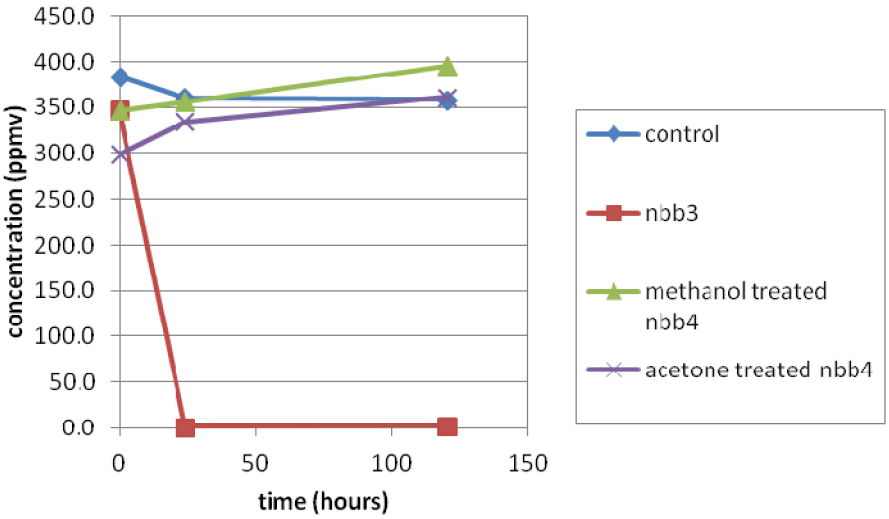

Figure 87. Effect of altering the cell surface of adhered bacteria on ethylene removal.

Ethylene levels in serum bottles containing the control (empty bottle except for ethylene) and biofilters with NBB4 cells treated with solvent washes did not decrease from 350ppm (Figure 87). This means these biofilters could not degrade ethylene. The solvents were likely too harsh and solubilised the NBB4 cell membrane lysing the cells. This made the enzymes necessary to facilitate ethylene degradation inactive. The benefits of adhesion over gel entrapment are a decreased processing time and higher cell survival rate [126]. The treatment of NBB4 cells with solvents does increase their adhesion efficiency as presented in Results & Discussion 4.2.2.4, but at the expense of an extra processing step and loss of cell viability and activity thus mitigating the advantages of an adhesion immobilization design.

NBB3 biofilters caused a drop in ethylene below the detectable limit within 24 hours. However, it was noticed that NBB3 cells had become detached from the scaffold. This was indicated by the yellow liquid that gathered at the bottom of the serum bottle. Although this biofilter confirmation successfully removed ethylene, the NBB3 was not properly immobilised to the scaffold. Cell leakage and re-distribution of bacterial cells has been previously reported in adhesion systems [126, 203]. For biofiltration it is important that bacteria are strongly immobilised to both ensure stable activity and to prevent contamination of the filtered environment. This is particularly important for the application of fruit preservation where poorly immobilized bacteria may come into contact with food and produce poor health outcomes. For this reason NBB3-scaffold biofilters are ultimately unsuitable.

4.4 Device Pilot Studies

4.4.1 In vitro wound modelling of Synthetic Skin Graft

4.4.1.1 Validation of PCR and qPCR standards

For the purpose of the co-culture model we were using qPCR not for determining the relative amount of a particular gene, but the total amount of a gene that would be linked to cell number and be a marker for cell survival. Thus standard aliquots of the genes needed to be prepared. These could be run in each qPCR set to determine the actual amount of DNA in each reaction. Standard PCR was used to amplify the product. This was then purified and run on a gel to check the purity. Finally serial dilutions of the purified product were used in qPCR reactions to form a standard curve.

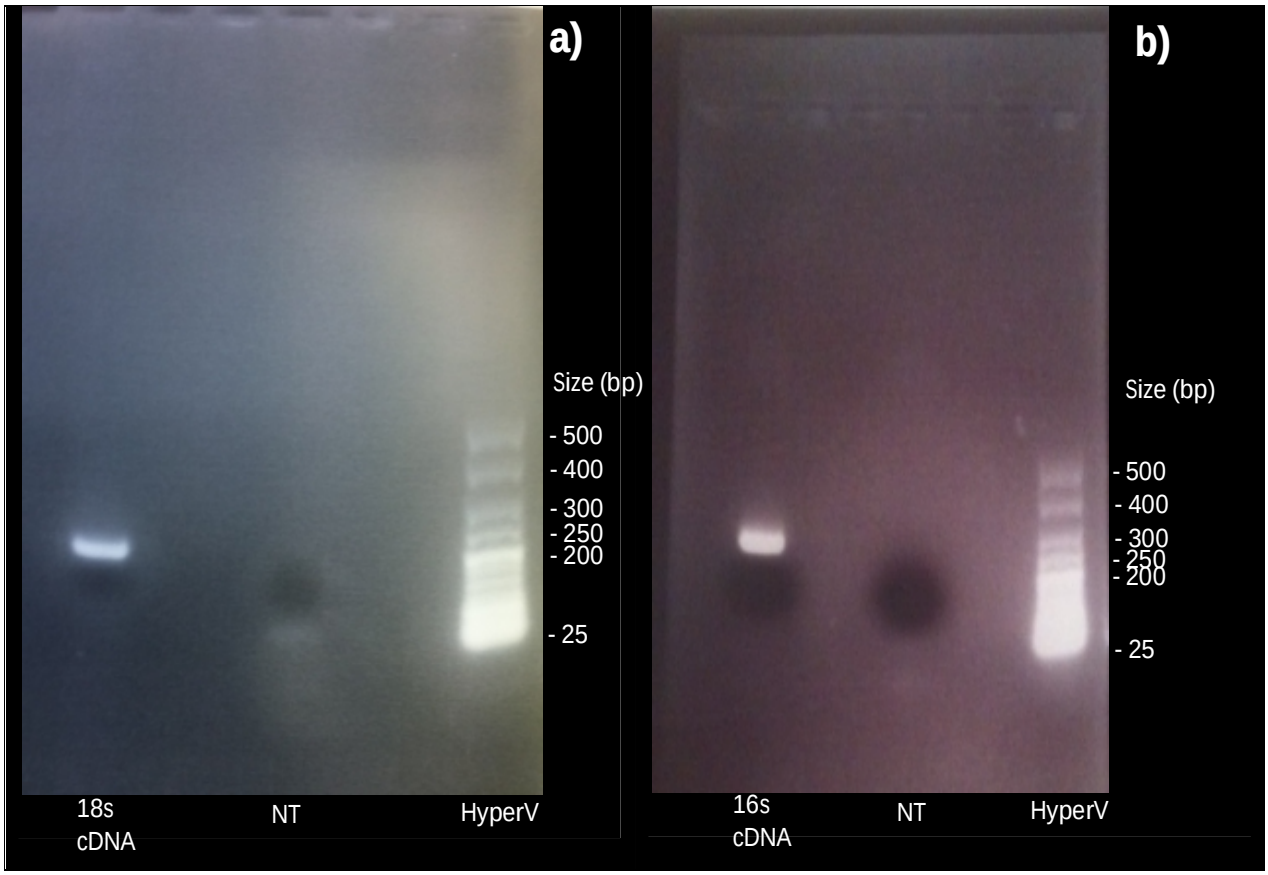

Figure 88. Gel electrophoresis of PCR amplified and purified ribosomal cDNA. PCR products were run with no-template controls (NT) and Hyperladder V (HyperV) as a reference. a) 18s cDNA single band at ~200bp; NT registered very faint band at ~50bp. b) 16s cDNA single band at ~250bp; NT registered no visible band.

Gel electrophoresis divides the DNA strands based on their length in base pairs (bp). When simultaneously run with a reference 'ladder' of known strand lengths, an unknown sample's length can be determined. The relative amount of DNA strands in a sample can also be qualitatively seen by the brightness of the bands. In this way, the PCR product can be validated by comparing the bands seen to the expected product size for a given primer-target pair. Both 18s and 16s PCR products were run on the gel to check to PCR specificity and purity.

Figure 88 shows the gel electrophoresis results. 18s PCR product was a single band at around 200bp in length and the 16s PCR product produced a single band at approximately 250bp. This agrees well with the known PCR product length (as predicted by the primer design) for 18s and 16s cDNA: 187bp and 247bp respectively. No other bands were seen in either cDNA lanes, which prove the specificity of the PCR primers – only the target strand was amplified in the PCR.

No-template control (NT) lanes contained samples that underwent the PCR reaction but with no cDNA. This is a test that all the PCR reagents are devoid of cDNA contamination which would effect the final concentrations of the standard curve. The 18s PCR NT lane exhibited only a very faint band at approximately 50bp. This is probably a primer-dimer, which is small amounts of primer have preferentially bound together in the absence of cDNA. This is why this band is not seen in the 18s cDNA lane. The 16s NT lane shows no distinguishable band. The NT results confirm that the PCR reactants are pure and free of contamination.

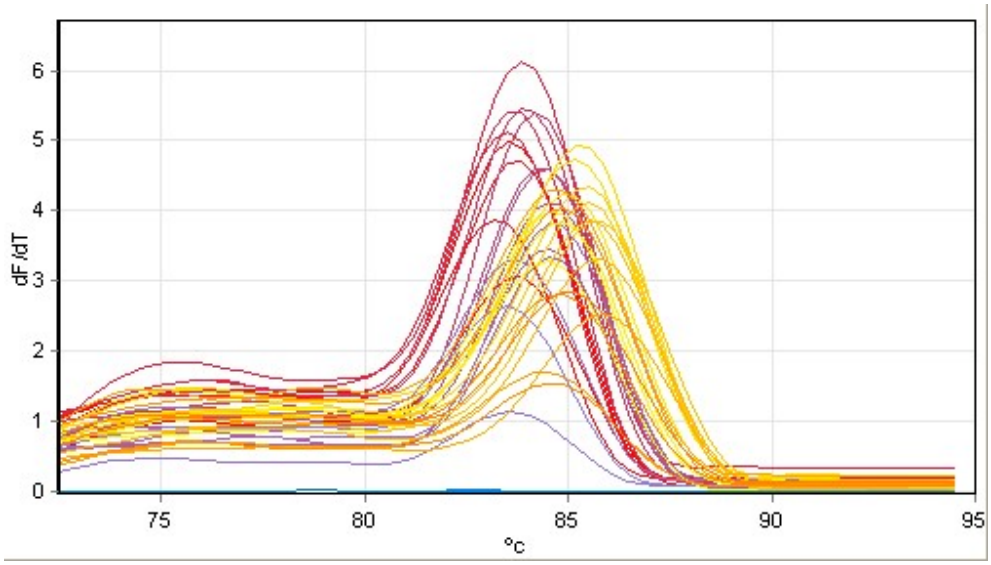

Figure 89. Melt curve analysis for 18s and 16s PCR standard curves. Red lines are 18s reactions; yellow/orange lines are 16s reactions.

Purified cDNA concentration was quantified spectrophotometrically and converted to copies per µl by applying the product sequence molecular weight. A ten-fold serial dilution was performed on the purified cDNA sample. qPCR was then carried out to form standard curves for 16s and 18s cDNA. A melt analysis was performed along with the qPCR.

The melt curve analysis in Figure 89 shows the melting temperature for the 18s and 16s standards. The single peak in each curve shows that only the target section of DNA was being melted and validates the specificity of the PCR reaction [184].

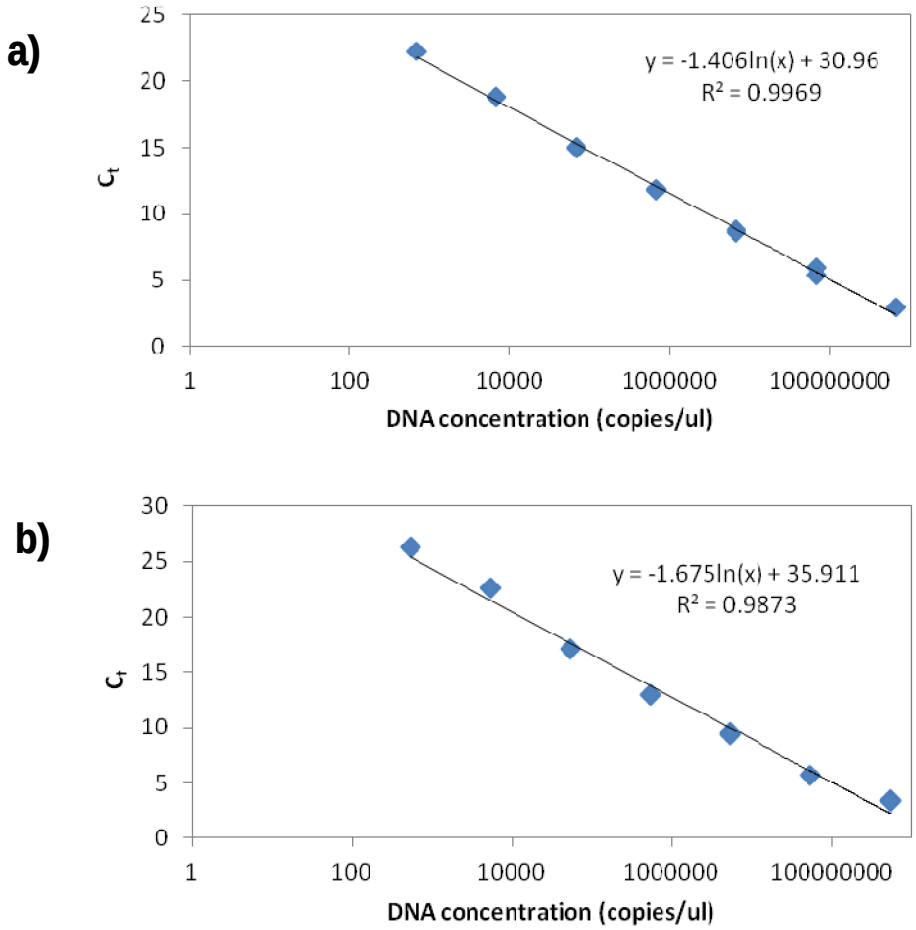

Figure 90. qPCR standard curves relating cycle threshold (Ct) to cDNA concentration (gene copies/µl). PCR reactions were performed in duplicate. a) 18s standard curve; b) 16s standard curve.

The standard curves produced from the qPCR can be seen in Figure 90. Both 18s and 16s curves produced logarithmic relations that would allow the concentration of an unknown cDNA sample from either fibroblasts or *S. aureus* to be determined. The standardised logarithmic relation with correlation coefficient (R^2) approaching 1, shows that the standards are diluting at even log intervals.

This experiment validated the qPCR measurement technique for HFb 18s rRNA and S. aureus 16s rRNA. The purity and specificity of the PCRs was confirmed and standard curves were produced which could be run in the future experiments to determine the ribosomal DNA concentration from a fibroblast or S. aureus sample.

4.4.1.2 Addition of Fibroblasts to the Scaffold

The large interconnected macropores of the PCL scaffold means adding a reliable number of cells for an assay becomes problematic due to cells falling through the pores to the bottom of the culture plate. For this co-culture model, the aim was to measure differences in ribosomal RNA which reflects the number of cells attached to the scaffold. Being able to reliably grow a known number of fibroblasts on the scaffold is essential given changes in RNA concentration was expected when demonstrating different scaffold design iterations. A method had to be validated to ensure a known number of cell numbers were able to attach to the scaffold.

The normal method of cell culture for the PCL scaffold has been to pre-wet the scaffold in sterile media, transfer the scaffold to a 24 well-plate, fill the well with 500ul of media, then add the cells in a small volume onto the scaffold [256]. This is suspected to cause the cells to fall through to the bottom causing low numbers and variable attachment. Three new methods were developed:

1. Pre-wet the scaffold as in the normal case, dried with sterile filter paper, then transfer to a cell culture well and add the cells in 100ul of DMEM+10%FCS. The thought was to put the cells in a smaller volume giving them a better chance of attachment.

2. Transfer a dry scaffold (not pre-wet) to a well then drop 100ul of cells in DMEM+10%FCS on top. This was thought to prevent the cells from falling to the surface and giving them a chance to adhere.

3. Exactly the same as in 2, but cells were delivered in a 50ul volume.

In all of the three new methods, the cells were given 12 hours to adhere before transferring to a new well, adding 500ul of media and continuing normal cell culture.

In new method 1, despite the scaffold looking dry after dabbing with filter paper, the droplet was readily absorbed by the scaffold and sat snugly inside it with little excess coming out the sides. Residues left on the hydrophobic scaffold after drying must have facilitated this.

In new method 2, the 100ul droplet overbalanced the scaffold causing it to flip and become dispersed over the plate. This occurred in both duplicates.

In new method 3, the 50ul droplet sat perfectly balanced on the top of the scaffold, propped up by surface tension and hydrophobic forces. The next day, the droplet looked to have sunk slightly into the scaffold but was still intact.

After the initial 24 hour culture period and the scaffolds were transferred to the new plate, the wells were imaged using a conventional phase microscope to qualitatively examine the number of cells that fell through to the bottom of the well.

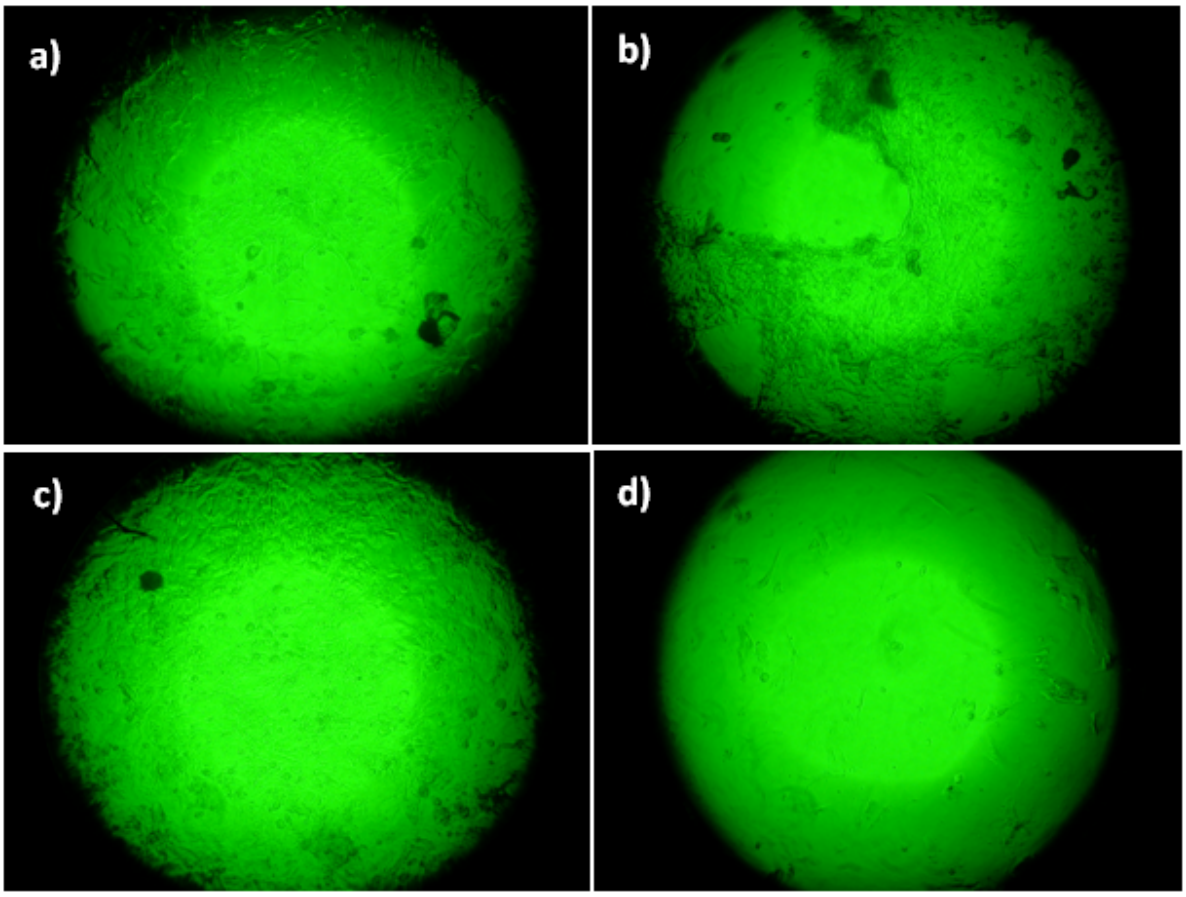

Figure 91. Unattached Cells. Phase microscope images of the bottom of the well after removing the cell-seeded scaffold: a) Normal method; b) New method 1 – pre-wet scaffold, 100ul drop; c) New method 2 – dry scaffold, 100ul drop; d) New method 3 – dry scaffold, 50ul drop. 200x magnification.

Although, the centre of the images is somewhat obscured due to the camera flash reflecting back up the aperture, the more peripheral zones exhibit a clear difference is the cell numbers. Figure 91a shows the result of the normal loading method, using a pre-wet scaffold and seeding the cells only just before filling the well with media. The cells are virtually confluent with the exception of a few bare zones. The acellular zones account for areas where the scaffold was touching the bottom of the cell preventing cells from attaching. Figure 91b exhibits even more confluent cells, which is consistent with the new method, of delivering the cells in a smaller volume. Acellular zones can be seen in this image very clearly due to the confluence of the cells. Figure 91c shows confluent cells. As mentioned earlier, the large 100ul drop

over balanced the scaffold so that the drop contacted the bottom of the well and dispersed over a greater area. This is why the image appears very similar to Figure 91a. Figure 91d) shows a much less dense layer of fibroblasts. This is a marked difference compared with the other images - one could almost count the number of cells. This may indicate that a far higher proportion of cells are attaching to the scaffold using New method 3, as oppose to falling to the bottom of the well in the liquid media.

After 2 weeks of cell culture, scaffolds and adherent cells were digested and the total RNA was extracted purified and measured using spectroscopy. Figure 92 shows the RNA yields from duplicate testing of each separate HFb seeding method. The Normal method shows the highest RNA yield followed by the Dry Drop 50ul, the Pre-wet Drop100ul and the Dry Drop 100ul. However only the Dry Drop 50ul method exhibited repeatability as the standard deviation of all other methods approximately equal to the mean. This shows that a larger and more consistent proportion of cells were becoming attached to the scaffold and not falling to the bottom of the plate. In contrast, the other methods had less attachment which was also less reliable as many variable parameters like pore size, pore saturation and pore topography would affect the level of attachment as cells were allowed to fall through the liquid media.

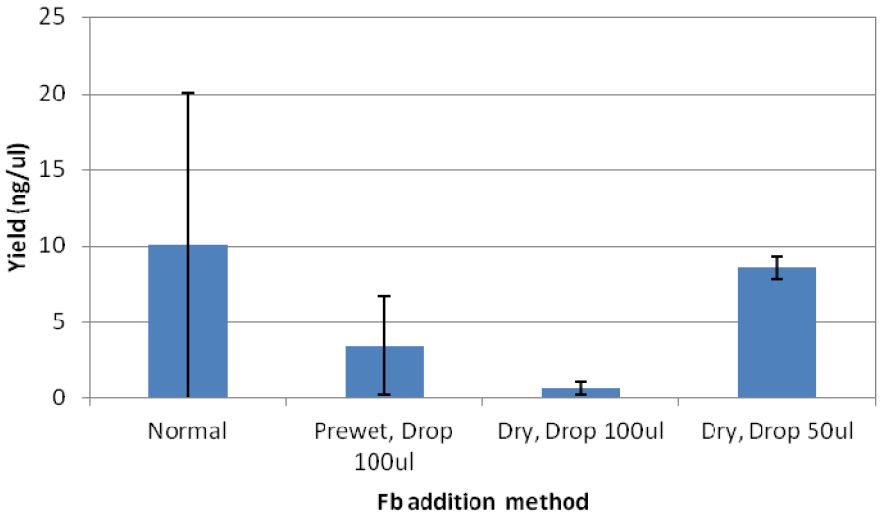

Figure 92. RNA yield from Fibroblast (HFb)-seeded scaffolds using different HFb addition methods. Error bars = Standard deviation. Each method was tested in duplicate.

4.4.1.3 Bacterial Growth in DMEM and Toxic Media

An experiment was performed to establish whether *S. aureus* bacteria could grow uninhibited in the cell growth media (DMEM + 10% FCS). This was an essential control for the co-culture model. A further experiment was then conducted to determine whether presence the *S. aureus* cells made the growth

media toxic for fibroblasts. This second study would help tune important parameters in setting up the final co-culture experiment.

S. aureus was cultured in the growth media overnight and showed strong growth which was determined by turbidity (OD600 > 1). The resulting cultures appeared very cloudy and the media colour changed from pink to yellow indicating a pH change. The resulting liquid culture was streaked onto TSA plates. After 24 hours of culture, single bright yellow colonies appeared confirming the culture purity and the viability *S. aureus* cells.

The resulting media from the overnight *S. aureus* cultures was filter sterilised and added to cell culture wells containing confluent HFbs. A prominent phenotypic change was observed in HFbs treated in this way: Cytoplasm was greatly reduced and the nucleus darkened suggesting cell death (Figure 93). This is an unsurprising result considering all strains of *S. aureus* secrete exotoxins containing a number of cytotoxic enzymes and exoproteins [257]. It is also possible the pH change played a part in the demise of the treated HFbs.

These experiments showed:

1. That *S. aureus* could grow in the same growth media as HFbs.
2. The presence of *S. aureus* in the media made the media cytotoxic for HFbs.

The first finding proved that DMEM + 10% FCS could be used as the co-culture growth media as both *S. aureus* and HFbs could be grown successfully independently in the media. There was no need to develop a modified culture media as was done in previous co-culture models [141]. This is also more biomimetic as when infections occur, bacteria are entering the host environment which is tuned for cell growth not bacterial growth.

The second finding showed that the presence of the *S. aureus* in the media turns the media cytotoxic to HFbs. This cytotoxicity would play a role in vivo wound sepsis and thus is a desirable phenomenon to have in the co-culture. Despite the change in phenotype there were cells that were still attached to the bottom of the well suggesting a level of survival despite the harsh conditions imposed by the *S. aureus*. Previous co-cultures performed employed flowing systems to decrease the cytotoxic effect of the bacteria in the media. Subbiahdoss *et al* [141] said that under static co-culture conditions “cells did not have a chance to win the race for the [biomaterial] surface”. Flowing conditions are experienced in vivo but these are expected to be slow-flow environments and static cultures may better represent the

localised build up of exotoxins from invading bacteria. Further, Subbiahdoss proposed his in vitro model for functionalised surfaces and coatings [141]. Our model has been developed with antibacterial-eluting systems in mind. It may be that the rapid destruction of bacteria from eluted antibiotics gives cells a chance to "win" in our model. Finally the simplicity of a static system makes it preferential to widespread adoption.

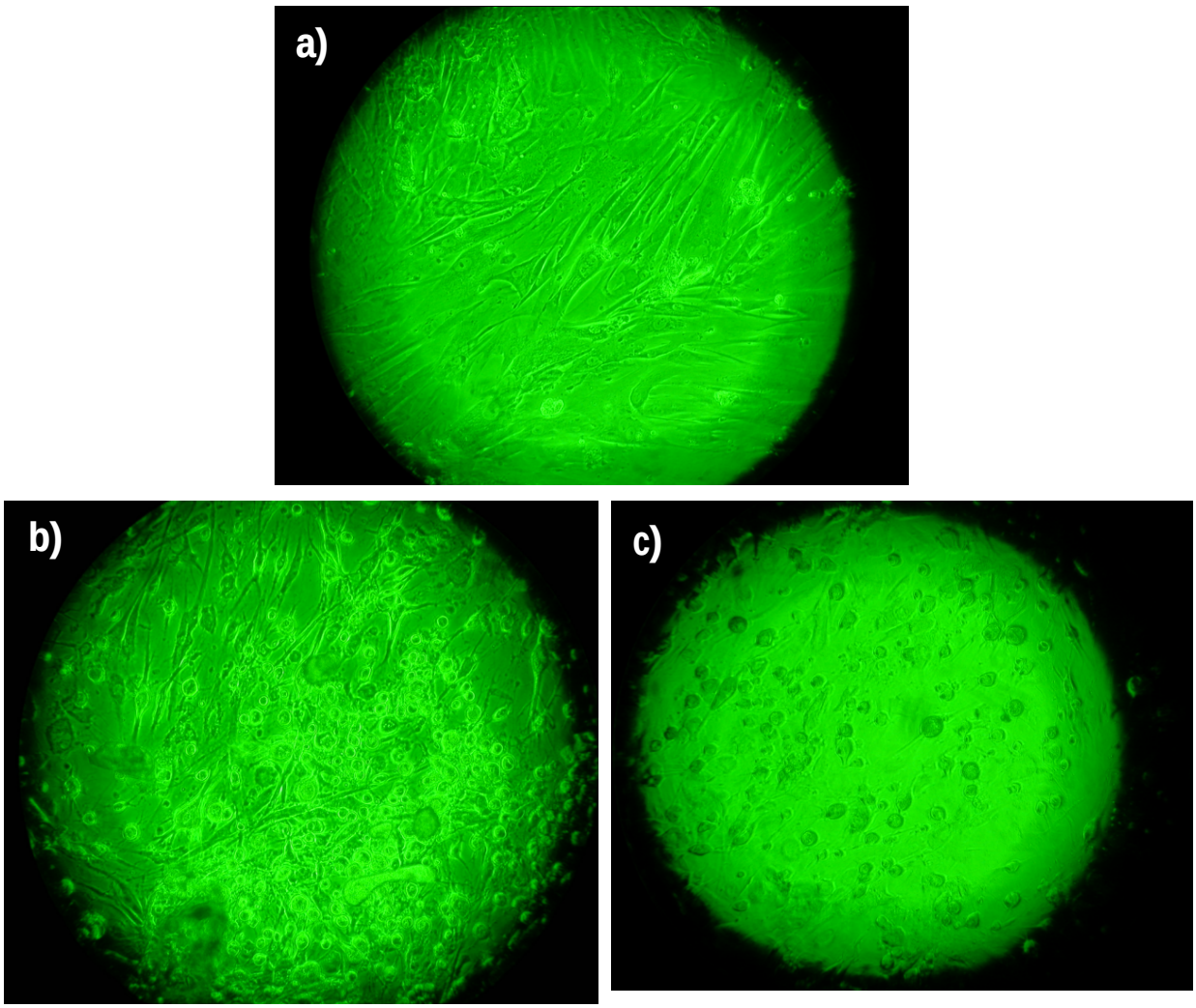

Figure 93. Phenotypic effect of toxic media on Human Fibroblasts. a) Control group: Confluent HFbs in normal growth media exhibiting healthy phenotype. b) & c) HFbs exposed to S. aureus toxic media exhibit abnormal phenotype with a substantial decrease in cytoplasm. 200x magnification.

4.4.1.4 Cell and Bacterial Growth on bi-Phasic Scaffold

Before the septic wound model could be attempted a preliminary experiment was required to validate whether the basic bi-phasic PVA-PCL scaffold could support growth of fibroblasts and staphylococcus in

their own right. It was also important to check that the isolation and quantification of rRNA from bacteria and cells would produce quantifiable results.

Cells and bacteria were added to each scaffold and harvested after 1 and 4 days of culture. Cells were stored in TriReagent at -80°C to preserve RNA until ready for extraction. Reverse transcription and qPCR were carried out to quantify number of target gene copies.

18s gene copies indicating fibroblasts were approx 4000/µl for the scaffolds harvested after 1 day of culture. After 4 days of culture this dropped to approx 10/µl (Figure 94). The expected result would be for 18s levels to remain constant or slightly increase as fibroblasts attach and grow on the scaffold. The decrease in fibroblasts could relate to a cytotoxic effect from the scaffold. However, this is unlikely because of the track-record in wound biocompatibility of the materials components of the scaffold: PVA [101] and PCL [107]. Only duplicates were performed to try and conserve samples so it is possible that this unexpected result stems from natural variation, however the results were consistent within the small sample size. Records show the day 4 cultured cells were stored for around 5 weeks in TriReagent. It is possible that the RNA may have degraded during this time accounting for the low 18s yields.

The 16s gene copies indicating *S. aureus* increased from approx 5000 to 50000 copies/µl. This exponential increase was expected as it corresponds with the exponential growth of bacteria. The results were consistent within the biological duplicate marked by the small error bars (Figure 94). This shows that S. aureus colonies were able to survive in the DMEM media and in the presence of the scaffold degradation products such as PVA and trace ethanol. The results also validated the RNA isolation and quantification methods as sensitive enough to illustrate this growth event.

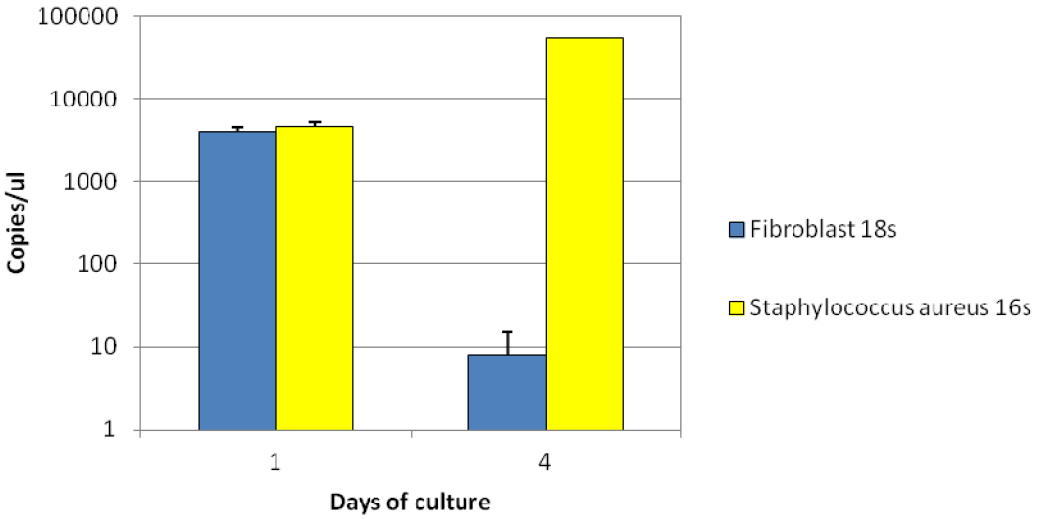

Figure 94. Individual culture of Fibroblasts and *S. aureus* on PVA-PCL scaffolds. Results show qPCR quantification of rRNA from extracted cells (18s) and bacteria (16s) removed from scaffolds after 1 and 4 days cell culture. Error bars = Std; n=2.

The possible cytotoxic effect of the PVA-PCL scaffold on fibroblasts was deemed unlikely. The bacteria were able to grow uninhibited on the scaffold. Both fibroblasts and bacteria could be detected with enough sensitivity to illustrate growth or decline. Therefore the protocol was deemed successful and approved for use in the final co-culture septic wound model.

4.4.1.5 Final Co-culture

Human fibroblasts were co-cultured with Staphylococcus aureus in the presence of different scaffold designs. The co-culture was used to simulate a septic wound, whereby both human cells and bacterial cells are interacting and competing with one another for the biomaterial surface.

Fibroblasts-only cultures were necessary controls for normal fibroblasts growth and attachment onto the different scaffolds. These sample sets were isolated from the co-culture samples to minimise the chance of bacterial contamination from the co-cultures. Bacterial contamination of culture wells can easily be seen because DMEM media contains a pH indicator which will turn from pink to yellow in the presence of bacterial acidic metabolic products. The media turning cloudy is another common sign of contamination. No cloudiness or colour change was seen in fibroblast only controls throughout the 5 day culture period. In contrast the co-cultures became yellow and cloudy after 24 hours with the exception of those containing scaffolds with entrapped erythromycin. This suggests that the erythromycin antibiotic was preventing bacterial metabolism, possibly by directly inactivating the

bacteria, while the other co-cultures allowed bacterial growth and metabolism. The sample set containing Bioglass but not erythromycin exhibited only minor colour change. This could be due to bioglass' antibacterial and/or its alkali nature (Figure 95).

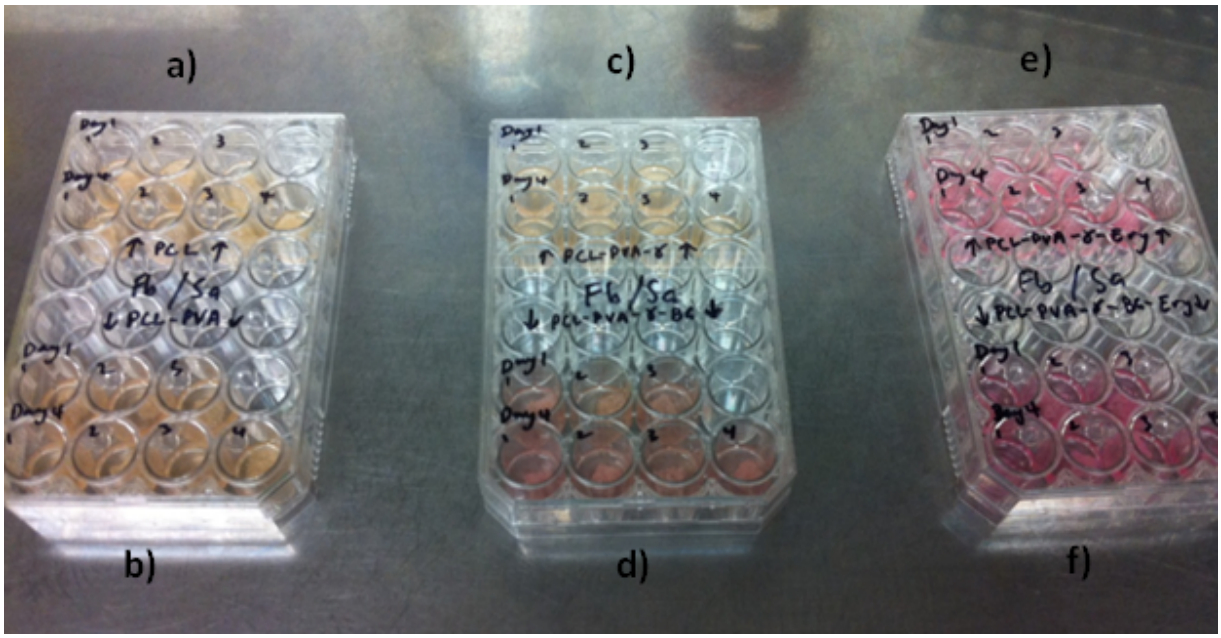

Figure 95. Colour change of DMEM media in the presence of bacterial acidic metabolites. a) PCL scaffold; b) PCL-PVA; c) PCL-PVA-γ; d) PCL-PVA-BG- γ; e) PCL-PVA-Ery- γ; f) PCL-PVA-Ery-BG- γ.

By day 5 there was no stark difference in the media colour of co-culture samples. However, the sample sets without erythromycin still appeared more turbid. This may be due to biofilm formation with a change in bacteria growth and metabolism and less production of acidic metabolites.

After 24 hours and 120 hours of culturing the scaffolds were washed and the adhered cellular matter harvested by trypsinisation followed by sonication. Trypsinisation was performed first to remove adherent fibroblasts, which may have become lysed during the sonication process needed to remove bacterial biofilms. RNA extraction followed with utilisation of bead beating to release bacterial RNA from within the tough *S. aureus* cell wall. RNA concentration was quantified using the nanodrop (Figure 96).

a)

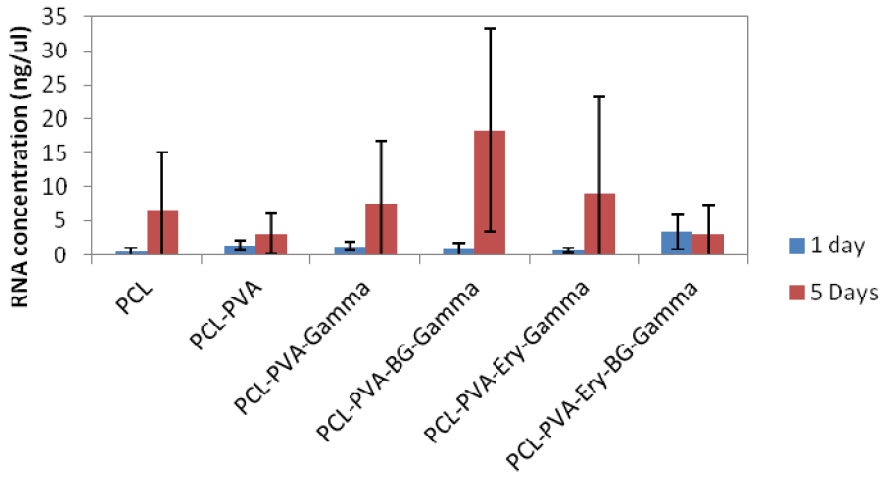

b)

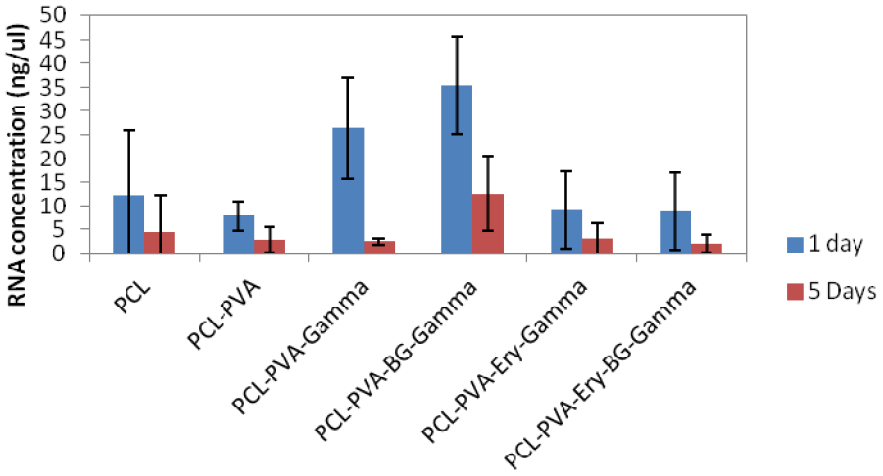

Figure 96. Nanodrop RNA quantification of cells cultured on different scaffold types. Cells were harvested form scaffolds after 1 and 5 days of culture. a) Fibroblast only controls; b) Fibroblast, *S. aureus* co-cultures. Error bars = Std; n=3.

The nanodrop data showed large variation as seen by the large error bars. This is likely due to the 'normal method' addition of fibroblasts which as previously mentioned has high variability (4.4.1.1). However, a trend could still be seen. The fibroblast only cultures RNA concentration increased over time. This is expected, as fibroblasts grow and proliferate on the scaffold. The co-culture RNA concentration seemed to decrease over time. It is difficult to postulate why, without data on both bacterial and fibroblast RNA (which will be discussed below in the qPCR results).It is also worth noting that the RNA concentrations were higher for the co-culture samples. This makes sense as there are more cells in these cultures due to the bacterial inoculation. Bacteria are also smaller cells and stay suspended more easily. This would increase the RNA concentration in two possible ways:

1. The more planktonic bacteria remained in the scaffold after washing and had their RNA extracted.
2. The suspended bacteria were more adept at adhering to the scaffold than the fibroblasts.

a)

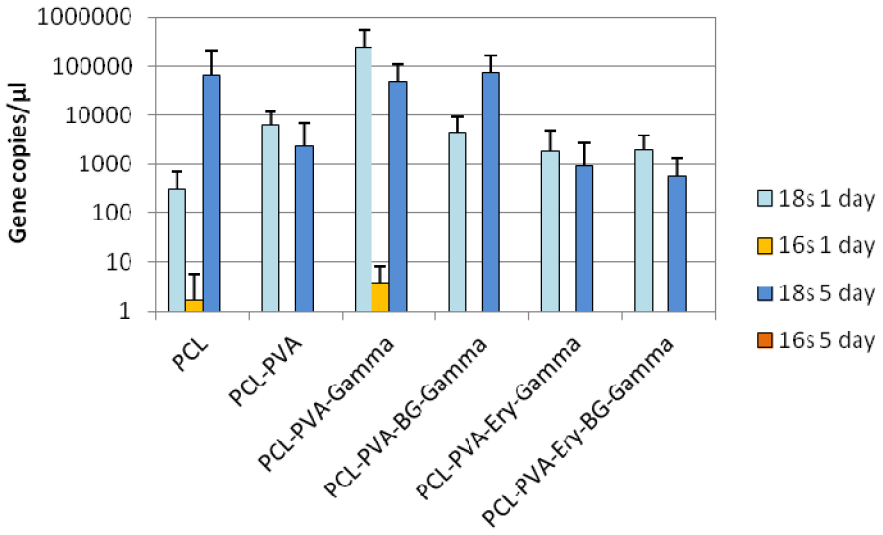

b)

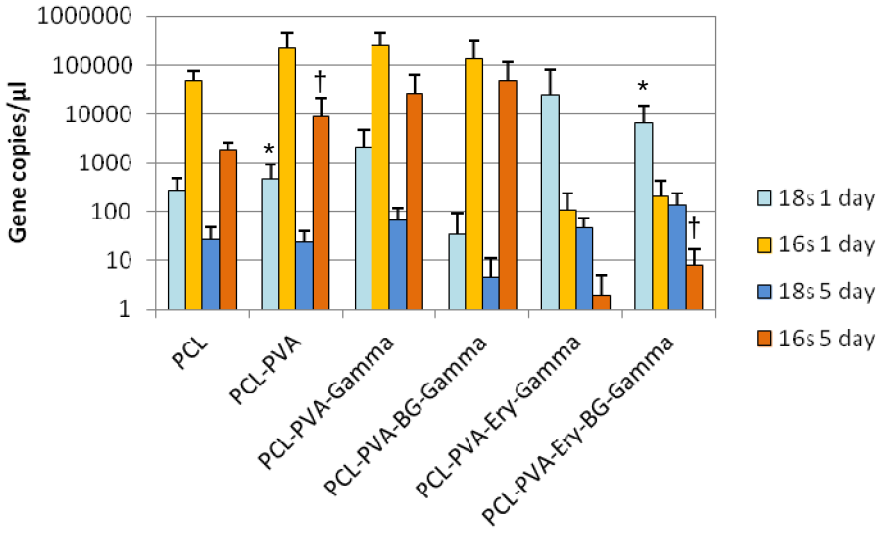

Figure 97. qPCR 18s and 16s gene quantification of cell cultured on different scaffold types. Cells were harvested form scaffolds after 1 and 5 days of culture. 18s gene indicates human fibroblasts while 16s gene indicates S. aureus bacteria. a) Fibroblast only controls; b) Fibroblast, S. aureus co-cultures. Error bars = Std; n=3. Differences between day 1 and day 5 within the same sample sets were all statistically significant (p <0.05). In addition, * and † represent significant differences (p <0.05) across sample sets.

Reverse transcription was carried out normally followed by qPCR using both 18s and 16s primers on each sample set to quantify animal and bacterial rRNA respectively (raw data can be viewed in Appendix A.4). Standards of purified 18s and 16s genes were run has internal controls for each PCR and used to quantify the gene copies/µl from the cycle threshold value obtained. The threshold of each run was set manually in the interest of keeping the internal standard curves consistent. Gene copies were the chosen metric as opposed to cell numbers as quantification of cell numbers based on rRNA is invalid in this wound model given the fluctuations in rRNA gene copies per cell when under severe stress. Meanwhile, rRNA gene copies remain a suitable marker for cell viability for both human cells and bacteria [184]. Despite this standard curves relating gene copies to cell number for both HFb and S. aureus were developed, which may be able to be used in future studies (Appendix Appendix B).

A stark difference is seen between the fibroblast only controls and the co-cultures: The yellow and orange columns indicating 16s RNA are virtually absent in the fibroblast only controls (Figure 97). This was the desired outcome, as no bacteria were added to these cultures and thus no bacterial RNA was anticipated. The yellow columns in the PCL and PCL-PVA-Gamma scaffolds were probably due to contamination after cells were harvested.

The fibroblast only cultures exhibited relatively high concentrations of 18s rRNA after both 1 day and 5 days of culture. Two scaffolds, PCL and PCL-PVA-BG-Gamma, showed an increase in 18s concentration over the culture period, whereas the others showed a very slight decrease. In particular the PCL scaffold showed the greatest increase in fibroblast growth. However, this is probably because the day 1 18s concentration is substantially lower than in the other scaffolds. This is likely due to the PCL scaffolds having larger porosity and more hydrophobic surface area making it difficult for initial fibroblast adhesion. The other scaffolds are PVA coated which as discussed earlier decreases scaffold porosity and may trap more fibroblasts added directly into the scaffold. Only minor growth was actually expected over the 5 day culture period. Trinh *et al* [256] performed a metabolic assay to measure fibroblast growth on the PCL scaffold. It was found that only minor growth occurred until 11 days culture (Figure 98). The increased 18s RNA seen in the PCL-PVA-BG-Gamma scaffold may have to do with its increased bioactivity from the 45S5 bioglass particles. But if this were the case one would also expect increased 18s RNA between the PCL-PVA-Ery-Gamma and PCL-PVA-Ery-BG-Gamma samples; which did not occur.

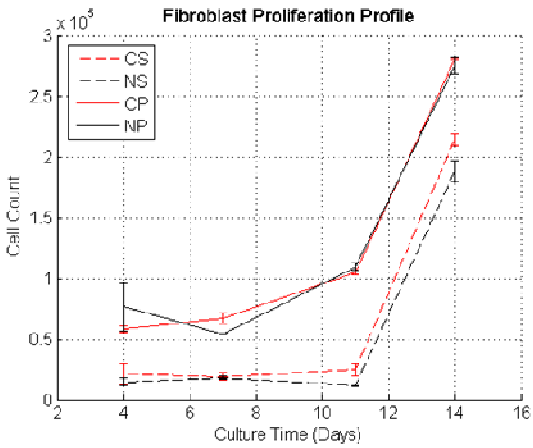

Figure 98. Fibroblast proliferation data. CS=coated scaffold, NS=non coated scaffold, CP=coated plate, NP= non coated plate [256].

The PCL-PVA-Ery-Gamma and PCL-PVA-Ery-BG-Gamma samples exhibited lower day 5 18s RNA than other scaffolds in fibroblast only culture. Erythromycin has been shown to be cytotoxic at high concentrations. The soak-off period in PBS was meant to account for this; bringing the erythromycin concentration to less than 500ug/ml. It is possible the sustained exposure to erythromycin at lower concentrations may still have a cytotoxic effect which accounts for this result.

The qPCR results clearly show the competition between the bacteria and fibroblasts in co-culture. After 24 hours of co-culture the 18s RNA concentration is lower than seen in the fibroblast only controls for all scaffolds that do not contain erythromycin. In the PCL-PVA-Ery-Gamma and PCL-PVA-Ery-BG-Gamma samples the 18s RNA was found to be greater than the fibroblast only control after 24 hours of co-culture. This is likely due to variations in scaffold size, erythromycin loading and fibroblast loading. Conversely, the 16s RNA concentration is very high in all samples except the PCL-PVA-Ery-Gamma and PCL-PVA-Ery-BG-Gamma samples in which 16s RNA was a thousand-fold less. Comparing this with the fibroblast only data shows the cytotoxic effect of the *S. aureus* bacteria. *S. aureus* grows comfortably in the DMEM-10% FCS growth media and competes with fibroblasts for nutrients. In addition, S. aureus produce exotoxins that negatively affect fibroblast proliferation and morphology. The erythromycin eluted into the co-culture environment with bacteriostatic and bactericidal effects on S. aureus, limiting the amount of exotoxins produced and allowing the fibroblasts to better compete.

After 5 days of culture the 16s rRNA decreased in all samples. However, the amount of 16s rRNA in PCL-PVA-Ery-Gamma and PCL-PVA-Ery-BG-Gamma were far lower, resembling the contamination levels seen in some of the fibroblast only controls. This suggests less bacteria are present and fits with the

observation that there was less of a colour change in the media after 5 days co-culture. The drop in 18s rRNA across the non-antibiotic samples may be a result of the culture reaching a stationary phase of growth or increased biofilm formation making the removal of bacterial cells more difficult. In the samples containing erythromycin, the drug would have been eluted throughout the 5 day period accounting for the extended bactericidal effect and further drop in 16s RNA.

18s RNA after 5 days of co-culture decreased compared with the day 1 co-culture results and the day 5 fibroblast only controls. This was the case for all scaffold samples, including the erythromycin-containing PCL-PVA-Ery-Gamma and PCL-PVA-Ery-BG-Gamma, which exhibited only slightly higher 18s RNA than the other samples. The decrease in 18s RNA between 1 and 5 days co-culture was anticipated in samples that were not eluting erythromycin as *S. aureus* could grow unopposed and exotoxins could continue to kill fibroblasts. Taking this into account, the 18s RNA was higher than expected in PCL, PCL-PVA and PCL-PVA-Gamma samples. It was thought that live fibroblasts and thus 18s RNA would be virtually non-existent after 5 days culture in the toxic environment. Nevertheless, comparing the co-culture results with the fibroblast only controls shows a marked decrease in 18s RNA, indicating fibroblast cell-death. The PCL-PVA-Ery-Gamma and PCL-PVA-Ery-BG-Gamma 18s RNA were hypothesized to reach similar levels as those seen in the fibroblast only cultures, but were about ten-fold lower. This may be because of the combination of *S. aureus* exotoxins and erythromycin has an increased cytotoxic effect that is time-dependent – more cytotoxic over the 5 day period.

This wound model was designed to closely mimic clinical conditions. The bacterial load of 100,000 cells was chosen to reflect a debrided wound. *S. aureus* was chosen as it is by far the most relevant bacteria in chronic wounds [101, 114]. Fibroblast cells are the main constituent cell in the dermis. A static culture of small volume (500ul) was used to simulate the poor perfusion seen in chronic wounds. The co-culture goes beyond most in vitro wound models that consider bacteria and human cells separately but very rarely together where the direct interactions between the cell types can be seen [140, 171, 176]. This co-culture did allow such insights giving it a higher level of complexity and relevance. The co-culture as a model for septic wound healing responded predictably to the therapeutic scaffolds and that in itself is validating.

One sample from each set of fibroblast only and co-cultured scaffolds were placed in glutaraldehyde as the initial fixative and prepared for SEM. Non-cultured samples were also examined by SEM as controls. These were not prepared with biological specimen preparation as they had the added purpose of

exhibiting what the scaffold surface looked like before culture. For this purpose, it was better that the samples were not exposed to the multiple chemical washes used in biological specimen preparation.

SEM is a common way to image scaffolds as other microscopy techniques do not achieve the same depth of field resulting in blurry images. The draw-back of SEM is that specialized stains cannot be used to illuminate biological features. The electron beam does not discriminate between different materials and will show all surfaces in varying shades of grey as seen below. This makes it difficult to identify biological features in particular which appear very similar to specks of dust or other artefacts on the surface.

The PCL scaffold appeared to be covered in biological matter in both the fibroblast-only culture and co-culture. Struts were almost completely covered in fibroblast-sized globules (20-50um) which appeared as a rough texturing on the normally smooth struts. In some places the confluence of fibroblasts makes the observer question whether they are just surfaces of the struts that have reacted to the specimen preparation. However, there are some breaches in the cellular layer where the PCL surface of the scaffold can be seen (Figure 99d). Further, the PVA coated scaffolds do not exhibit this dramatic surface change and normal PCL surfaces can be seen.

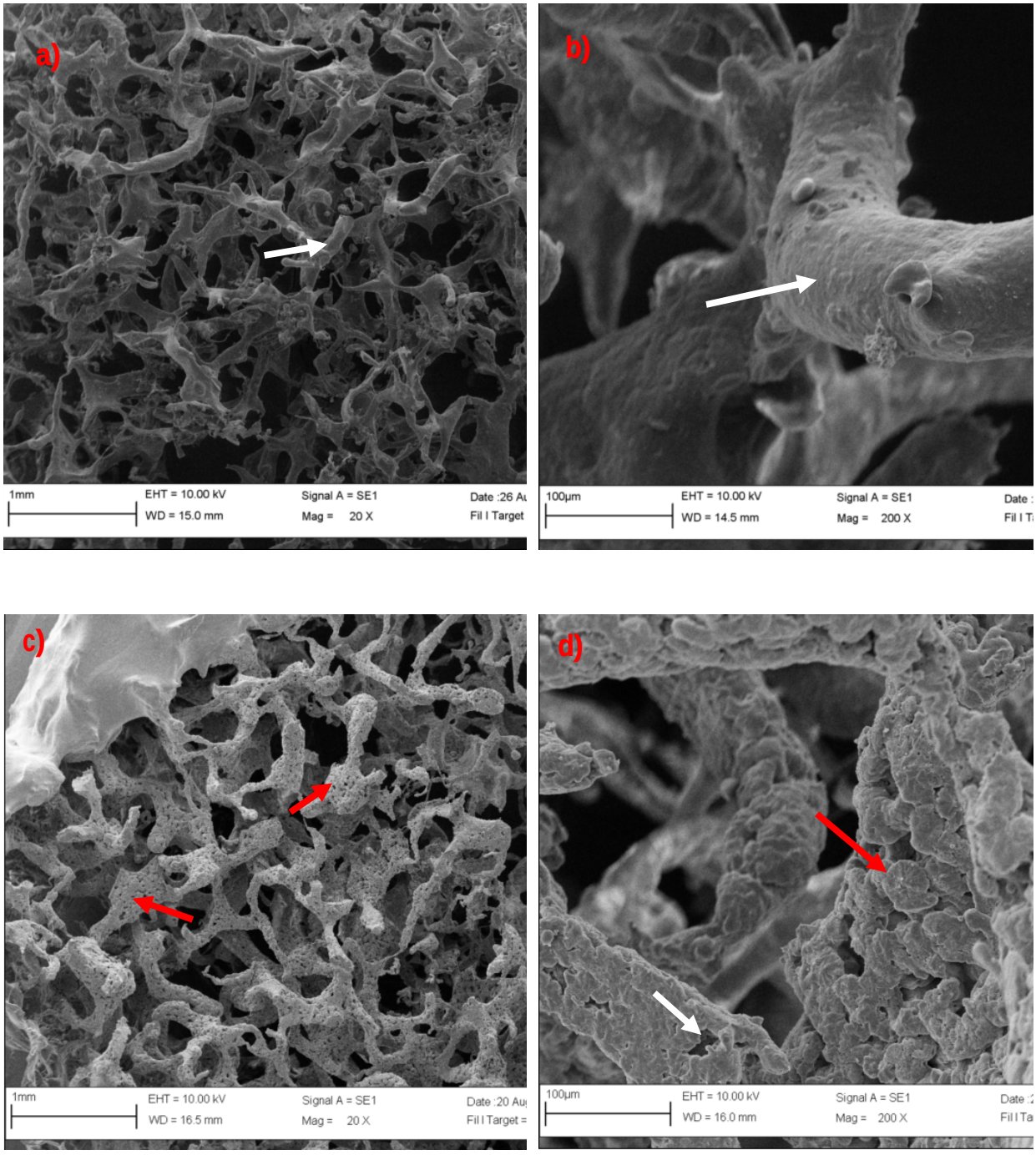

Figure 99. Fibroblast binding to PCL scaffold. a) Not cultured PCL scaffold (x20) and b) scaffold strut close-up (x200); c) Fibroblast cultured PCL scaffold (x20) and d) scaffold strut close up. White arrows = PCL surface, Red arrows indicate fibroblasts.

The co-cultured PCL scaffold had similar morphology to the fibroblast only scaffold (Figure 100). This was not expected given the qPCR results showing a large decrease in 18s rRNA compared to the control

after 5 days culture. Therefore, the cellular matter on the co-cultured scaffold is likely to be non-viable cell debris that adhered to the PCL surface due to physical adhesion.

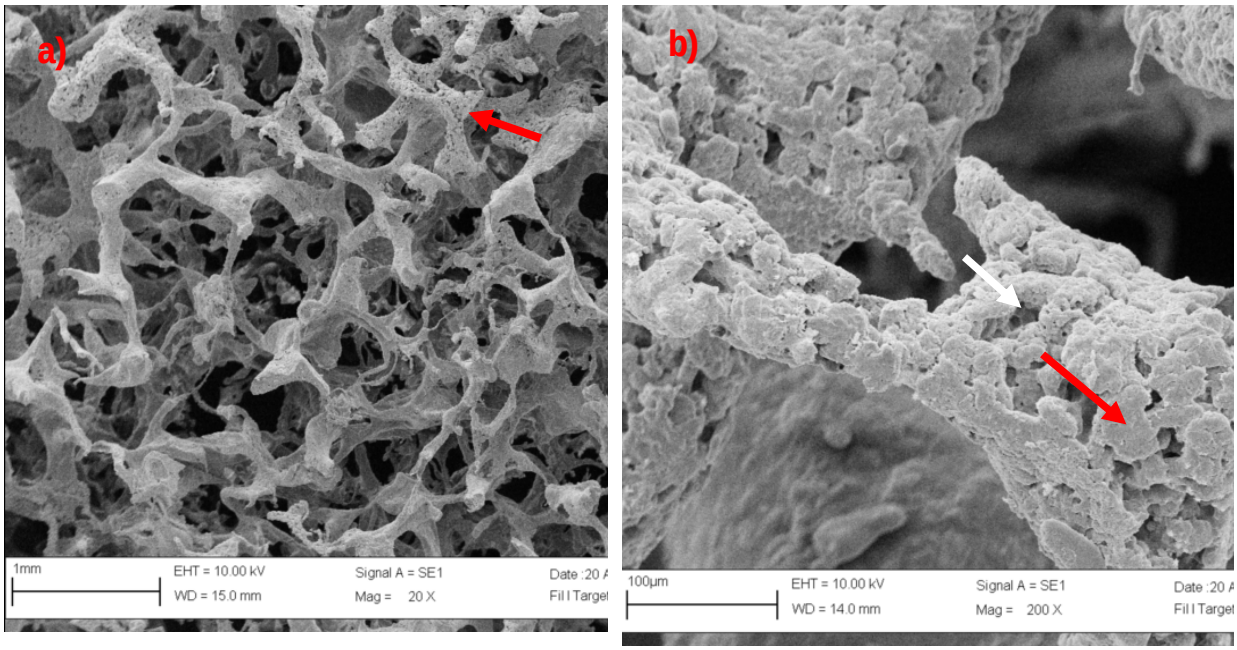

Figure 100 Cell binding to Co-cultured PCL scaffold. a) Co-cultured PCL scaffold (x20) and b) scaffold strut close-up (x200). White arrows = PCL surface, Red arrows indicate fibroblasts.

In the PVA-coated scaffolds, the general architecture appeared more regular as cells were sparser and did not form an obvious confluent mat as seen in the PCL scaffolds. This is despite the fact that 18s rRNA concentrations in PVA-coated scaffolds were similar to PCL scaffolds. Fibroblasts were difficult to detect because their distinguishing features (tendrils and stretched shape) appear similar to the hydrogel coating. It is also possible that the mechanical strains from swelling and dehydration during sample preparation damaged the cellular features on the surfaces of these scaffolds. Figure 101c shows a cell indicated by the particularly fine tendril structure.

Bacterial cells were much easier to visualise. Surface fouling could be seen as lighter patches of tiny small specs even at relatively low magnification (Figure 102a). *S. aureus* has a very regular spherical cocci-appearance and are easily distinguishable from other features on the scaffolds. The other characteristic adding to the ease of identification is the small size of *S. aureus* cells; approximately 1um diameter (Figure 102b). These cells were seen in PCL-PVA, PCL-PVA-Gamma and PCL-PVA-BG-Gamma samples. *S. aureus* cells were often seen in colonies that were partially enveloped in biofilm (Figure

102c-d). In these scaffold samples the bacteria overwhelmed any fibroblasts initially present as none could be found on the surfaces.

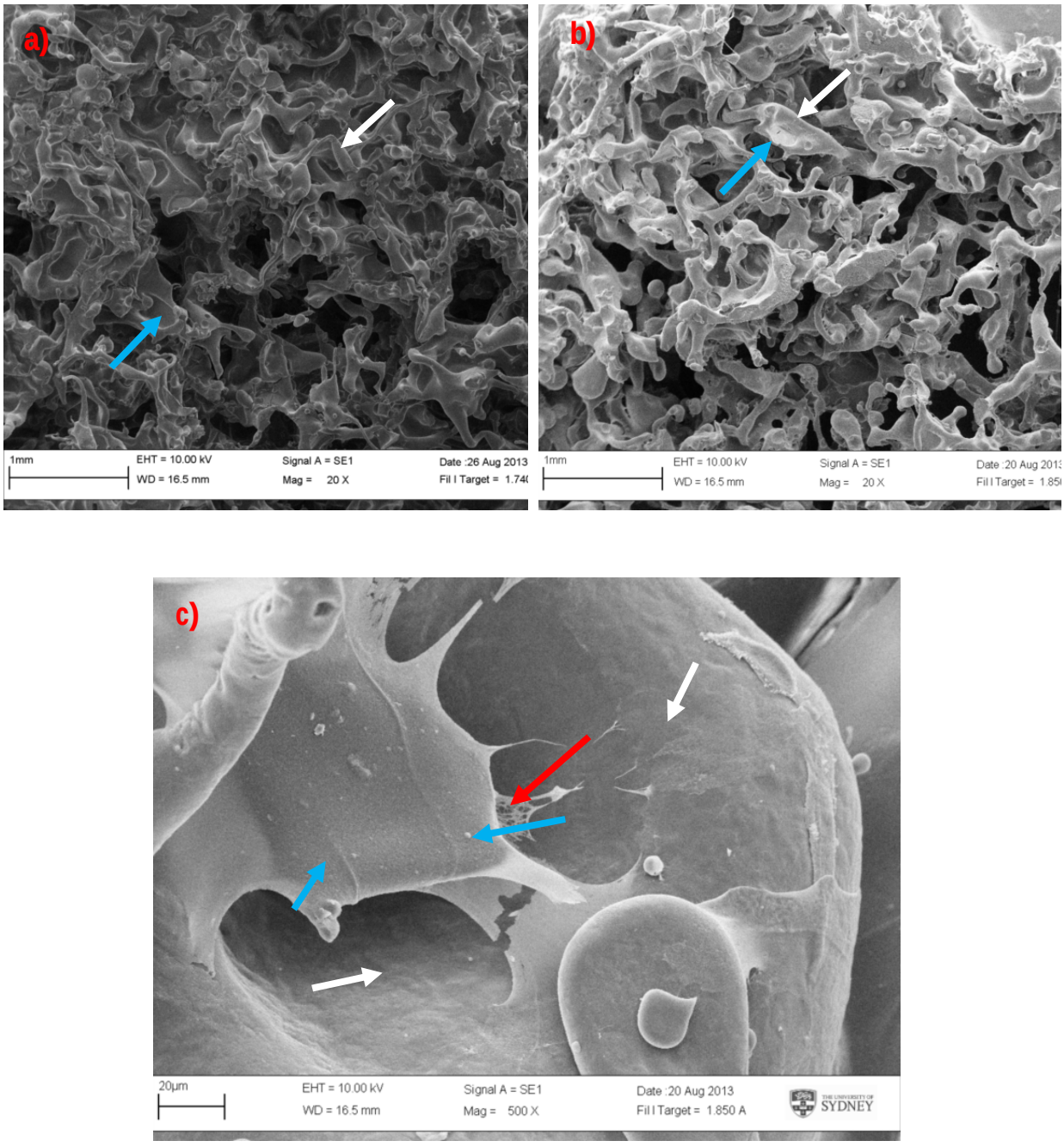

Figure 101.Cell Binding to PVA-coated scaffolds. a) PCL-PVA-Gamma no-cell control; b) PCL-PVA Fibroblast only culture (x20); c) PCL-PVA Fibroblast only culture (x500). White arrows = PCL surface, Red arrows = fibroblasts, Blue arrows = PVA surface.

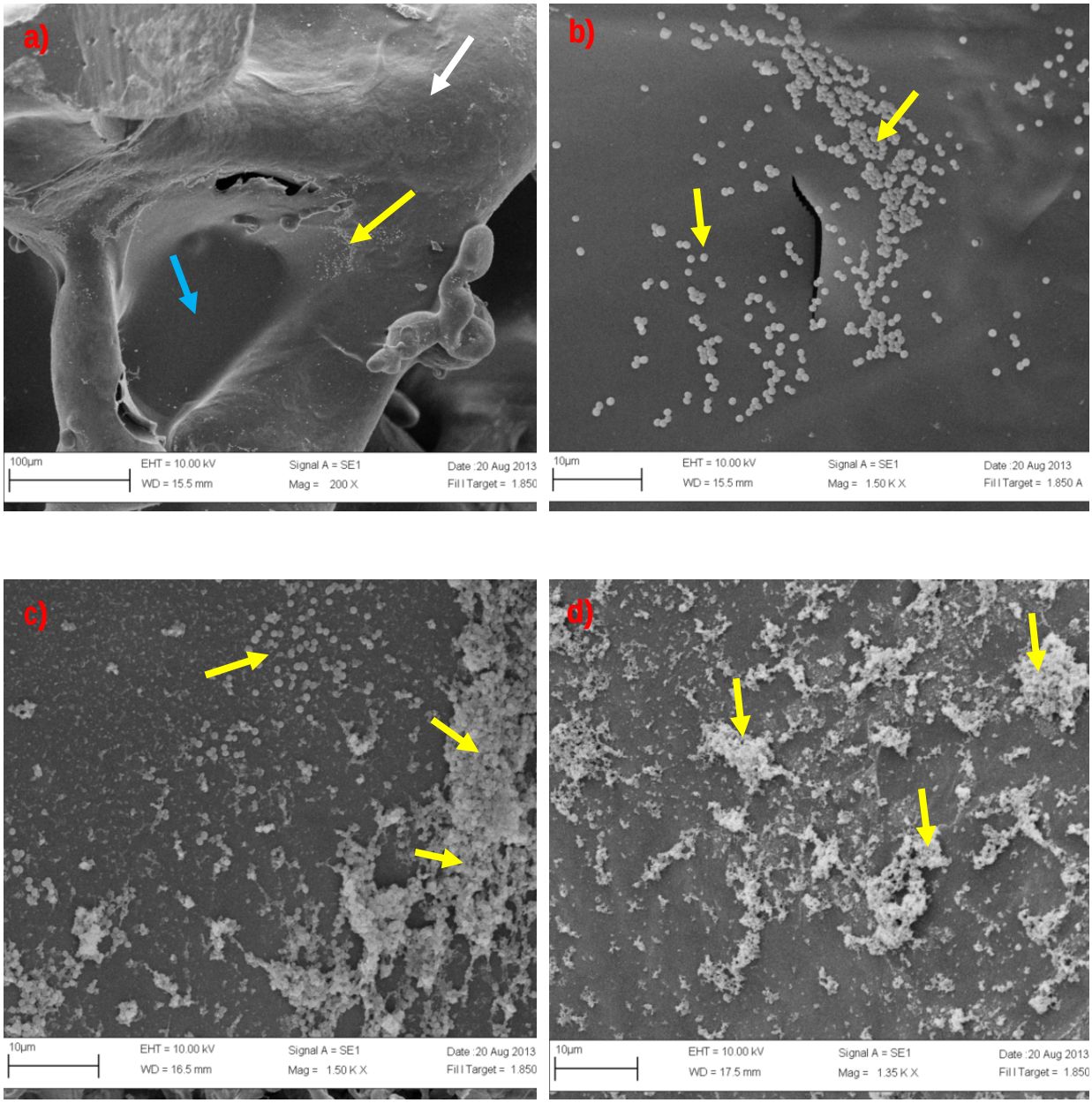

Figure 102. *Staphylococcus aureus* cells seen on co-cultured scaffolds. a) PCL-PVA scaffold (x20); b) PCL-PVA (x1500); c) PCL-PVA-Gamma (x1500); d) PCL-PVA-BG-Gamma (x1350). White arrows = PCL surface,Yellow arrows = *S. aureus*, Blue arrows = PVA surface.

The scaffolds containing erythromycin were distinctive from other PVA-coated scaffolds after manufacture. These scaffolds exhibited a hydrogel structure of thin shard-like strands which was homogenous throughout the architecture giving a roughened appearance in contrast to the very smooth regular PVA-coated scaffolds (Figure 103a/b). This is likely due to recrystalisation of erythromycin after

the scaffold is dehydrated. The shards are crystals of erythromycin entrapped within the PVA hydrogel. This morphology was not seen in samples that were cultured for 5 days. This validates the interpretation, as erythromycin would have been almost completely eluted from scaffold by this point.

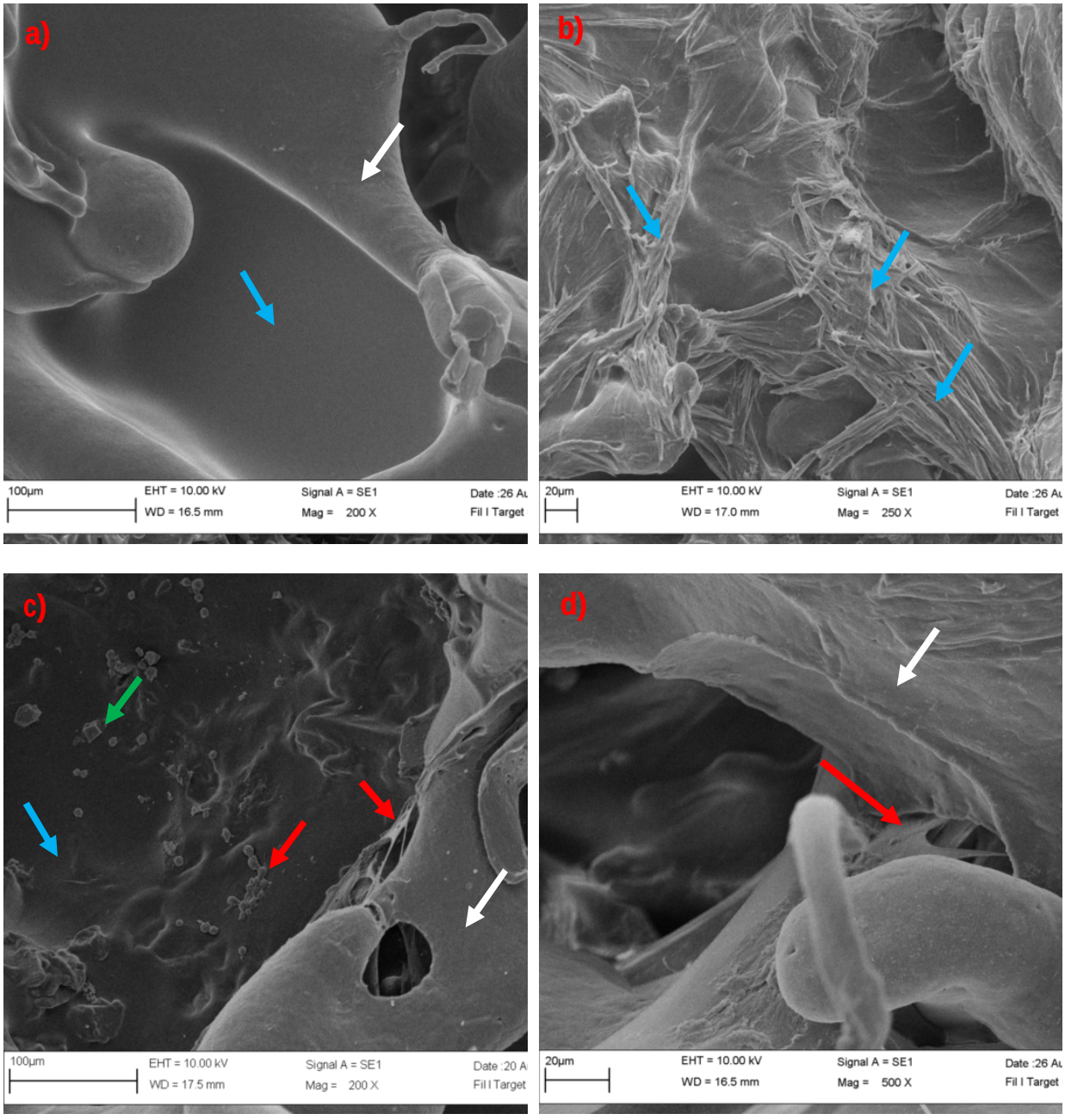

Figure 103.Morphology of Antibiotic scaffolds. a) PCL-PVA scaffold not-cultured, here for comparison (x200); b) PCL-PVA-Ery-Gamma not-cultured (x200); c) PCL-PVA-Ery-BG-Gamma fibroblast only cultured (x200); d) PCL-PVA-Ery-Gamma co-cultured (x500). White arrows = PCL surface, Red arrows = fibroblasts, Blue arrows = PVA surface, Green arrows = 45S5 bioglass.

Fibroblasts could be seen on the erythromycin scaffolds. Figure 103c shows the PCL-PVA-Ery-BG-Gamma scaffold with a number of different features within the field of view. Fibroblasts can be seen with two different morphologies. Fibroblasts show a rounded morphology on the hydrogel surface and a flattened, spread-out morphology on the PCL surface. Different material surface properties are known to influence cell differentiation. Parker *et al* [252] demonstrated a flat morphology of chondrocytes on a PCL surface and a rounded morphology on a alginate hydrogel coating. A similar pattern is seen here. The flat morphology is desirable for fibroblasts. This may be a disadvantage of the PVA coating and why the only thin hydrogel webbing is preferable: To maintain PCL surface area for fibroblast adhesion and differentiation. A Bioglass particle can also be seen coming through the surface of the hydrogel.

In both co-cultured erythromycin composite scaffolds no *S. aureus* cells or biofilm were visible. This shows that bacteria were not able to adhere and proliferate on the surface of this scaffold. Fibroblasts could be found in these co-cultured scaffolds with regular morphology (Figure 103d). This is further validation of the designed scaffold's ability to fight infection while allowing for new dermal growth. Therefore this design may be important for chronic wound healing and treating sepsis.

4.4.2 Mechanical Properties of Synthetic Skin Graft

Scaffold samples were tested by DMA in compression to quantify relevant mechanical properties for use in diabetic foot ulcers.

The DMA set up was a compressive plate coupled with a load cell. The computer program recorded relevant signals such as force and height, which it then used to calculate stress and strain respectively. In calculating the stress, the computer needs the user to input the cross-sectional area of the sample. The cross-sectional area of scaffold samples is incredibly complex due to their porosity and complex architecture. Because of the difficulties of calculating this true surface area, the bulk geometry of the samples was used to assume the cross-sectional area as square.

Stress-strain curves were obtained. Curves had two characteristic sections: an initial high strain section and a later low strain section. The initial section relates to elastic and plastic deformation of the pore structure. The second section reflects when the material can be thought of as non-porous. (Olah *et al*). Only the initial section was analysed as this would be the working strain range of the device in vivo and accounts for the porous structure of the scaffolds. A relation for the linear portion of this initial section of the curve was used to determine the compressive modulus. The compressive modulus can be given by the following equation:

$$E_{comp} = \sigma/\varepsilon \quad (12)$$

Where Ecomp is the compressive modulus, σ is the stress developed in the porous scaffold and ε is the scaffold strain state (dimensionless).

The average Ecomp of the basic PCL scaffold was 54.43 kPa (Figure 104). The addition of PVA hydrogel in its hydrated form yielded much unchanged compressive properties; 53.066 kPa. Addition of the bioglass coating increased the Ecomp; PCL-PVA-BG had an Ecomp of 72.672 kPa. Gamma irradiation had little effect on the Ecomp with PCL-PVA-Gamma and PCL-PVA-BG-Gamma samples registering 54.462 kPa and 74.03 kPa respectively; almost identical to their non-sterilised counterparts. The addition of erythromycin seemed to slightly decrease the Ecomp. The modulus for the PCL-PVA-Ery-BG-Gamma scaffold was 62.978 kPa, approximately 11 kPa less than the PCL-PVA-BG-Gamma sample. The starkest result was the PCL-PVA-Dry scaffold with a Ecomp of 237.11 kPa, which is at least 3 times greater than all other samples.

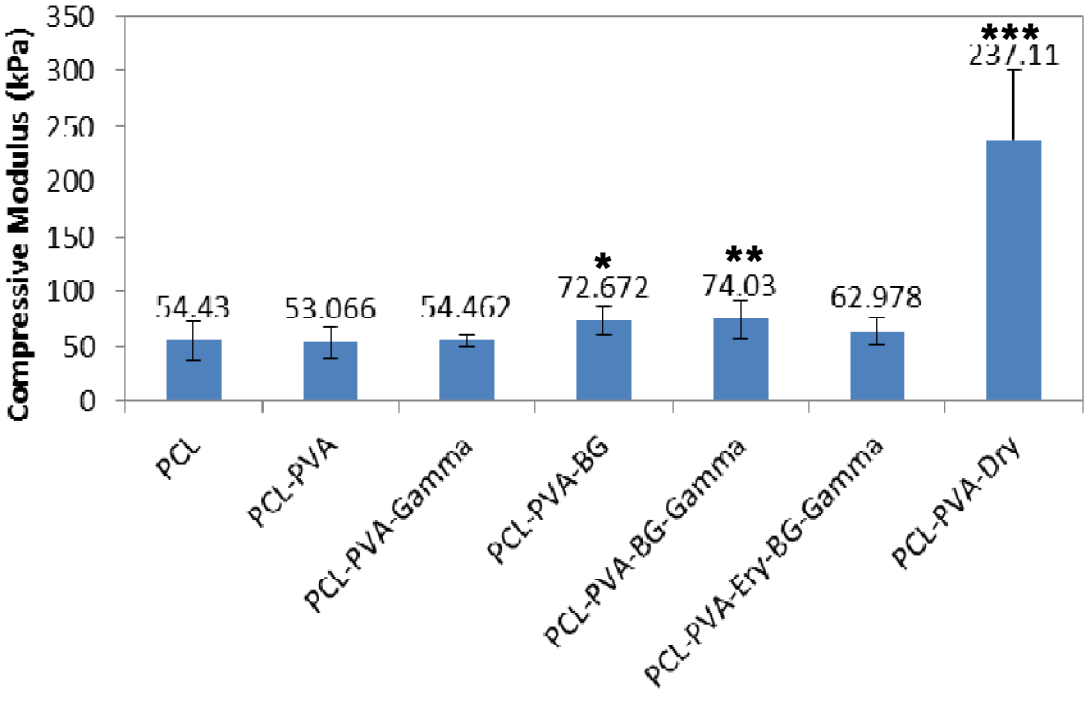

Figure 104. Compression DMA of square scaffold samples. Error bars = Standard deviation; n=5. Significant difference compared with: *PCL-PVA, **PCL-PVA-Gamma and ***All other samples; using Student's t-test ($p \leq 0.05$)

The PCL was tested “hydrated” as a matter of consistency but in reality the hydrophobic PCL absorbed almost zero water after drying on paper. The average mass for the PCL samples was 10.21 mg which is typical for a non-soaked scaffold sample of the same size. The PCL scaffolds tested had been gamma sterilised.

The hydrated PVA coating made no significant difference to the compressive properties of the scaffold ($p > 0.05$). This is an unexpected result given the increased porosity from the coating. The thin web-like coating architecture and its poor mechanical properties compared to the PCL may explain the phenomenon. It is clear the PCL phase controls the mechanical properties of the scaffold.

The bioglass coating caused a statistically significant increase in compressive modulus ($p \leq 0.05$). This is an expected result. Bioglass is a stiff and brittle material similar to typical glasses (albeit not as strong). The surface becomes hydrated and forms a gel when in aqueous solution and softens. But the bulk particles that coat the surfaces of these scaffolds retain their glassy material properties and stiffen the structure against compression.

Gamma irradiation had no appreciable effect on the scaffold compressive modulus ($p > 0.05$). This agrees well with previous hydrogel data that showed negligible changes to hydrogel properties (swelling and gel fraction) after gamma sterilization.

The addition of erythromycin slightly decreased compressive modulus albeit not significantly ($p > 0.05$). This may be because the erythromycin addition to the PVA solution during manufacturing increases its viscosity. This in turn could have caused the delamination of bioglass attached to the PCL surface. Unfortunately, no more samples were available to test PCL-PVA-Ery-Gamma. The non-bioglass sample would have helped better explain this result. The decrease was not significant and the erythromycin may have no effect. This is what was hypothesised; that erythromycin would be almost completely eluted during hydration of samples before DMA and would have no effect on scaffold mechanics.

The unhydrated PCL-PVA-Dry sample had a much higher compressive modulus than the hydrated PVA scaffolds ($p \leq 0.05$). This is due to the PVA being below its glass transition point and polymer chains have little freedom to move. In this state it has mechanical properties like a stiff, brittle, hard plastic.

The scaffolds were tested for compressive modulus as this was considered the key mechanical property for diabetic ulcer healing. Many diabetic ulcers occur due to long term pressure sores that the patient in not aware of due to peripheral neuropathy [106]. Thus the scaffold should not be too stiff compared to

the surrounding tissue lest it act as a pressure point itself. However, the scaffold must not be too weak in compression that it becomes squashed and its porous structure is lost.

Previous studies on testing pig skin in compression found that at 25% strain the modulus was 35kPa [106]. The scaffolds tested here were quite close to this value (with the exception of the non-hydrated scaffold). Scaffolds with bioglass were a little stiffer, although it is difficult to conclude whether this is a negative without further testing. It may be the scaffold should be stiffer to protect pores from collapse. The non-hydrated state greatly increased the stiffness of scaffold and if utilised in this way may create a pressure point which may exacerbate the wound. This gives further need to a soak down step that a clinician may perform before administering to the patient. However, if the wound bed is kept moist enough, the scaffold may swell quickly enough for these poor mechanical properties to have little impact. In fact, this swelling effect may be beneficial in fitting the scaffold to the wound bed; the swelling filling up any spaces and ensuring good contact with the wound bed. To summarise the scaffolds tested had similar mechanical properties to biological skin and are therefore likely to perform well mechanical in the skin wound environment.

4.4.3 Long-term degradation of Ethylene

The batches of 10 biofilter scaffolds were able to reduce a 200-600ppm injection to below the detectable limit even after 86 days of operation (Figure 105). The control serum bottle containing only 300ppm of ethylene remained at this level with no further injections.

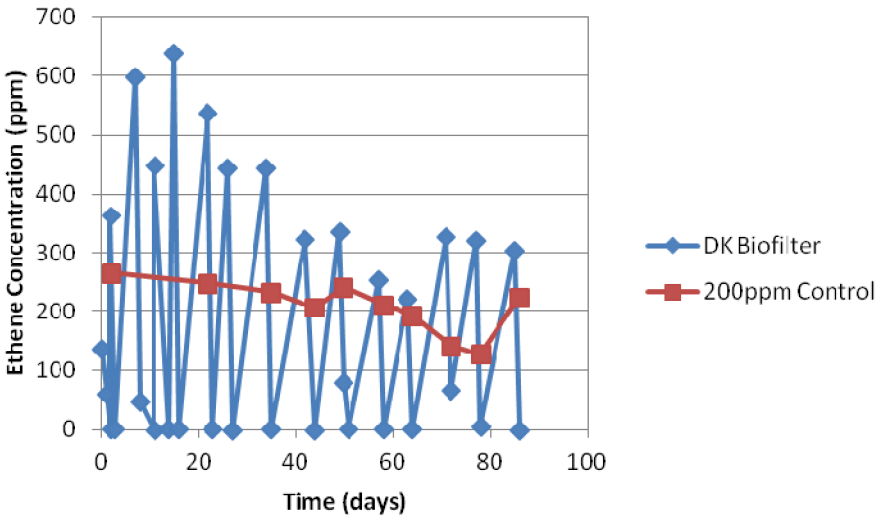

Figure 105. Long-term degradation of ethylene by NBB4-Biofilter. Ethylene was injected at regular time intervals (maximum 7 days) and the ethylene concentration was monitored using GC analysis. The continued breakdown of ethylene is seen in NBB4 biofilter samples. The control, 200ppm ethylene in bottle, was unable to degrade the ethylene.

Although shorter time points were not tested, the rate on the 85th day seemed to be similar to the 1st day of testing with all ethylene degraded within 24 hours. This suggests the biofilter retains operational stability to at least 3 months. Some sample points did not see full depletion of the ethylene in 24 hours. This did not seem to be isolated to the diminished activity of one particular batch and is more likely due to a sampling error or drift of the standard curve from changes in the flame ionisation detector of the GC.

In this experiment the biofilters undergo numerous starvation periods between degrading the ethylene load and the next injection. The biofilters continued to degrade the ethylene despite these starvation periods. Therefore the device has a level of reusability following a period of ethylene starvation. Most biofilter investigations deliver a constant stream of ethylene influent to the biofilter [196-197, 203, 208, 210] as opposed to the simplified re-injection method used here.

Biofilters processing and ethylene injection were done in a sterile manner to prevent contamination. No visual signs of contamination such as fungal growth were seen during the testing period. The white scaffolds eventually turned yellow due to NBB4 growth (Figure 106). Growth of viable cells in a biofilter has been previously reported [203] and is likely to increase operational stability.

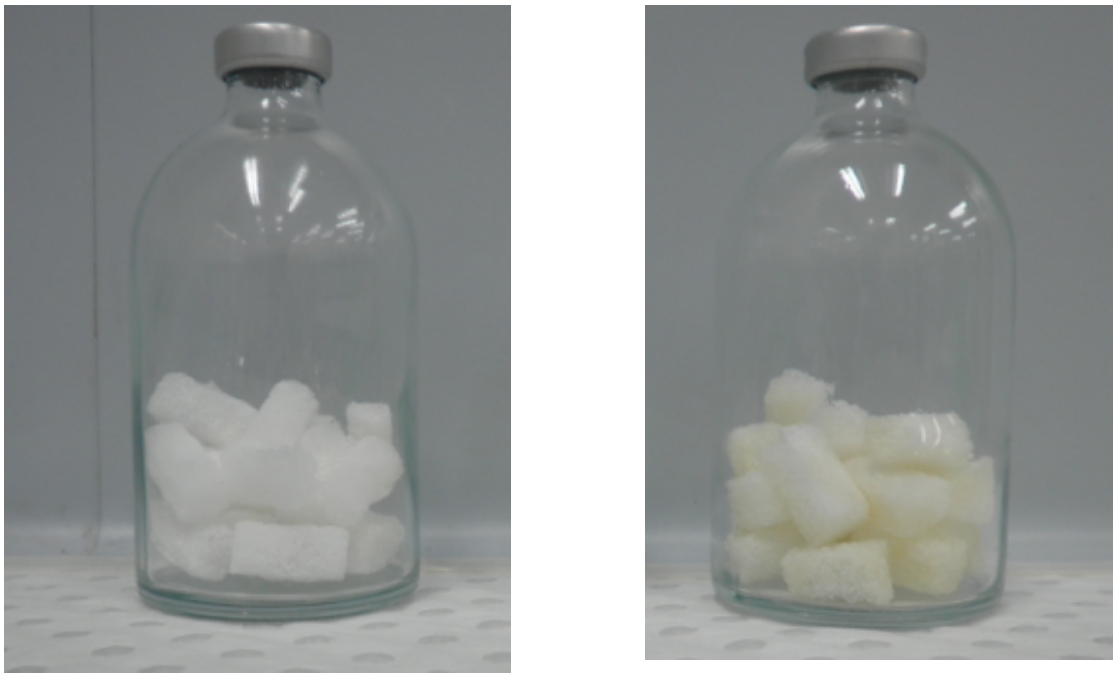

Figure 106. Growing NBB4 in biofilters. Left: NBB4 biofilter 1 day after immobilization. Right: NBB4 biofilter after 90 days of long-term ethylene degradation.

4.4.4 Storage Life of Biofilter

4.4.4.1 Starvation Conditions and Activity

After starvation scaffold batches were put in seal serum bottles along with 100ppm of ethylene and measured by GC until the ethylene peak was below the detectable limit. The ethylene peak occurred between 1.2-1.5 minutes into the run at oven temperature 200C.

All scaffold batches starved in a humidified environment depleted the concentration of ethylene within the serum bottles to below the detectable limit (Figure 107). Slower degradation exhibited after only 2 days starvation is likely due to no sampling point being examined over the first 3 days after ethylene injection. At 62 days the ethylene degradation rate was reduced and it took two days for ethylene levels to go below the detectable limit. Interestingly the 30 day starved sample took 3 days, longer than the 62

day sample. This may be due to differing levels of moisture within these scaffolds. The 30 day sample may have been stored dryer (as humidity inside the bottles could not easily be measured) explaining the loss of activity. The explanation for a loss in cellular activity correlates well with the apparent loss of capacity of these samples with the 30 day sample only able to reduce the ethylene levels to 20ppm.

No appreciable stall time was seen before commencement of ethylene depletion. This suggests that the NBB4 mono-oxygenase enzyme activity is preserved during starvation in a humidified environment up to 62 days.

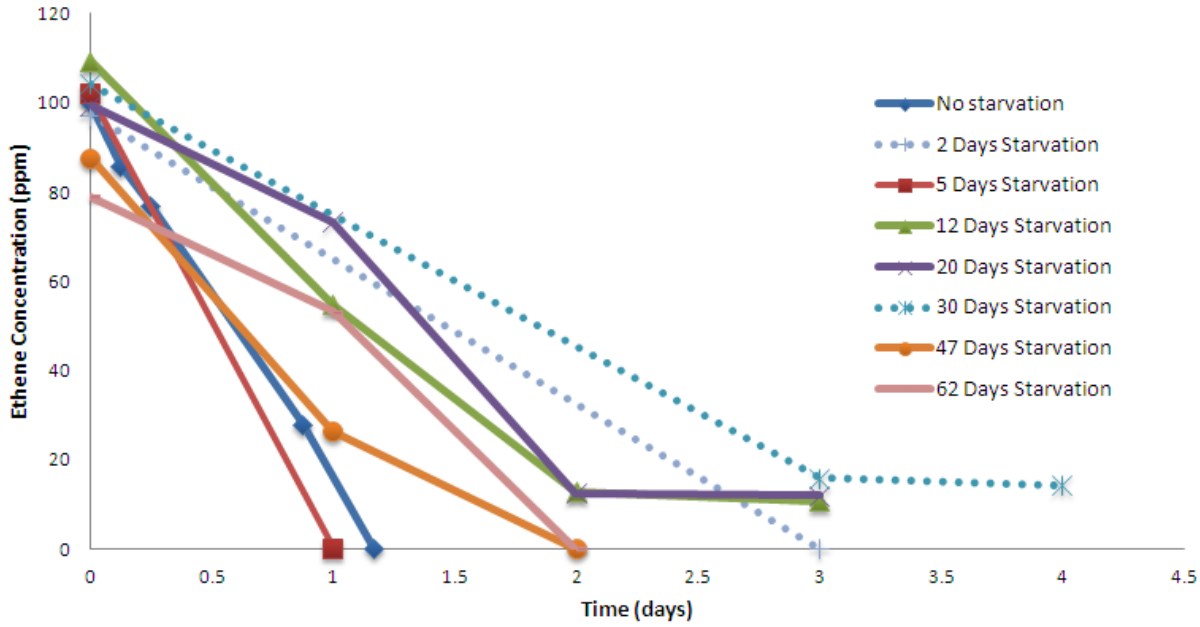

Figure 107. Depletion of ethylene **by NBB4-scaffolds that were starved of ethylene for different periods in a humidified environment.**

Scaffolds starved up to 12 days in a dry environment showed a stall time before commencing to deplete the ethylene in the serum bottle (Figure 108). Scaffold batches starved for 25 days and longer could not deplete the ethylene load in 14 days of monitoring. The desiccation during storage likely rendered most cells unviable and inactive. This is supported by biofilters and trickling systems maintaining a moist environment for bacterial cell survival [205]. The very slow decrease in ethylene is probably due to losses from the serum bottle during injections.

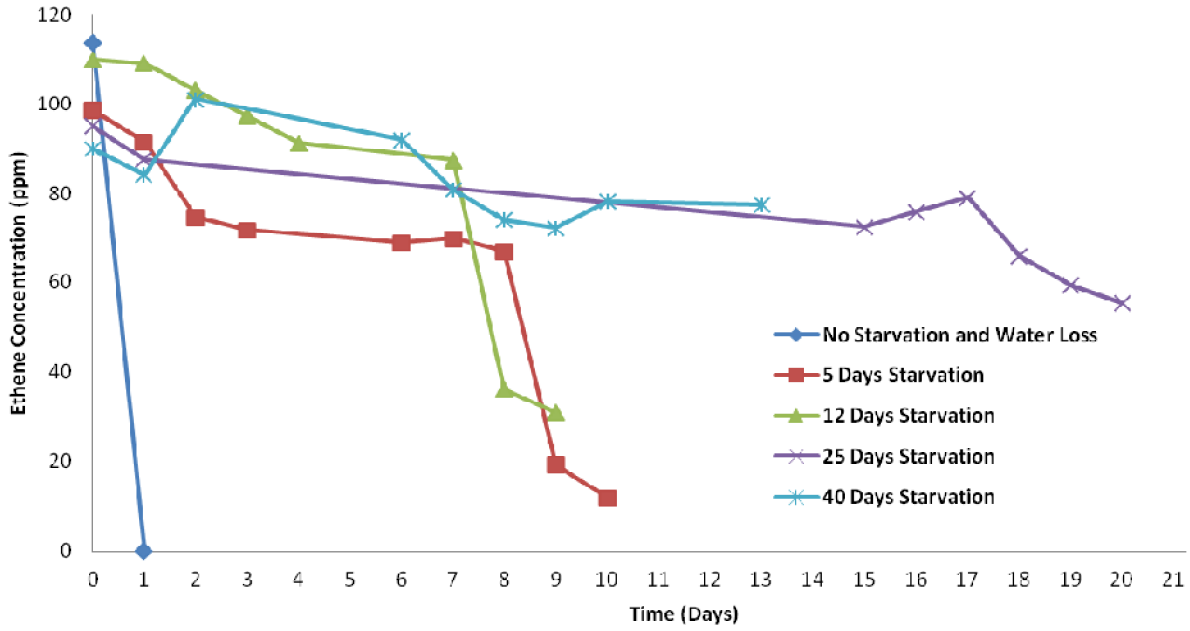

Figure 108. Depletion of ethylene by NBB4-scaffolds that were starved of ethylene for different periods in a dry environment.

The humidified environment had a stark effect on ethylene depletion compared with a dry environment during NBB4 starvation. In a humidified environment scaffolds were able to degrade ethylene even after 2 months ethylene starvation with the ethylene degrading activity dropping 50% compared with no storage time. This biofilter system shows favourable storage performance compared with previous biofilters: Elsgaard *et al* stored biofilters for up to 4 weeks with a > 75% drop in activity [196]. The excellent storage performance is likely due to the MSM agar maintaining a moist environment and providing a reservoir of nutrients for the bacteria.

These results provide a valuable insight into the storage conditions and packaging design of an ethylene biofilter. The successful operation of the biofilter may also rely on retaining a moist environment to prevent NBB4 cells from drying out and losing activity and viability.

4.4.4.2 Viable Cell Recovery

The viable cell number on the scaffold was determined by removing the adhered cells by sonication and vortexing, plating and viable counts. This cell recovery technique was previously tested and showed a 35%-40% recovery rate (data not shown). The 10-fold dilution series went from undiluted to 1000-fold, with the countable plate (30-300 colonies) occurring at 100-fold.

The cell recovery rate was calculated by first determining the initial number of cells trapped in each scaffold. This was done by weighing scaffolds before (m_0) and after (m_1) processing, to calculate the volume of inoculated agar (which had an assumed density of 1) added to each scaffold. This was then multiplied by the known concentration of NBB4 cells in the agar (c_0) (Table 27). The ratio of the viable count after starvation to the initial cell number gave the recovery rate:

$$Cell\ Recovery\ Rate\% = \frac{Viable\ Count}{(m_1 - m_0) \times c_0} \quad (13)$$

It is important to note that the cell recovery rate as calculated this way encompasses both the loss of cells due to decreased cellular viability as well as losses due to the recovery technique.

Table 27. Viable NBB4 cell recovery from scaffolds starved in a humidified environment.

Experimental Condition	Cell per millilitre of Initial Agar Suspension	Cells per Scaffold at Zero time	Cells per Scaffold at Sample time	Cell Recovery rate (%)
No Starvation	3.25×10^6	2.90×10^6	1.11×10^6	38.07%
12 Days Starvation	3.25×10^6	1.54×10^6	4.00×10^5	25.90%
20 Days Starvation	3.25×10^6	1.13×10^6	3.30×10^5	29.29%
30 Days Starvation	3.25×10^6	5.30×10^5	1.00×10^5	18.87%
47 Days Starvation	3.25×10^6	2.33×10^6	3.85×10^5	16.54%

The cell recovery rate showed a continual decrease from 38.07% for non-starved scaffolds to 16.54% after 47 days of starvation. Over a period of 47 days starvation in a humidified atmosphere, NBB4-scaffolds showed a steady loss of the cell recovery rate. Given the recovery method was identical across all samples this loss suggests a genuine loss of viability which fits well with data attained above (Results & Discussion 4.4.4.1) and with other previous studies [196].The 30 day sample had the lowest number of viable cells but also the lowest initial cells per scaffold, explaining the lower than expected ethylene-degrading activity of this sample (Results & Discussion 4.4.4.1). The initial low cells per scaffold is likely due to batch to batch variance in the manufacturing process. A sample at 62 days starvation was not

included in the data because the viable counts were too high even after a 1000-fold dilution. This could suggest growth on the scaffold during starvation period.

The low recovery rate at day 0 was expected as the act of removing pathogens from scaffolds is not particularly efficient even without gel entrapment [181]. This could tentatively be used to determine the daily loss in cell viability, however other mechanisms could affect recovery rate such as increased biofilm thickness having a negative effect and loss of gel structure possibly increasing recovery rate with time [131].

Another analytical approach was employed to isolate the loss in NBB4 viability with increasing starvation times. The recovery rate when scaffolds were not starved (Table 27) was used to calculate the 'true number' of cells on the scaffold by taking into account losses during processing. Relating this to the initial cell number determined by weighing gives the following equation:

$$Relative\ Cell\ Viability\% = \frac{Viable\ Count\ \times\ {}^{1}/_{38.07\%}}{(m_1 - m_0)\ \times\ c_0} \qquad (14)$$

As predicted the relative cell viability decreases with extended starvation times. However after 47 days starvation there is still 43.46% cell viability. This correlates to the ethylene degradation data in Results & Discussion 4.4.4.1 which shows approximately half activity after 47 days starvation. A linear trend is seen, from which the rate of decreasing cell viability with starvation time was calculated to be 1.16% loss in viability per day (Figure 109). Obviously though the possible NBB4 growth seen in the 62 day sample puts this relationship into question.

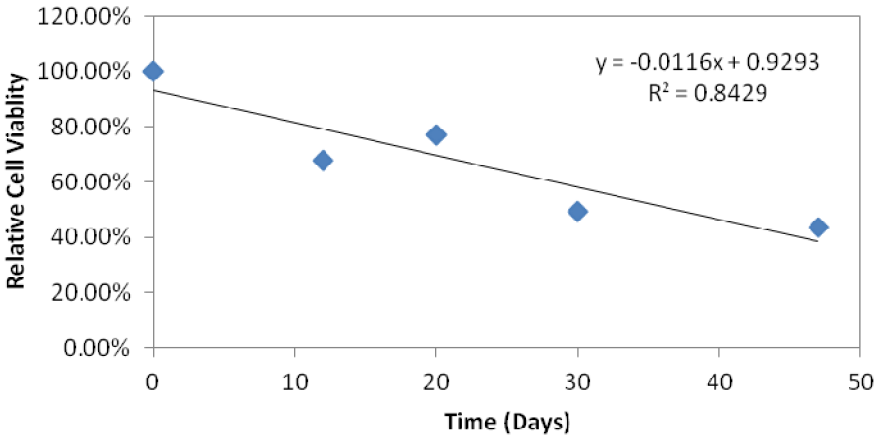

Figure 109. Loss of NBB4 viability on scaffolds starved for different periods in a humidified environment.

4.4.5 Fruit Preservation

Batches of three un-ripe bananas were put into air tight jars along with ten NBB4 biofilter scaffolds. This was compared to batches of bananas with no biofilters, so the action of the biofilter could be seen (Figure 110). After 4 weeks, banana batches that were in the presence of biofilters were a healthy yellow colour. In contrast bananas that did not have biofilters in the air tight jars appeared brown and black. These bananas exhibited other symptoms of physiological damage such as liquidation. These bananas also were colonized by fungal infections, which are also reported to be in part ethylene mediated along with the increased susceptibility to other pathogens [198-199].

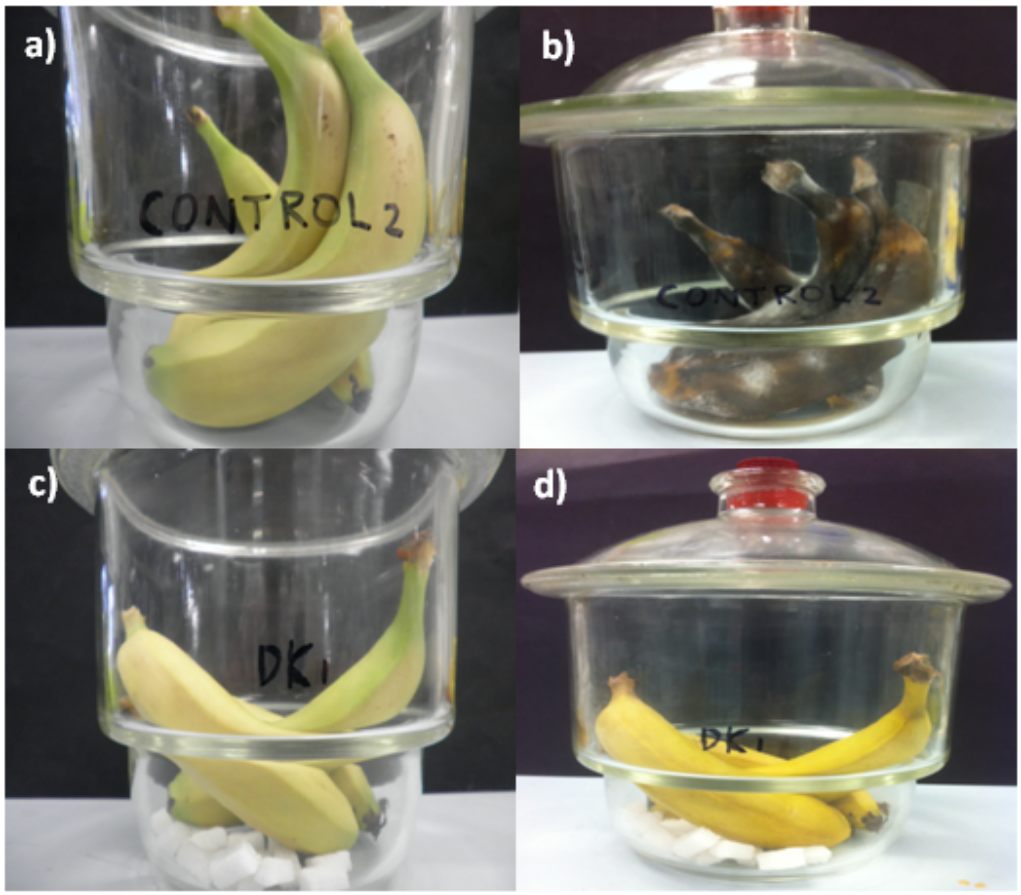

Figure 110. Preservation of Bananas. a) Control bananas time = 0; b) Control bananas time = 4 weeks, browning, fungus and liquidation can be seen; c) NBB4 Biofiltered bananas time = 0; d) NBB4 Biofiltered bananas time = 4 weeks, still yellow and healthy.

A NBB4 concentration dependent assay was set up to observe the minimum amount of active NBB4 immobilized on scaffolds to preserve bananas over a period of 4 weeks. Biofilters were constructed with varying OD_{600} absorbencies in the NBB4-agar suspension. This resulted in biofilters with varying numbers of immobilised NBB4 and thus varying ethylene degradation efficiency. Cell densities of OD_{600} = 0, 0.01, 0.1 and 0.8 were used. The OD_{600} = 0 sample was an agar coated scaffold without any NBB4 cells added.

The biofilter activity can clearly be seen by the results with the higher OD_{600} biofilters able to better preserve the post-harvest bananas (Figure 111). In particular there is a stark comparison between the OD_{600} = 0.8 sample and the no-cell samples. The former was able to maintain a yellow colour on the bananas for 30 days whereas in the latter, bananas were black after 15 days. In theory, the cell density could be increased further to produce biofilters of even greater ethylene degrading activity. Indeed, gel entrapment bioreactor systems can have very high biomass loading, up to 700mg/g [126]. The limit to

this would probably be when the number of cells increased the viscosity of the agar, affecting the optimised coating. There may also be a point where addition of more NBB4 is inefficient as cells become overcrowded in the thin agar layer and are unable to contact the gas interface and consume ethylene.

This experiment also shows how small the filter could potentially be. For example, four scaffolds at OD_{600} = 0.8 were effective at preserving three bananas. Four scaffolds accounts for a volume of approximately 7.5 cm^3 with dimensions: 15 x 17 x 11 mm. As explained above there is no reasons why the cell concentration in scaffolds could not be increased exponentially. This could result in either an even smaller design to fit into supermarket packaging or a similar sized filter which could potentially preserve a large container of produce.

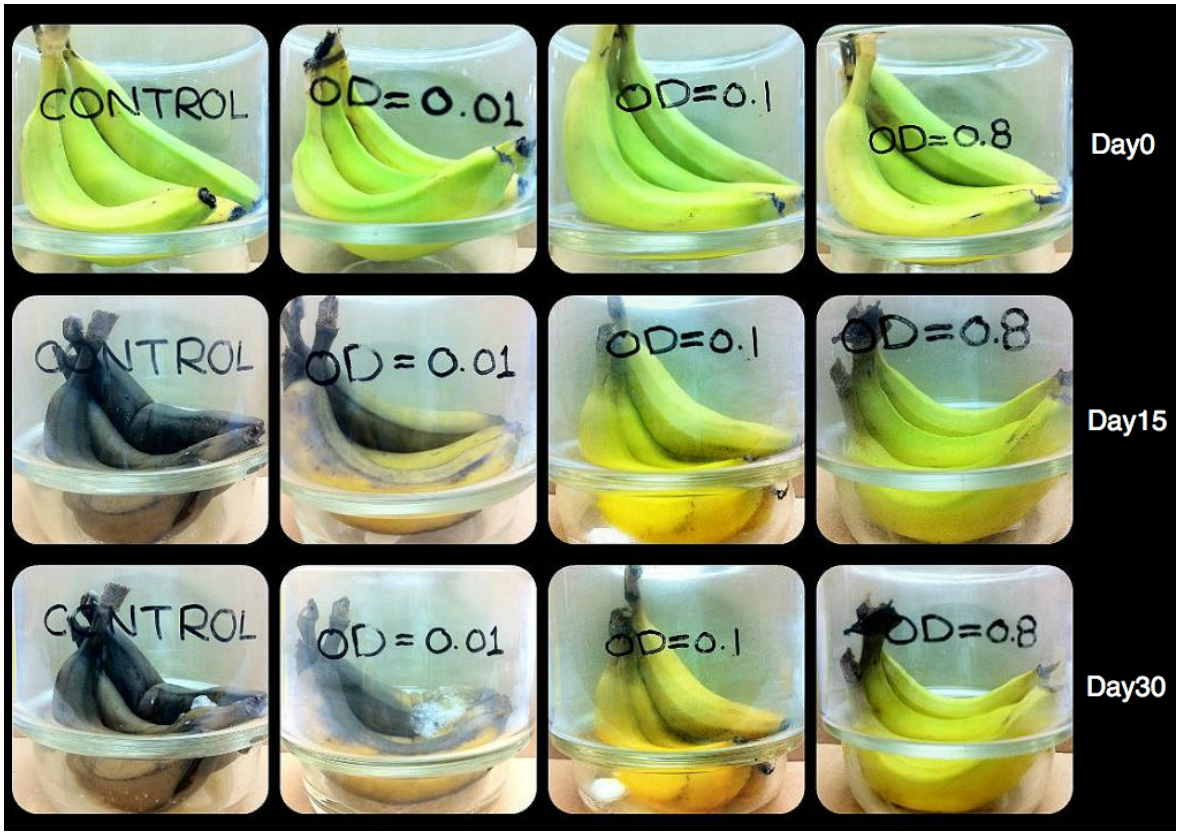

Figure 111. Preservation of bananas dependent on NBB4 concentration. Different cell densities as measured by optical density (OD600=0, 0.01, 0.1 and 0.8), tested on bananas ripening activity after 0, 15 and 30 days.

5 Device Design Summary

5.1 Antibacterial Synthetic Skin Graft

5.1.1 User Requirements/Design Inputs

A chronic skin ulcer is a debilitating condition for patients. They are a result of poor blood flow to the injured dermis resulting in slow healing. These wounds are regularly subject to chronic bacterial and fungal infections which cause inflammation and prolong healing as well as imposing their own pathogenic effects. These ulcers are becoming more common due to the increase in diabetes and an aging population.

For many years clinical treatment for chronic skin ulcers was contentious and generally ineffective. The wound was kept clean and dry and dressings were applied in an attempt to prevent biofouling. Systemic antibiotics were also administered as a prophylactic against infection. More recently dressings have become more advanced; containing antibiotics, antibacterial factors, dermal stem cells and growth factors. Some tissue engineering solutions exist on the market but these are expensive and have not demonstrated a correspondingly large increase in healing rates. Herein I have designed a synthetic skin graft device that improves on past treatments in terms of both clinical efficacy and cost efficiency.

Clinicians and Patients are technically both the 'users' of this device. Clinicians must understand, possibly alter and implant the device while the Patient is the host of the implanted device. As such the different user requirements for each will be addressed separately for simplicity. Consideration of these requirements shows the end users are being considered.

Clinician user requirements:

1. Simple handling and implantation of device
2. Limit maintenance or revision of device
3. Produce good patient outcomes (see Patients)

Patient user requirements:

1. Limit maintenance or revision of device

2. Minimal pain or discomfort from implant
3. Prevents infection over an extended period
4. Reduced time of hospitalisation and wound treatment

Regulatory requirements are constraints imposed by regulatory bodies and are usually related to the safety of the device. For implanted tissue engineering devices this usually relates to the safety, efficacy and sterility of the product:

Regulatory requirements:

1. Device conforms to international standards regarding sterility and validation of sterility; Prove device maintains a sterility assurance level (SAL) of less than 10^{-6}.
2. Device conforms to international standards regarding sterile packaging and its and validation.
3. Device is adequately traceable and identifiable through use of labelling and quality systems.

The User and Regulatory Requirements have been combined to form distinct and specific design inputs for the wound healing scaffold. These have been summarised into the table below (Table 28). It has to be mentioned, that design inputs in some circumstances be subject to validation and verification in unison. This is intentional as different aspects of the device must be tested to understand possible and anticipated synergistic effects.

5.1.2 Design Evolution

To meet user requirements a synthetic skin graft was envisioned. This graft would be a leave-in solution, distinct from a wound dressing that needs to be changed regularly. The graft would be bioactive for skin tissue and accelerate healing while simultaneously fighting infection in a sustained manner. To ease the costs on health systems the graft would be batch manufactured, use inexpensive synthetic materials and terminally sterilized.

The initial design concept was based around the PCL scaffold developed by Elizabeth Boughton [237] but with attenuated antibacterial and bioactive coatings. The PCL scaffold would first be coated with Chloramphenicol by a soak-in process then coated with 45S5 bioglass. This increases the bioactivity of the scaffold for soft tissue while entrapping Chloramphenicol due to the closing of micropores from the heat-based coating method. The release of chloramphenicol would be controlled by a biodegradable

metallic envelope (MgZnCa amorphous alloy). This bulk-metallic glass (BMG) layer is itself antibacterial in nature and as it degrades it would allow the slow, controlled elution of the chloramphenicol coating beneath. The bioactivity and mechanical properties of this scaffold encourage host skin cells to attach and proliferate.

The chloramphenicol soak-in method initially showed promise as a high antibacterial loading efficiency was achieved on porous scaffolds [240]. However testing the chloramphenicol soak-in on PCL discs revealed only superficial adhesion which explained the extremely rapid release on chloramphenicol in previous antibiotic elution studies [240].The BMG coating was determined to be non-homogenous over the scaffold surface and inadequate as a degradable envelope to control the release of chloramphenicol. This drug delivery mechanism would not be able to maintain an inhibiting concentration of antibiotics for an extended period. However, BMG as an antibacterial agent may have its use in the future. It was found to be bactericidal against *S. aureus*. Further, metals have been shown to be effective against biofilms where antibiotics are less so [76, 134].

A new drug delivery system was required to address the sustained release design input. A new composite scaffold was designed with two distinct phases. The first: the PCL matrix with interconnected pores, >95% porosity and mechanical properties mimicking the dermis. The second: phase is a poly(vinyl-alcohol) (PVA) webbing that coats the PCL matrix. This webbing is a dehydrated crosslinked hydrogel, which when *in vivo* conditions swells releasing bioactive and antibacterial substances entrapped within. PVA has been used and tested extensively for drug delivery applications [25-26, 31, 35, 38, 165, 168, 258-259]. Creating the PVA web-like coating was inspired by results from the gel entrapment of agar. Some parameters had to be tweaked to account for the change in material but the base concept is very similar. The porosity could be controlled by varying the PVA concentration but in the same way as the NBB4 biofilter, a high porosity was required but was inversely proportional to the active ingredient in this case the amount of antibiotic. A PVA concentration of 10% w/v was decided upon which corresponded to only 33µl of gel coated onto each scaffold for possible drug loading. Because of this the activity of the antibiotic and drug loading methods were reassessed to ensure sustained activity.

MIC/MLC assays shows that chloramphenicol was not bactericidal and is consistent with the literature [150]. Although the bacteriostatic nature of the drug does not necessarily affect their clinical performance [150], it does affect results of long-term *in vitro* studies where a full resurgence on bacteria may be seen after the concentrations of the bacteriostatic antibiotic fall below the MIC. On the other

hand, this may allow very obvious confirmation of sustained release of antibiotics. Erythromycin was used to replace chloramphenicol. Erythromycin in mainly reported as bacteriostatic [149-150], but has been shown to have a much lower MIC than chloramphenicol when tested against 60 MRSA isolates [157] making it more relevant for wounds. This means it is more likely to have sustained antibacterial activity in comparison to chloramphenicol.

Design changes needed to be made to increase the drug loading efficiency given the very thin PVA coating (a mere 33 µl of gel per scaffold). To further increase the drug loading efficiency of the PVA coating, PVA solutions were formed with ethanol. Erythromycin is much more soluble in ethanol than water [154] and PVA solutions could be formed and remained homogenous using up to 50% ethanol [165]. PVA hydrogels were cross-linked by freeze thawing – a common technique which introduces physical cross-links in the polymer structure [25-26, 30-32, 165] without the use of harmful chemical cross-linkers [27, 38, 260] or ionizing agents that would inactivate the antibiotics [163-164, 253]. After cross-linking the scaffolds were dried and ethanol volatised out of the system. Erythromycin diffused from the PVA hydrogel coating in a sustained manner. Manufacturing scaffolds with a higher ethanol concentration in the PVA solution allowed higher loading of erythromycin. PVA scaffolds made with 50%v/v ethanol were able to prevent the growth of *S. aureus* for up to 5 days.

The erythromycin release profile from the scaffold was standard for drug delivery devices – a burst release followed by sustained release [31, 35, 169].This phenomenon caused the scaffold to initially release very high concentrations of erythromycin that were determined to have some cytotoxicity. To overcome this a soak-off method was designed to bring the initial concentration down to biocompatible levels. A 15 minute soak in sterile PBS proved enough to accomplish this. This simple procedure could be conducted by the clinician just prior to implantation of the device. This also softens the PVA in the scaffold allowing it to be cut to size if needed and applied to the wound.

5.1.3 Final Design

Table 28. Design Outputs of Synthetic Skin Graft final design iteration.

Design Input	Design Output	References	Validation
Biocompatible/Bioactive	PCL, PVA are biocompatible and FDA approved in medical devices. 45S5 Bioglass is bioactive	[107, 261]	4.4.1.5
Bioabsorbable	PCL, PVA and 45S5 bioglass are all bioabsorbable	[15], [262]	-
Sustained Bactericidal	Erythromycin is broad spectrum antibiotic. Especially susceptible to MRSA. Entrapped in thin film of PVA for slow release	[157], [263]	4.3.1, 4.3.2, 4.4.1.5
Skin-like mechanical properties	Thin film PVA will have very little effect on mechanics. PCL scaffold already has properties that mimic skin.	[264], [237]	4.4.2
Sterile and packaged	Dehydrated, Gamma sterilized, for simple packaging	[163], [181]	4.3.1.2
Inexpensive	All synthetic materials that are readily available, simple scalable manufacturing procedure	[28, 116]	3.1.2.2
Good Shelf Life	Dehydrated, encapsulated bioactive components to extend shelf life	[28, 116]	4.3.1.2

The final design is a composite scaffold designed for accelerating the healing of chronic wounds. This scaffold should be thought of as a synthetic skin graft. It is a leave-in solution unlike wound dressings which need to be continually reapplied which increases the risk of infection. Each of the design inputs has been addressed through the final design (Table 28), encompassing a complete solution.

The composite scaffold contains two distinct phases (Figure 112):

1. Polycaprolactone (PCL) matrix with interconnected pores, >95% porosity and mechanical properties mimicking the dermis. It is coated with 45S5 bioglass - a known bioactive compound which increases fibroblast attachment and angiogenesis [71, 237].

2. Poly(vinyl-alcohol) (PVA) webbing that coats the PCL matrix. This webbing is a dehydrated crosslinked hydrogel, which when *in vivo* conditions swells releasing bioactive and antibacterial substances entrapped within. Erythromycin diffuses from the hydrogel in a sustained manner preventing opportunistic pathogens such as methicillin resistant staphylococcus aureus. The PVA webbing also serves to preserve a moist wound environment, shown to be vital for healing.

The scaffold is removed from its sterile packaging and soaked in a sterile solution of PBS for 15 minutes to optimise the antibacterial load and to soften the scaffold. Meanwhile the wound is debrided and cleaned of necrotic tissue. The clinician can then cut the scaffold to a size to match the dimensions of the wound cavity with sterile scissors. The scaffold is then implanted directly into the wound and secured by application of a secondary wound dressing. Once in vivo the PVA hydrogel phase swells to deliver antibiotics in a sustained manner. Meanwhile, fibroblasts are attracted to the bioactive glass and adhere to the PCL matrix. As time goes on, fibroblasts proliferate and begin to make extracellular matrix resulting in wound closure. After the wound has healed the scaffold breaks down naturally leaving only healthy tissue behind .

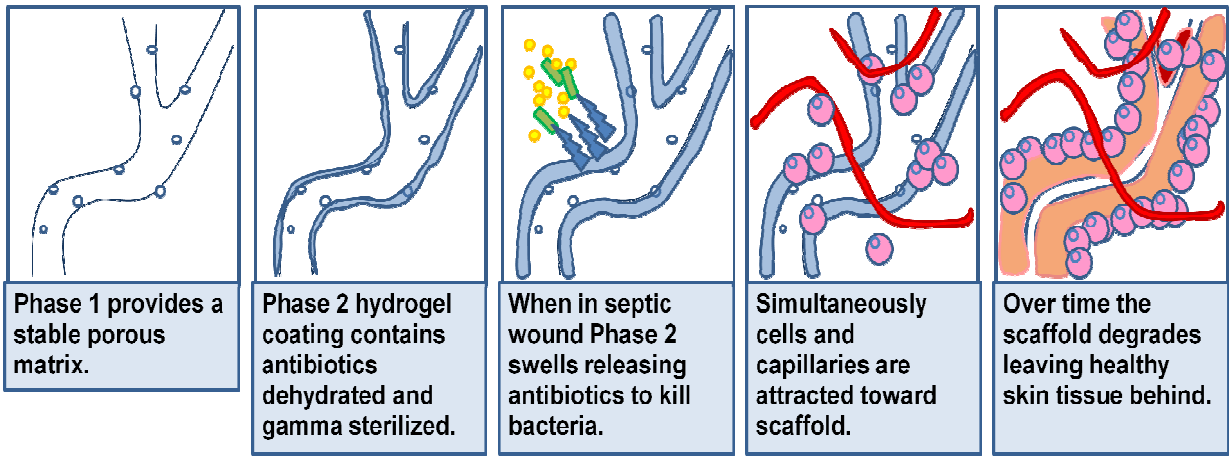

Figure 112.The structure and in vivo function of the novel synthetic skin graft. The schematic focuses on a single strut of the overall porous network.

All the materials used in the composite scaffold are biocompatible and non-toxic. Further all the material are bioabsorbable [15, 262] meaning that implant will eventually be naturally broken down in the patient which is necessary for a leave-in solution and allows the natural tissue to takeover. The materials are also all synthetic and readily available – A downfall of many wound healing scaffolds in the past has been due to prohibitive costs due to use of expensive natural polymers and growth factors [28]. The composite uses both hydrophobic adherent PCL to house cells and hydrophilic anti-fouling PVA to prevent biofilm formation – a beneficial tissue engineering design that has been previously described [142-143] but never carried out in this way.

The manufacturing method is simple, elegant and scalable. Gamma irradiation is employed for terminal sterilization which omits the need for expensive aseptic processing methods that are so common in tissue engineered products [163, 181, 265]. The scaffold is packaged dehydrated which ensures a long shelf life and further drives down costs.

The efficacy of the final design was tested in the most sophisticated *in vitro* co-culture wound model to date. The scaffold was validated to attract dermal cells to attach and proliferate while inhibiting the growth and biofilm formation of *S. aureus*, the most common pathogen in chronic wounds [101]. The antibiotic protection against bacteria was sustained and local which is preferred over the use of systemic antibiotics which require high doses and have harmful side effects [101]. The scaffold has mechanical properties that very closely match skin and provides support against further trauma.

This scaffold overcomes limitations of current wound healing treatments. The scaffold is a leave-in solution which does not require frequent changes like wound dressings. This reduces health care costs and improves patient life style [12]. Tissue engineered skin substitutes have shown great potential for wound healing, but in the past they have suffered due to high cost [28], antigenicity and infection carry over [101]. Many studies have reported tissue engineering scaffolds that allow dermal cell growth and may be candidates for wound healing. However, many of these use expensive naturally-derived polymers, cellular components or growth factors [55, 110, 119, 182] and of the more cost-effective scaffold designs very few can deal with infection [107]. Antibacterial wound healing scaffolds commonly contain cytotoxic agents like silver [41, 55], or employ enzymes [266] and peptides [116] which cannot be terminally sterilized or dehydrated which consequently elevates production costs. My design promotes healing through dermis cell adhesion and angiogenesis while simultaneously fighting bacteria. It is inexpensive compared to other tissue engineered grafts due to smart synthetic material selection, a scalable manufacturing route, terminal sterilization and long shelf life. In summary I have designed a synthetic skin graft that overcomes shortcomings of previous traditional treatments and tissue engineered scaffolds making it a realistic candidate for chronic wound care.

5.2 Probacterial NBB4 Ethylene Biofilter

5.2.1 User Requirements/Design Inputs

The price of fresh fruit is increasing due to a number of factors such as a growing population and climate change. Despite this a large proportion of fruit goes to waste. A key reason for this is ethylene mediated spoilage [201-202]. Ethylene is a gaseous pollutant and plant hormone that is emitted by fruits and in turn accelerates their ripening and degradation. This is particularly a problem in closed environments where elevated ethylene concentrations can greatly increase spoilage.

Many methods already exist to remove ethylene. Of these, biofiltration presents a method with potential: Active bacteria are immobilized and metabolically breakdown ethylene to harmless products while sustaining themselves. This allows biofilters to remain active theoretically indefinitely offering a distinct advantage over chemical scrubbers. Herein I design a biofilter using an existing scaffold as a support to immobilize bacteria.

For this device the end user is not as obvious as for the wound healing scaffold. Ethylene mediated food spoilage occurs at all parts of the fresh fruit supply chain meaning users will require different designs based on the scale of the problem. For example, a biofilter for fruit distributors have different requirements and properties to a biofilter for supermarkets. Because of this I focussed on the base technology – the active biofilter component.

User Requirements:

1. Non-toxic and non-pathogenic
2. Active agents are totally immobilized
3. Sustained efficient degradation of ethylene
4. Cost-competitive compared with other ethylene removers

The User Requirements have been further distilled to form specific design inputs for biofiltration of ethylene. These have been summarised into the table below (Table 29). As mentioned above design inputs in some circumstances be subject to validation and verification in unison via device pilot studies.

5.2.2 Design Evolution

To meet user requirements a biofilter was envisioned that used environmental *Mycobacterium* as the active ethylene degrading agents. Environmental *Mycobacteria* are non-pathogenic and can survive on minimal nutrients for long periods. *Mycobacterium chubuense* strain NBB4 is an environmental bacteria isolated by ethylene enrichment from estuarine sediments. NBB4 has the ability to survive solely on ethylene as an energy source [233-235] making it an ideal candidate for biofiltration. Ethylene-active live NBB4 cells were to be immobilized on the PCL scaffold, taking advantage of the support structures large surface area and 95% porosity allowing high activity and diffusion efficiency respectively [181, 237].

The method of immobilization initially decided upon was adhesion. The thinking was the hydrophobic PCL scaffold would allow NBB4 cells to be adsorbed [123, 128]to its surface and the cells would later form biofilms, immobilizing themselves to the scaffold [122, 131]. Adhesion immobilization requires only very simple processing (a cell suspension is agitated in the presence of the immobilization support) making it a cost effective method. Adhesion has the additional advantage that the processing procedure is not harmful to bacteria and hence maximises activity of the cells [126].

The adhesion method proved to be unreliable with levels of bacterial adhesion efficiency varying wildly between batches. Additional studies proceeded to test designs that would improve the efficiency and reliability of the NBB4 adhesion. In an attempt to improve the adhesion of NBB4, modifications to the scaffold surface and the NBB4 cell wall were attempted.

Modifications to the scaffold surface were attempted first because altering materials is generally more predictable than altering biology. Given the development of a bioglass coating method for the scaffold a similar method was employed to apply coatings of glass and silica coatings. Inorganic ceramic immobilization supports have been used extensively [126, 215, 224], and as a particulate coating the surface area would be greatly increased. Whether it was due to the increased surface area or a favourable change of surface interactions, adhesion efficiency was increased by these coatings. However, the coatings involved an extra step of manufacturing and made the scaffolds more difficult to handle, which somewhat negated the advantages of adhesion immobilization.

Modifications to the NBB4 cell surface were carried out by varying the growth phase, which had been reported to influence the capsular material that forms around the bacterial cell wall. It was found that harvesting NBB4 at an earlier phase of growth did increase the adhesion efficiency, a result that corresponded to prior work on the adhesion of *Mycobacterium marinum* [120]. However preferential binding to the glass vessels in which the adhesion assays were conducted did suggest the adhesion of NBB4 was not necessarily preferential toward the scaffold.

Given the reasonable success of varying growth phase, solvent treatment processes were designed to solubilise and remove capsular material from the NBB4 cell wall. Washes of acetone and methanol were trialled which greatly increased the adhesion efficiency but unfortunately inactivated the cells such that they could not degrade ethylene. *Mycobacterium rhodesiae* strain NBB3 was substituted for NBB4 because its roughened macroscopic morphology and clumping nature suggested little capsular material and a more hydrophobic surface. NBB3 also contains monooxygenase enzymes allowing it to subsist solely on ethylene. The NBB3 had much higher adhesion efficiency than NBB4 and was able to degrade ethylene. However, the adhesion was not homogenous and very clumpy suggesting cell-cell adhesion was preferential over cell-scaffold. Adhesion was also found to be distinct from immobilization as adhered cells were sloughed off the scaffold as they were handled during testing. This cell leakage has been reported in adhesion immobilization systems [126, 131, 208] and is an intolerable characteristic for biofilter applications with food.

Exhaustive design iterations and experiments were unsuccessful in improving the efficiency and reliability of adhesion immobilization. A new design was conceived using the gel entrapment immobilization method. The concept was to entrap active NBB4 cells in a thin coating of agar on the scaffold surface. It was hypothesised that there would be a balance between the porosity and the gel volume to load NBB4 cells that would give an optimum efficiency. It was found that these parameters could be controlled by varying the agar concentration and thus the viscosity of the gel solution. Ethylene degradation studies then confirmed the hypothesis and 0.4% w/v agar was found to give optimum ethylene-degrading efficiency. Later pilot studies revealed that increasing the concentration of the NBB4 cells in the agar solution increased the activity of the biofilter.

Shelf-life studies showed the importance of a humidified packaging system for storing the biofilter. Packaging that was exposed to the air allowed the biofilter to dry out such that the cells were not active and could not degrade ethylene. Biofilters that were stored still containing some moisture and packaged in air tight containers could degrade ethylene even after 60 days of storage in the presence of no gaseous energy source. A simple packaging solution could be designed to maintain a long shelf life for the biofilter.

5.2.3 Final Design

Table 29. Design Outputs of Ethylene biofilter final design iteration.

Design Input	Design Output	References	Validation
Non-pathogenic	NBB4 fast growing, environmental *Mycobacterium*.	[232, 236]	-
Immobilization of active bacteria	NBB4 are entrapped in physically crosslinked agar gel	[102, 205, 213, 216]	4.1.1, 4.2.3
Efficient removal of ethylene	Ethylene is degraded by active NBB4; high porosity for excellent diffusion characteristics	[128, 196, 233, 235]	4.3.3.1, 4.4.3, 4.4.5
Long term removal of ethylene	Living NBB4 grow and survive on ethylene as sole carbon source; Agar used to deliver key nutrients and moist environment	[233, 235, 239]	4.4.3, 4.4.5
Inexpensive	Readily available materials; simple scalable manufacturing procedure	[128, 201]	4.1.1
Good shelf life	Hardy environmental microbes requiring minimal energy; humidified packaging.	[232-233, 235]	4.4.4

The final design is a composite scaffold for the biofiltration of ethylene. The composite consists of a PCL matrix which serves as the immobilization support material. It has > 95% porosity allowing rapid diffusion of ethylene through the filter and providing a very high surface area for gas exchange and bacterial metabolic activity. The PCL matrix has excellent mechanical properties which prevents collapsing of pores to minimize mass transfer resistance. This is coated in a 0.4% MSM-agar gel which carries ethylene-active NBB4 cells. When the agar sets the NBB4 are entrapped in a thin layer of agar allowing unimpeded diffusion of ethylene to the cells. The MSM-agar can be kept liquid at low temperatures and sets without the need for chemical crosslinkers which preserves the viability and activity of the bacteria. The additional benefit of the MSM agar is it can be used to deliver trace elements to the bacteria to extend their survival. It also attracts and stores water to maintain a hydrated environment crucial for cell viability. NBB4 cells efficiently break down ethylene to produce carbon dioxide and water. NBB4 is a non-pathogenic strain of *Mycobacterium* and is firmly immobilized onto the scaffold surface by the gel coating.

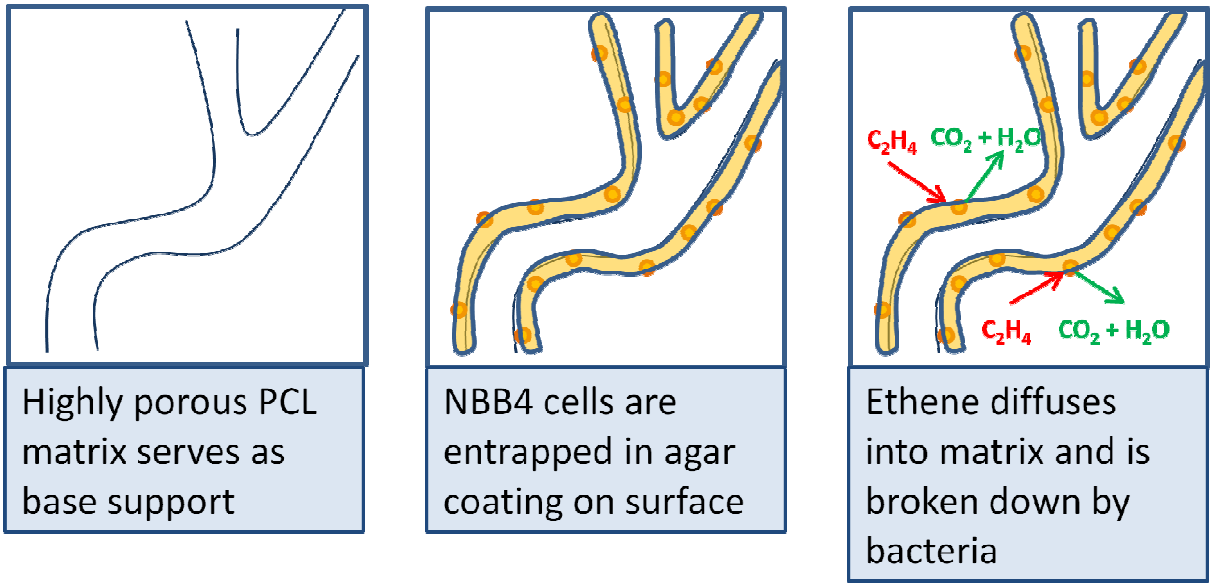

Figure 113. The structure and function of the novel ethylene biofilter. The schematic focuses on a single strut of the overall porous network.

The biofilter is manufactured using a simple, scalable process so as to stay cost-competitive with other ethylene removal systems. A humidified airtight packaging system can be achieved by enclosing semi-dry biofilters in airtight packaging. In this state, the biofilter can remain active up to 60 days.

The operational stability of the biofilter was tested in a long-term ethylene degradation assay. The biofilter continued to break down ethylene for up to 85 days (latest tested time point) with no perceivable difference in the rate of degradation over the time period. This biofilter design showed an operational stability similar to that of other ethylene biofilters [196, 203, 208, 210]. The efficacy of the final design was tested in a fruit preservation study. To my knowledge there have been no studies that test the effects of ethylene biofiltration directly on fruit [198]. At ambient temperature, the biofilter was able to keep bananas yellow and fresh for up to 30 days compared to the control in which the bananas rotted in 15 days. It can be concluded that the mechanism of this preservation is through the removal of ethylene by immobilized NBB4 of ethylene. As ethylene is a fruit hormone that is produced by many different fruits [196, 198], it follows that the biofilter designed here could be used for preserving a large variety of fruits.

This biofilter design represents an effective alternative to chemical and physical ethylene scrubbers. The active NBB4 bacteria continue to survive and proliferate on the PCL support material, meaning the biofilter will continue operating while other filter systems would require their active ingredients to be replaced [196-197, 203, 205, 208]. To my knowledge this is only the second ethylene biofiltration system that uses the gel entrapment method to immobilize bacteria with the majority of biofilter designs using natural adhesion [196-197, 203]. The gel entrapment method in my design may be advantageous as the agar coating can be used to deliver essential trace nutrients to the cells and create a moist environment which may increase the working life-time of the biofilter compared to those using adhesion. Further, I have demonstrated control over the agar coating properties which allows close control of biofilter characteristics. This concept has not previously been reported and would be difficult to adapt using natural adhesion immobilization [126, 205]. The NBB4 cells used are non-pathogenic fast growing *Mycobacterium* [232, 236] and are tightly immobilized within the agar coating. The biofilter demonstrated fruit preserving properties even when small amounts of active biofilter was used. The majority of previous studies on ethylene biofilters had been concerned with larger filter system designs [196-197, 203, 208], but this study suggests biofilters may also be used for smaller scale designs like active packaging [202]. Fruit preservation may not be the only use of this design as NBB4 has been used for bioremediation of industrial waste [235]and epoxidation for the chemical industry [233]. In both cases the immobilization of NBB4 on a porous structure would be ideal for improving reaction efficiency, which suggests multiple applications for the biofilter design. In summary, I have designed a novel and effective ethylene biofilter for the preservation of fruit and other possible applications.

6 Conclusions & Recommendations

6.1 General

- A highly porous PCL scaffold was used as the base for the dichotomous design of composite scaffold systems.
- A procedure for applying thin web-like hydrogel adjunct coatings to scaffolds was developed and the porosity of the resulting composites could be controlled.
- The formation of composites using specialised bioactive coatings allowed the modulation of biotic activity and biofilm formation enabling formation of both antibacterial and pro-bacterial systems.

6.2 Wound Healing Device

- The PVA coating was optimised for drug carrying capacity and composite porosity.
- The drug carrying capacity was further increased by ethanol into the PVA hydrogel solution. The PVA hydrogel coating was cross-linked by freeze-thaw cycling with a density of approximately 90% and swelling ratio of around 300%.
- A microbial assay using *Staphylococcus aureus* revealed that increasing the ethanol content to 50% allowed maintenance of an inhibitory concentration of erythromycin for up to 5 days. This was not affected by gamma sterilizing the scaffolds in their dehydrated and packaged form.
- The burst release of erythromycin proved to be cytotoxic to fibroblasts (> 500µg/ml), thus a soak-down procedure was designed and validated. A 15 minute soak-down of scaffolds in sterile PBS ensured erythromycin concentration was below the cytotoxic limit, but continued to inhibit bacterial growth for 5 days.
- An *in vitro* septic wound model was designed in which *S. aureus* and human dermal fibroblasts were cultured on 3D porous scaffolds simultaneously. RT-qPCR was used to quantify the bacterial and cellular colonisation of the scaffold surface. This septic wound model is the most advanced to date.
- A bioglass manufacturing route was designed to synthysise and adhere bioglass microparticels to the scaffold. The bioglass had no positive or negative affect on fibroblast or *S. aureus* growth.

- The septic wound model was used to validate that the composite scaffold containing erythromycin was able to simultaneously fight bacteria, prevent biofilms and allow fibroblasts to attach and grow. This makes the wound healing scaffold a suitable candidate for septic wound care.

6.2.1 Recommendations

- Given the success of the synthetic skin graft design an animal model is recommended as future work to assess the efficacy of the scaffold in the presence of a working immune system.
- Erythromycin was a convenient model drug for this study, but testing the drug carrying capacity and drug delivery kinetics with a more clinically relevant drug would further the potential of the scaffold system. Further, testing the delivery of growth factors from the PVA coating may have potential.

6.3 Biofilter Device

- Natural adhesion was ineffective in immobilizing ethylene-degrading Mycobacterium despite attempts to improve adhesion interactions by modifying the cell wall and the scaffold surface.
- *Mycobacterium chubuense* strain NBB4 was successfully immobilized in an ultra thin coating of agar on the surface of a porous PCL matrix. This method of immobilization encompasses the benefits of gel entrapment such as high biomass loading and mitigates the key disadvantage of diffusion limitations.
- The agar coating thickness was controlled and optimised for ethylene degradation rate, balancing diffusional limitations and biomass loading capacity.
- Batches of biofilters were able to continually remove ethylene for > 85 days. This operational stability was similar to other ethylene biofilter systems.
- The biofilters shelf life depended very much on a humidity: In packaging that was open to the air and allowed to dry the shelf life was a maximum of 12 days. In a closed, humidified package the biofilter shelf life was > 47 days.
- The biofilters could preserve bananas for up to one month compared to unprotected fruits that degraded within two weeks. The maintenance of freshness was due to removal of ethylene by NBB4 bacteria and the preservation could be improved by increasing the biomass loading of the biofilters.

6.3.1 Recommendations

- Biofilter should best tested on many different types of fruit to prove its efficacy. In addressing commercial requirements the fruits tested should be high cost items such as tropical fruits and temperate-growing stone fruits. Tests should also be side-by-side with common chemical scrubbers such as potassium permanganate.
- The biofilter has potential for removal of other hazardous hydrocarbon and chlorinated pollutants. Thus it should be tested for its removal efficiency of pollutants from gaseous and liquid streams.

7 References

1. Lui, C., *Design and development of three dimensional Scaffolds for Tissue Engineering.* Chemical Engineering Research and Design 2007. **85**(7): p. 1051-1064.
2. Rezwan, K., et al., *Biodegradable and bioactive porous polymer/inorganic composite scaffolds for bone tissue engineering.* Biomaterials, 2006. **27**(18): p. 3413-3431.
3. E Sachlos, J.C., *Making Tissue Engineering Scaffolds Work. Review on the Application of Solid Freeform Fabrication Technology to the Production of Tissue Engineering Scaffolds.* European Cells and Materials, 2003. **5**: p. 12.
4. Patrick Jr, C.W., et al., *Prospectus of Tissue Engineering*, in *Frontiers in Tissue Engineering*. 1998, Pergamon: Oxford. p. 3-11.
5. Hutmacher, D.W., *Scaffolds in tissue engineering bone and cartilage.* Biomaterials, 2000. **21**(24): p. 2529-2543.
6. Kohane, D.S., *Polymeric Biomaterials in Tissue Engineering.* International Pediatric Research Foundation, Inc., 2008. **63**(5): p. 5.
7. Zhang, Y.Z., et al., *Tissue response to commercial silicone and polyurethane elastomers after different sterilization procedures.* Biomaterials, 1996. **17**(23): p. 2265-2272.
8. Cottam, E., et al., *Effect of sterilisation by gamma irradiation on the ability of polycaprolactone (PCL) to act as a scaffold material.* Medical Engineering & Physics, 2009. **31**(2): p. 221-226.
9. Oláh, L., et al., *Changes of porous poly([epsilon]-caprolactone) bone grafts resulted from e-beam sterilization process.* Radiation Physics and Chemistry, 2007. **76**(8-9): p. 1430-1434.
10. Ma, L., et al., *Collagen/chitosan porous scaffolds with improved biostability for skin tissue engineering.* Biomaterials, 2003. **24**(26): p. 4833-4841.
11. Cuhna-Reis, C., *A New Method for Tailoring the Degradation Rate of Chitosan Fibre-mesh Scaffolds.* European Cells and Materials, 2006. **11**(3): p. 1.
12. Clark, R.A.F., K. Ghosh, and M.G. Tonnesen, *Tissue Engineering for Cutaneous Wounds.* J Invest Dermatol, 2007. **127**(5): p. 1018-1029.
13. Haycock, J.W., *3D cell culture: a review of current approaches and techniques.* Methods Mol Biol, 2011. **695**: p. 1-15.
14. Vail, N.K., et al., *Materials for biomedical applications.* Materials & Design, 1999. **20**(2-3): p. 123-132.
15. Tormala, P., T. Pohjonen, and P. Rokkanen, *Bioabsorbable polymers: materials technology and surgical applications.* Proc Inst Mech Eng H, 1998. **212**(2): p. 101-11.
16. Bajgai, M.P., et al., *In vitro hydrolytic degradation of poly([var epsilon]-caprolactone) grafted dextran fibers and films.* Polymer Degradation and Stability, 2008. **93**(12): p. 2172-2179.
17. Plikk, P., et al., *Finalizing the properties of porous scaffolds of aliphatic polyesters through radiation sterilization.* Biomaterials, 2006. **27**(31): p. 5335-5347.
18. Burkersroda, F.v., L. Schedl, and A. Göpferich, *Why degradable polymers undergo surface erosion or bulk erosion.* Biomaterials, 2002. **23**(21): p. 4221-4231.
19. Gan, Z., et al., *Enzymatic degradation of poly([var epsilon]-caprolactone) film in phosphate buffer solution containing lipases.* Polymer Degradation and Stability, 1997. **56**(2): p. 209-213.
20. Zhang, Y.Z., et al., *Characterization of the Surface Biocompatibility of the Electrospun PCL-Collagen Nanofibers Using Fibroblasts.* Biomacromolecules, 2005. **6**(5): p. 2583-2589.
21. Gupta, P., K. Vermani, and S. Garg, *Hydrogels: from controlled release to pH-responsive drug delivery.* Drug Discovery Today, 2002. **7**(10): p. 569-579.
22. Peppas, N.A. and A.R. Khare, *Preparation, structure and diffusional behavior of hydrogels in controlled release.* Advanced Drug Delivery Reviews, 1993. **11**(1–2): p. 1-35.

23. Pillai, O. and R. Panchagnula, *Polymers in drug delivery.* Current Opinion in Chemical Biology, 2001. **5**(4): p. 447-451.
24. Salama, R., et al., *Preparation and characterisation of controlled release co-spray dried drug–polymer microparticles for inhalation 1: Influence of polymer concentration on physical and in vitro characteristics.* European Journal of Pharmaceutics and Biopharmaceutics, 2008. **69**(2): p. 486-495.
25. Hassan, C.M. and N.A. Peppas, *Cellular PVA hydrogels produced by freeze/thawing.* Journal of Applied Polymer Science, 2000. **76**(14): p. 2075-2079.
26. Hassan, C. and N. Peppas, *Structure and Applications of Poly(vinyl alcohol) Hydrogels Produced by Conventional Crosslinking or by Freezing/Thawing Methods*, in *Biopolymers · PVA Hydrogels, Anionic Polymerisation Nanocomposites*. 2000, Springer Berlin Heidelberg. p. 37-65.
27. Drury, J.L. and D.J. Mooney, *Hydrogels for tissue engineering: scaffold design variables and applications.* Biomaterials, 2003. **24**(24): p. 4337-4351.
28. Place, E.S., N.D. Evans, and M.M. Stevens, *Complexity in biomaterials for tissue engineering.* Nat Mater, 2009. **8**(6): p. 457-470.
29. Hwang, M.R., et al., *Gentamicin-loaded wound dressing with polyvinyl alcohol/dextran hydrogel: gel characterization and in vivo healing evaluation.* AAPS PharmSciTech, 2010. **11**(3): p. 1092-103.
30. Fumio, U., et al., *Swelling and mechanical properties of poly(vinyl alcohol) hydrogels.* International Journal of Pharmaceutics, 1990. **58**(2): p. 135-142.
31. Li, J.K., N. Wang, and X.S. Wu, *Poly(vinyl alcohol) nanoparticles prepared by freezing–thawing process for protein/peptide drug delivery.* Journal of Controlled Release, 1998. **56**(1–3): p. 117-126.
32. Lian, Z. and L. Ye, *Structure and properties of PVA/PEO hydrogel prepared by freezing/thawing method.* Journal of Thermoplastic Composite Materials, 2011.
33. Sung, J.H., et al., *Gel characterisation and in vivo evaluation of minocycline-loaded wound dressing with enhanced wound healing using polyvinyl alcohol and chitosan.* International Journal of Pharmaceutics, 2010. **392**(1–2): p. 232-240.
34. Nikolic, V.M., et al., *On the use of gamma irradiation crosslinked PVA membranes in hydrogen fuel cells.* Electrochemistry Communications, 2007. **9**(11): p. 2661-2665.
35. Bourke, S., et al., *A photo-crosslinked poly(vinyl alcohol) hydrogel growth factor release vehicle for wound healing applications.* AAPS PharmSci, 2003. **5**(4): p. 101-111.
36. Rouxhet, L., et al., *Adsorption of albumin, collagen, and fibronectin on the surface of poly(hydroxybutyrate-hydroxyvalerate) (PHB/HV) and of poly(ε-caprolactone) (PCL) films modified by an alkaline hydrolysis and of poly(ethylene terephtalate) (PET) track-etched membranes.* Journal of Biomaterials Science, Polymer Edition, 1998. **9**(12): p. 1279-1304.
37. Wei, G. and P.X. Ma, *Structure and properties of nano-hydroxyapatite/polymer composite scaffolds for bone tissue engineering.* Biomaterials, 2004. **25**(19): p. 4749-4757.
38. Basak, P. and B. Adhikari, *Poly (vinyl alcohol) hydrogels for pH dependent colon targeted drug delivery.* Journal of Materials Science: Materials in Medicine, 2009. **20**(1): p. 137-146.
39. Oliveira, M.J.A., et al., *Hybrid hydrogels produced by ionizing radiation technique.* Radiation Physics and Chemistry, 2012. **81**(9): p. 1471-1474.
40. Pok, S., et al., *A multilayered scaffold of a chitosan and gelatin hydrogel supported by a PCL core for cardiac tissue engineering.* Acta Biomaterialia, 2012(0).
41. Blaker, J.J., S.N. Nazhat, and A.R. Boccaccini, *Development and characterisation of silver-doped bioactive glass-coated sutures for tissue engineering and wound healing applications.* Biomaterials, 2004. **25**(7-8): p. 1319-1329.

42. Hench, L.L., *Bioceramics: From Concept to Clinic.* Journal of the American Ceramic Society, 1991. **74**(7): p. 1487-1510.
43. Arcos, D. and M. Vallet-Regí, *Sol-gel silica-based biomaterials and bone tissue regeneration.* Acta Biomaterialia, 2010. **In Press, Corrected Proof**.
44. Lin, C.-C., L.-C. Huang, and P. Shen, *Na2CaSi2O6-P2O5 based bioactive glasses. Part 1: Elasticity and structure.* Journal of Non-Crystalline Solids, 2005. **351**(40-42): p. 3195-3203.
45. Vrouwenvelder, W.C.A., C.G. Groot, and K. de Groot, *Better histology and biochemistry for osteoblasts cultured on titanium-doped bioactive glass: Bioglass 45S5 compared with iron-, titanium-, fluorine- and boron-containing bioactive glasses.* Biomaterials, 1994. **15**(2): p. 97-106.
46. Balamurugan, A., et al., *An in vitro biological and anti-bacterial study on a sol-gel derived silver-incorporated bioglass system.* Dental Materials, 2008. **24**(10): p. 1343-1351.
47. Bellantone, M., N.J. Coleman, and L.L. Hench, *Bacteriostatic action of a novel four-component bioactive glass.* Journal of Biomedical Materials Research, 2000. **51**(3): p. 484-490.
48. Bellantone, M., H.D. Williams, and L.L. Hench, *Broad-Spectrum Bactericidal Activity of Ag2O-Doped Bioactive Glass.* Antimicrob. Agents Chemother., 2002. **46**(6): p. 1940-1945.
49. Chen, W., et al., *In vitro anti-bacterial and biological properties of magnetron co-sputtered silver-containing hydroxyapatite coating.* Biomaterials, 2006. **27**(32): p. 5512-5517.
50. Ciceo Lucacel, R., et al., *Structural characterization of phosphate glasses doped with silver.* Journal of Non-Crystalline Solids, 2009. **355**(7): p. 425-429.
51. Matsumoto, N., et al., *Preparation and characterization of [beta]-tricalcium phosphate co-doped with monovalent and divalent antibacterial metal ions.* Acta Biomaterialia, 2009. **5**(8): p. 3157-3164.
52. Robinson, D.A., et al., *In vitro antibacterial properties of magnesium metal against Escherichia coli, Pseudomonas aeruginosa and Staphylococcus aureus.* Acta Biomaterialia, 2009. **In Press, Corrected Proof**.
53. Allan, I., H. Newman, and M. Wilson, *Antibacterial activity of particulate Bioglass® against supra- and subgingival bacteria.* Biomaterials, 2001. **22**(12): p. 1683-1687.
54. Hu, S., et al., *Study on antibacterial effect of 45S5 Bioglass®.* Journal of Materials Science: Materials in Medicine, 2009. **20**(1): p. 281-286.
55. Kumar, P.T.S., et al., *Preparation and characterization of novel β-chitin/nanosilver composite scaffolds for wound dressing applications.* Carbohydrate Polymers, 2010. **80**(3): p. 761-767.
56. Saboori, A., et al., *Synthesis, characterization and in vitro bioactivity of sol-gel-derived SiO2-CaO-P2O5-MgO bioglass.* Materials Science and Engineering: C, 2009. **29**(1): p. 335-340.
57. Sheng, J., P.T.M. Nguyen, and R.E. Marquis, *Multi-target antimicrobial actions of zinc against oral anaerobes.* Archives of Oral Biology, 2005. **50**(8): p. 747-757.
58. Yoshinari, M., et al., *Influence of surface modifications to titanium on antibacterial activity in vitro.* Biomaterials, 2001. **22**(14): p. 2043-2048.
59. Ortega-Lara, W., et al., *Antibacterial properties, in vitro bioactivity and cell proliferation of titania-wollastonite composites.* Ceramics International, 2010. **36**(2): p. 513-519.
60. Kim, H.-W., et al., *Effect of fluoridation of hydroxyapatite in hydroxyapatite-polycaprolactone composites on osteoblast activity.* Biomaterials, 2005. **26**(21): p. 4395-4404.
61. Lin, F.-H., et al., *Preparation and in vivo evaluation of a newly developed bioglass ceramic.* Journal of Biomedical Engineering, 1993. **15**(6): p. 481-486.
62. Cannillo, V., et al., *Production of Bioglass® 45S5 - Polycaprolactone composite scaffolds via salt-leaching.* Composite Structures, 2010. **92**(8): p. 1823-1832.
63. Krajewski, A., et al., *Structural modifications and biological compatibility of doped bio-active glasses.* Biomaterials, 1988. **9**(6): p. 528-532.

64. Hench, L.L., et al., *Bonding mechanisms at the interface of ceramic prosthetic materials.* Journal of Biomedical Materials Research, 1971. **5**(6): p. 117-141.
65. Gidwani, P., *Commercial & Manufacturing Recommendations for a Soft Tissue Scaffold Development*, in *School of Aeronautical, MEchanical and Mechatronic Engineering*. 2009, University of Sydney: Sydney, Australia.
66. Bharati, S., et al., *Studies on a novel bioactive glass and composite coating with hydroxyapatite on titanium based alloys: Effect of [gamma]-sterilization on coating.* Journal of the European Ceramic Society, 2009. **29**(12): p. 2527-2535.
67. Kundu, D., A. Patra, and D. Ganguli, *Study of γ-radiation induced defects in fumed silica-alkoxide derived silica glasses.* Journal of Materials Science Letters, 2000. **19**(1): p. 37-39.
68. Hong, Z., R.L. Reis, and J.F. Mano, *Preparation and in vitro characterization of scaffolds of poly(l-lactic acid) containing bioactive glass ceramic nanoparticles.* Acta Biomaterialia, 2008. **4**(5): p. 1297-1306.
69. Verrier, S., et al., *PDLLA/Bioglass® composites for soft-tissue and hard-tissue engineering: an in vitro cell biology assessment.* Biomaterials, 2004. **25**(15): p. 3013-3021.
70. Ramakrishna, S., et al., *Biomedical applications of polymer-composite materials: a review.* Composites Science and Technology, 2001. **61**(9): p. 1189-1224.
71. Day, R.M., et al., *Assessment of polyglycolic acid mesh and bioactive glass for soft-tissue engineering scaffolds.* Biomaterials, 2004. **25**(27): p. 5857-5866.
72. Helen, W., et al., *Three-dimensional culture of annulus fibrosus cells within PDLLA/Bioglass® composite foam scaffolds: Assessment of cell attachment, proliferation and extracellular matrix production.* Biomaterials, 2007. **28**(11): p. 2010-2020.
73. Wang, W.H., C. Dong, and C.H. Shek, *Bulk metallic glasses.* Materials Science and Engineering: R: Reports, 2004. **44**(2–3): p. 45-89.
74. Gu, X., et al., *Corrosion of, and cellular responses to Mg–Zn–Ca bulk metallic glasses.* Biomaterials, 2010. **31**(6): p. 1093-1103.
75. Zberg, B., P.J. Uggowitzer, and J.F. Loffler, *MgZnCa glasses without clinically observable hydrogen evolution for biodegradable implants.* Nat Mater, 2009. **8**(11): p. 887-891.
76. Harrison, J.J., et al., *Biofilm susceptibility to metal toxicity.* Environmental Microbiology, 2004. **6**(12): p. 1220-1227.
77. Kelly, P.J. and R.D. Arnell, *Magnetron sputtering: a review of recent developments and applications.* Vacuum, 2000. **56**(3): p. 159-172.
78. Rossnagel, S.M., *Magnetron plasma deposition processes.* Thin Solid Films, 1989. **171**(1): p. 125-142.
79. Rossnagel, S.M., I. Yang, and J.J. Cuomo, *Compositional changes during magnetron sputtering of alloys.* Thin Solid Films, 1991. **199**(1): p. 59-69.
80. Rigaku. *Application Sputtering Systems*. 2009 [cited 2013 28/2].
81. Oláh, L., et al., *Changes of porous poly([epsilon]-caprolactone) bone grafts resulted from e-beam sterilization process.* Radiation Physics and Chemistry. **76**(8-9): p. 1430-1434.
82. Odelius, K., P. Plikk, and A.-C. Albertsson, *The influence of composition of porous copolyester scaffolds on reactions induced by irradiation sterilization.* Biomaterials, 2008. **29**(2): p. 129-140.
83. Dado, D. and S. Levenberg, *Cell-scaffold mechanical interplay within engineered tissue.* Seminars in Cell & Developmental Biology, 2009. **20**(6): p. 656-664.
84. Ghosh, K., et al., *Cell adaptation to a physiologically relevant ECM mimic with different viscoelastic properties.* Biomaterials, 2007. **28**(4): p. 671-679.
85. A Miko, G.S., S Leite, J Vacanti, R Langer, *Laminated three-dimensional biodegradable foams for use in tissue engineering.* Biomaterials, 1993. **14**: p. 8.

86. Chen, U.a.T., *Development of Biodegradable porous scaffolds for tissue engineering.* Materials Science and Engineering, 2001. **17**: p. 7.
87. Cao, G.M., A Messina, *The influence of arcitecture on degradation and tissue ingrowth into three-dimensional poly(lactic-co-glycolic acid) scaffolds in vitro and in vivo.* Biomaterials, 2006. **27**: p. 11.
88. Cooper, J.A., et al., *Fiber-based tissue-engineered scaffold for ligament replacement: design considerations and in vitro evaluation.* Biomaterials, 2005. **26**(13): p. 1523-1532.
89. Freed, L.E. and G. Vunjak-Novakovic, *Culture of organized cell communities.* Advanced Drug Delivery Reviews, 1998. **33**(1-2): p. 15-30.
90. Xu, C.Y., et al., *Aligned biodegradable nanofibrous structure: a potential scaffold for blood vessel engineering.* Biomaterials, 2004. **25**(5): p. 877-886.
91. Andrews, K.D., J.A. Hunt, and R.A. Black, *Effects of sterilisation method on surface topography and in-vitro cell behaviour of electrostatically spun scaffolds.* Biomaterials, 2007. **28**(6): p. 1014-1026.
92. Das, S., et al., *Tissue Engineering Scaffolds*, in *Encyclopedia of Materials: Science and Technology*. 2003, Elsevier: Oxford. p. 1-7.
93. Calvert, P., J. O'Kelly, and C. Souvignier, *Solid freeform fabrication of organic-inorganic hybrid materials.* Materials Science and Engineering: C, 1998. **6**(2-3): p. 167-174.
94. Standards, I., *Sterilization of health care products - Radiation*, in *Part 1: Requirements for development, validation and routine control of a sterilization process for medical devices*. 2006, Standards Australia.
95. Standards, I., *Sterilization of health care products - Radiation*, in *Part 2: Establishing the sterilization dose*. 2006.
96. FDA, *GEM 21S (Growth-factor Enhanced Matrix) - P040013*, in *Labelling*. 2005, U.S. Food and Drug Administration.
97. Noah, E.M., et al., *Impact of sterilization on the porous design and cell behavior in collagen sponges prepared for tissue engineering.* Biomaterials, 2002. **23**(14): p. 2855-2861.
98. Parenteau-Bareil, R., R. Gauvin, and F. Berthod, *Collagen-Based Biomaterials for Tissue Engineering Applications.* Materials, 2010. **3**(3): p. 1863-1887.
99. Croonenborghs, B., M.A. Smith, and P. Strain, *X-ray versus gamma irradiation effects on polymers.* Radiation Physics and Chemistry, 2007. **76**(11-12): p. 1676-1678.
100. Lewis, S., *Cleaning, disinfection and sterilisation of equipment.* Equipment and Clinical Physics, 2004: p. 360-364.
101. Boateng, J.S., et al., *Wound healing dressings and drug delivery systems: A review.* Journal of Pharmaceutical Sciences, 2008. **97**(8): p. 2892-2923.
102. Klein, J. and M. Kluge, *Immobilization of microbial cells in polyurethane matrices.* Biotechnology Letters, 1981. **3**(2): p. 65-70.
103. Schaedler, T.A., et al., *Ultralight metallic microlattices.* Science, 2011. **334**(6058): p. 962-5.
104. Kirker, K.R., et al., *Loss of viability and induction of apoptosis in human keratinocytes exposed to Staphylococcus aureus biofilms in vitro.* Wound Repair and Regeneration, 2009. **17**(5): p. 690-699.
105. Brandon, H. *Skin Anatomy*. 2014; Available from: http://dermatology.about.com/cs/skinanatomy/a/anatomy.htm.
106. Wang, Y., et al., *Hyperelastic Material Properties of Mouse Skin under Compression.* PLoS ONE, 2013. **8**(6): p. e67439.
107. Chong, E.J., et al., *Evaluation of electrospun PCL/gelatin nanofibrous scaffold for wound healing and layered dermal reconstitution.* Acta Biomaterialia, 2007. **3**(3): p. 321-330.

108. Agache, P.G., et al., *Mechanical properties and Young's modulus of human skin in vivo.* Archives of Dermatological Research, 1980. **269**(3): p. 221-232.
109. Silver, F.H., J.W. Freeman, and D. DeVore, *Viscoelastic properties of human skin and processed dermis.* Skin Research and Technology, 2001. **7**(1): p. 18-23.
110. Breen, A.M., et al., *The use of therapeutic gene eNOS delivered via a fibrin scaffold enhances wound healing in a compromised wound model.* Biomaterials, 2008. **29**(21): p. 3143-3151.
111. Omar, A.A., et al., *Treatment of Venous Leg Ulcers with Dermagraft®.* European Journal of Vascular and Endovascular Surgery, 2004. **27**(6): p. 666-672.
112. Bergin, S.M., et al., *Australian Diabetes Foot Network: management of diabetes-related foot ulceration - a clinical update.* Med J Aust, 2012. **197**(4): p. 226-9.
113. Sen, C.K., et al., *Human skin wounds: a major and snowballing threat to public health and the economy.* Wound Repair Regen, 2009. **17**(6): p. 763-71.
114. Jeffcoate, W.J. and K.G. Harding, *Diabetic foot ulcers.* The Lancet, 2003. **361**(9368): p. 1545-1551.
115. Leung, P.C., *Diabetic foot ulcers — a comprehensive review.* The Surgeon, 2007. **5**(4): p. 219-231.
116. Song, A., A.A. Rane, and K.L. Christman, *Antibacterial and cell-adhesive polypeptide and poly(ethylene glycol) hydrogel as a potential scaffold for wound healing.* Acta Biomaterialia, 2012. **8**(1): p. 41-50.
117. D. D. Rhoads, R.W.W., K.F. Cutting and S.L. Percival, *Evidence of Biofilms in Wounds and the Potential Ramifications.* Biofims: coming of age, 2007.
118. Hood, A., *RPA Wound Clinic*, A. Baume, Editor. 2013: Sydney.
119. Kim, K.L., et al., *Enhanced dermal wound neovascularization by targeted delivery of endothelial progenitor cells using an RGD-g-PLLA scaffold.* Biomaterials, 2009. **30**(22): p. 3742-3748.
120. Alavi, M., et al., *Attachment and Biofilm Formation of <i>Mycobacterium marinum</i> on a Hydrophobic Surface at the Air Interface.* World Journal of Microbiology and Biotechnology, 2007. **23**(1): p. 93-101.
121. Beer, D. and P. Stoodley, *Microbial Biofilms*. 2006. p. 904-937.
122. Bryers, J.D., *Bacterial biofilms.* Current Opinion in Biotechnology, 1993. **4**(2): p. 197-204.
123. Hori, K. and S. Matsumoto, *Bacterial adhesion: From mechanism to control.* Biochemical Engineering Journal, 2010. **48**(3): p. 424-434.
124. Pavithra, D. and D. Mukesh, *Biofilm formation, bacterial adhesion and host response on polymeric implants—issues and prevention.* Biomedical Materials, 2008. **3**(3): p. 034003.
125. Hosseinkhani, S., et al., *Adsorptive immobilization of bacterial luciferases on alkyl-substituted Sepharose 4B.* Enzyme and Microbial Technology, 2003. **32**(1): p. 186-193.
126. Klein, J. and H. Ziehr, *Immobilization of microbial cells by adsorption.* Journal of Biotechnology, 1990. **16**(1-2): p. 1-15.
127. Mazumder, S., et al., *Role of hydrophobicity in bacterial adherence to carbon nanostructures and biofilm formation.* Biofouling: The Journal of Bioadhesion and Biofilm Research, 2010. **26**(3): p. 333-339.
128. Robledo-Ortíz, J.R., et al., *Bacterial immobilization by adhesion onto agave-fiber/polymer foamed composites.* Bioresource Technology, 2010. **101**(4): p. 1293-1299.
129. Colón-González, M., M.M. Méndez-Ortiz, and J. Membrillo-Hernández, *Anaerobic growth does not support biofilm formation in Escherichia coli K-12.* Research in Microbiology, 2004. **155**(7): p. 514-521.
130. Bjergbæk, L.A., et al., *Effect of oxygen and growth medium on in vitro biofilm formation by Escherichia coli.* Biofilms, 2006. **3**(01): p. 1-10.
131. Lindsay, D. and A. von Holy, *Bacterial biofilms within the clinical setting: what healthcare professionals should know.* Journal of Hospital Infection, 2006. **64**(4): p. 313-325.

132. Toté, K., et al., *Inhibitory efficacy of various antibiotics on matrix and viable mass of Staphylococcus aureus and Pseudomonas aeruginosa biofilms.* International Journal of Antimicrobial Agents, 2009. **33**(6): p. 525-531.
133. Gao, G., et al., *The biocompatibility and biofilm resistance of implant coatings based on hydrophilic polymer brushes conjugated with antimicrobial peptides.* Biomaterials. **In Press, Corrected Proof**.
134. Teitzel, G.M. and M.R. Parsek, *Heavy Metal Resistance of Biofilm and Planktonic Pseudomonas aeruginosa.* Appl. Environ. Microbiol., 2003. **69**(4): p. 2313-2320.
135. Toté, K., et al., *A new colorimetric microtitre model for the detection of Staphylococcus aureus biofilms.* Letters in Applied Microbiology, 2008. **46**(2): p. 249-254.
136. Götz, F., *Staphylococcus and biofilms.* Molecular Microbiology, 2002. **43**(6): p. 1367-1378.
137. Yarwood, J.M., et al., *Quorum Sensing in Staphylococcus aureus Biofilms.* Journal of Bacteriology, 2004. **186**(6): p. 1838-1850.
138. Klausen, M., et al., *Biofilm formation by Pseudomonas aeruginosa wild type, flagella and type IV pili mutants.* Molecular Microbiology, 2003. **48**(6): p. 1511-1524.
139. Sperandio, V., A.G. Torres, and J.B. Kaper, *Quorum sensing Escherichia coli regulators B and C (QseBC): a novel two-component regulatory system involved in the regulation of flagella and motility by quorum sensing in E. coli.* Mol Microbiol, 2002. **43**(3): p. 809-21.
140. Subbiahdoss, G., et al., *Microbial biofilm growth versus tissue integration on biomaterials with different wettabilities and a polymer-brush coating.* Journal of Biomedical Materials Research Part A, 2010. **94A**(2): p. 533-538.
141. Subbiahdoss, G., et al., *Microbial biofilm growth vs. tissue integration: "The race for the surface" experimentally studied.* Acta Biomaterialia, 2009. **5**(5): p. 1399-1404.
142. Al-Ahmad, A., et al., *Comparison of bacterial adhesion and cellular proliferation on newly developed three-dimensional scaffolds manufactured by rapid prototyping technology.* Journal of Biomedical Materials Research Part A, 2011. **98A**(2): p. 303-311.
143. Wang, Q., X. Yu, and M. Libera, *Reducing Bacterial Colonization of 3-D Nanofiber Cell Scaffolds by Hierarchical Assembly of Microgels and an Antimicrobial Peptide.* Advanced Healthcare Materials, 2012: p. n/a-n/a.
144. Kuijer, R., et al., *Assessing infection risk in implanted tissue-engineered devices.* Biomaterials, 2007. **28**(34): p. 5148-5154.
145. Recht, J. and R. Kolter, *Glycopeptidolipid Acetylation Affects Sliding Motility and Biofilm Formation in Mycobacterium smegmatis.* J. Bacteriol., 2001. **183**(19): p. 5718-5724.
146. Rivardo, F., et al., *Synergistic effect of lipopeptide biosurfactant with antibiotics against Escherichia coli CFT073 biofilm.* International Journal of Antimicrobial Agents, 2011. **37**(4): p. 324-331.
147. Kostenko, V., et al., *Staphylococcus aureus biofilm formation and tolerance to antibiotics in response to oscillatory shear stresses of physiological levels.* FEMS Immunology & Medical Microbiology, 2010. **59**(3): p. 421-431.
148. Patel, J. and M. Sharma, *Differences in attachment of Salmonella enterica serovars to cabbage and lettuce leaves.* International Journal of Food Microbiology, 2010. **139**(1-2): p. 41-47.
149. Hackbarth, C.J., H.F. Chambers, and M.A. Sande, *Serum bactericidal activity of rifampin in combination with other antimicrobial agents against Staphylococcus aureus.* Antimicrobial Agents and Chemotherapy, 1986. **29**(4): p. 611-613.
150. Pankey, G.A. and L.D. Sabath, *Clinical Relevance of Bacteriostatic versus Bactericidal Mechanisms of Action in the Treatment of Gram-Positive Bacterial Infections.* Clinical Infectious Diseases, 2004. **38**(6): p. 864-870.

151. Schwarz, S., et al., *Molecular basis of bacterial resistance to chloramphenicol and florfenicol.* FEMS Microbiology Reviews, 2004. **28**(5): p. 519-542.
152. Bartlett, J.G. *Chloramphenicol*. 2010 [cited 2011 5/6].
153. ECONOCHLOR®, *Chloramphenicol*, Chloramphenicol-2D-skeletal.svg, Editor. 2009.
154. Sigma, *Erythromycin - Product Information*. 2013, Sigma-Aldrich.
155. Walash, M.I., et al., *Spectrophotometric determination of four macrolide antibiotics in pharmaceutical formulations and biological fluids via binary complex formation with eosin [corrected].* Journal of Aoac International, 2007. **90**(6): p. 1579-87.
156. Bekele, L.K. and G.G. Gebeyehu, *Application of Different Analytical Techniques and Microbiological Assays for the Analysis of Macrolide Antibiotics from Pharmaceutical Dosage Forms and BiologicalMatrices.* International Scholarly Research Network Analytical Chemistry, 2012: p. 17.
157. Welch, W.D. and P.M. Southern, *Unusual susceptibility of methicillin-resistant Staphylococcus aureus to erythromycin, clindamycin, gentamicin, and tetracycline at 30 degrees C but not at 35 degrees C.* J Clin Microbiol, 1984. **19**(6): p. 831-3.
158. Byarugaba, W., et al., *Toxicity of antibiotics on cultured human skin fibroblasts.* Humangenetik, 1975. **28**(3): p. 263-267.
159. Zimmerman, H.J., J. Kendler, and S. Libber, *Studies on the in Vitro Cytotoxicity of Erythromycin Estolate.* Experimental Biology and Medicine, 1973. **144**(3): p. 759-761.
160. Walash, *Spectrophotometric determination of four macrolide antibiotics in pharmaceutical formulations and biological fluids via binary complex formation with eosin (vol 90, pg 1579, 2007).* Journal of Aoac International, 2008. **91**(2): p. 48a-48a.
161. Danielson, N.D., et al., *Simple methods for the qualitative identification and quantitative determination of macrolide antibiotics.* Journal of Pharmaceutical and Biomedical Analysis, 1993. **11**(2): p. 121-130.
162. Jacobs, G.P., *A Review of the Effects of Gamma Radiation on Pharmaceutical Materials.* Journal of Biomaterials Applications, 1995. **10**(1): p. 59-96.
163. Ražem, D. and B. Katušin-Ražem, *The effects of irradiation on controlled drug delivery/controlled drug release systems.* Radiation Physics and Chemistry, 2008. **77**(3): p. 288-344.
164. Sakurada, I. and Y. Ikada, *Effects of Cobalt-60 Gamma Radiation on Poly(vinyl alcohol) (III).* 1960.
165. Hyon, S.-H. and Y. Ikada, *Porous and transparent poly(vinyl alcohol) gel and method of manufacturing the same*. 1987.
166. 962, S. *Solid - liquid phase diagram of ethanol water mixtures (melting points, freezing points)*. 2010 [cited 2013 12 March]; Available from: http://commons.wikimedia.org/wiki/File:Phase_diagram_ethanol_water_s_l_en.svg.
167. Yang, X., et al., *Investigation of PVA/ws-chitosan hydrogels prepared by combined γ-irradiation and freeze-thawing.* Carbohydrate Polymers, 2008. **73**(3): p. 401-408.
168. Sasaki, S., et al., *Elution of polymers from poly(vinyl alcohol) cast gels with different degrees of polymerization and hydrolysis.* Journal of Applied Polymer Science, 2012. **126**(S2): p. E233-E241.
169. Adi, H., et al., *Controlled release antibiotics for dry powder lung delivery.* Drug Dev Ind Pharm, 2010. **36**(1): p. 119-26.
170. Gottrup, F., M.S. Ågren, and T. Karlsmark, *Models for use in wound healing research: A survey focusing on in vitro and in vivo adult soft tissue.* Wound Repair and Regeneration, 2000. **8**(2): p. 83-96.
171. Moulin, V., et al., *In vitro models to study wound healing fibroblasts.* Burns, 1996. **22**(5): p. 359-362.

172. Loo, A.E.K. and B. Halliwell, *Effects of hydrogen peroxide in a keratinocyte-fibroblast co-culture model of wound healing.* Biochemical and Biophysical Research Communications, 2012. **423**(2): p. 253-258.
173. Schor, S.L., *Cell proliferation and migration on collagen substrata in vitro.* Journal of Cell Science, 1980. **41**(1): p. 159-175.
174. Kirker, K.R., et al., *Differential effects of planktonic and biofilm MRSA on human fibroblasts.* Wound Repair and Regeneration, 2012. **20**(2): p. 253-261.
175. Werthen, M., et al., *An in vitro model of bacterial infections in wounds and other soft tissues.* APMIS, 2010. **118**(2): p. 156-64.
176. Oberringer, M., et al., *A new in vitro wound model based on the co-culture of human dermal microvascular endothelial cells and human dermal fibroblasts.* Biol Cell, 2007. **99**(4): p. 197-207.
177. Herman, I.M. and A. Leung, *Creation of human skin equivalents for the in vitro study of angiogenesis in wound healing.* Methods Mol Biol, 2009. **467**: p. 241-8.
178. Xie, Y., et al., *Development of a three-dimensional human skin equivalent wound model for investigating novel wound healing therapies.* Tissue Eng Part C Methods, 2010. **16**(5): p. 1111-23.
179. Mempel, M., et al., *Invasion of human keratinocytes by Staphylococcus aureus and intracellular bacterial persistence represent haemolysin-independent virulence mechanisms that are followed by features of necrotic and apoptotic keratinocyte cell death.* Br J Dermatol, 2002. **146**(6): p. 943-51.
180. Nuzzo, I., et al., *Apoptosis of human keratinocytes after bacterial invasion.* FEMS Immunol Med Microbiol, 2000. **27**(3): p. 235-40.
181. Baume, A.S., N.V. Coleman, and P. Boughton, *Methods for Achieving Soft Tissue Scaffold Sterility.* Journal of Biomimetics, Biomaterials, and Tissue Engineering, 2009. **4**: p. 10.
182. Li, B., J.M. Davidson, and S.A. Guelcher, *The effect of the local delivery of platelet-derived growth factor from reactive two-component polyurethane scaffolds on the healing in rat skin excisional wounds.* Biomaterials, 2009. **30**(20): p. 3486-3494.
183. Seth, A.K., et al., *In vivo modeling of biofilm-infected wounds: A review.* Journal of Surgical Research, 2012. **178**(1): p. 330-338.
184. Matsuda, K., et al., *Sensitive quantitative detection of commensal bacteria by rRNA-targeted reverse transcription-PCR.* Appl Environ Microbiol, 2007. **73**(1): p. 32-9.
185. Baker, G.C., J.J. Smith, and D.A. Cowan, *Review and re-analysis of domain-specific 16S primers.* Journal of Microbiological Methods, 2003. **55**(3): p. 541-555.
186. Rosato, A.E., W.A. Craig, and G.L. Archer, *Quantitation of mecA transcription in oxacillin-resistant Staphylococcus aureus clinical isolates.* J Bacteriol, 2003. **185**(11): p. 3446-52.
187. Tan, J.T.M., et al., *Connective tissue growth factor inhibits adipocyte differentiation.* American Journal of Physiology - Cell Physiology, 2008. **295**(3): p. C740-C751.
188. Wang, X., et al., *Regulation of pro-inflammatory and pro-fibrotic factors by CCN2/CTGF in H9c2 cardiomyocytes.* J Cell Commun Signal, 2010. **4**(1): p. 15-23.
189. Young, C.N., et al., *Reactive Oxygen Species in Tumor Necrosis Factor-[alpha]-Activated Primary Human Keratinocytes: Implications for Psoriasis and Inflammatory Skin Disease.* J Invest Dermatol, 2008. **128**(11): p. 2606-2614.
190. Giricz, O., J.L. Lauer-Fields, and G.B. Fields, *The normalization of gene expression data in melanoma: Investigating the use of glyceraldehyde 3-phosphate dehydrogenase and 18S ribosomal RNA as internal reference genes for quantitative real-time PCR.* Analytical Biochemistry, 2008. **380**(1): p. 137-139.

191. Dobinsky, S. and D. Mack, *[22] Efficient rna isolation method for analysis of transcription in sessile staphylococcus epidermidis biofilm cultures*, in *Methods in Enzymology*, J.D. Ron, Editor. 2001, Academic Press. p. 255-262.
192. Altuzar, V., et al., *Atmospheric ethene concentrations in Mexico City: Indications of strong diurnal and seasonal dependences.* Atmospheric Environment, 2005. **39**(29): p. 5219-5225.
193. Burg, S.P. and E.A. Burg, *Relationship between Ethylene Production and Ripening in Bananas.* Botanical Gazette, 1965. **126**(3): p. 200-204.
194. Høyer, L., *Investigations of the ethylene build-up during transport of pot plants in controlled temperature trucks.* Postharvest Biology and Technology, 1995. **5**(1–2): p. 101-108.
195. Scott, K., W. McGlasson, and E. Roberts, *Potassium permanganate as an ethylene absorbent in polyethylene bags to delay ripening of bananas during storage.* Australian Journal of Experimental Agriculture, 1970. **10**(43): p. 237-240.
196. Elsgaard, L., *Ethylene Removal by a Biofilter with Immobilized Bacteria.* Applied and Environmental Microbiology, 1998. **64**(11): p. 6.
197. Elsgaard, L., *Ethylene Removal at Low Temperatures under Biofilter and Batch Conditions.* Appl. Environ. Microbiol., 2000. **66**(9): p. 3878-3882.
198. Martínez-Romero, D., et al., *Tools to Maintain Postharvest Fruit and Vegetable Quality through the Inhibition of Ethylene Action: A Review.* Critical Reviews in Food Science and Nutrition, 2007. **47**(6): p. 543-560.
199. Bleecker, A.B. and H. Kende, *ETHYLENE: A Gaseous Signal Molecule in Plants.* Annual Review of Cell and Developmental Biology, 2000. **16**(1): p. 1-18.
200. Blidi, A.E., et al., *Ethylene removal for long term conservation of fruits and vegetables.* Food Quality and Preference, 1993. **4**(3): p. 119-126.
201. Verdouw, C.N., et al., *Process modelling in demand-driven supply chains: A reference model for the fruit industry.* Computers and Electronics in Agriculture, 2010. **73**(2): p. 174-187.
202. Parfitt, J., M. Barthel, and S. Macnaughton, *Food waste within food supply chains: quantification and potential for change to 2050.* Philosophical Transactions of the Royal Society B: Biological Sciences, 2010. **365**(1554): p. 3065-3081.
203. Fu, Y., et al., *Ethylene removal efficiency and bacterial community diversity of a natural zeolite biofilter.* Bioresource Technology, 2011. **In Press, Corrected Proof**.
204. Guardian, E.G. *EGG Produce Freshness.* 2013 [cited 2011 3 March]; Available from: http://producefreshness.com/home.php.
205. Cohen, Y., *Biofiltration - the treatment of fluids by microorganisms immobilized into the filter bedding material: a review.* Bioresource Technology, 2001. **77**(3): p. 257-274.
206. Deshusses, M.A., *Biological waste air treatment in biofilters.* Current Opinion in Biotechnology, 1997. **8**(3): p. 335-339.
207. Chu, L. and J. Wang, *Comparison of polyurethane foam and biodegradable polymer as carriers in moving bed biofilm reactor for treating wastewater with a low C/N ratio.* Chemosphere, 2011. **83**(1): p. 63-68.
208. Kim, J.-O., *Degradation of benzene and ethylene in biofilters.* Process Biochemistry, 2003. **39**(4): p. 447-453.
209. De Heyder, B., et al., *Ethene removal from a synthetic waste gas using a dry biobed.* Biotechnology and Bioengineering, 1994. **44**(5): p. 642-648.
210. Lee, S.-h., et al., *Biofiltration of a mixture of ethylene, ammonia, n-butanol, and acetone gases.* Bioresource Technology, 2013. **127**(0): p. 366-377.
211. Wu, S.-C. and Y.-K. Lia, *Application of bacterial cellulose pellets in enzyme immobilization.* Journal of Molecular Catalysis B: Enzymatic, 2008. **54**(3-4): p. 103-108.

212. de-Bashan, L.E. and Y. Bashan, *Immobilized microalgae for removing pollutants: Review of practical aspects.* Bioresource Technology, 2010. **101**(6): p. 1611-1627.
213. Fukui, S. and A. Tanaka, *Immobilized Microbial Cells.* Annual Review of Microbiology, 1982. **36**(1): p. 145-172.
214. Anisha, G.S. and P. Prema, *Cell immobilization technique for the enhanced production of [alpha]-galactosidase by Streptomyces griseoloalbus.* Bioresource Technology, 2008. **99**(9): p. 3325-3330.
215. Karel, S.F., S.B. Libicki, and C.R. Robertson, *The immobilization of whole cells: Engineering principles.* Chemical Engineering Science, 1985. **40**(8): p. 1321-1354.
216. Junter, G.-A. and T. Jouenne, *Immobilized viable microbial cells: from the process to the proteome... or the cart before the horse.* Biotechnology Advances, 2004. **22**(8): p. 633-658.
217. Jouenne, T., et al., *Cell immobilization in composite agar layer microporous membrane structures: growth kinetics of gel-entrapped cultures and cell leakage limitation by a microporous membrane.* Applied Microbiology and Biotechnology, 1993. **38**(4): p. 478-481.
218. Jouenne, T., O. Tresse, and G.-A. Junter, *Agar-entrapped bacteria as an in vitro model of biofilms and their susceptibility to antibiotics.* FEMS Microbiology Letters, 1994. **119**(1–2): p. 237-242.
219. Zhu, H., et al., *Entrapment of Rhodobacter sphaeroides RV in cationic polymer/agar gels for hydrogen production in the presence of NH4+.* Journal of Bioscience and Bioengineering, 1999. **88**(5): p. 507-512.
220. Chen, D., et al., *Degradation of methyl tert-butyl ether by gel immobilized Methylibium petroleiphilum PM1.* Bioresource Technology, 2008. **99**(11): p. 4702-4708.
221. Messing, R.A. and R.A. Oppermann, *Pore dimensions for accumulating biomass. I. Microbes that reproduce by fission or by budding.* Biotechnology and Bioengineering, 1979. **21**(1): p. 49-58.
222. Flygare, S. and P.-O. Larsson, *Steroid transformation using magnetically immobilized Mycobacterium sp.* Enzyme and Microbial Technology, 1987. **9**(8): p. 494-499.
223. Doran, P.M. and J.E. Bailey, *Effects of immobilization on growth, fermentation properties, and macromolecular composition of <I>Saccharomyces cerevisiae</I> attached to gelatin.* Biotechnology and Bioengineering, 1986. **28**(1): p. 73-87.
224. Dias, A.C.P., J.M.S. Cabral, and H.M. Pinheiro, *Sterol side-chain cleavage with immobilized Mycobacterium cells in water-immiscible organic solvents.* Enzyme and Microbial Technology, 1994. **16**(8): p. 708-714.
225. Degiorgi, C.F., et al., *Hydrogels for immobilization of bacteria used in the treatment of metal-contaminated wastes.* Radiation Physics and Chemistry, 2002. **63**(1): p. 109-113.
226. Claudino, M.J.C., et al., *Immobilization of mycobacterial cells onto silicone - Assessing the feasibility of the immobilized biocatalyst in the production of androstenedione from sitosterol.* Bioresource Technology, 2008. **99**(7): p. 2304-2311.
227. Kuyukina, M.S., et al., *Selective adsorption of hydrocarbon-oxidizing Rhodococcus cells in a column with hydrophobized poly(acrylamide) cryogel.* Journal of Microbiological Methods, 2009. **79**(1): p. 76-81.
228. Lyew, D., et al., *Comparison of different support materials for their capacity to immobilize Mycobacterium austroafricanum IFP 2012 and to adsorb MtBE.* Enzyme and Microbial Technology, 2007. **40**(6): p. 1524-1530.
229. Wick, L.Y., et al., *Influence of the growth substrate on ester-linked phospho- and glycolipid fatty acids of PAH-degrading Mycobacterium sp. LB501T.* Environmental Microbiology, 2003. **5**(8): p. 672-680.
230. de Bont, J.A.M., et al., *Ethylene oxide production by immobilized Mycobacterium Py1 in a gas-solid bioreactor.* Enzyme and Microbial Technology, 1983. **5**(1): p. 55-59.

231. Li, F., et al., *Microbial Desulfurization of Gasoline in a Mycobacterium goodii X7B Immobilized-Cell System.* Applied and Environmental Microbiology, 2005. **71**(1): p. 276-281.
232. Hartmans, S., J.A.M. DE BONT, and E. STACKEBRANDT, *The Genus Mycobacterium—Nonmedical*, in *Prokaryotes*. 2006.
233. Cheung, S., *Biocatalytic epoxidation of alkenes using Mycobacterium sp. strain NBB4*, in *School of Chemistry, Faculty of Science*. 2009, University of Sydney.
234. Coleman, N.V., et al., *Untangling the multiple monooxygenases of Mycobacterium chubuense strain NBB4, a versatile hydrocarbon degrader.* Environ Microbiol Rep, 2011. **3**(3): p. 297-307.
235. Le, N. and N. Coleman, *Biodegradation of vinyl chloride, cis-dichloroethene and 1,2-dichloroethane in the alkene/alkane-oxidising Mycobacterium strain NBB4.* Biodegradation, 2011. **22**(6): p. 1095-1108.
236. Houben, E.N.G., et al., *Differential expression of a virulence factor in pathogenic and non-pathogenic mycobacteria.* Molecular Microbiology, 2009. **72**(1): p. 41-52.
237. Boughton, E., *Development of Novel Wound Healing Scaffold*, in *School of Aeronautical, Mechanical and Mechatronic Engineering*. 2010, University of Sydney: Sydney. p. 452.
238. Coleman, N.V., N.B. Bui, and A.J. Holmes, *Soluble di-iron monooxygenase gene diversity in soils, sediments and ethene enrichments.* Environmental Microbiology, 2006. **8**(7): p. 1228-1239.
239. Normand, V., et al., *New Insight into Agarose Gel Mechanical Properties.* Biomacromolecules, 2000. **1**(4): p. 730-738.
240. Benjamin Chow, et al., *Development of 3D Antibiotic-Eluting Bioresorbable Scaffold with Attenuating Envelopes.* Journal of Biomimetics, Biomaterials, and Tissue Engineering 2012. **15**: p. 55-62.
241. Chang, H.I., Y. Perrie, and A.G.A. Coombes, *Delivery of the antibiotic gentamicin sulphate from precipitation cast matrices of polycaprolactone.* Journal of Controlled Release, 2006. **110**(2): p. 414-421.
242. Dagalakis, N., et al., *Design of an artificial skin. Part III. Control of pore structure.* Journal of Biomedical Materials Research, 1980. **14**(4): p. 511-528.
243. Pharmacopoeia, B., *Appendix XIV A. Microbiological Assay of Antibiotics*, in *Appendix XIV Biological Assays and Tests*. 2014, Crown.
244. Bonner, F.J., G. Kordas, and D.L. Kinser, *Sol-gel glasses by non-aqueous processes.* Journal of Non-Crystalline Solids, 1985. **71**(1-3): p. 361-371.
245. Tsybeskov, L., J.V. Vandyshev, and P.M. Fauchet, *Blue emission in porous silicon: Oxygen-related photoluminescence.* Physical Review B, 1994. **49**(11): p. 7821-7824.
246. Hagedorn, D., F. Löffler, and R. Meeß, *Magnetron sputter process for inner cylinder coatings.* Surface and Coatings Technology, 2008. **203**(5-7): p. 632-637.
247. XRF. *Product Selection - XRF Scientific*. 2013 [cited 2014 19 January]; Available from: http://www.xrfscientific.com/en/products-list/platinum-labware/product-selection.html.
248. Hench, L.L., *The story of Bioglass.* J Mater Sci Mater Med, 2006. **17**(11): p. 967-78.
249. Kuisma-Kursula, P., *Accuracy, precision and detection limits of SEM–WDS, SEM–EDS and PIXE in the multi-elemental analysis of medieval glass.* X-Ray Spectrometry, 2000. **29**(1): p. 111-118.
250. Goller, G., et al., *Processing and characterization of bioglass reinforced hydroxyapatite composites.* Ceramics International, 2003. **29**(6): p. 721-724.
251. Jones, J.R., *Review of bioactive glass: From Hench to hybrids.* Acta Biomaterialia, 2013. **9**(1): p. 4457-4486.
252. Parker, A., *Development and Validation of a Novel Tissue Engineering System for Cartilage and Osteochondral Regeneration*. 2010, University of Sydney.
253. Oliveira, M.J.A., et al., *Effects of Sterilization on poly(vinyl alcohol) (PVAl) Hydrogels Matrices*, in *International Nuclear Atlantic Conference*. 2007: Santos, SP, Brazil.

254. Li, A. and S.H. Yalkowsky, *Solubility of organic solutes in ethanol/water mixtures.* J Pharm Sci, 1994. **83**(12): p. 1735-40.
255. Riss, T.L. and R.A. Moravec, *Use of multiple assay endpoints to investigate the effects of incubation time, dose of toxin, and plating density in cell-based cytotoxicity assays.* Assay Drug Dev Technol, 2004. **2**(1): p. 51-62.
256. Trinh, A., *THE APPLICATION OF TISSSUE ENGINEERING PRINCIPLES IN THE DEVELOPMENT OF WOUND HEALING MODELS*, in *Biomedical Engineering*. 2010, University of Sydney: Sydney.
257. Dinges, M.M., P.M. Orwin, and P.M. Schlievert, *Exotoxins of Staphylococcus aureus.* Clin Microbiol Rev, 2000. **13**(1): p. 16-34, table of contents.
258. Kaczmarek, H. and A. Podgórski, *The effect of UV-irradiation on poly(vinyl alcohol) composites with montmorillonite.* Journal of Photochemistry and Photobiology A: Chemistry, 2007. **191**(2–3): p. 209-215.
259. Qin-Yuan, Z., et al. *Tailoring of poly(vinyl alcohol) hydrogels properties by incorporation of crosslinked acrylic acid*. in *Defense Science Research Conference and Expo (DSR), 2011*. 2011.
260. Patel, V. and M. Amiji, *Preparation and Characterization of Freeze-dried Chitosan-Poly(Ethylene Oxide) Hydrogels for Site-Specific Antibiotic Delivery in the Stomach.* Pharmaceutical Research, 1996. **13**(4): p. 588-593.
261. Keshaw, H., A. Forbes, and R.M. Day, *Release of angiogenic growth factors from cells encapsulated in alginate beads with bioactive glass.* Biomaterials, 2005. **26**(19): p. 4171-4179.
262. Rahaman, M.N., et al., *Bioactive glass in tissue engineering.* Acta Biomater, 2011. **7**(6): p. 2355-73.
263. Zhang, L.F., et al., *An ionically crosslinked hydrogel containing vancomycin coating on a porous scaffold for drug delivery and cell culture.* International Journal of Pharmaceutics, 2008. **353**(1-2): p. 74-87.
264. Baume, A., *Sterilisation Design for a Soft Tissue Engineering Scaffold*, in *AMME*. 2009, University of Sydney: Sydney.
265. Holy, C.E., et al., *Optimizing the sterilization of PLGA scaffolds for use in tissue engineering.* Biomaterials, 2000. **22**(1): p. 25-31.
266. Adhirajan, N., et al., *Functionally modified gelatin microspheres impregnated collagen scaffold as novel wound dressing to attenuate the proteases and bacterial growth.* European Journal of Pharmaceutical Sciences, 2009. **36**(2–3): p. 235-245.

Appendix A Method Development & Validation

A.1 Bacterial Strains

The following table shows the bacterial strains, some relevant characteristics and their corresponding growth conditions used in this thesis.

Table 30. Bacterial strains, characteristics and growth conditions.

Bacteria species	Strain	Gram's stain (+/-)	Biofilm Former (y/n)	Growth Media	Plate Media
Escherichia coli	ATCC 11775	-	y	LB	LB-agar
Mycobacterium chubuense	NBB4	+	y	MSM	TSG-agar
Mycobacterium rhodesiae	NBB3	+	y	MSM	TSG-agar
Pseudomonas aeruginosa	NCTC 7244	-	y	LB	LB-agar
Staphylococcus aureus	'Oxford' NCTC 7244	+	n	TSB	TSA
Staphylococcus aureus	ATCC 29213	+	y	TSB	TSA

NOTE: *Staphylococcus aureus* 'Oxford' strain was only used for the Zone of Inhibition (Method 3.3.2.1) and the MIC/MLC assays (Method 3.3.2.2) as it was unable to form appropriate biofilms. All other experiments used *S. aureus* ATCC 29213 as this is a known biofilm former [76].

A.2 Biofilm measurement validation

A.2.1.Method

Both the sonication time and the number of washes needed to be validated for accurate biofilm quantification.

Overnight cultures of *E.coli*, *S. aureus* and *P. aeruginosa* were grown up in there specified culture conditions. A PCL disc (Method 3.1.2.1.3) was put in the bottom of wide-mouth McCartney 15ml Bottles. 2ml of bacteria specific biofilm media (Method 3.2.1, Table 16) was brought to OD600 = 0.1 and transferred to bottles. Stoppers were left loose to ensure good aeration. Bottles were incubated shaken at 100rpm for 24 hours at 37°C. Disc were removed with sterile tweezers and transferred to a petri dish filled with 20ml sterile PBS for to wash off excess media and un-attached cells.

Discs were gently washed three times in sterile PBS, transferred to Eppendorf tubes containing 1ml of PBS and sonicated at maximal frequency for varying amounts of time: 30 seconds, 1, 2 and 5 minutes. A control for each bacterial strain was left un-sonicated. The OD600 of the removed biofilm suspension was measured.

S. aureus biofilms grown up on PCL discs were washed in 20ml sterile PBS up to 3 times to determine the appropriate number of washes. The discs were then transferred to fresh PBS and sonicated. 100 µl of the sonicated PBS was used for serial dilutions of which 50ul were drop plated on appropriate media (see Methods 3.2.1, Table 16). Drop plates were incubated for 18 hours (to ensure small colonies) and counted to determine the viable number of cells in the biofilm recovered. Triplicates were used to test samples treated by varying number of wash steps.

A.2.2.Results

The OD600 for all strains increased dramatically after sonication (Figure 114). The increase in turbidity (OD600) is due to more microbes being removed from the surface of the PCL disc and dispersed in the PBS solution. Varying the time of sonication had little effect on the amount of biofilm removed. The highest turbidity for *E. coli, P. aeruginosa* and *S. aureus* were after 30 seconds, 5 minutes and 5 minutes respectively. The increased *E. coli* biofilm removal at 30 seconds and 2 minutes compared with at 5 minutes is probably due to increased biofilm growth on these discs, as the sonication removal is believed to be time-dependent. 5 minutes was chosen as the sonication time for all microbes used to

simplify processing and because this time achieved efficient biofilm removal in all microbes compared to the non-sonicated controls.

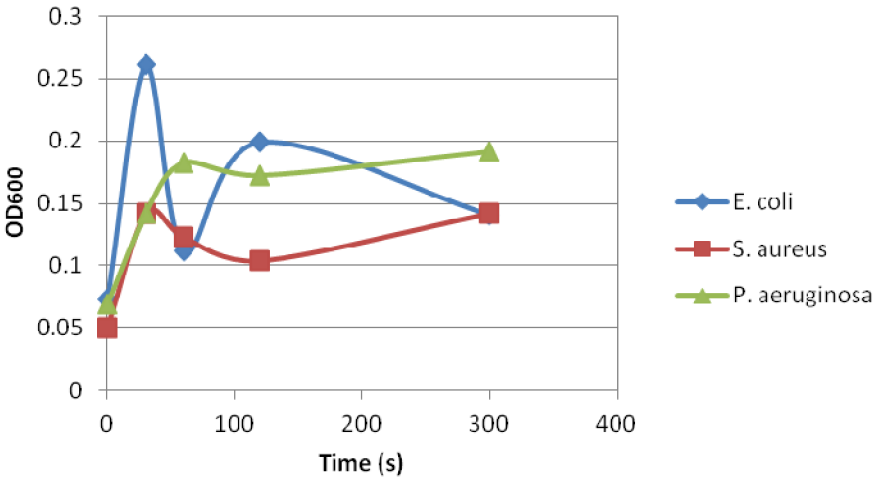

Figure 114. Turbidity (OD600) of removed biofilm after varying sonication treatment times.

After the varied washing steps, biofilms were sonicated for 5 minutes and serial dilutions and drop plating were used to enumerate the biofilms collected. No washing resulted in the recovery of at least 10 times more cells than the washed samples (Figure 115). This is because these samples would include a large number of non-adhered bacteria that were inadvertently transported from the biofilm culture media. Therefore the cells recovered do not selectively represent the biofilm.

One wash decreased the cells recovered by a factor of ten, but further washes did not dramatically decrease the cells recovered. This is because the majority of the biomass loading after washing is strongly adhered to the disc in biofilms and requires sonication removal. Three washes did decrease the number of bacterial cells recovered but considering there was no difference between one and two washes; this is likely due to accidental mechanical removal of biofilm from tweezer manipulations of the discs. As such, two washes was selected as the optimal number to best represent the biofilm grown on discs.

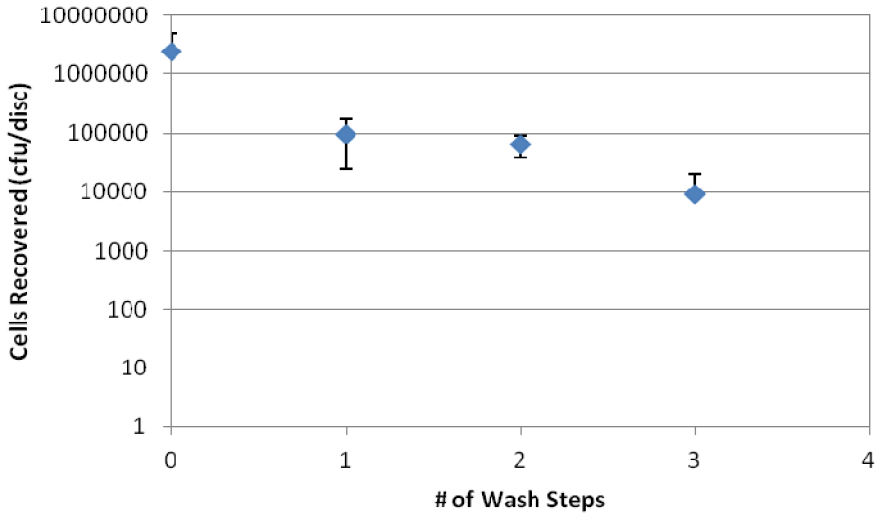

Figure 115. *S. aureus* bacterial cells recovered after varying numbers of wash steps in petri dishes of PBS. Error bars = Std; n = 3.

A.3 Scaffold Interference

A.3.1. Method

HFb were grown up according to the method in 3.4.1.1.1. Cells were harvested and counted as described in 3.4.1.1.2. 100,000 HFb cells were aliquotted into Eppendorf tubes. Sterile PCL scaffolds (dimensions: 7x6x2mm; Method 3.1.1.1) were added to the bottom of the tubes. A set of tubes was left without scaffolds as the cell-only control.

From the cell-only controls and a set of cells + scaffold RNA was extracted and quantified as in 3.4.1.1.2. For the other set of cells + scaffold a slight modification to the method was used: The 1-bromo-3-chloropropane was added first. Tubes were gently swirled until the scaffold appeared completely dissolved. Then the Tri-reagent was added and the extraction and quantification proceeded normally. Different samples and controls were tested in triplicate.

A.3.2.Results

Ideally the *in vitro* wound model that was being designed should quantify the number of HFb and bacterial cells on the scaffold by qPCR of rRNA. This meant that all of the rRNA had to be extracted from cells adhered to the scaffold. The thinking was that if the scaffold could be completely digested in the RNA extraction reagents, then all the rRNA could be collected and would reflect the true cell numbers attached to the scaffold. The full digestion of the scaffold also had the advantage of not having to remove the cells from the scaffold, especially bacterial cells enveloped in biofilm which may be difficult to remove. Because of this, removal of cells from the scaffold would likely add extra variability to the results. Therefore, the full digestion of the scaffolds was reasoned to be the most efficient and reliable way to extract RNA is this system.

The RNA extraction method that was used on the cell-only controls, when the TriReagent was added first, caused the scaffold in the cell + scaffold samples to go translucent but not dissolve. When the 1-bromo-3-chloropropane was added the scaffold only partly contacted this reagent and hence only partially dissolved. After vortexing, globs of partially dissolved scaffold were seen stuck to the walls of the tubes. Conversely when 1-bromo-3-chloropropane was added to the scaffold first, the scaffold completely dissolved with gentle agitation. With addition of TriReagent and after vortexing, no undissolved globs could be seen.

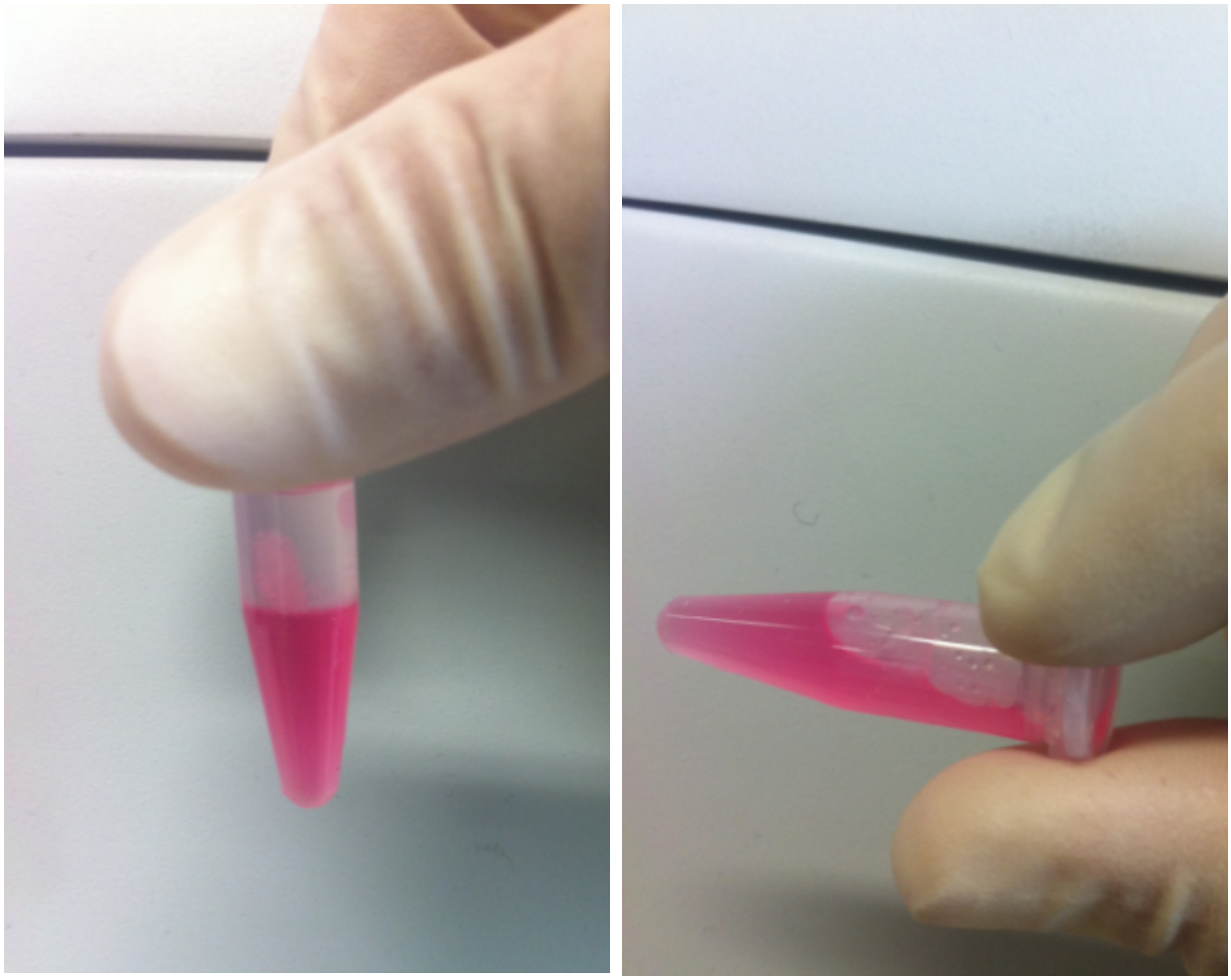

Figure 116. Dissolution of scaffold in RNA extraction reagents. a) TriReagent added first resulting in glob formation. b) 1-bromo-3-chloropropane added first resulting in complete dissolution of the scaffold.

Spectrophotometric quantification results of the different RNA extraction methods are seen in Figure 117. The addition of the scaffold decreased the RNA yield compared to the cell-only control for both methods, however this difference was not significant when the new extraction method was employed.

It is thought that the globs formed from the incomplete dissolution of the scaffold seen in Figure 116 trap nucleic acids preventing them from being extracted and decreasing the yields. The addition of 1-bromo-3-chloropropane first, completely dissolves the scaffold and allowed RNA yields that were not significantly different than the extractions from cells alone.

The very hydrophobic PCL scaffolds dissolved readily in the 1-bromo-3-chloropropane. No globs of PCL remained to entrap RNA. After the addition of TriReagent and phase separation the PCL subsided into the organic phase leaving the nucleic acids uncontaminated in the aqueous phase.

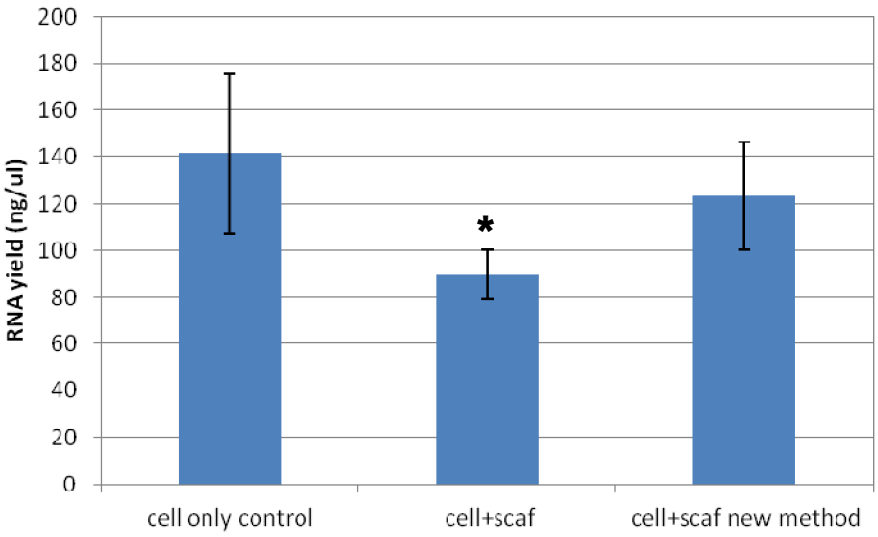

Figure 117. RNA yield from different extraction methods. The 'new method' is the addition of the 1-bromo-3-chloropropane first as oppose to TriReagent. Samples were extracted in triplicate and every sample was quantified in duplicate. * p < 0.05, significantly different to cell-only control (T-test, two tails).

Unfortunately, despite the aforementioned benefits of the new method, it was found that it was ultimately unsuitable for RNA extracting from bi-Phasic scaffolds. When the 1-bromo-chloropropane was added the scaffold seemed to dissolve well and no globules were seen after vortexing the mixture. However, when the aqueous phase was added to isopropanol a white cotton-like precipitate formed (Figure 118). The precipitate is hydrophilic PVA that was extracted along with the aqueous phase and contaminated the RNA. This could not easily be filtered out using standard syringe and hepafilters. Further, the extra manipulations of the RNA would lead to degradation and contamination of the nucleic acids along with lower yields.

The full digestion of the scaffold with 1-bromo-3-chloropropane before addition of TriReagent to extract RNA yielded concentrations that were not significantly different to extractions from cells alone. This is an efficient and reliable method for RNA extraction and was employed when un-altered PCL scaffolds were used for cell-culture. This method may also be possible using other hydrophobic scaffold systems. Due to hydrophilic components in the bi-Phasic scaffolds which contaminated the RNA, the method was

not used in experiments using PVA scaffolds. Instead a method of removing cells and biofilm was developed to use in these studies.

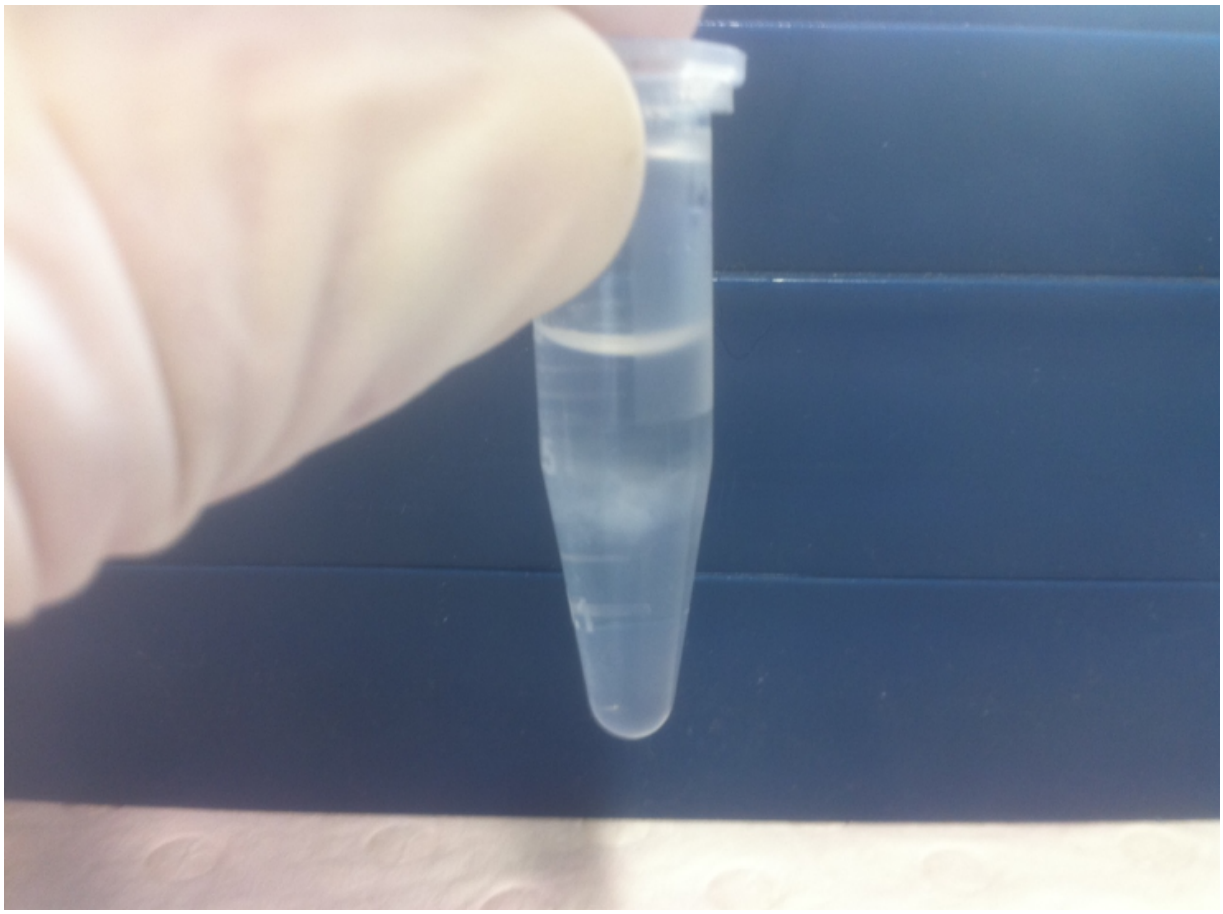

Figure 118. RNA extraction from PVA scaffolds. Cloudy PVA precipitate in the isopropanol, contaminating the RNA.

A.4 Co-culture raw qPCR data

Herein is the collection of qPCR raw data from the Final Co-culture (Results and Discussion 4.4.1.5). The raw data is presented in the original graphs from the qPCR program. The x-axis is the number of PCR cycles and the y-axis is the relative fluorescence reflecting the amount of 16s or 18s PCR product. The fluorescence threshold was determined by pre-generated standard curves for known amounts of the target gene. The relative concentration of 16s and 18s cDNA (relating to the presence of fibroblasts and *S. aureus* respectively) can be seen on the graphs below by the position of the coloured curves. Curves on the left have higher concentration and curves on the right have lower concentration. This is because less starting concentration of the gene requires more PCR cycles to achieve a given fluorescence signal.

The absence of curves entirely suggests no starting gene to amplify. The different coloured curves represent the different scaffold types, while the ever-present red curves are the internal standard curve controls. This raw data is provided here to validate the results aforementioned.

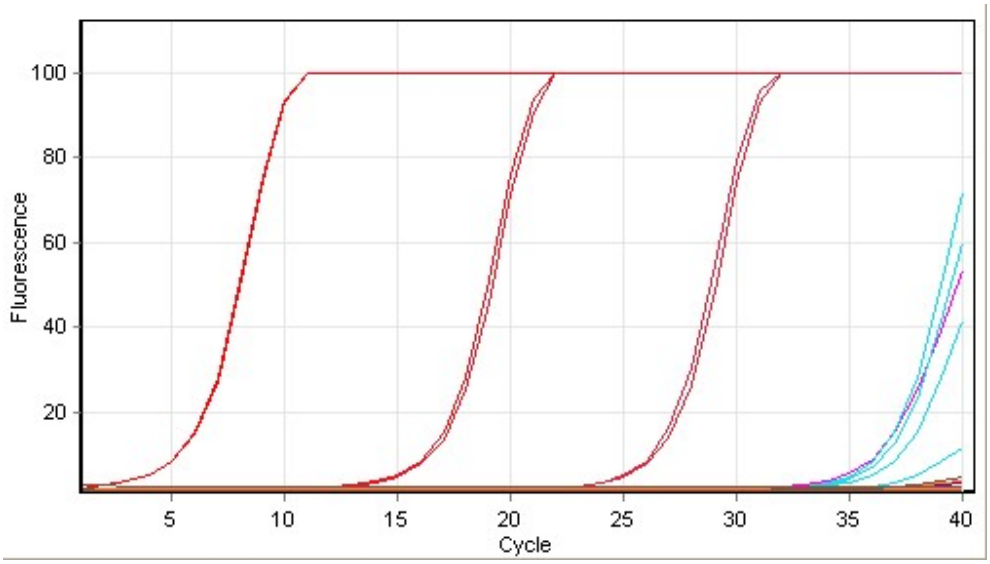

Figure 119. Co-culture qPCR curves: Fibroblast Only control 16s Day 1

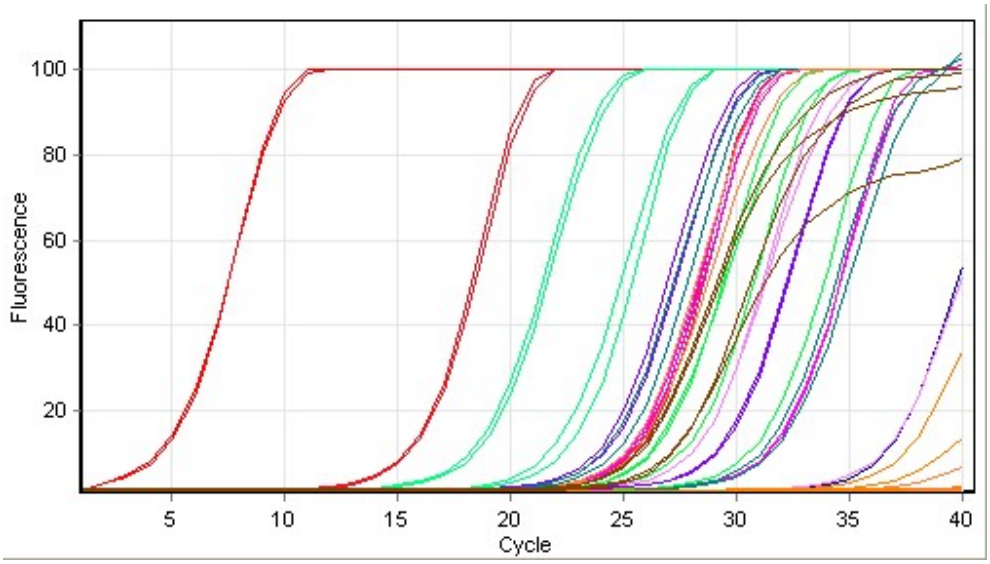

Figure 120 Co-culture qPCR curves: Fibroblast only control 18s Day 1

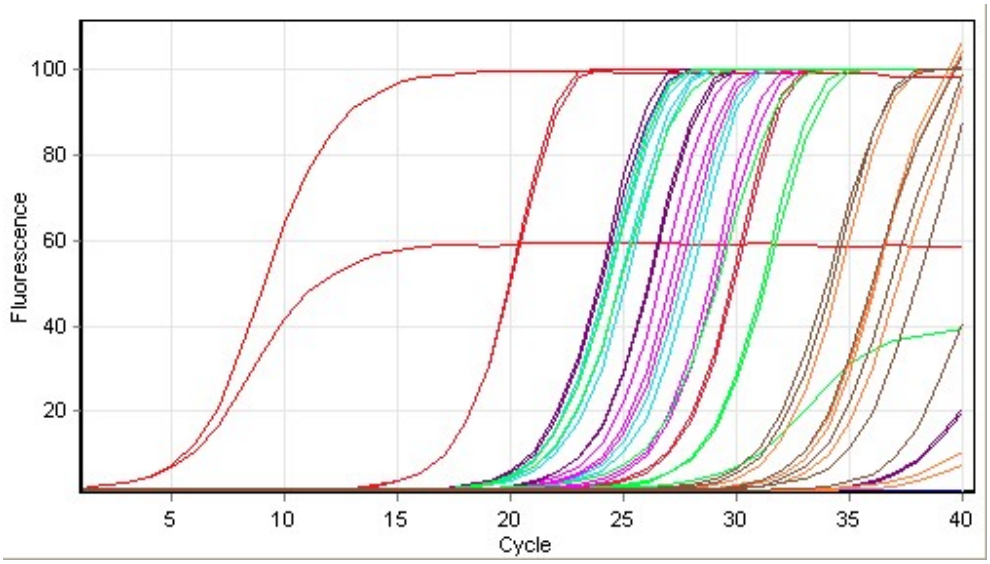

Figure 121. Co-culture qPCR curves: Co-culture 16s Day 1

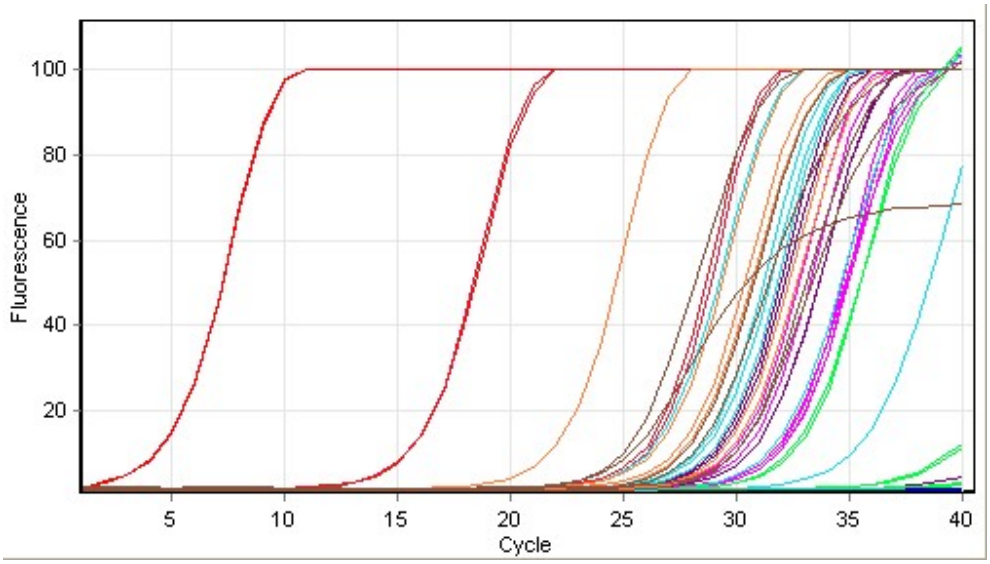

Figure 122. Co-culture qPCR curves: Co-culture 18s Day 1

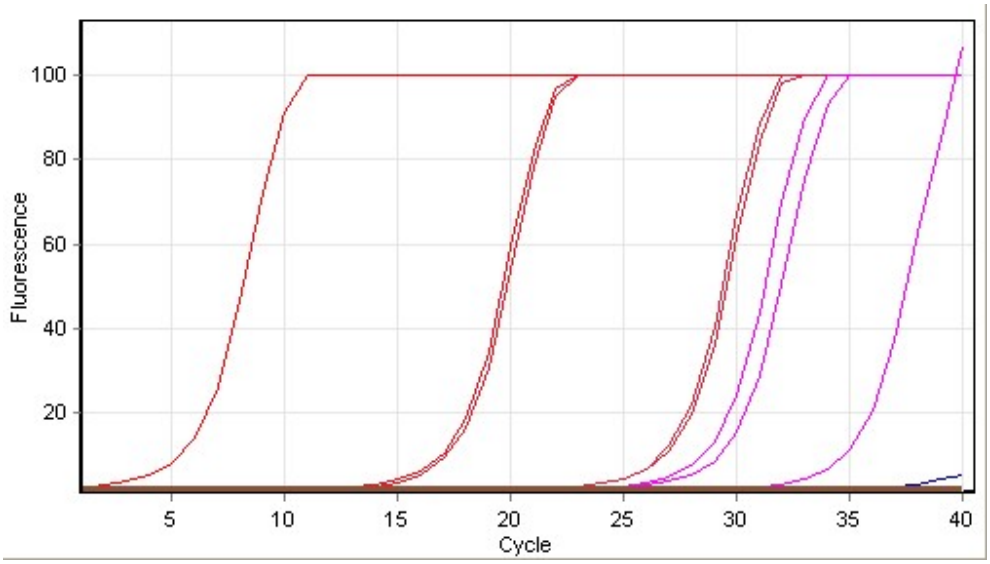

Figure 123. Co-culture qPCR curves: Fibroblast Only control 16s Day 5.

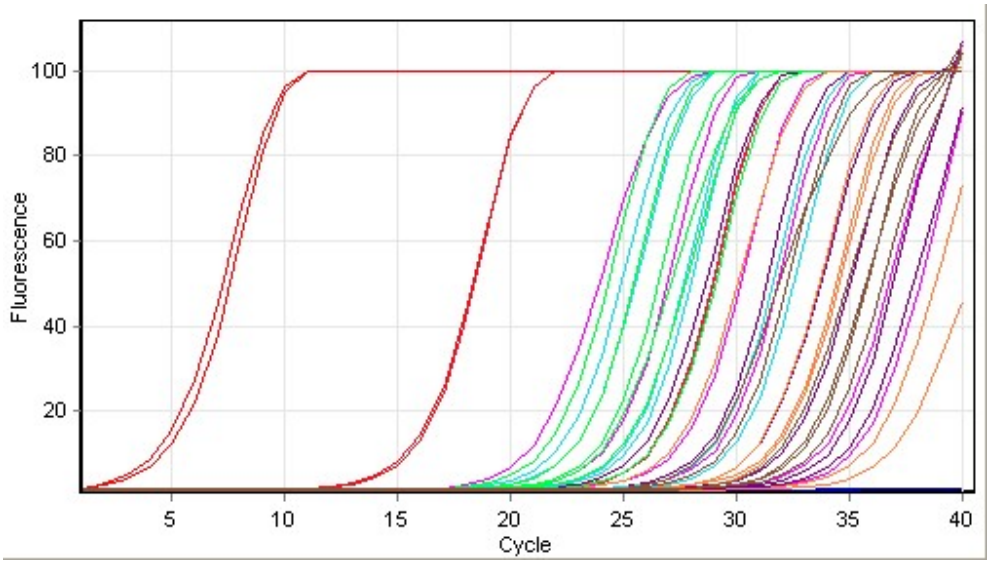

Figure 124. Co-culture qPCR curves: Fibroblast only control 18s Day 5.

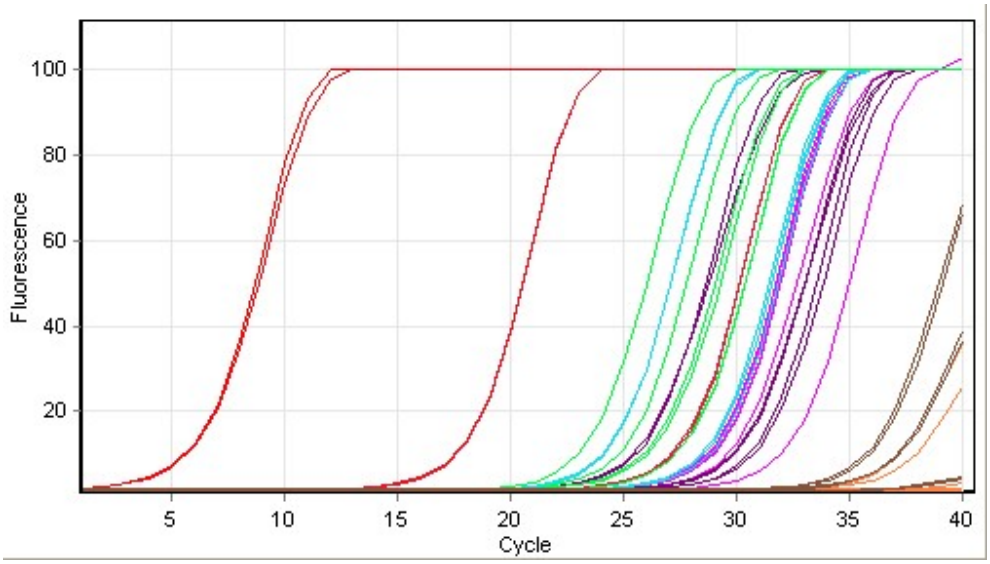

Figure 125. Co-culture qPCR curves: Co-culture 16s Day 5.

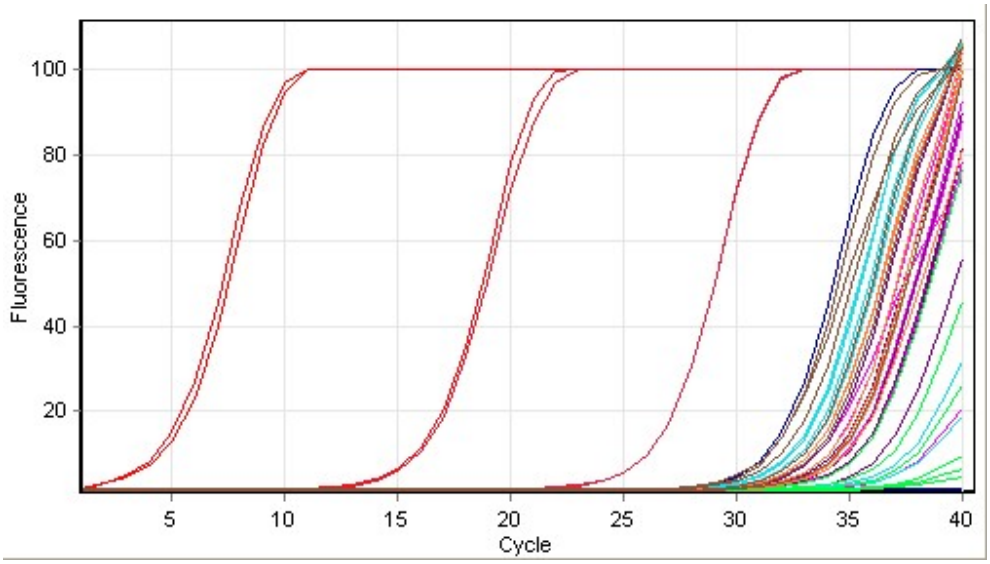

Figure 126. Co-culture qPCR curves: Co-culture 18s Day 5.

Appendix B Inconclusive Results

B.1 Modulating DSC

B.1.1.Method

Hydrogel samples of 5-10mg were weighed into aluminium sample pans and crimp sealed. Modulated Differential Scanning Calorimetry (DSC) experiment was performed (DSC 2920 Modulated DSC, TA Instruments). Dried samples of PVA and cross linked PVA weighing 5-10 mg, were put into aluminium sample pans, crimp sealed then placed in the DSC instrument. Samples were first heated from 35°C to 150°C (first heating cycle); then cooled to 35°C followed by heating up to 120°C (second heating cycle), all at a heating rate of 2.5°C min^{-1} under nitrogen and with oscillations of +/- 2°C every 60 seconds. Results were taken from the second heating runs of the experiments in order to avoid experimental effects arising from the previous thermal history, structural relaxation and incomplete chemical reactions [38]. The reversible heat flow signal was analysed to attempt to extract a glass transition temperature.

B.1.2.Results

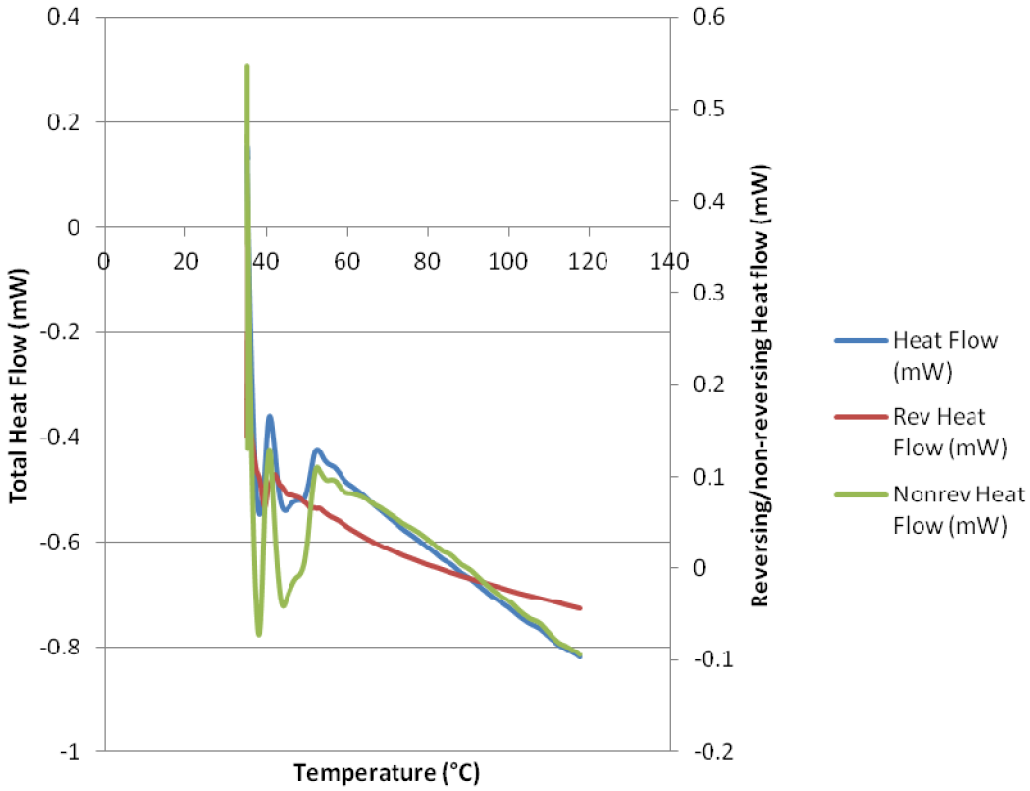

Modulated DSC uses small oscillations to simultaneously measure reversible and non-reversible heat flow signals. This is sometimes effective when the total heat flow as measured by regular DSC over shadows due to superposition. Reversible heat flow signals show the glass transition temperature.

In the figure above the reversible heat flow signal shows what looks like a step-down feature between 60-100°C. This could reflect the glass transition of PVA which is around 80°C. However, the feature is over a large temperature range and pin-pointing the Tg, from this data is dubious.

Due to the lack of confidence in determining the Tg in the control sample, it was decided that it would be invalid to try and compare changes in Tg between samples treated with ethanol. Thus this line of experimentation was discontinued. However, more work in this area is suggested as Tg is a key thermal property of hydrogel functionality and is not determined for most new hydrogel devices and materials.

B.2 Enumeration of Cells by qPCR

B.2.1.Method

HFb and *S. aureus* cells were grown up and enumerated as described in methods section 3.4.1.1.1. Cells were combined into tubes in specific numbers (Table 31). Each tube was prepared in triplicate.

Table 31. HFb/S. aureus combination tubes for enumeration.

Tube #	Fibroblast (cell #)	*S. aureus* (cell #)
1	100,000	$2.5x10^8$
2	50,000	$5x10^8$
3	10,000	$2.5x10^9$
4	5,000	$5x10^9$

RNA was extracted from cells using the method for *S. aureus* in 3.4.1.1.2. Then 8µl of RNA from tubes was converted to cDNA (Method 3.4.1.1.3). qPCR was carried out on cDNA samples from combined tubes (Method 3.4.1.1.8). Neat samples were tested as well as 100-fold dilutions of each sample. Internal controls containing a standard curve of the purified 18s and 16s gene of interest of known gene copy concentration (dilutions: 10^{-1}, 10^{-4}, 10^{-7}) were run in each qPCR. This was used to calculate the gene concentration of each sample and form a relationship between cell number and gene concentration. All reactions were run in duplicates.

B.2.2.Results

The Ct results from qPCR were converted to DNA concentration (copies/µl) by comparing with internal standards from the same run. Values from either the neat or 100-fold dilution were chosen based on Ct value. A Ct value of 10-20 was considered in the optimal range. Chosen values were then plotted against the number of cells in the starting sample to produce curves correlating DNA concentration to cell number (Figure 127).

Linear correlations were expected as each cell type will have a given set of rRNA genes that are independent of cell number. rRNA should be converted to cDNA in a 1:1 manner during reverse transcription. It was assumed that no cells would have no rRNA and hence the DNA concentration would be zero. As such the y-intercept of these standard curves was set at zero.

The standard curve for quantifying fibroblasts was seen in Figure 127a. A weak linear correlation can be seen ($R^2 < 0.95$). This may be due to overestimation of cell numbers. HFb do not stay well suspended in solution which may account for less cells being added to tubes, hence the overestimation. The equation from the curve suggests there are ~60 copies of the 18s gene per fibroblast (after accounting for a 15µl qPCR reaction volume). Although there may actually be more as this data does not account for losses that inevitably take place during processing.

Figure 127b shows the standard curve for *S. aureus*. Only three points can be seen on the curve as the results for Tube 4 counter-intuitively produced the lowest DNA concentration values. This is attributed to human error. A strong linear correlation was seen ($R^2 > 0.95$). Each cell would have multiple copies of this essential gene – thus a linear relationship was expected. It is known that *E. coli* has around 1000 copies of its 16s rRNA gene [184]. This suggests that there are substantial losses throughout the process, likely as a result of incomplete RNA extraction from the tough *S. aureus* cells. *S. aureus* are notorious for producing low RNA yields [191]. The difference in the linear correlations between the bacteria and cells is due to the difference in cell size and therefore volume.

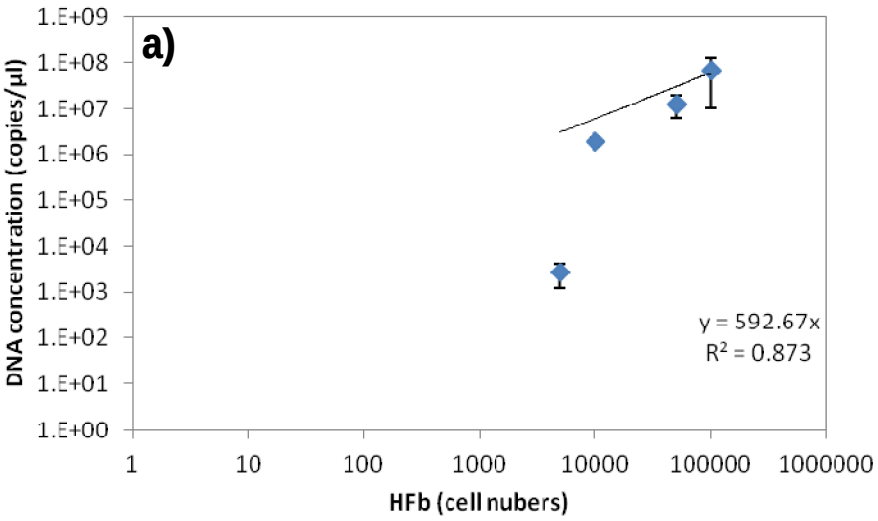

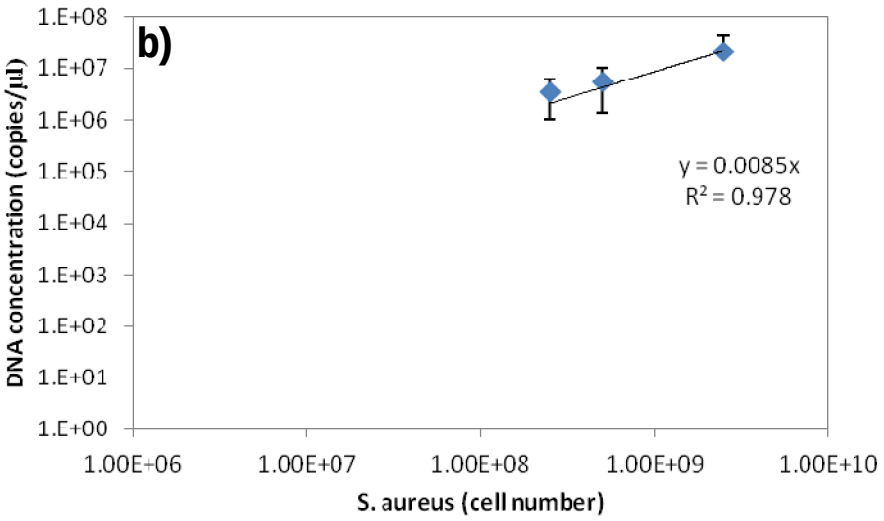

Figure 127. Standard curves relating DNA concentration to cell number for a) HFb and; b) S. aureus. Error bars = Std; n=3.

The results suggest a level of unreliability as such the curves can be used for determination of absolute cell number in future experiments, only tentatively. It may be an over complication to calculate cell number from DNA concentration. Matsuda *et al*, produced a linear correlation between a cell number of different bacteria (including S. aureus) and Ct that was very reliable ($R^2 > 0.99$). The benefit of our method is in cases where the copies of rRNA per cell will likely fluctuate, e.g. under severe stress or different growth phases, it may not be valid to determine cell number based on rRNA quantification, but the rRNA quantification itself will still be a marker for viability. Hence, the method for quantifying ribosomal DNA using this 2-step RT-qPCR method can be used for modelling diseased states like chronic skin ulcers.